Tampere University

CHRISTINE GERING

Design Strategies for Polysaccharide Hydrogels Used in Soft Tissue Engineering

Modification, Testing and Applications of Gellan Gum

Tampere University Dissertations 803

Tampere University Dissertations 803

CHRISTINE GERING

Design Strategies for Polysaccharide Hydrogels Used in Soft Tissue Engineering

Modification, Testing and Applications of Gellan Gum

ACADEMIC DISSERTATION
To be presented, with the permission of
the Faculty of Medicine and Health Technology
of Tampere University,
for public discussion in the auditorium TB109
of the Tietotalo building, Korkeakoulunkatu 1, Tampere,
on 16 June 2023, at 12 o'clock.

ACADEMIC DISSERTATION
Tampere University, Faculty of Medicine and Health Technology
Finland

Responsible supervisor and Custos
Professor Minna Kellomäki
Tampere University
Finland

Pre-examiners
Professor Pietro Matricardi
Sapienza University of Rome
Italy

Professor Berit L. Strand
Norwegian University of Science and Technology
Norway

Opponent
Professor João F. Mano
University of Aveiro
Portugal

The originality of this thesis has been checked using the Turnitin OriginalityCheck service.

Cover design: Roihu Inc.

ISBN 978-952-03-2900-6 (print)
ISBN 978-952-03-2901-3 (pdf)
ISSN 2489-9860 (print)
ISSN 2490-0028 (pdf)
http://urn.fi/URN:ISBN:978-952-03-2901-3

Carbon dioxide emissions from printing Tampere University dissertations have been compensated.

PunaMusta Oy – Yliopistopaino
Joensuu 2023

"Man's quest for knowledge is an expanding series whose limit is infinity, but philosophy seeks to attain that limit at one blow, by a short circuit providing the certainty of complete and inalterable truth. Science meanwhile advances at its gradual pace, often slowing to a crawl, and for periods it even walks in place, but eventually it reaches the various ultimate trenches dug by philosophical thought, and, quite heedless of the fact that it is not supposed to be able to cross those final barriers to the intellect, goes right on."

— from *His Master's Voice* by Stanisław Lem

ACKNOWLEDGEMENTS

This study was performed at the Biomaterials and Tissue Engineering Group within the Faculty of Medicine and Health Technology of Tampere University. This work was funded by the TAU doctoral school, the Jenni & Antti Wihuri foundation, as well as the Academy of Finland through the Center of Excellence – Body on Chip project, for which I am extremely grateful.

I wish to express my sincerest gratitude to my supervisor Professor Minna Kellomäki, for providing me the opportunity and time to carry out research in the extraordinary and inspiring field of biomaterials for medical engineering. Further, I want to profoundly thank the members of my doctoral follow-up group, including PhD Jenny Párraga, Professor Vesa Hytönen, and Associate Professor Oommen P. Oommen, for their support throughout the years, valuable advice on project planning, and encouragement to stick to my goals.

This dissertation is based on five original publications, which would not have been possible without the contributions from my co-authors: Janne Koivisto, Jenny Párraga, Anum Rasheed, Sampo Tuukkanen, Jenni Leppiniemi, Kaisa Vuornos, Vesa Hytönen, Susanna Miettinen, Jennika Karvinen, Reeja Maria Cherian, Birhanu Belay, Jari Hyttinen, Katriina Aalto-Setälä, Hanna Vuorenpää, Lucía Botero, and of course Minna Kellomäki. Foremost, however, I want to highlight the roles of Janne and Jenny, who initiated the hydrogel projects at our laboratory and were invaluable guidance throughout my Master thesis and doctoral research.

This work was further supported through fruitful collaboration with other groups at Tampere University and the former BioMediTech. These include the Neuro Group around Adjunct Professor Susanna Narkilahti for help in handling the tissue samples in Publication IV, as well the Heart Group of Professor Katriina Aalto-Setälä assisting with the cardiac cells and technical support in Publication IV. The Adult Stem Cell group around Professor Susanna Miettinen for providing adipose and bone-marrow stem cells, as well as fantastic technical assistance for Publications III and V. The SEC MALS data in Publication I was provided through collaboration with Stepan Podzimek and Milena Bennewitz at Wyatt Technology, who carried out the analysis and assisted with their interpretation.

Finally, I would like to thank all colleagues who provided technical help and beneficial discussions surrounding data analysis and academic writing. Namely, PhD Vijay Parihar for recording ^{1}H-NMR spectra; Professor Michiel Postema for advice on rheology evaluation; Professor Jonathan Massera for providing the ICP-OES data; PhD Kirsi Penttinen for carrying out the gelatin coating experiments; the Laboratory of Chemistry and Bioengineering at Tampere University for providing NMR and FT-IR devices and sample preparation advice; all the help and instructions from our laboratory personnel including Heikki Liejumäki, Anna-Maija Honkkala, Elina Lehtinen, Juha Heikkilä, and Sari Kalliokoski; Tampere CellTech Laboratories and Tampere Imaging Facility (TIF) for their services; and of course Peter Heath for proof-reading and editing several of the published manuscripts.

I could not have undertaken this journey without the support of my friends and family. It is a wealth to be surrounded by such wonderful and unique people, both online and offline, who, without their knowledge, are and inspiration and support structure to me, but also provided much needed distraction from thesis writing. A special thanks must go to Sami, who was with me in every step of this journey, and has lent an open ear for all issues, especially for software struggles. Much like catching a whale, writing a thesis is done with persistence and joy: For forty days or even more, the line went slack then tight once more. All boats were lost, there were only four, but still that whale did go. Soon may the Wellerman come and bring us sugar and tea and rum. And one day, when the tonguing is done, we'll take our leave and go.

Tampere, December 2022

Christine Gering

ABSTRACT

Hydrogels are water-swollen polymer networks which provide an aqueous, three-dimensional environment and can mimic the biological cell environment and tissue architecture. Therefore, hydrogels are a valuable class of biomaterials for tissue engineering purposes that can be modified to support a specific application, such as the encapsulation of cells or as implantable device. Gellan gum is a microbial polysaccharide that readily forms self-supporting hydrogels in the presence of ions, and that has been investigated for medical applications due to its biocompatibility. However, due to its lack of innate cell recognition sites in its structure, gellan gum is highly inert and does not elicit any cell response required for *in vitro* cell culture or *in vivo* tissue integration

Here, the possibilities to chemically modify gellan gum and render it bioactive for cell culture purposes are explored. The investigated modifications include purification, oxidation, reductive scissoring, as well as blending and chemical crosslinking, and are initially reviewed for their biocompatibility and ability to form hydrogels. The modified materials were assessed for their mechanical and viscoelastic properties, and basic cell response using the human fibroblast line WI-38. The cells were seeded either 2D on the surface of a gelated sample or encapsulated in the 3D hydrogel. Similarly, more advanced cell lines, such as human adipose stem cells, bone marrow-derived stem cells and a vascular co-culture model, were investigated using some of the formulations, and evaluated using different microscopic techniques. Furthermore, extrusion bioprinting was investigated as biofabrication method, and tissue response *in vivo* of cell-free hydrogels was ascertained by subcutaneous implantation.

In conclusion, the aim of thesis was to examine different modification approaches for the hydrogel gellan gum, but also to present a wholistic assessment protocol of modified hydrogel. Gellan gum acts as model polymer with the intent of projecting the design strategies and evaluation insights onto other polysaccharides and hydrogels. It has proven to be a suitable base polymer to create a material library with various mechanical and bioactive properties.

CONTENTS

List of Figures

List of Tables

ABBREVIATIONS

2D	two-dimensional
3D	three-dimensional
ADH	adipic acid hydrazide
ALP	alkaline phosphatase
avd	avidin
BSA	bovine serum albumin
CDH	carbohydrazide
CNCA	charge neutralized chimeric avidin
DAPI	4',6-diamidino-2-phenylindole
d.i.	de-ionized
DNA	deoxyribonucleic acid
DPBS	Dulbecco's phosphate buffered saline
EBM-2	endothelial basal medium
EC	endothelial cells
ECM	extracellular matrix
EGM-2	endothelial growth medium
FRAP	fluorescence recovery after photo-bleaching
FT-IR	Fourier transform infrared spectroscopy
gela	gelatin
GAG	glycosaminoglycans
GG	gellan gum (low acyl form)
GGox	oxidized gellan gum
GGsciss	reductively cleaved gellan gum
GLP	good laboratory practices
hASC	human adipose stem/stromal cells
hBMSC	human bone marrow derived stem/stromal cells
hCM	human cardiomyocytes
HUVEC	human umbilical vein endothelial cells
HPLC	high performance liquid chromatography
ICP-OES	inductively coupled plasma optical emission spectroscopy

LAOS	large amplitude oscillatory sweep
LVER	linear viscoelastic range
MMP-1	matrix metalloproteinase
NaGG	sodium purified gellan gum
NaGG-avd	sodium purified gellan gum coupled with avidin
NDS	normal donkey serum
NMR	nuclear magnetic resonance
PDI	polydispersity index
PFA	paraformaldehyde
RGD	peptide sequence arginine (R) glycine (G) aspartate (D)
RNA	ribonucleic acid
RT-PCR	reverse transcription polymerase chain reaction
SAOS	small amplitude oscillatory sweep
SC	stem/stromal cells
SEC	size exclusion chromatography
SMA	smooth muscle actin
SPD	spermidine trihydrochloride ($C_7H_{19}N_3 \cdot 3\ HCl$)
SPM	spermine tetrahydrochloride ($C_{10}H_{26}N_4 \cdot 4\ HCl$)
TERM	tissue engineering and regenerative medicine
TEMPO	2,2,6,6-tetramethylpiperidinyl-1-oxyl
TPC	tissue culture plastic
TRITC	tetramethylrhodamine
u.p.	ultra-pure
UV	ultraviolet light
VEGF	vascular endothelial growth factor
WI-38	human fibroblast line WI-38

ORIGINAL PUBLICATIONS

Publication I Gering, C., Rasheed, A., Koivisto, J. T., Párraga, J., Tuukkanen, S., & Kellomäki, M. (2021). Chemical modification strategies for viscosity-dependent processing of gellan gum. Carbohydrate Polymers, 269, 118335. https://doi.org/10.1016/j.carbpol.2021.118335

Publication II Gering, C., Koivisto, J.T., Parraga, J.E., Kellomäki, M. (2018). Reproducible preparation method of hydrogels for cell culture applications – case study with spermidine crosslinked gellan gum. In: Eskola, H., Väisänen, O., Viik, J., Hyttinen, J. (eds) EMBEC & NBC 2017. EMBEC NBC 2017 2017. IFMBE Proceedings, vol 65. Springer, Singapore. https://doi.org/10.1007/978-981-10-5122-7_203

Publication III Gering, C., Koivisto, J. T., Párraga, J., Leppiniemi, J., Vuornos, K., Hytönen, V. P., Miettinen, S., & Kellomäki, M. (2019). Design of modular gellan gum hydrogel functionalized with avidin and biotinylated adhesive ligands for cell culture applications. PLoS ONE, 14(8), 1–22. https://doi.org/10.1371/journal.pone.0221931

Publication IV Koivisto, J. T., Gering, C., Karvinen, J., Maria Cherian, R., Belay, B., Hyttinen, J., Aalto-Setälä, K., Kellomäki, M., & Parraga, J. (2019). Mechanically Biomimetic Gelatin-Gellan Gum Hydrogels for 3D Culture of Beating Human Cardiomyocytes. ACS Applied Materials and Interfaces, 11(23), 20589–20602. † https://doi.org/10.1021/acsami.8b22343

Publication V Gering, C., Párraga, J., Vuorenpää, H., Botero, L., Miettinen, S., Kellomäki, M., 2022. Bioactivated gellan gum hydrogels affect cellular rearrangement and cell response in vascular co-culture and subcutaneous implant models. Biomaterials Advances 143, 213185. https://doi.org/10.1016/j.bioadv.2022.213185

† This publication has previously been included in the doctoral dissertation of Janne T. Koivisto "Development and Characterization of Gellan Gum Based Hydrogels for Soft Tissue Engineering Applications" at Tampere University in November 2019.

CONTRIBUTIONS

I The study was design by all co-authors, while the methodology was refined, and actualization of the project carried out by CG. CG wrote major part of the manuscript and validated the data evaluation together with JTK.

II The study was designed together by CG and co-authors, the preparation method was devised and refined by CG. The work and evaluation were carried out by CG. The abstract was written by CG.

III The study was designed by CG and co-authors. The material synthesis and characterization were carried out by CG. The manuscript was written by CG.

IV CG is the second author and has contributed substantially to the work. The study was conceptualized, and the materials were designed and synthesized by JTK and JP. Material degradation was characterized and evaluated by CG. Further, CG assisted in writing the manuscript and graphical work. In contrast to the dissertation from JTK, here the degradation of the formulations, as well as their cross-comparison to hydrogels in other publications is established, and the scientific contribution is well distinguished.

V The study was originally conceptualized by JP, and the final design was established by all co-authors. CG prepared the materials, designed, and carried out mechanical analysis. The cell culture study was designed by HV and SM and carried out and analyzed by CG. The animal test was designed and handled by JP, while the analysis was supported by CG. The manuscript was written in majority by CG.

1 INTRODUCTION

In the endeavor to study life and living organisms, researchers are developing tools and technologies to mimic tissues and organs for medical engineering (Langer and Vacanti, 1993). It has been well accepted that there are three components of tissue engineering: cells, a surrounding matrix, and stimulating factors such as growth factors, nutrients, and mechanical stimulation (Caddeo *et al.*, 2017). Material scientists thus have the task to create such matrix material that supports the growth and viability of living cells, but also supports the experiment and analysis in a meaningful way and is an accurate reflection of the native cell environment. These artificial matrices are needed not only to circumvent ethical and economic issues of animal and clinical testing, but more crucially to critically advance the relevance and the overall understanding of the biological system in the fields of stem cell research, disease modelling, and personalized healthcare.

Hydrogels are water-swollen network-forming polymers, and inherently suited to the task of encapsulating cells while providing biochemical and biomechanical stimulation. Many polymers are capable of forming hydrogels, including those from natural, synthetic, microbial sources, and their mode of network formation, referred to as crosslinking and gelation, is equally diverse (Barbucci, 2009). Typically, hydrogels are engineered specifically for one purpose or one tissue model, and no universal hydrogel material exists. There is particular interest to create modular hydrogels as facile tools to easily adapt specific properties within the hydrogels, such as biological factors, or gelation speed, or final stiffness, without causing great inconvenience to the cell biologist and while also retaining other properties of the material.

Here, the polysaccharide gellan gum (GG) is investigated as hydrogel material for cell encapsulation and tissue engineering, where it serves suitably as a model compound for different chemical modification and mechanical reinforcement. GG provides an advantageous base material for this subject, because it is abundantly available, relatively inexpensive, biocompatible and inert, non-immunogenic due to its microbial source, outstanding capacity to form rigid hydrogels at low concentration, and optical transparency (Morris *et al.*, 2012; Smith *et al.*, 2007).

However, the aforementioned inertness must be overcome by compounding and bioactivation, in order to provoke any positive cell response. A core subject of this thesis is hence to investigate different modification strategies to improve and activate this hydrogel material, alongside a profound analysis of the resulting properties, such as mechanical stiffness, degradation, and cytocompatibility. Further, the available analytical tools to thoroughly describe hydrogel properties and performance as tissue engineering construct are described, and their relationship to application observation is discussed.

Relevant background on hydrogels for tissue engineering, GG, as well as modification strategies will be explored initially. The results and discussion are organized in the order of hydrogel modification, characterization, and application throughout. Firstly, different modification strategies are discussed, according to their purpose and application onto polysaccharides. Both the biological and mechanical properties of a hydrogel are crucially important for their application in tissue engineering, and the characterization of both aspects will be analyzed alongside each other. Finally, the applications of such modified gellan gum will be discussed, and the translation of experimental results to the creation and mimicking of different tissue types.

2 LITERATURE REVIEW

This literature review will explore the basis of hydrogels used in tissue engineering and regenerative medicine, with a larger focus on *in vitro* cell culture and disease modeling application. General aspects of hydrogel design will be discussed, including adjustment of physical properties and bioactive functionalization strategies. A special highlight is on the polysaccharide gellan gum, nonetheless other polysaccharide hydrogels will be briefly introduced. Further, modification strategies for polysaccharides presented in the literature are listed and critically evaluated.

2.1 Hydrogel polymers for tissue engineering purposes

Hydrogels have been identified as excellent materials to mimic the native extracellular matrix of cells, thus providing artificial tissue platforms for *in vitro* cell culture, disease modeling, general tissue engineering applications and regenerative medicine (Drury and Mooney, 2003; Liaw *et al.*, 2018; Madl and Heilshorn, 2018; Park and Gerecht, 2015; Peppas *et al.*, 2006; Tibbitt and Anseth, 2009). All hydrogels are understood as water-swollen polymeric networks, however their structure and origin are highly diverse (Barbucci, 2009). Typically, hydrogels are distinguished by either their sourcing, e.g., mammalian tissue, bacterial product, plant-based, or synthetic, or through their chemical building blocks, e.g., polypeptide, polysaccharide, or polyvinyl, but often also by their network formation strategy, e.g., chemical, photon, physical, or thermal crosslinking.

From this broad spectrum of hydrogel varieties, we can easily derive their fascinating range of properties in mechanics and biology. Specifically, hydrogels are great to mimic native tissues, due to the possibility to cultivate cells in 3D for disease and tissue models, as well as the possibility to fill volumetric defects in regenerative applications (Drury and Mooney, 2003). They further provide an aqueous, non-toxic environment and typically a low-density non-restricting matrix, so that cells can expand and migrate as needed (Kraehenbuehl *et al.*, 2009; Walters and Gentleman, 2015). There are two main aspects to consider for the design of any biomaterial: biological response and mechanical features. Essentially, a balance must be struck

between the introduction of cell recognition site, cytocompatibility, material stiffness and degradability (Brandl *et al.*, 2007; Kyburz and Anseth, 2015; Mason *et al.*, 2013; Peng *et al.*, 2018; Santos *et al.*, 2015; Wong *et al.*, 2019).

Most hydrogels are indeed not inherently toxic to cells, and will not actively impair their vitality. However, it should be noted that the correct design features, namely biological interaction, can further advance and direct certain cell growth and response, such as the differentiation of stem cells down the desired path, or the elongation of attachment-dependent cells (Alakpa *et al.*, 2016; Broguiere *et al.*, 2018; Castillo Diaz *et al.*, 2016; Li *et al.*, 2012; McKee and Chaudhry, 2017). There are common drawbacks to hydrogel polymers that must be appreciated and raise the needs for modification. On one hand of the spectrum there are synthetic polymers, which typically are easy to modify and form robust hydrogels in controlled manner. However, biological functionality has to be introduced separately in the majority of the cases, and degradation has to be strategized for as well. On the other end of the spectrum there are tissue-derived materials such as collagen and decellularized basement membranes, which are natively recognized by cells, but are challenging to modify and fabricate into self-supporting hydrogels, and also have rapid degradation profile. Modification strategies to achieve the desired properties within a hydrogel will be discussed in more detail in the following chapter 2.3.

The polymer GG is at the center of this research work and is featured throughout the Publications I-IV. Undoubtedly, GG has some outstanding material properties and certain advantages, however it essentially functions as a model polymer. Its structure and related properties will be discussed in more detail in chapter 2.2. This first chapter will introduce design parameters of hydrogels, general notes on polysaccharide hydrogels, as well as analysis techniques relevant to hydrogels.

2.1.1 Relevant aspects of hydrogel design

In order to discuss rational design, the application requirements have to be considered. These requirements stem from both the target cell or tissue type, as well as the user and fabrication needs before, during and after the experiment or respective application. To illustrate, for a simple *in vitro* cell encapsulation experiment, the user will have to prepare the so-called hydrogel precursor, form the hydrogel at the target location, sustain the culture for the desired period and analyze the construct thereafter. Thus, in a hypothetical world, the ideal hydrogel for a cell encapsulation experiment would have the following properties:

- The hydrogel precursor and components are affordable and have long shelf-life.
- Both the chemical structure, molecular weight, purity, and the possible degree of modification of the polymer are well-known.
- The polymer is sterile, or it can easily be sterilized before application.
- The polymer dissolves in various aqueous solutions and cell culture media without detrimental effects on known properties.
- Hydrogels are formed either in a suitable time frame after the addition of crosslinker, or upon trigger such as UV-light.
- The network possesses suitable diffusion characteristics, so that waste and nutrients are exchanged as necessary, and no necrotic cell core would develop.
- The hydrogel is mechanically stable in the sense that cells will not contract the hydrogel beyond recognition. Further, the hydrogel is rigid enough to allow for flow of cell culture medium past its surface without detrimental erosion.
- The hydrogel has adequate mechanical characteristics for the cell type in question, ideally so that the modulus can be adjusted *via* crosslinking mechanism to the cells' needs without changing hydrogel properties or density.
- The architecture provides attachment sites for attachment-dependent cells such as fibroblasts, so that the cells could interact with the hydrogel matrix and feel the inferred mechanical characteristics.
- Other cell-guiding factors are provided as needed, if necessary for these to be tethered to the network rather than provided in the culture medium.
- The hydrogel has a suitable degradation profile or provides degradation sites that allow for the remodeling by the cells, in order for them to divide and migrate.
- Alternatively, there would be an external trigger to induce complete matrix degradation, which allows for the cells to be assessed post-culture period
- It is transparent to allow for visualizing the encapsulated cells during culture and after optional staining procedure

Unfortunately, such a hydrogel is likely to remain fiction. While the literature provides a host of attractive formulations and ingenious designs, some compromises must be made. This subchapter aims to delve further into key design features of a hydrogel for tissue engineering and regenerative medicine (TERM) applications.

The biological relevance of a hydrogel is dictated by the presence of bioactive sites and the absence of harmful or toxic substances. Firstly, the inherent cytocompatibility and non-cytotoxicity of a material is established, commonly with an extract or direct contact *in vitro* cell test. According to the European standard EN ISO 10993-IV for biomedical device evaluation, the investigated biomaterial should achieve a cell viability of at least 70% viability as compared to a positive control material (ISO 10993-1, 2009). From a synthetic polymer perspective, typically small monomer or oligomer fragments, residual crosslinking agents or polymerization chemicals can be the source of toxicity and cell damage. On the other hand, natural hydrogels pose the risk of endotoxins and other allogenic risks (Magnusdottir *et al.*, 2013; Ménard *et al.*, 2010). It should be noted that this, however, is not a marker of a "good" tissue mimic, but rather the basis of cell viability. Otherwise, the generic tissue culture plastic (TCP) and styrene would be ideal biomaterials.

Moreover, cells interact with their native environment, the extracellular matrix (ECM) in highly complex ways through ubiquitous signaling arrays. The adhesion between a cell and its surrounding matrix provides the basis for cell migration, tissue organization, and differentiation, through which remodeling and tissue homeostasis are enabled (Berrier and Yamada, 2007; Li *et al.*, 2017). Integrins are transmembrane cell receptors that provide these adhesion sites between cells and their matrix. There are 24 distinct integrin receptors that bind various ECM ligands with different affinities, but all provide bi-directional signaling between the receptor and the cytoskeleton (Luo *et al.*, 2007). This bi-directional signaling is the basis for mechanotransduction, which is the communication of mechanical environment to the cell. To complicate things further, it has been found that also the overall ligand density and their spacing can greatly affect cell recognition in two-dimensional (2D) as well as in three-dimensional (3D) environments (Walters and Gentleman, 2015).

Native tissue and ECM contain certain peptide sequences that can be identified by integrins from components such as fibronectin, vitronectin, collagen and laminin. The full biochemical makeup of ECM can partially be recapitulated in an artificial environment, however knowledge of the matching peptide sequence has been shown to be successful (dos Santos *et al.*, 2019; Ferris *et al.*, 2015; Macková *et al.*, 2016). Peptide motifs utilized for functionalization are abundant, but include for example various fibronectin fragments (Fn III9-10) (Li *et al.*, 2017), the laminin fragments Tyr–Ile–Gly–Ser–Arg (YIGSR) (Kubinová *et al.*, 2014; Su *et al.*, 2019), Ile-Lys-Val-ala-Val (IKVAV) (dos Santos *et al.*, 2019; Kubinová *et al.*, 2014; Patel *et al.*, 2019) and "C16" (CGGKAFDITYVRLKF), or fragments of other proteins such as the "T1" peptide sequence from the domain III of Cysteine-rich 61 (Cyr61/CCN1) protein

(GQKCIVQTTSWSQCSKS) (da Silva *et al.*, 2018). However, the tripeptide sequence of arginine-glycine-aspartate (RGD) is perhaps the most commonly used cell recognition motif (Ferris *et al.*, 2015; Macková *et al.*, 2016; Silva *et al.*, 2012; Zhu *et al.*, 2009), as it is the minimal peptide sequence recognized by the integrins. Similarly, growth factors have been covalently coupled to a hydrogel's polymer network to function as cell recognition sites, for example the vascular endothelial growth factor (VEGF) has been shown to support cell attachment and function (Miyagi *et al.*, 2010; Rouwkema and Khademhosseini, 2016). Also the introduction of larger, natively cell-adhesive compounds such as collagen and gelatin has been found to increase cell recognition (Bello *et al.*, 2020; Tallawi *et al.*, 2015; Zhou *et al.*, 2021).

Degradation is linked to a material's capacity to be remodeled by cells. However, the degradation profile of a hydrogel is often investigated independently of its final application. Typically, three design approaches are distinguished: hydrolysis, enzymatically controlled degradation, or user-controlled disassembly triggers. However, the degradation kinetics, products and mechanism have to be well understood universally (Leijten *et al.*, 2017; Tibbitt and Anseth, 2009). In an ideal scenario of a cell encapsulation study, the cells enact the needed degradation and remodeling, for example *via* the incorporation of enzyme-recognizable motifs within the polymer network structure, such as matrix metalloproteinase (MMP) cleavable sites (Anderson *et al.*, 2011; Sridhar *et al.*, 2015). After the encapsulated cells have successfully taken up residence in the hydrogel matrix, they can be expected to deposit their own ECM, thus partially and gradually replacing the initial matrix, but ideally retaining the 3D hierarchy. Similarly for implantable hydrogels, the degradation rate must be finely tuned or biologically driven, so that the surrounding tissue will gradually replace the implant material with body-own tissue. Degradable sites within the hydrogel architecture also influence the original mechanical stability, as well as the temporal stability, *i.e.*, degradation or remodeling. It should be understood that degradation, or simply aging, of a hydrogel will affect the mechanical properties as well. While typically degradation will destabilize the network and weaken a hydrogel overall, there are also cases in which a hydrogel does not degrade, but instead increases its stiffness by either continuous crosslinking or sedimentation of other products (Prajapati *et al.*, 2013; Silva-Correia *et al.*, 2013). Again, the desired hydrogel design would be highly application dependent, however the user should have control over such property evolution.

Hydrogels developed for *in vivo* applications have to be designed and tested for their biocompatibility and tissue response. It should be noted that cytocompatibility

and biocompatibility are two different features of a material, and the *in vivo* tissue response is independent, if not contradicting, the cytocompatibility behavior of a material. Certainly, the cytocompatibility and biocompatibility of a hydrogel material are assessed using different methods, as outlined in chapter 2.1.3. The systemic response is steered by the fibrous capsule formation and general foreign body response of the tissue to the implant (Amer *et al.*, 2019). Here, it may be preferred for the implant material to be rather inert, as opposed to stimulating cell interaction, in order to avoid intense and chronic inflammation reaction. The initial, acute inflammation reaction is typically neither avoidable nor detrimental, but the long-term effect will have to be considered. Additionally, the phenomenon of tissue adhesion should be considered as design feature for implantable hydrogels. Tissue adhesion is based on different mechanisms compared to cell adhesion, as it is achieved through covalent catechol bonds, non-covalent hydrogen bridge bonding or mechanical interlocking (Ghobril and Grinstaff, 2015; Hofman *et al.*, 2018). The interface formed between hydrogel implant and biological tissue is highly interesting for several applications, such as wound dressings and bioelectronic patches (Li *et al.*, 2021). Without a doubt, the immunogenicity of a material, e.g., the ability to provoke or avoid a strong host immune response, is of utmost relevance for cell and tissue engineering purposes.

The demands on mechanical properties of a hydrogel formulation are, once again, highly application dependent. In comparison to other classes of materials for biotechnology, such as steel and solid plastics, hydrogels are considered soft materials, owing to their water-based loose network structure. However, there is indeed a wide range within the descriptor of "soft" and aspects such as elastic modulus, compression modulus, creep, brittle-ductile fracture behavior, viscoelasticity, shear thinning, etc. have to be examined. Furthermore, this topic has to be approached from two sides: the biological requirements of encapsulated cells or interfacing tissues, and the requirements for hydrogel fabrication and end use.

As mentioned previously, cells experience their mechanical surrounding *via* mechanotransduction, and thus there is a crucial interplay between their preferred matrix properties and cell response including ECM secretion. A soft hydrogel matrix is evidently needed for soft tissues, such as fat, brain, mammary glands with elastic moduli between 0.01-0.5 kPa. While on the other end of the spectrum there are more resilient tissues that require low compliance and rigid support, such as cartilage, skeletal muscle, and tendon with elastic moduli of up to 50-1000 kPa (Levental *et al.*, 2007). If the matrix stiffness is outside of the range required for a cell type, it can lead to malfunction of cell development or indicate disease states. For instance,

myoblasts will differentiate to form myotubes resembling healthy muscle tissue only in stiff enough substrates but fail to do so in soft environment. On the other hand, lung fibrosis for example is characterized by a stiffer lung tissue (Levental *et al.*, 2007; Walters and Gentleman, 2015). It must be noted, however, that any macroscopically determined mechanical property, such as bulk compressive modulus, may not be relevant on the microscopic scale of cells (Crosby and Zoldan, 2019; Savina *et al.*, 2009; Tibbitt and Anseth, 2009).

Outside of biological mechanical requirement, hydrogels are developed towards certain macroscopic demands as well, including both the initial fabrication as well as long-term stability. In hydrogel fabrication, it is important to distinguish between true, crosslinked hydrogels and shear-thinning formulations. Shear thinning hydrogels are semi-solid and shape-retaining at rest, but due to their non-Newtonian flow behavior decrease their viscosity under shear force, thus allowing for extrusion and shaping (Jongprasitkul *et al.*, 2021; Moeinzadeh *et al.*, 2021). In contrast, true hydrogels are typically defined as the combination of a so-called hydrogel precursor that is made to form a 3D network with a crosslinking agent during a distinct crosslinking step. The precursor solution may also be shear-thinning, but the final hydrogel is formed *via* a chemical or physical reaction. Typically, crosslinked hydrogels possess a higher stiffness than shear-thinning hydrogel pastes, even though an insufficient amount of crosslinking can also result in so-called "weak" hydrogels whose network crosslinking does not support shape fidelity (Morris *et al.*, 2012). Nevertheless, all of these should be considered hydrogels, albeit with limited application areas.

The gelation kinetics, *i.e.*, the speed of crosslinking, are important for cell encapsulation, coatings, and injection. A too fast gelation may prevent casting or passing through a needle gauge, and much delayed gelation can impair true 3D encapsulation. After the hydrogel has fully formed and arrived at its final mechanical features, we can consider some applications to require relatively high stability, for example wound patches, microparticles, and implantable drug delivery devices merely due to their nature of having to withstand erosion and external pressure. Additive manufacturing, or 3D bioprinting of hydrogels is a hot topic in the recent literature of the field (He *et al.*, 2016a; Kim *et al.*, 2022; Leppiniemi *et al.*, 2017; Rasheed *et al.*, 2021), and especially here shape fidelity of the printed constructs is of concern, as the technique itself shines with the ability to produce small scale features. While the parameters or the printing process must be finely tuned, also the rigidity and viscoelastic properties of the hydrogel, or bioink, must be suitable to uphold the printing design. On the other hand, shape fidelity is not necessarily needed for

example in microfluidic devices, however the resistance against flow along or through the gel should be monitored.

Finally, there is a host of other, perhaps smaller, aspects to consider when designing a hydrogel or considering different formulations. For instance, transparency of a hydrogel is a boon to microscopical evaluations and also an important requirement for ophthalmic applications. Certainly, the availability and cost of a hydrogel and its polymer material will influence the economic viability of a wider application. In the same vein, the storage and long-term stability of a hydrogel formulation will influence the usability of a hydrogel, especially those with complex modifications. Sterilization presents an issue at all steps of hydrogel design and application area, even more so to ensure a clean and sterile product immediately before application. Several sterilization techniques are applicable to hydrogels, such as filtration and ethylene oxide treatment, however detrimental effects on the polymer itself must be considered.

2.1.2 Hydrogels prepared from polysaccharides

There is a considerable number of hydrogel-forming polymers in the literature that have been developed for TERM applications. They may be categorized into synthetic polymers, polysaccharides, and polypeptides here. Certainly, the distinction could be made between synthetic and natural polymers, but it is more straight-forward to discuss these hydrogels based on their chemical structure rather than origin. For example, polypeptides can be derived either from biological tissue (top-down) or polymerized from their amino acid building blocks. Polysaccharides on the other hand tread the line between being produced in an industrial process (bottom-up), while still being natural polymers. Here, we will briefly discuss the chemical structure, modifications, and applications of these hydrogel-forming polysaccharides.

Polysaccharides are a truly vast and diverse family, which features pyranoses (6-ring sugar) or furanoses (5-ring sugars) linked *via* glycosidic linkages, in either linear or branched polymer chains. The structures of different polysaccharide family members are shown in **Figure 1**. Polysaccharides are the most abundant carbohydrate in food, and they can be produced free of pathogens and allogenic factors influencing their immunogenicity.

The term 'gum' refers to the large group of polysaccharides produced during the growth of organisms, including bacteria, fungi, and yeasts (Alizadeh-Sani *et al.*, 2019). Gellan gum will be discussed in detail in the following chapter 2.2, but its ubiquitous

opportunities for modification can be abstracted to other types of polysaccharides as well. For example, oxidation of gums to create reactive aldehyde groups has been shown for guar gum (Dai *et al.*, 2017), pullulan (Zhang *et al.*, 2019), and dextran (Nonsuwan *et al.*, 2019; Su *et al.*, 2021), but also other modifications strategies have been explored, such as thiol-ene modification of dextran (Mergy *et al.*, 2012) and methacrylation of xanthan (Tulegenovna *et al.*, 2022) and guar gum (Tiwari *et al.*, 2009). Blending with other polymers is evidently successful strategy for gums, as shown using gelatin and pullulan (Zhang *et al.*, 2019), xanthan and methylcellulose (Liu and Yao, 2015), and bioactive glass incorporation to dextran (Nikpour *et al.*, 2018).

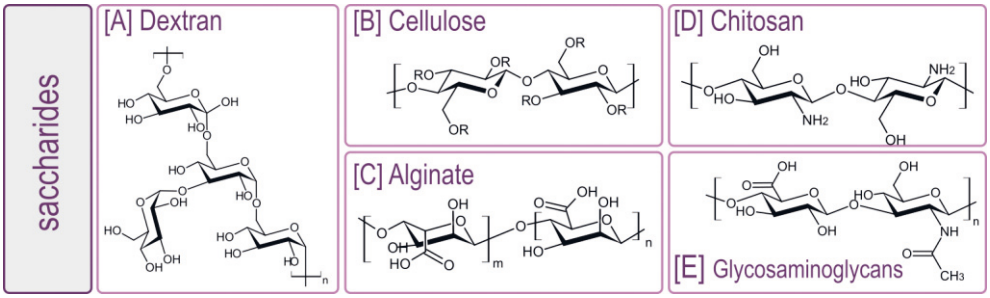

Figure 1. Molecular structures of polysaccharides. [A] dextran; [B] cellulose; [C] alginate; [D] chitosan; [E] glycosaminoglycan.

Polysaccharides derived from plant sources include alginate and cellulose, with various types of subtypes from cellulose such as cellulose nanocrystals (CNC), cellulose nanofibrils (CNF) and bacterial cellulose (BC), most of which have been converted to hydrogels. Nanocellulose has been well established in bioprinting, due to its outstanding shear thinning behavior (Rasheed *et al.*, 2021). Cellulose-alginate combinations have been shown by Leppiniemi *et al.* (2017) as well as Wei *et al.* (2020), who utilized avidin-functionalization and oxidation respectively to render it more bioactive (Leppiniemi *et al.*, 2017; Wei *et al.*, 2020). Alginate has been extensively used in bacterial culture and was proposed already in the 1990s for TERM applications with bioactive modifications (Rowley *et al.*, 1999). Various functionalization have been introduced since, such as end-group modifications using oxime (Bondalapati *et al.*, 2014), norbornene coupling for photocrosslinking (Desai *et al.*, 2015), and the addition of *N*-cadherin to control stem cell differentiation (Lee *et al.*, 2017). Due to its good physical properties and stability, alginate is often compounded with other bioactive polymers to improve their mechanical resilience, such as alginate-gelatin microspheres (Ke *et al.*, 2021), or injectable alginate-collagen (Moeinzadeh *et al.*,

2021). GrowDex is a commercial preparation of nanocellulose produced by UPM (UPM-Kymmene Corporation, Helsinki, Finland), and despite its perceived biological inertness has shown successful application for spheroid culture (Chang *et al.*, 2020). Crucially, it excels at printing applications due to its shear thinning nature (Rasheed *et al.*, 2021) and can be rendered transparent through anionic treatment.

The most prominent example of animal-derived polysaccharides is perhaps chitosan, which is the deacetylation product of chitin, which is obtained from crustaceans and insects. Modification of chitosan is required not only to increase its bioactivity, but also to overcome its insolubility in water. Combing different polymers, double networks can be formed between chitosan and, for example, PEG-aldehyde (Yan *et al.*, 2021), alginate, or fucoidan (Hao *et al.*, 2021) synergistically improving the mechanical and biological properties of the composites. Self-healing hydrogel systems based on chitosan were described by Yang *et al.* (2021) using aldehyde-modified PEG, and Khan *et al.* (2022) using 4-arm PEG and Au nanoparticles (Khan *et al.*, 2022; Yang *et al.*, 2021). Rendering chitosan photocrosslinkeable by introducing methacrylate pendants is also possible, as shown by Samani *et al.* (2019) and Valmikinathan *et al.* (2012) (Samani *et al.*, 2020; Valmikinathan *et al.*, 2012). A pure chitosan hydrogel was used by Pakzad *et al.* (2020) for drug delivery to the eye, based on improved transparency and thermal gelation by combination with *β*-glycerophosphate (Pakzad *et al.*, 2020).

The family of glycosaminoglycans (GAGs) is found in vertebrates, invertebrates, and bacteria, and includes hyaluronic acid, chondroitin sulfate, and heparan sulfate which are commonly used to prepare hydrogels for biomedical purposes. Structurally, GAGs are composed of disaccharide repeat units (Fig. 1E) and play an important role for the development, growth, and adult life of organisms by facilitating the interaction with proteins and cellular binding (DeAngelis, 2002). However, the extraction of GAGs from animal sources or from Streptococcus carries the risk of endotoxin contamination, but fermentation *via* different, bioengineered microorganisms has been used to circumvent this risk (Sze *et al.*, 2016). Hyaluronic acid is often modified in order to create double, or interpenetrating networks. For instance, hydrazide-modified hyaluronic acid can be combined with either oxidized gellan gum or oxidized hyaluronic acid to form soft, injectable hydrogels for stem cell culture and delivery (Karvinen *et al.*, 2017; Koivusalo *et al.*, 2018). An interpenetrating network was created by Guo *et al.* (2021), based on the orthogonal crosslinking of two differently modified hyaluronic acid hydrogels, with a thermoreversible PNIPAAm and a swellable, covalently crosslinked component (Guo *et al.*, 2021). A dual-degradation system was proposed

by Sahoo *et al.* (2008) through the grafting of methacrylated polylactic acid (PLA) pendants. While the hydrogel is thus formed through photo-crosslinking, the degradation is governed by both hydrolysis of the lactic acid, as well as enzymatic degradation of the hyaluronic acid (Sahoo *et al.*, 2008). Hydrogels for TERM applications can also be prepared from chondroitin sulfate (Anjum *et al.*, 2016) and heparan sulfate (Chopra *et al.*, 2019), but interestingly there seems to be no hydrogel formulation using keratan sulfate.

2.1.3 Assessment of hydrogel properties

A thorough analysis of a created hydrogel materials is required to verify the polymer modification, and to validate the targeted application. Here, we will discuss broadly the various analysis techniques employed throughout the literature to assess hydrogels, including chemical structure, the success of modification, mechanical properties, gelation and fabrication modalities, degradation, as well as the conclusion of cell and tissue response. A visual guideline for the analysis classification is shown in **Figure** 2. The special focus remains to be polysaccharides, although this largely general discussion should be applicable to any hydrogel formulation.

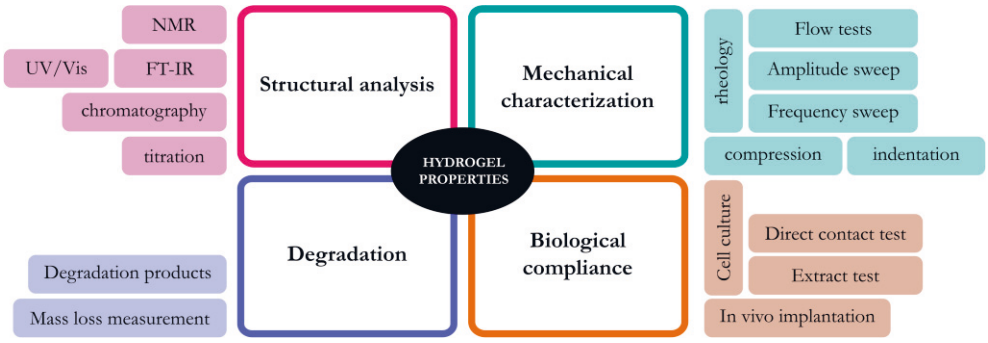

Figure 2. Assessment flow chart for hydrogel properties.

2.1.3.1 Structural analysis

To assess the chemical structure and repeat units of a polysaccharide, standard polymer assessment methods are available, such as nuclear magnetic resonance (^{1}H and ^{13}C-NMR), chromatography (HPLC, GPC), and spectroscopy (FT-IR, UV/Vis). The chemical structure of a polysaccharide is defined by its monosaccharide

composition, molecular weight, the linkage pattern of the glycosidic bonds, degree of branching and branching position, and the molecular folding due to α- or β-configurations (Guo *et al.*, 2018). Especially for modified polysaccharides, the native and added functional groups, molecular weight and molecular weight distribution must be determined. The microstructure of a swollen hydrogel can be indirectly assessed *via* diffusion and rheological characteristics (Antoine *et al.*, 2014; Caliari and Burdick, 2016; Soto *et al.*, 2016; Yan *et al.*, 2018). However, it remains challenging to directly image, e.g., pores and fibrillar structures, because standard techniques are operating in vacuum and thus hydrogels are dehydrated one way or another, changing their properties and microstructure. Certainly, direct comparisons between two formulations can still be made, but their limitation has to be critically discussed.

Depending on the research question and the presence of chemical functionalities, titration and chemical derivatization can be a powerful tool to assess hydrogel structure and functionalization. For example, the thiol content in either a polymer (Nonsuwan *et al.*, 2019; Tam *et al.*, 2012) or small degradation products (Su *et al.*, 2021) can be determined using the Ellmans assay. The reagent, 5,5'-dithio-bis-(2-nitrobenzoic acid) or DTNB, gives a stoichiometric absorption in the UV/Vis spectra and can universally quantify sulfhydryl, disulfides, and other thiols. To determine aldehyde concentration. they can be derivatized using tert-butyl-carbazate (TBC) for ^{1}H-NMR analysis, because the tert-butyl peak gives a clear, stand-out signal in the spectrum (Martínez-Sanz *et al.*, 2011; Pandit *et al.*, 2019). Aldehyde concentration can also be determined using potentiometric titration with NaOH, after reaction with hydroxylamine hydrochloride. This titration method was successfully employed for pullulan dialdehyde (Zhang *et al.*, 2019) as well as oxidized dextran (Su *et al.*, 2021). Similarly, carboxylic groups of nanocellulose can be quantified using NaOH, with the change in pH being monitored (Rasheed *et al.*, 2021). Evidently, there exists a myriad of analysis methods to investigate compounds in the formulation besides the polymer. For instance, counterion concentration in polysaccharides that form ionic hydrogels can be assessed by inductively coupled plasma optical emission spectroscopy (ICP-OES) (Ferris *et al.*, 2015; Kirchmajer *et al.*, 2014).

2.1.3.2 Mechanical analysis

Mechanical features of a hydrogel are described through its viscoelastic response, fracture type and modulus. These features are analyzed using methods such as compression testing, indentation, tensile testing, rheology with its various modes,

dynamic mechanical analysis (DMA), and creep compression testing (Callister and Rethwisch, 2007; Oyen, 2014). From the point of view of the entirety of material science, hydrogels are perceived as very soft materials. However, within this class of material there exists a wide range from flowing, weak network hydrogels to highly rigid, almost rubber-like formulations. Here, we will consider mostly the mechanical properties of true hydrogels, *i.e.*, those that have been crosslinked in any fashion. Nevertheless, also weak hydrogels find application in TERM, and should be assessed towards their mechanical properties, such as their flow and viscosity.

Rheology is the study of flow and deformation of complex fluids and viscoelastic materials (Barbucci, 2009; Mezger, 2006), such as hydrogels, which represent a type of material that is solid (elastic) at rest, but begins to flow when a certain shear force is exceeded (viscous). Oscillatory time sweeps are carried out with a fixed amplitude and frequency and are used to observe the evolution of the mechanical properties of a hydrogel sample, for example during gelation. At the onset of gelation, induced either by addition of a crosslinker or the action of UV light in photocrosslinkable systems, storage modulus quickly increases until the storage modulus reaches a plateau, and the hydrogel network has fully formed (Zuidema *et al.*, 2014). Such time sweeps have been used to describe the hydrogel formation of ionically crosslinked gellan gum (Silva *et al.*, 2013), chemically crosslinked PEG-chitin gels (Yang *et al.*, 2021), and UV-crosslinkable dextrans (Mergy *et al.*, 2012). However, many publications concentrate on demonstrating amplitude (Jongprasitkul *et al.*, 2021; Koivisto *et al.*, 2017), frequency (Su *et al.*, 2021), or thermal sweeps (Liu and Yao, 2015; Reis *et al.*, 2012) to characterize their hydrogel formulations. Most commonly, shear rate sweeps to measure viscosity of hydrogel precursors or shear-thinning formulations are carried out to validate applications for 3D printing (Jongprasitkul *et al.*, 2021; Rasheed *et al.*, 2021; Wei *et al.*, 2020) and injection (Bellini *et al.*, 2015; Liu and Yao, 2015). Overall, flow testing has proven to be a versatile and robust method for fluid hydrogels, and can be implemented in facile setup, allowing e.g., for the measurement with suspended cells (Cao *et al.*, 2012), the observation of fluid gel gelation (Chouhan *et al.*, 2019), as well as temperature dependent viscosity measurements (Bartnikowski *et al.*, 2015).

2.1.3.3 Degradation analysis methods

To support and validate the mass loss measurement, a wide selection of other analytical methods can be used, which further allow to investigate the underlying degradation mechanism. The applicability of these other methods depends on the

design and type of hydrogel (Meyvis *et al.*, 2000). For example, spectroscopic methods may not be suitable to study the polymer degradation or degradation products in the supernatant, if the compound cannot easily be detected with standard methods. Moreover, degradation products in the supernatant may not directly correlate with the rate of degradation, e.g. due to diffusion effects if the detectable compound is an oligomer (Bryant and Anseth, 2003; Martens *et al.*, 2001; Taylor *et al.*, 2012). Thus, while a complimentary technique should be used to validate the mass change results, its suitability needs to be carefully selected.

The degradation medium supernatant can conveniently be utilized in conjunction with mass analysis, as it does not perturb the hydrogel sample. Thus, colorimetric, protein, and other standardized UV/Vis assays from the supernatant are conducted frequently. For example, the release of protein-crosslinker through matrix metalloproteinase (MMP-1) enzymatic degradation can be quantified using a commercial, micro-BCA (bicinchoninic acid) kit (da Silva *et al.*, 2018). Similarly, Sahoo *et al.* (2008) quantified the uronic acid concentration, a degradation product of their engineered pHEMA-HA hydrogel, *via* carbazole reaction and colorimetric assay (Sahoo *et al.*, 2008), while Su *et al.* (2021) utilize the Ellman's assay (Ellman, 1959) to quantify the free thiol groups, correlating to the undegraded disulfide crosslinks (Su *et al.*, 2021). To exemplify the detection of network dissociation and polymer chain detection, there are two exemplary approaches quantifying the presence of gellan gum chains in the supernatant: Hossain and Nishinari (2009) used the phenol-sulfuric acid method (DuBois *et al.*, 2002) to digest the polysaccharide structure and detect the resulting UV-absorbent product using colometry (Hossain and Nishinari, 2009). Silva *et al.* (2013) on the other hand employed circular dichroism, an absorption spectroscopy method based on polarized light, to calculate the polymer chains in solution (Silva *et al.*, 2013). An elegant example of degradation design is given by Sridhar *et al.* (2015), who equip their hydrogel with an MMP-cleavable sequence that is fluorescent only upon cleavage, thus fluorescence can be observed to track ongoing specific enzymatic activity (Sridhar *et al.*, 2015). Spectroscopic methods, as mentioned for the structural analysis of hydrogel polymers, are suitable and frequently applied to determine polymer fragments and other hydrogel degradation products (Johnson *et al.*, 2007; Wang *et al.*, 2018).

2.1.3.4 Biological analysis

Perhaps the ultimate testing and proof of concept for a biomaterial is to bring it into contact with a living system and to study the results. On one hand, this serves to

validate the targeted application and demonstrate a benefit for the studied system, in the attempt to also learn about, *e.g.*, the cell model or regeneration of tissue lesions. From a materials science perspective on the other hand, *in vitro* and *in vivo* testing is a means to evaluate the material only, and the biological behavior is considered as analytical tool. Within the scope of this thesis, cell culture is used to study bioactivity and cytocompatibility of the material, rather than phenotypical or morphological changes in the cells. However, it can also serve as an indication for the proposed application. For the testing of hydrogels, it is crucial to consider whether to plate the cells onto the hydrogel surface (2D), or to make full use of the concept of hydrogels and encapsulate the cells during gelation (3D) (Justice *et al.*, 2009; Tibbitt and Anseth, 2009). Both of these approaches are valid concepts, where the relevance of testing and application is under the digression of the researcher.

Bright-field, fluorescence and confocal microscopy have been successfully implemented for hydrogel cell cultures generally, and 3D imaging specifically. The cell staining procedure has to be adapted from of 2D protocols, typically by increasing the staining time and concentration, in order to assure diffusion throughout the hydrogel volume. Common cell staining approaches that have been adapted for hydrogel culture include Live/Dead™ (based on calcein-AM and ethidium homodimer-1), immunocytochemical fluorescent staining, alizarin red staining for calcium production of osteocytes, and so forth. Quantitative assays can, with some limitations, also be carried out with encapsulated cells, as has been shown with Trypan Blue (Bondalapati *et al.*, 2014; Bonifacio *et al.*, 2020; Pan *et al.*, 2009; Silva *et al.*, 2012), alamarBlue™ (Ermis, 2021), luciferase-based assays such as CellTiter-Glo™ (Rasheed *et al.*, 2021) and MTT assays (Joy *et al.*, 2020; Pacelli *et al.*, 2015; Zhang *et al.*, 2019). Direct visualization of cells is also possible using scanning electron microscopy (SEM), but only to identify the shape and placement of cells, as the applied vacuum dries the hydrogel and is thus not representative of its microstructure. If the DNA, RNA, or other biological characteristics of the cells should be investigated, the cells must be extracted from their encapsulating matrix to proceed with the required steps for, e.g., reverse transcription polymerase chain reaction (RT-PCR). Fortunately, this can be achieved without preserving the cells as such, and the entire specimen can be fragmented and digested, forcefully breaking the hydrogel matrix (Vuornos *et al.*, 2020). If the cells are required to remain intact, for example for flow cytometry, a gentle dissolution or degradation of the hydrogel must be implemented. This is exceedingly challenging, and hydrogels must be designed with such feature requirements in mind, as will be discussed in chapter 2.3.4.

Albeit ethical issues, biomaterial implantation into animal models remains to be most relevant testing procedure for biocompatibility verification. Quantitative and qualitative observations of such studies should typically include capsule formation, angiogenesis, tissue-specific repair capability, inflammation, and the general biocompatibility, *i.e.*, absence of detrimental host response. Different implant sites may be used for different research question, such as subperiosteal injection sites und the bone membrane (Martínez-Sanz *et al.*, 2011), a defect in the lumbar vertebrae (Kim *et al.*, 2022), a calvaria defect in the skull of rats (Moeinzadeh *et al.*, 2021), replacement of the right ventricular heart of rats (Miyagi *et al.*, 2010) , or chondral lesion repair of rabbit knee cartilage (Vilela *et al.*, 2018). Most commonly however, hydrogel specimen are implanted to a subcutaneous site, regardless of tissue indication (dos Santos *et al.*, 2019; Liu *et al.*, 2019; Tsaryk *et al.*, 2014; Wu *et al.*, 2017). To make full use of the shear-thinning and gelation abilities of hydrogels, injection to the target site has become a popular objective, with the added benefit of a minimally invasive procedure (Liu and Yao, 2015; Martínez-Sanz *et al.*, 2011; Yao *et al.*, 2013). As for analysis methods of *in vivo* hydrogel transplantation studies, the commonly used methods are used to characterize the explants and tissue surrounding. These include thinly sectioning the retrieved tissue and histological staining with, for example Masson trichrome to stain mucus and collagen fibers, hematoxylin and eosin which stains basophilic and acidophilic cells, or Oil Red O for lipids (Suvarna *et al.*, 2019). Besides analyzing the cells and tissue features, also the material degradation state and animal welfare should be noted in the observations to record a complete image of the *in vivo* experiment.

2.2 Gellan gum as model hydrogel in tissue engineering

We will now take a closer look at the hydrogel-forming compound called Gellan Gum, which is central in and around the publications presented herein. Indeed GG is an advantageous choice for hydrogel engineering due to its high-yield production, stability and superior gelation properties (Fialho *et al.*, 2008; Smith *et al.*, 2007). Its molecular structure and mechanical details are relatively well established and there is relatively low batch-to-batch variation. As it is produced by a non-mammalian source it holds no immunogenic capacity, which is a crucial aspect for any biomedical application (Fialho *et al.*, 2008). Regardless, while this thesis work is structured around using gellan gum, it should be understood as model polymer. General

thoughts and discussion should be applicable to a wider selection of hydrogel polymers, as presented in the next subchapter.

2.2.1 Origin, structure, and gelation of gellan gum

GG is an anionic exopolysaccharide produced by the bacterium *Sphingomonas elodea* (ATCC31461) in aerobic conditions (Fialho *et al.*, 2008). Bacteria produce these exopolysaccharides as part of their external biofilm, which acts as protective diffusion barrier (Harimawan and Ting, 2016). The gellan gum producing bacterium had been isolated from the surface of a plant in the *Elodea* genus, which is a species of submerged aquatic plants. In the late 1970 the company CP Kelco U.S. Inc (then Kelco, San Diego, U.S.A.) drove efforts to identify polysaccharides produced by bacteria and soil for commercial gain. Besides GG, other exopolysaccharides from *Sphingomonas* strains were identified, including Welan gum, Rhamsan gum, and Diutan gum. These gums are hence classified as "Sphingans" and many have found commercial applications, however, only GG readily forms self-supporting hydrogels (Fialho *et al.*, 2008). The compound Gellan gum is distributed under several different tradenames. For example, Gelrite® and Gelzan™ CM are both trademarks of Kelco designed for use in microbiological assay and tissue culture media, while Kelcogel® is the food-grade version, and Phytagel™ is a trademark of Sigma-Aldrich Co. LLC.

On the cellular level, the fermentation and production of GG observes three sequential steps: First the sugar precursors are synthesized intracellularly, followed by the assembly of the tetrasaccharide repeat units, which are connected to the inner cell membrane. Finally, the separate repeat units are polymerized while being transported through the periplasmic space and excreted into the outer membrane. After the fermentation process, which may take about 72 h, the polymeric substance must be separated from the bacterial broth. A high viscosity production bath makes it somewhat difficult to separate the exopolysaccharide from the bacterial cells, but it is achieved *via* dilution and precipitation in *iso*-propanol. The lyophilized product is then treated in a strong alkaline bath, in order to deacetylate the (1→3) D-glucose rest and produce the commonly used version of low-acyl GG.

The cardinal factors influencing the biosynthesis of GG are broth temperature and nutrient source. With fermentation temperatures of 30°C or higher, polysaccharide production will decrease, as the bacterial cells will increase their cell wall synthesis and fewer 'supplies' are available for exopolysaccharide production. Thus, lower temperatures around 20-25°C result in higher yield, and higher M_w.

Nutrient supply on the other hand appears to affect the yield mostly, with the type of carbon source also being able to affect the acyl substitution and susceptibility to enzymatic degradation (Fialho *et al.*, 2008).

Kelco aimed to develop these exopolysaccharides and other materials for food applications, and indeed GG has been approved as food product by the FDA (U.S.A) and EFSA (EU) (E418) in 1990 (Younes *et al.*, 2018). It serves as gelling, stabilizing, and suspending agent in various products such as milkshakes, sports drinks, tooth pastes, and desserts (Giavasis *et al.*, 2000). Additionally, it can be noted that GG excels as a material choice due to its inertness, gelation capacity, as well as transparency which are properties that translate well for some TERM applications. GG has further found application within the medical field, for example as nasal sprays, pharmaceutics coating, and contact lenses. These medical applications have been reviewed by Osmałek *et al.*, 2014 (Osmałek *et al.*, 2014).

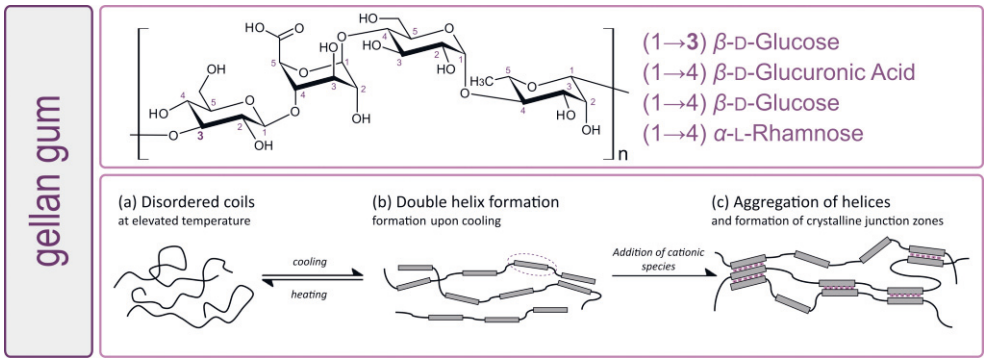

Figure 3. Structure and gelation of gellan gum. [A] Tetrasaccharide repeat unit of deacetylated gellan gum; [B] gelation mechanism of native gellan gum.

The tetrasaccharide repeat unit of gellan gum comprises of β-D-glucuronic acid, α- L-rhamnose, and two β-D-glucose, as shown in **Figure 3**. Its crystal structure has been investigated and described in detail by Chandrasekaran *et al.* (1988) using x-ray diffraction (Chandrasekaran *et al.*, 1988). It was revealed that when dissolved at high temperatures (70-80°C) the polymer chains exist as random coils, but upon cooling to ambient temperature they will arrange into a double helix structure, with the two chains running parallel to each other, but in inverse direction and translated by half a repeat unit. This double helix formation is caused by the occurrence of the single 1→3 sugar linkage between glucose and rhamnose, introducing a twist in the otherwise linear chain of 1→4 linkages. One repeat unit was found to be 5.64 nm long in this conformation. Further, it is crucial to point out that the carboxylic groups on the glucuronic acid are pointed outwards from the double helix, and are thus

sterically available for counterions (Morris *et al.*, 2012). These double helices are not continuous but are offset by chain sections without conformation. This double helix formation is possible only for deacetylated gellan gum, as the acetyl group causes steric hindrance and prevents the association of the chain. Throughout this thesis and always the deacetylated version is used and referred to as gellan gum. There are publications investigating the use of acetylated GG as well (Silva *et al.*, 2013), however its use is heavily limited by its difficulties to form gels.

However, double helix formation upon cooldown does not imminently form self-supporting hydrogels, but the presence of cations is required to agglomerate the double helices into crystalline junction zones, as shown in Figure 1b. This agglomeration then is facilitated by the presence of divalent cations, with calcium (Ca^{2+}) being the native and dominant choice. Divalent cations succeed by directly bridging two double helices in what has been described as "eggbox" model. Monovalent ions on the other hand can only offset the anionic aggregates *via* charge screening and do not provide as efficient crosslinking, yet readily increasing the viscosity of a GG solution (Morris *et al.*, 2012). Indeed, the tendency to gelate in the presence of any cation has impaired the structural identification of GG due to many chromatographic methods requiring ionic liquids.

2.2.2 Mechanical properties of gellan gum

It is challenging to discuss the mechanical properties of any hydrogel material, as they are always highly dependent on the production process, dissolution strategy, concentration, and of course any modification that has been introduced. Especially for exopolysaccharides from bacterial culture, the molecular weight (M_w), polydispersity and available counterions, are closely related to the fermentation and harvesting procedure. Regardless, it is important to investigate mechanical properties of precursor and final hydrogel for all types of application, be it texture for food applications, viscosity for injection and extrusion, viscoelasticity and modulus for implants and tissue models. While there may be no definitive values available, a critical comparison between literature sources has to be carried out for each variable.

Before considering the mechanical properties of true, self-supporting hydrogel samples, the viscosity of GG precursor solution should be evaluated. If unmodified, the typical operating range of GG is 0.2 – 2% w/v, which is capable of forming hydrogels. However, these solutions can be quite viscous, and this viscosity is highly temperature dependent. Chouhan *et al.* (2019) measured the viscosity of GG fluid

gels with a Na^+ concentration of up to 0.2 M. At 20°C, all formulations had a specific viscosity around 0.030 Pa·s, but experience a rapid drop above 30°C down to 0.005 Pa·s (Chouhan *et al.*, 2019). While the investigated Na^+ concentrations do not result in self-supporting hydrogels, they still affect the viscosity and form weak gels. As is characteristic for polymeric solutions, GG solutions are weakly shear thinning, yet again the extend of this behavior is dependent on the exact formulations and counterions. Shear thinning observed by measuring the apparent viscosity (MPa·s) as a function shear rate, with reduced viscosity at increased shear. Ferris *et al.* (2015) compared the apparent viscosities of native gellan gum and two ion-purified formulations, where one was kept as acid form (A-GG) and the other supplemented with Na^+ (NaGG). Formulations with higher counterion-crosslinking strength indeed had higher viscosity throughout, and stronger shear thinning features (Ferris *et al.*, 2015). The viscosity of gellan solutions can further be reduced by oxidative scissoring, which effectively cleaves the polymer chain. Thus, it is useful to consider the intrinsic viscosity, which is directly related to the molar mass of the solute and given as inverse concentration (mL/g). For example, Gong *et al.* (2009) reduced the intrinsic viscosity of native GG from 9.06 x1000 mL/g down to 0.18 x1000 mL/g *via* Malaprade reaction for 120 h (Gong *et al.*, 2009).

Compression testing is the preferred technique over tensile testing for hydrogels, and quite a number of research groups have chosen this uniaxial, unconfined compression to assess the bulk properties of gellan gum. Koivisto *et al.* (2017) determined a range of compression modulus for native GG, albeit physically crosslinked with the divalent bioamine SPD or tetravalent bioamine SPM, between 3.9 – 23.0 kPa dependent on the crosslinker concentration. For comparison the authors compressed rabbit brain tissue samples, however they concluded that compression testing should be used as screening rather than deducing micromechanical features (Koivisto *et al.*, 2017). Calcium crosslinking of native GG results in much tougher hydrogels with a compression modulus of 108 kPa, as published by Kirchmajer *et al.* (2014). Similar to the observed viscosity decrease upon purification, they showed that Na-purified NaGG only achieved a modulus of 78 kPa with identical crosslinking concentration (Kirchmajer *et al.*, 2014). As for chemically modified GG hydrogels, Xu *et al.* (2018) compared methacrylated GG with high (HM-GG, 0.5 methacrylate/repeat unit) and low (LM-GG, 2 methacrylate/repeat unit) modification degrees. While the formulations had similar compression ranges of 6.4 to 11.3 kPa (LM-GG) and 7.4 to 17.2 kPa (HM-GG), the authors noted that modification affects gelation in the way that high modification degrees prevent calcium crosslinking., LM-GG hydrogel formation was more readily

affected by calcium concentration, in conjunction with the photocrosslinking (Xu *et al.*, 2018). Magnitudes higher compression moduli were achieved by Douglas *et al.* (2012) by mineralizing GG using alkaline phosphatase (ALP), with moduli from about 600 kPa up to 1500 kPa. Further, incubation in polymerizing dopamine solution increased the modulus up to 5 MPa, but only if the hydrogel disks had previously been mineralized with ALP (Douglas *et al.*, 2012).

The effect of sugar in the solvent on compression behavior of GG was investigated by Evageliou *et al.* (2010). While they point out that firmness and gel strength is affected by the addition of different sugars, the overall modulus increase compared to sugar-free formulation is minimal. The reported moduli are approximately 190 kPa without any sugar, 100 kPa with glucose, 200 kPa for both fructose and sucrose, and nearly independent of the sugar concentration between 5 -15% w/v (Evageliou *et al.*, 2010).

Rheology is an excellent technique for viscoelastic materials because the duality of viscous and elastic deformation is a key feature of hydrogels. However, it may be challenging to achieve reliable measurements for preformed, gelated samples, as opposed to the flowing, viscous precursor solution for viscosity testing. The frequency sweeps carried out by Matricardi *et al.* (2009) revealed largely frequency independent behavior of their lysine-crosslinked GG formulations, with oscillation frequency up to 10 Hz. While native GG formulations were observed to have a storage modulus (G') of 1000 Pa and loss modulus (G") of 200 Pa, the presented lysine modification achieved increased modulus of about G' 4000 Pa and G" 2000 Pa (Matricardi *et al.*, 2009). Koivisto *et al.* (2017) reported a complex modulus, which is the ratio of storage and loss modulus and a measure of gelation, between 18 – 42 kPa for their bioamine crosslinked formulations (Koivisto *et al.*, 2017). Ferris *et al.* (2015) took a more detailed look at the linear viscoelastic region (LVER) of the amplitude sweep, with a maximum amplitude of 100% oscillatory strain. Within the linear region of the curves, native GG observed a slightly higher modulus than the Na^+-purified (NaGG) formulation with a G' of 105 kPa (G" 10.0 kPa) and 86 kPa (G" 4.5 kPa) respectively. Again, this is due to higher native ion concentration within the non-purified version, contributing to higher counterion concentration. In stark contrast, their presented RGD-modification had a very low modulus with G' 6.0 kPa and G" 0.4 kPa, because the modification reaction utilized the carboxylic group as reaction site, directly preventing the ionic crosslinking mechanism (Ferris *et al.*, 2015).

2.2.3 Tissue engineering applications of gellan gum

Initially developed for food applications, GG has found a wide variety of applications also in the medical research field. Soon after its commercialization, it was readily adopted as substitute for Agar in microorganism culture (Rule and Alexander, 1986). One of the earliest applications in mammalian cell culture presented by Smith *et al.* in the year 2007. As a proof of concept, the authors used the cell culture medium α-MEM to crosslink GG and encapsulated rat bone marrow stem cells. The cells remained viable for the culture period of 21 days, and GG was deemed as suitable 3D matrix with mild formation conditions (Smith *et al.*, 2007)

Bone tissue engineering and osteogenesis continue to be interesting avenues for the application of GG, due to its relatively high strength and biomimetic features. For example, Oliveira *et al.* (2016) demonstrated the osteogenic differentiation of human adipose stem/stromal cells (SC) in methacrylated gellan gum. Interestingly, they were able to show an autonomous differentiation capacity in GG even without addition of any cell adhesive or soluble mineralization factors. However, when blended with collagen, the mineralization capacity, as well as cell spreading. is further increased (Oliveira *et al.*, 2016). The same group also investigated the formation of beads from methacrylated gellan gum for bone regeneration *in vivo*. The Ca-enriched macroscopic beads were loaded with dexamethasone and subcutaneously implanted to mice. The beads showed excellent immune response and mineralization, further underlining the prospect of GG for bone tissue engineering (Vieira *et al.*, 2019).

A profound issue for both implantable regenerative devices, as well as disease models and organ-on-chip applications is the formation of functional blood vessels, *i.e.,* vascularization, throughout and between the tissues. Vuornos *et al.* (2020) investigated a blend of GG and collagen for the simultaneous microvascularization and osteogenic differentiation of human adipose SC in *co*-culture with endothelial cells. All medium conditions expressed strong osteogenic markers, however hydroxyapatite deposition *in vitro* was supported by bioactive glass extract (Vuornos *et al.*, 2020). In an effort to tune GG hydrogels towards endothelial cell recognition and enzymatic degradation by introducing MMP-1 cleavable crosslinker, da Silva *et al.* (2018) employed divinylsulfone (DVS) modification and two different peptide sequence additions. While the angiogenic peptide T1, derived from the cysteine-rich 61 (Cyr61/CCN1) protein, promoted endothelial cell invasion and elongation, the authors did not observe vessel maturation (da Silva *et al.*, 2018). Rocha *et al.* (2020) functionalized native GG with the peptide sequence RGD (GG-GRGDS) and examined the encapsulation of adipose SC and endothelial cells towards vascularized

neuronal tissue. Their aim to was to develop a regenerative therapy for traumatic spinal cord injury, in which SC are encapsulated in the hydrogel and transplanted. The hydrogel is required to promote both vascularization and innervation to ensure longevity and success of the transplant. The presented chick chorioallantoic membrane (CAM) assay indicates the potential of the cell-laden functionalized hydrogel to induce a revascularization of injured tissue and the recovery of nerve function (Rocha *et al.*, 2020).

The group around Shoichet and Salgado had previously developed this GG-GRGDS hydrogel for neural stem cell culture aimed for central nervous system regeneration with the co-culture of olfactory ensheathing glia (OEG) and neural SC fate. The work by Silva *et al.* (2013) showcases the effect of peptide-cell adhesion from the functionalized hydrogels, which supports the proliferation of neural SC and demonstrates a therapeutic benefit for spinal cord injury repair (Silva *et al.*, 2013). Koivisto *et al.* (2017) showed that also unmodified GG hydrogels are suitable for *in vitro* neuronal tissue engineering, with certain modifications closely resembling the mechanical properties of rabbit brain. The culture of hPSC-derived neuronal cells was carried out on top of the bioamine crosslinked hydrogels, below, as well as encapsulated within, but surprisingly only for the 2D culture on the top of the hydrogels the addition of laminin up to 10% v/v to the hydrogel showed any effect (Koivisto *et al.*, 2017).

One application and tissue type that is exceedingly suitable for GG materials is cartilage and chondrocyte culture, as vascular ingrowth is not observed but mechanical stimulation plays a major role (Vinatier and Guicheux, 2016). Gong *et al.* (2009) used their scissored GG to culture primary porcine chondrocytes for up to 150 days *in vitro*. The modification helped to control the molecular weight of GG and improved its injectability and gelation point. Compared to the culture in agarose, the chondrocytes showed an increased glycosaminoglycan (GAG) and collagen production (Gong *et al.*, 2009). The chondrogenic potential of GG was established further by Tsaryk *et al.* (2014), who compared the encapsulation of nasal chondrocytes and bone marrow SC in photocrosslinkable methacrylated and physically crosslinkable GG. The subcutaneous implantation of cell-laden hydrogels indicated chondrogenic potential, however photocrosslinking was found to have higher cell compatibility in this study, perhaps due to higher rigidity and stability (Tsaryk *et al.*, 2014). The same research group went on to use NaGG methacrylation, and then demonstrated the encapsulation of human nasal cartilage or human adipose SC *in vitro* and *in vivo* for cartilage repair. The material implantation to a cartilage lesion in a rabbit model demonstrated the successful cell delivery of rabbit adipose

SC, adhesion to native cartilage and ultimately a full thickness regeneration (Vilela *et al.*, 2018). Bonifacio *et al.* (2020) showed that the performance of GG hydrogels can further be improved by the incorporation of inorganic clays and the compounding with Manuka honey. While the inorganic clay phase serves as physical reinforcement and improves the biomimetic morphology, the Manuka honey acts as antibacterial agent, preventing the infection at the injury site and protecting what little autonomous healing capacity cartilage has. Chondrogenic differentiation capacity of human mesenchymal SC was shown for *in vitro* culture up to 45 days, as well as biocompatibility *in vivo* for only one week (Bonifacio *et al.*, 2020).

Due to its outstanding transparency, GG has also found application within ophthalmology and ocular tissue engineering. Lee *et al.* (2021) investigated the possibility to deliver retinal pigment epithelial cells to the diseased eye *via* subretinal injection. The adhesion to wet surfaces, such as the eye, was achieved by the catechol groups of the dopamine functionalization of GG. The dopamine functionalization does not prevent the crosslinking with calcium, however it decreases the viscosity, injection force, and compression modulus (Lee *et al.*, 2021). Chouhan *et al.* (2019) created a hydrogel eye drop system based on GG to counteract the scarring and opacity of the eye after infection and disease. The application as such is based on the suspension hysteresis and self-healing capacity of GG fluid gel, releasing decorin, which is a glycoprotein that has previously been shown to attenuate intraocular fibrotic scarring (Chouhan *et al.*, 2019).

Ultimately, GG has been established as intriguing and versatile biomaterial in a wide range of TERM applications in the recent decades. Various literature examples demonstrate the facile modification of mechanical properties, viscosity, modulus, and morphology. GG is readily combined with other materials and phases, and there are several functional sites within the molecular structure that can serve as modification targets. However, direct modification with bio-functional markers has yet to eclipse the bioactivity of natural polymers such as gelatin or collagen. Nevertheless, promising regenerative, tissue forming results have been achieved using GG *in vivo* and *in vitro*.

2.3 Polysaccharide hydrogel modification strategies

Modification of hydrogel polymers stands in the foreground of this dissertation, and thus some of the strategies employed specifically for polysaccharides are reviewed in this chapter and listed in **Appendix A1**. While not intending to be a comprehensive

list, the most common approaches are summarized, with the aim to understand the reason of modification. Typically, the aim for modification is to adjust either the biological functionality or the mechanical properties of a hydrogel, while the respective other is considered as fixed. It should be kept in mind, however, that alteration of one aspect, can have consequences for the other. For example, crosslinking to increase the temporal stability of a hydrogel can diminish cell response because crucial binding sites are blocked. Another desired aspect is often modularity, which enables a facile adaption of the desired properties to the application ad hoc without changing the base properties much and retaining essentially the same material, so that comparison of results is achievable.

2.3.1 Chemical modification

Here, the chemical modification of a polysaccharide is understood as a direct alteration of the chemical structure of the polymer chain by means of organic synthesis. The aim to do so may include attachment of bioactive factors, such as small peptides or growth factors, or the alteration of the polymer chain to include higher functionality, or to include indirect modification such as the biotin-avidin strategy and other orthogonal approaches. Chemical modifications to allow for a wider spectrum of crosslinking strategies are discussed in the next chapter, however the approaches often overlap.

Chemical modification of polysaccharides in general is a well-established topic for several industrial research fields, for example the modification of cellulose to overcome its hydrophobicity. Thus, the chemical modification of hydrogels can rely on long experience and knowledge in chemical synthesis (Cumpstey, 2013). When designing a polysaccharide hydrogel, the repeat units and native functional groups of that polysaccharide should be considered, for example glucuronic acid carries a single carboxyl group, and there are amine pendants in glucosamine. A common issue for polysaccharides may be their solvent, as many do not dissolve readily in aqueous or organic solvents, and inorganic salts and buffers must be used (Cumpstey, 2013). On the other hand, hydrogel-forming polysaccharide may encounter issues with viscous slurries due to ionic interactions

The carbodiimide coupling strategy is borrowed from peptide synthesis and achieves conjugation between a carboxyl group and an amine compound without additional crosslinking structure, thus often termed a 'zero-length' bond. As a reagent either *N,N'*-dicyclohexylcarbodiimide (DCC) or the water-soluble 1-ethyl-3-

(3-dimethylaminopropyl)carbodiimide (EDC) are used to activate a carboxyl group. This group is then converted to an amide or ester *via* an O-acylisourea intermediary structure, and an isourea by-product that is removed *via* dialysis. While this coupling strategy excels with good conversion rates and well-established protocols, it is also prone to hydrolysis and sensitive to pH changes, which may make it challenging to adapt for hydrogel synthesis. The use of a buffer advised and *N*-hydroxysuccinide (NHS) is often used to stabilize intermediary product and reduce side reactions (Hermanson, 2013). Carbodiimide conjugation has been used for instance to couple the peptide RGD to GG (Ferris *et al.*, 2015; Lee *et al.*, 2021) and alginate (Rowley *et al.*, 1999), or to attach the protein avidin to nanocellulose (Leppiniemi *et al.*, 2017), or to attach gallic acid to chitosan (Khan *et al.*, 2022).

Cyclo-addition and click reactions are used to achieve chemoselective ligation, implying they do not undergo reactions with other functional groups, but only react with specific dienes which are not found in biological molecules. Famous examples include the Diels-Alder reaction and so-called 'click chemistry', which is a Cu^{1}-catalyzed azide-alkyne cycloaddition. The copper catalyst allows for the reaction to occur at room temperature and ambient pressure, thus opening it for bioconjugation reactions. For instance, Silva *et al.* (2012) used the Diels-Alder cycloaddition between furan-modified GG and maleimide-functionalized peptide pendant to decorate GG under mild conditions. The furan modification of GG was achieved through etherization of the carboxyl group using the triazine coupling reagent 4-(4,6-Dimethoxy-1,3,5-triazin-2-yl)-4-methylmorpholinium chloride (DMT-MM). With a total reaction time of 48 h, the authors achieved a furan substation of 27% and final peptide concentration of 0.3 mM per mg of GG (Silva *et al.*, 2012).

Polysaccharides can be oxidized in order to introduce aldehyde functional groups to their structure, which offer great reactivity and ample opportunities for further functionalization, especially to alter crosslinking capacity. Most polysaccharide oxidations in the literature make use of the Malaprade reaction using sodium periodate $NaIO_4$ (Malaprade, 1928). The oxidation of vicinal diols using relatively high concentrations of sodium periodate leads to a ring-opening of the sugar. The thus created aldehydes are often used for further conjugation, for example *via* Schiff-base formation with an amine or hydrazide, or *via* reductive amination. Ring-opened oxidized polysaccharides are rarely not further reacted, because the molecular folding of the polymer chain is disrupted through the oxidation, and native crosslinking mechanisms are typically impaired. Alternatively, the amino groups on sugars such as glucosamine and galactosamine can be oxidized. As an example, Martinez-Sanz *et*

al. (2011) attached an amino-glycerol side chain to hyaluronic acid *via* amidation reaction, and further oxidized this pendant selectively (Martínez-Sanz *et al.*, 2011).

There are, of course, many other chemical approaches to modify a polysaccharide, and possibilities have to be explored for each type of polysaccharide independently. For high molecular weight polysaccharides for example, the scissoring of the polymer chain can be advantageous to reduce the solution viscosity. This can be achieved *via* reductive cleavage after ring-opening oxidation (Gong *et al.*, 2009). A highly intriguing strategy was presented by Bondalapati, who proposed the exclusive modification of the polymer chain end groups using oxime-mediated chemistry. Depending on the polymer and its molecular weight, there can be several thousand repeat units in one polymer chain, but only two end groups, which explain how this approach does not affect the chemical structure of the polymer chain, and thus does not alter any crosslinking groups or bioactive functionalities present by it. Nevertheless, the authors showed relevant peptide modification degrees for alginate to improve cell adhesion and organization, while retaining similar viscoelastic properties to native alginate. The ring opening of the aldehyde in the terminal saccharide is catalyzed by nucleophile action of aniline, shifting the acetal balance, and allowing for oxime bond formation under addition of an aminoxy-capped functional species (Bondalapati *et al.*, 2014).

2.3.2 Crosslinking modification

While different crosslinking mechanisms of polysaccharides will be discussed here, the use of different crosslinking species acting through essentially the same mechanism will not be exhausted. For example, native GG can be crosslinked with mono- and multivalent cations, as well as amine compounds, and the crosslinking mechanism differs slightly for each (chelation, charge-screening, partial Schiff-base), however GG does not need to be modified for this to occur. Further, crosslinking modification should be understood as subset of chemical modification with specific purpose to affect the crosslinking, and hence the mechanical and temporal properties, rather than the biological response. Small, reactive chemical crosslinkers such as glutaraldehyde are usually avoided due to their cytotoxicity and potential unspecific side reactions. But examples using epichlorohydrin have been shown by Meybodi *et al.* (2013) and Nikpour *et al.* (2018) for crosslinking of dextran (Meybodi *et al.*, 2013; Nikpour *et al.*, 2018).

Photocrosslinking gives high user control over the gelation point, provides robust crosslinking densities, and has established itself as popular choice for hydrogel modification if the network formation needs to be adjusted. Photocrosslinking sites must be introduced artificially, but this in turn typically improves mechanical rigidity of hydrogels without detrimentally affecting biological competences, as the reaction occurs orthogonally to chemical reaction *in vivo*, thus not affecting tissue-, and cyto-compatibility. A photon, *i.e.*, light exposure, is needed to initiate the chemical crosslinking reaction and depending on the photoinitiator used either ultraviolet (UV) or visible (Vis) wavelengths are used. Broadly, two types of photocrosslinking reactions can be distinguished: acrylates and photo-click-reactions. Acrylates exhibit a chain growth pattern, and the reaction may be sensitive to O_2, while click-reaction follow a step growth pattern and are comparably insensitive to O_2. Methacrylated polysaccharides in the recent literature include hyaluronan (Muir *et al.*, 2021; Spearman *et al.*, 2020), GG (Jongprasitkul *et al.*, 2021; Oliveira *et al.*, 2016; Pacelli *et al.*, 2016; Tsaryk *et al.*, 2014; Vieira *et al.*, 2019; Vilela *et al.*, 2018), guar gum (Tiwari *et al.*, 2009) and alginate (Jongprasitkul *et al.*, 2021). In these, the free-radical-initiated chain polymerization requires a photo-initiator (Irgacure, VA086, LAP) which absorbs a photon and releases a radical, thus starting the radical reaction and opening the double bonds of the vinyl groups. A disadvantage of methacrylate-photocrosslinking is the presence of free radicals, which may be harmful to cells, and the reaction is sensitive to O_2 and other radical catchers (Hermanson, 2013).

Besides methacrylate photo-addition reaction, thiol-ene reactions between a thiol (SH) and an alkene (C=C) have been exploited as reactions to modify polysaccharide hydrogels. Often, they are referred to as 'photoclick' reactions because the formation of the thio-ether bond is triggered by radicals and requires photoinitiators similar to the methacrylate strategy. Mergy *et al.* (2012) investigated the modification of hyaluronic acid and dextran with pentenoic anhydride *via* esterifaction. Networks were formed in presence of a dithiol (HS-R-SH) and photoinitiator Irgacure, alongside attachment of thiolated peptide to increase bioactivity (Mergy *et al.*, 2012).

Using a Michael type addition reaction, da Silva *et al.* (2018) exploited the modification of the hydroxymethyl group in glucose of gellan gum using divinyl sulfone. The remaining divinyl group could then be used to efficiently bind either bioactive sites or degradable crosslinkers (da Silva *et al.*, 2018). While also a click-reaction, this strategy is not photo-mediated and the thiol-ene reaction triggers on contact of the components. Another click reaction as crosslinking strategy was used by Desai *et al.* (2015), who showed the facile combination of norbornene-modified alginate (Alg-N) and tetrazine-modified alginate (Alg-T). The cycloaddition reaction

between the two components releases only N_2 as side product and completes within about 1 h. Unreacted Alg-N remaining in the hydrogel could be used to further attach thiolated peptides to the network *via* thiol-ene reaction (Desai *et al.*, 2015).

Carbohydrazide modification has been established to be popular strategy in recent years due to its great selectivity and bio-orthogonality. It involves the reaction between a dihydrazide (-(C=O)-NH-NH_2) and aldehyde group (-CH=O) forming a hydrazone bond (-(C=O)-NH-N=CH-). The dihydrazide group must be added synthetically, as it does not occur on polysaccharides or other native polymers, however the aldehyde can either be present natively or require modification. Using carbodiimide coupling, for example hyaluronic acid can be modified to carry dihydrazide group, and can then be crosslinked with an carbonyl-carrying polymer (Karvinen *et al.*, 2017; Koivusalo *et al.*, 2018; Martínez-Sanz *et al.*, 2011). Hydrazone crosslinking could also be used to create an injectable chitin hydrogel for stem cell delivery (Yang *et al.*, 2021). Also, primary amines (-NH_2) react quite readily with aldehydes as Schiff-base coupling, however they are less stable than the hydrazone bond. As such, amine functionality in chitosan was exploited to form Schiff-base linkages with oxidized gellan gum (Osmałek *et al.*, 2014) and oxidized hyaluronic acid (Thomas *et al.*, 2017).

2.3.3 Blending

Finally, we will briefly consider two types of blended hydrogel systems, based on their material class: Combination with inorganic particles and the formation of an interpenetrating network between two polymers. Mixing of any two polymers, or any two components can be a highly feasible strategy, yet material design strives to achieve a synergistic effect between two phases, in order to exceed the mechanical, and maybe biological, properties of either of the individual components. For example, Goyal *et al.* (2011) created a hydrogel for gene delivery from GG and polyethylenimine (PEI). The two components form a nanocomposite based on their ionic interaction between the negatively charged GG (-COO^-) and the positive PEI (-NH_3^+) and a reduced cytotoxicity of PEI was demonstrated, while retaining its transfection capacity (Goyal *et al.*, 2011). Typically, a strong interaction between the two constituents of a composite is needed to achieve the most robust outcomes.

There is a multitude of dual-phase hydrogel systems in the literature using an inorganic material as filler, benefitting from the complimentary performance of soft, hydrated, cell-adhesive hydrogel network and the tough, ion-rich ceramic substances

such as clays and bioactive glasses. Clays are layered mineral silicates of varying composition and crystallinity and microstructure. They can be osteoinductive materials and capable of inducing hydroxyapatite layer formation *in vivo*, which is mediated by their porosity, lamellar structure, as well as ion release profile. In comparison to clays, bioactive glasses (BAG) are sintered silicate ceramics and typically transparent (Hupa, 2018). Also, their exact composition varies widely, but generally the ratio between Ca and P released from the glass determines their biological effect, such as bone formation and protein adsorption. BAG can be produced as sintered bulk, nano- or micro-particles (nBAG and mBAG), or as amorphous sol-gel. Besides their bioactive features, these ceramic particles are typically blended to hydrogel networks in order to improve the mechanical stability of the composite, however an aggregation of the particles will result in a harsh deterioration of the mechanical properties. Through addition of different inorganic clay phases, Bonifacio *et al.* (2020) prepared composites structures for cartilage repair from GG. The hydrogel had already been modified with the addition of manuka honey to improve the antibacterial action, but no further chemical modification was carried out to incorporate the clays, namely mesoporous silica, sodium calcium bentonite, and halloysite nanotubes, to the scaffold. The mechanical reinforcement increased the compression modulus from GG-manuka honey of 85 kPa up to 139 kPa for the clay composites (Bonifacio *et al.*, 2020). Also the incorporation of BAG greatly increased the stiffness of hydrogel samples, as for example shown for GG-BAG with compressive modulus of up to 1160 kPa (Gantar *et al.*, 2014), or epichlorohydrin crosslinked dextran-nBAG with compressive modulus of up to 76.6 kPa (Nikpour *et al.*, 2018).

The combination of two polymer species can be achieved either through crosslinking of the two polymers with another, or through the formation of an interpenetrating polymer network (IPN). Crucially, in an IPN the two polymer networks are topologically interlaced but are not chemically crosslinked with another (Myung *et al.*, 2008). This results, for example, in the decoupling of mechanical properties and degradation mode and affords intriguing possibilities for network design. Lee and Kurisawa (2013) demonstrated the reinforcement effect of a fibrin hydrogel network with tyramine-crosslinked hyaluronic acid network. While fibrin contributes excellent bioactivity and encourages HUVEC cell spreading, their excessive shrinkage and deformation is prevented by hyaluronan network (Lee and Kurisawa, 2013). Tyramine was conjugated to hyaluronic acid *via* carbodiimide strategy, and its crosslinking was achieved enzymatically using HRP and H_2O_2 (Kurisawa *et al.*, 2005). An IPN of two different hyaluronic acid hydrogel was

presented by Guo *et al.* (2021) as cell carrier for nucleus pulposus repair. One network was formed by covalent crosslinking of hyaluronic acid with 1,4- butanediol diglycidyl ether (BDDE), which is also used as a dermal filler for esthetic surgery. The other network is a thermoreversible, ionic hydrogel of PNIPAM brushes grafted to hyaluronic acid, which is injectable at room temperature but gelates at temperatures above 29°C. The covalent-ionic hybrid nature of this IPN endures physiological loading conditions in intervertebral disc model for up to one month (Guo *et al.*, 2021). Other polysaccharide IPNs haven been prepared from agar (Yan *et al.*, 2021), alginate (Wen *et al.*, 2014) and GG (Morris *et al.*, 2012).

2.3.4 Degradation modification

There are many approaches to classify the degradation of a polymer, based on either the type of hydrogel (natural, synthetic), the type of hydrogel crosslinking (chemical, physical), or the driving agent of the degradation (hydrolysis, enzymes) (Meyvis *et al.*, 2000). Here, we will consider the underlying molecular action of the degradation mode, thus differentiating to three cases: Solubilization, severing of the network crosslinks, and the cleavage of the polymer backbone. Solubilization is observed predominantly for physically and thermally crosslinked hydrogels. The latter two can be brought about *via* hydrolytic, enzymatic or physical means, and are mostly considered for chemically crosslinked hydrogels (Kamath and Park, 1993). In this chapter, some polysaccharide hydrogels that have either been modified or observed to follow these degradation schemes will be briefly introduced.

A dissociation of the hydrogel network is commonly seen in physical and thermal hydrogels. Since the network forming points, *i.e.*, crosslinks are not covalent or permanent, they are prone to rearranging and eventually uncoupling, which weakens the network. Small polymer chains are also prone to exit the formed network, thus decreasing the density of the total hydrogel. For ionically crosslinked hydrogels, this behavior can be caused by a reduction of ion concentration in the formulation, especially when the sample is incubated in a larger volume of a solution with lower ion concentration. GG is a good example for such behavior, as it forms hydrogels at low polymer concentration either by addition of cations such as calcium chloride, or even simply by cool-down from higher temperatures due to coiling and counterions present in the native product (Morris *et al.*, 2012). Thus, GG hydrogels are stabilized by a dual mechanism of electrostatic interaction and chain entanglement. The chain release behavior of GG hydrogels was first described by Tanaka and Nishinari, and

followed up by Hossain and Nishinari (Hossain and Nishinari, 2009). The authors provide an in-depth analysis of the phenomenon, where non-network forming, shorter polymer chains are released from the hydrogel when immersed to water. When immersed in pure water, the hydrogels swell and become stiffer, as shown by an increase in elastic modulus with time using a longitudinal rheometer. The erosion effects of chain release are offset if the samples are immersed in ionic solutions (KCl or $N(CH_3)_4Cl$). The authors point out, however, that within their short 8 h of incubation, this chain release does not lead to degradation, as the released chains never did contribute to the network formation (Hossain and Nishinari, 2009). In contrast, Silva *et al.* (2013) presented a long-term incubation study of high and low acyl GG hydrogels over 168 days (Silva *et al.*, 2013). It was found that these gels exhibited mass loss for 28 days and then remained stable for the remaining period of 140 days. The crosslinking strength within the hydrogels is maintained by immersion in phosphate buffered saline (PBS), which is in line to the previous finding by Hossain and Nishinari. The mass loss was attributed to polymer leaching, *i.e.*, chain release, which again is partially offset by the influx of ion because of cation exchange with the surrounding medium. Bellini *et al.* (2015) developed a hydrogel system by blending GG and hyaluronic acid for the treatment of bone defects. When incubating their hydrogel in simulated body fluid (SBF), they observed a very similar behavior. After an initial degradation period the hydrogels stabilize and do not degrade within 45 days of incubation. The initial degradation reduces the samples to about 50% of their original weight, which can be explained by a combined effect of swelling, chain release and additional crosslinking from the incubation medium. The authors further report a delay in degradation rate based on a higher initial crosslinker concentration (Ca^{2+}), further supporting this claim (Bellini *et al.*, 2015).

The most frequently observed hydrogel degradation mode is the chemical breaking of covalent crosslinking points. Indeed, it is similar to the previously discussed network dissociation as the destabilization of network originates from the crosslinking points, however the crosslinking was covalent, and thus a chemical hydrogel. Within this category, we can distinguish the two major pathways of enzymatic and hydrolytic cleavage, where the degradation is driven either by presence of proteases (peptidases) or merely the presence of water. Recently, a large number of hydrogels developed for TERM are designed to degrade *via* hydrolysis or enzymatic cleavage of the crosslinking point, and thus belong into this category.

To render the rather stable GG biodegradable, da Silva *et al.* (2014) equipped it with MMP-1 cleavable sites *via* divinyl-sulfone (DVS) functionalization (Silva *et al.*, 2014). Again, this DVS-functionality provides crosslinking sites, which are sensitive

to enzymatic cleavage, as well as the addition of cell adhesive sites. Interestingly, when incubated in either MMP-1 solution or pure PBS, the hydrogel weight change was fairly similar, and MMP-1 has seemingly no effect on the degradation rate. Moreover, very low concentrations of MMP-1 (here 5 mg/L) were observed to slow down the degradation even further. The authors argue that this is due to a complex interplay of swelling and absorption of more water in a looser network, rather than their modification being unsuccessful. Further, while the peptide crosslinker does apparently not increase the degradability of their GG hydrogel, they hope that cells are still given the opportunity to remodel the initially tight network by cleavage of extra crosslinks. The favorable cell culture results, however, are likely achieved by the addition of cell adhesive sites. Another GG modification to steer degradation was shown by Karvinen *et al.* (2017), who compound it with the glycosaminoglycan hyaluronic acid (HA) (Karvinen *et al.*, 2017). The primary mode of crosslinking in this hydrogel happens *via* chemical reaction between aldehydes of oxidized GG and adipic dihydrazide-modified hyaluronic acid. However, the ionic nature of GG remains and influences the swelling kinetics of the final hydrogel (Richbourg and Peppas, 2020). When incubated in pure water, the authors observe the unmodified, ionically crosslinked GG hydrogel to remain stable without swelling or noticeable degradation within 5 h. The GG-hyaluronic acid, on the other hand, shows strong swelling and weight increase of up to 2500% from the original weight. However, when incubating both hydrogels in an ionic solution such as PBS, shrinkage is observed. The modified GG-hyaluronic acid hydrogels show less severe shrinkage compared to the native GG which likely is a compromise of the counteracting effects: Degradation of the hyaluronic acid component and contraction due to GG ionic crosslinking. When incubated in hyaluronidase, GG-hyaluronic acid hydrogel again initially swelled, but then degraded in about 24 h.

A dually enzyme-responsive hydrogel was proposed by Lee and Kurisawa (2013), consisting of both fibrin and hyaluronic acid (Lee and Kurisawa, 2013). The polymers are made to form an interpenetrating network (IPN), with the goal to prevent rapid and premature degradation observed in pure fibrin constructs. IPNs are partially interlaced polymeric networks without covalent bonds between the two polymers, however they cannot be separated unless chemical bonds are broken. For the fibrin-hyaluronic acid hydrogel of Lee and Kurisawa, it was observed that the proteolytic degradation of fibrin still happens at same rate, but the hydrogel bulk remains because of the hyaluronic acid network. The fibrin network is degraded due to plasmin expressed by encapsulated human umbilical vein endothelial cells (HUVECs) within hours and causes the construct to contract slightly, but this

contraction effect is highly diminished due to the presence of the hyaluronic acid network. When needed, the entire construct can be degraded by addition of hyaluronidase.

In another dual-degradation approach, Sahoo *et al.* (2008) combined hydrolytic and enzymatic degradation of hyaluronic acid modified with lactic acid pendants (Sahoo *et al.*, 2008). While hyaluronic acid degrades natively *via* hyaluronidase, this enzyme is not commonly expressed in cell cultures and hyaluronic acid hydrogels have been found to be very stable. To increase the degradation rate *in vitro*, the authors introduce lactic acid crosslinking to enable hydrolysis of the ester groups in aqueous solutions. Rather than monitoring the weight, the degradation is followed by the release of coupled VEGF and its degradation product uronic acid. As a result, in an enzyme-free solution the hydrogels completely degrade within 9 days *via* hydrolysis, and the rate could be controlled by initial precursor concentration, where lower crosslinking density leads to a faster degradation. As opposed to enzymatic degradation, hydrolytic degradation provides the advantage of higher degree of control over the molecular mechanism and concentration of active species especially in cell culture settings. However, the degradation kinetics have to be specifically designed to match the formation of new tissue *in vitro* and *in vivo* (Drury and Mooney, 2003; Stosich and Mao, 2007). A somewhat more complex, dual-degradation system was described by Su *et al.* (2021), wherein oxidized dextran (dex-CHO) was crosslinked *via* Schiff-amine base pairing using cysteamine to form dex-SS hydrogels bearing disulfide bonds (Su *et al.*, 2021). After gelation, this hydrogel can degrade *via* two pathways: Either hydrolysis of the Schiff-base (imine) bond, or *via* disulfide (S–S) cleavage in a reducing environment. The imine bond is labile against acidic environment below pH 5, while the sulfide bond is opened in presence of L-glutathione (GSH). However, only using GSH presence proved to be insufficient to release the model drug doxorubicin (DOX) from the hydrogel, as the hydrogels remained too stable within the two days of observation. Only a dual action low pH and GSH efficiently released the drug.

If we consider hydrogels as polymer chains with discrete points of crosslinking, either physical or chemical in nature, then another option for degradation is scission of the polymer chain as opposed to dissociation at the crosslinking point (Meyvis *et al.*, 2000). This type of degradation mechanisms is observed mostly for chemically crosslinked hydrogels with very stable crosslinking sites. The polymer chains can be broken *via* enzymatic, proteolytic, and other chemical means. Albeit not meant for any tissue engineering application, Tayal *et al.* (1999) proposed a guar gum crosslinked by borate ion complexation to develop degradable transport sand

(proppant) used in oil and gas industry (Tayal *et al.*, 1999). While the borax complex is highly stable, the guar galactomannan rests are enzymatically degraded using endo-*β*-mannanase, an enzyme which cleaves the polymer chain backbone. Indeed, they manage to fully digest the hydrogel within 7 h and use rheology, as well as GPC, to correlate molecular degradation mechanisms. Ultimately, the complete degradation is combination of initial, rapid chain scission and a delayed breakdown of the remaining gel structure. Another example of enzymatic action on the polymer backbone is given by Yang *et al.* (2021). Through the formation of a double network from the natural polysaccharide chitin and the synthetic, non-degrading PEG, they achieve a robust system using adipic hydrazide functionalization (Yang *et al.*, 2021). The hydrogels were shown to be stable with a mass loss of less than 20% in PBS for longer than 15 days. In presence of lysozyme however, the hydrogels completely degrade within 7-15 days, depending on the initial ratio and degree of functionalization of the components.

Nonsuwan *et al.* (2019) showed a very elegant degradation through chemical rearrangement of the Mailliard reaction (Nonsuwan *et al.*, 2019). Oxidized dextran was crosslinked using dithiothreitol (DTT) to form hydrogels *via* Micheal-type addition reaction, leaving some aldehydes unreacted. These hydrogels are rather stable, only through addition of any amino-compound such as glycine, a Schiff-base reaction is induced, triggering the subsequent degradation of the saccharide chain. Essentially, the dextran polymer chain is destabilized through the oxidation modification, but initiation of chain scission is possible only through the presence of amines. Interestingly, the degradation speed could be controlled independently of the mechanical properties of the hydrogel because the chain scission sites are independent of the crosslinking sites.

3 AIMS

The aim of this thesis is to explore the modification strategies for gellan gum-based hydrogels and to verify their suitability for tissue engineering and biomedical purposes. While gellan gum has been established as a suitable material for soft tissue engineering it requires modification and bioactivation to provide desired properties. A wide range of testing methods is required to adequately describe a hydrogel and determine the relevant biochemical and biomechanical properties for tissue engineering applications. Furthermore, the processing and preparation strategies are given special attention in this thesis, as there is a significant correlation to the viscoelastic properties of a hydrogel. Similarly, the degradation profile, along with degradation testing principles of gellan gum hydrogels are being investigated, in an attempt to understand and highlight the importance of hydrogel temporal stability for both *in vitro* cell culture and *in vivo* regenerative applications. The research themes can be divided into the three following aspects:

(1) Exploration of suitable modification strategies for the polysaccharide hydrogel gellan gum. These strategies include chemical alteration of the polymer chain, functionalization, and addition of active compounds, as well as crosslinking strategy. The aim is to improve the hydrogel towards application in tissue engineering. Modification of gellan gum is presented in Publications I, III and IV.

(2) Evaluation of the modified hydrogel by assessment of its structural, mechanical, and biological properties. Material characterization and cytocompatibility are elaborated in Publications I, III, IV and V. A special focus is the interaction between the biomaterial and human cells in a 3D environment to assess cytocompatibility: What can be learned about the biomaterial? How is this interaction studied?

(3) Investigation of application areas of the modified hydrogels. In order to gauge the success of a modification, application-based testing is shown in Publications I, II, III and V, with the aim of the designed hydrogel properties benefitting the application. These applications span from sample fabrication and 3D printing, to implantation and medical application, and to cell encapsulation and preparation of 3D tissue models.

4 METHODS

4.1 Modification of gellan gum

4.1.1 Purification

For ion purification, GG (Gelzan™, Sigma Aldrich, 200 mg) was dissolved in ultra-pure (u.p.) water (Sartorius arium® mini, 0.055 µS/cm) at 0.5% w/v at 60 °C. According to the protocol by Doner *et al.* (1997), cation exchange resin (5 g, Dowex® 50W X8, hydrogen form, 50–100 mesh) was pre-rinsed in water and HCl (0.5M) and an excess was added to the hot GG solution. Using decantation, the resin was separated from the solution after 30 min and filtered. The pH was adjusted to 7.5 using NaOH (1M). The solution was precipitated in 3-fold volume of *iso*-propanol. The product (NaGG) pre-dried over vacuum and lyophilized over 2 days.

The success of purification was determined using ICP-OES. The polymers were digested according to the protocol by Kirchmajer *et al.* (2014). Therefore, NaGG and GG (100 mg) were treated with sulfuric acid (0.5 mL, H_2SO_4, 98%) under heating and subsequently hydrogen peroxide was added dropwise until the solution was translucent (Kirchmajer *et al.*, 2014). The diluted samples were analyzed using Agilent 5110 ICP-OES (Agilent Technologies).

4.1.2 Oxidation

GG was oxidized using sodium iodate according to Malaprade reaction (Gong *et al.*, 2009; Malaprade, 1928). Therefore, 100 mL of GG solution (Gelzan™, Sigma Aldrich, 0.5% w/v in u.p. water) was heated to 40 °C and placed under nitrogen atmosphere. Shielded from light sources, sodium periodate ($NaIO_4$, 12-48 mg) was dissolved in water (4 mL) and added to the GG solution dropwise. After 4 h at 40°C, the oxidation was quenched using ethylene glycol (300 µL). The product (GGox) was dialyzed against d.i. water (de-ionized water, Miele Aqua Purificator G 7795, Siemens) using cellulose membrane dialysis tubes (12-14 kDa MWCO,

Spectra/Por™ 4, Spectrum™ Labs) for three days with daily water exchange, after which it was lyophilized for four days.

4.1.3 Scissoring

Scissoring, the reductive cleavage at the oxidized sites, was carried out using the previously oxidized products. Oxidized GG (100 mg of GGox 1, 2, or 3) was dissolved in sodium borate buffer (46 mL, 0.05 M) at 60°C for one hour. Under nitrogen atmosphere, the solution was chilled to a temperature below 10°C. Consequently, sodium borohydride $NaBH_4$ (4 mL, 0.1% w/v in sodium borate buffer) was added dropwise to the GGox solution and kept overnight. The reaction was quenched using a mixture of acetic acid and methanol (5 mL; 1:4). The product (GGsciss) was dialyzed as described above against d.i. water for two days and subsequently lyophilized for four days. For nomenclature, scissoring transforms GGox(1) to GGsciss(1) and so forth, as static amount of $NaBH_4$ were used and only the type of GGox was changed.

4.1.4 Carbodiimide coupling of avidin

Carbodiimide functionalization of GG was based on the protocol by Ferris *et al.* (2015). Here, NaGG (10 mg/mL, 10 or 20 mL) was dissolved in HEPES buffer (50 mM, pH 6.5) at 40 °C and activated with 1-ethyl-3-(3-dimethylaminopropyl)-carbodiimide (EDC, 0.4 M) and sulfo- N-hydroxysuccinimide (sulfo-NHS, 1.0 M) for 15 min. This activation reaction was quenched using β-mercapthoethanol (28 µL, final concentration 20 mM). Finally, charge-neutralized chimeric avidin (CNCA, 1 mg/mL, 3.5 mL in HEPES 50 mM, pH 6.5) was added and the mixture was stirred for 5 h at 40 °C. The product (NaGG-avd) was dialyzed over 5 days (MWCO 12-14 kDa) and lyophilized over 4 days.

4.2 Hydrogel preparation

Hydrogel precursors used herein were dissolved in either in u.p. water, sucrose (10% w/v in water), HEPES/sucrose (25 mM, 10% w/v sucrose, pH 6.5), or serum-free cell culture medium as stated. The dry polymer was weighed and dissolved under

constant stirring at 37°C for up to 1 h. Once dissolved, the solutions were stored at 4°C and warmed to 37°C before hydrogel preparation.

4.2.1 Mold casting

To mold cast the majority of the here presented GG hydrogel formulations, a mixing technique was employed to improve the uniformity. All hydrogel components are warmed to 37 °C on a water bath. In a mixing vial, the components were combined typically in a ratio of 5:1 (precursor : crosslinker) and rapidly stirred (max. 300 rpm). Optional gel components are added to the polymer solution before adding the crosslinking agent. Within less than 60 sec, the mixture is transferred to the mold to set, as described in more detail in Publication II.

This method is not applicable for gelatin formulations, which were thus prepared directly in the mold or well plate by placing first the GG component (GGox) to the mold and pipetting the warmed gelatin into that volume. Mixing was achieved by few, swift pumps, without introduction of excess bubbles.

4.2.2 Extrusion-based printing

Printing features of ionic hydrogel formulations and a crosslinking bath were investigated in Publication I. Nordson EFD extrusion-based printer and software were used so that the precursor solutions were extruded through a 0.15 mm stainless steel nozzle onto a nylon mesh on a glass substrate. A concentrated crosslinking solution was applied onto the mesh to ensure an evenly distributed thin layer. The printed lines were immersed for about 1 min in the crosslinking solution. Writing speed was kept constant at 25 mm/s and the relative humidity was stable at 55% RH.

4.3 Testing methods

4.3.1 Degradation

To assess the degradation of cell-free hydrogels, samples were cast to ø 12 mm mold (500 µL volume) or ø 8.5 mm mold (200 µL) and left to fully gelate at 37°C overnight. Gelatin samples were typically chilled for a few hours in order to facilitate demolding.

After demolding, the samples were individually placed on pre-weighed mesh ring holder (nylon mesh fixed to acrylate ring, ø 1.8 cm) and their initial weight was recorded. The samples, on top of the mesh rings, are then placed into a small chamber that is filled with incubation media (PBS, lysozyme solution, DMEM, EBM, etc.) so that the sample is fully immersed. The mesh rings allowed for transportation of even delicate samples between the incubation chamber and the scale, as well as gentle blotting of excess incubation media. After weighing, the sample is placed back to the incubation chamber, allowing for continuous monitoring of the same sample throughout the degradation period.

For rheology degradation testing, the samples were cast to ø 2 cm molds, and the medium was added and refreshed in these molds without removing the hydrogel before its measuring point. The samples were then carefully removed from the mold, placed onto the lower geometry and analyzed using an amplitude sweep (0.01 – 500% oscillation strain) with a fixed frequency of 0.75 Hz and plate temperature of 30°C.

4.3.2 Compression

Mold-casted samples were compressed using Bose BioDynamic ElectroForce Instrument 5100 equipped with 22 N or 221 N load cell and WinTest software version 4.1 (Publication II and III) or 8.2 (Publication I and IV) software (TA Instruments, USA) Cylindrical samples were accurately measured for their diameter and height, and subjected to uniaxial, unconfined compression in ambient air. The sample was placed on the lower piston which was covered in parafilm and wet cellulose paper to prevent slippage of the sample, and the upper piston is brought into contact with the top surface manually. Compression was carried out at a speed of 10 mm/min up to 65% of the original sample height. Wherever possible, 5 replicates were measured (n=5). From the resulting force curve the stress is calculated as force over area of the sample. The stress is plotted against the applied strain and the slope from linear region (between 15-35% strain) of the resulting curve yields the compression modulus.

4.3.3 Rheology

For rheological experiment the Discovery HR-2 rheometer and TRIOS software (TA Instruments, USA) was used, which was equipped with a temperature control.

A 20 mm plate-plate geometry with smooth surfaces was used throughout. A solvent trap was used for measurements taking longer than 15 min.

For hydrogel precursor flow comparison, polymer solutions were warmed to facilitate the manipulation of the more viscous precursors. A steady state flow shear rate sweep test was performed with a gap of 1000 μm, using a logarithmic sweep at 25°C with a shear rate from 0.01 – 500 s^{-1}, with 5 points/s and a sampling period of 25 s. Experiments were carried out in triplicate (n=3).

Rheological analyses of the hydrogel gelation kinetics, *i.e.*, time sweeps, were performed so that the components, precursor and crosslinker, were combined on the bottom plate and the geometry was spun rapidly for mixing. In practice, the precursor solution was dispensed to the plate at 37 °C, the geometry was lowered to a gap of 1500 μm and the crosslinker solution was added during the mixing phase at 70 rad/s for 7 s. Consequently, the time sweep started with an amplitude of 0.75% oscillation strain, 0.75 Hz at 30 °C for at least 30 min (n≥3). After the sweep had concluded and the gel had formed, an amplitude sweep (30 °C, 0.75 Hz, 0.1 – 100% oscillation strain, n=3) or frequency sweep (30 °C, 0.75% oscillation strain, 0.1 – 100 Hz, n=3) was performed.

4.3.4 Structural analysis

The degree of oxidation was assessed based on the protocol by (Bouhadir, *et al.*, 1999) by derivatization of the aldehydes groups with *t*-butyl carbazate (TBC) and subsequent reaction with picryl sulfonic acid (TNBS) for UV-absorption quantification. Briefly, oxidized GG and controls were incubated overnight with an excess of TBC (10 mM in acetate buffer 0.1 M, pH 5.2). Then, the sample solutions were incubated with TNBS (2.5 mM in borate buffer 0.01 M, pH 8) at room temperature and quenched with hydrochloric acid (HCl, 0.5 M) after 30 min. The TNBS uptake was measured using UV-Vis-NIR spectrophotometer (Shimadzu UV-3600 Plus, slit width 5 nm) at 342 ±4 nm.

The molecular weight and size of native GG and selected derivatives were determined through size exclusion chromatography (SEC) and subsequent light scattering detection. Therefore, samples were dissolved in the mobile phase (DMSO with 0.2% LiBr) overnight, then heated at 70 °C for 2 h, and filtered (0.45 μm) before injection (100 μL, flow rate 0.5 mL/min). The solutions were separated using Agilent 1260 HPLC pump equipped with and autosampler and 2 PLgel Mixed-C 300×7.5 mm columns. The separated phases were detected using the multiangle light

scattering detector (DAWN, Wyatt Technology) in combination with a refractive index (RI) detector (Optilab).

Carbodiimide coupling yield between purified GG and avidin was indirectly investigated exploiting the avidin-biotin binding, using either fluorescence spectroscopy, gel electrophoresis, or an elution analysis. Firstly, a fluorescence titration curve was prepared from NaGG-avd (0.1% w/v in HEPES pH 7, 10% sucrose) and the biotinylated fluorescent dye b5F (biotin-5-fluorescein, 2 μM in DMSO and PBS). Control curves were prepared using NaGG and NaGG-avd blocked with biotin (3 μL, 0.17 mg/mL in 50 mM sodium-phosphate, 100 mM NaCl buffer, pH 7). Aliquots of b5F (25 μL) were added to the sample (2 mL) and measured after 2 min incubation using QuantaMaster PTI spectrofluorometer (Photon Technology International, Inc., Lawrenceville, NJ, USA) (excitation at 495 nm, emission at 520 nm, slits 2 nm). To demonstrate the covalent bonding, sodium dodecyl sulfate polyacrylamide gel electrophoresis (SDS-PAGE) was used, and urea was added to the samples and the cast gel to improve the resolution, where the PAGE gel was cast according to standard procedure, but urea (8 M) was added. All samples were incubated with biotin (85 μg/mL final concentration) to stabilize the avidin tetramer. After addition of the loading buffer, samples were heated to 50 °C for 15 min and urea was added. Electrophoresis was performed at +4 °C for 3 h at 100 V. Finally, the gel was stained with Oriole™ fluorescent gel stain (Bio-Rad) and imaged with a ChemiDoc MP imaging system (Bio-Rad Laboratories) and Image Lab software. For a more practical demonstration of avidin modification, hydrogel samples (NaGG-avd(H) 0.5% w/v and b5F 10 μm) were crosslinked with spermidine (SPD 2 mM). The samples were incubated overnight, demolded and then placed into 500 μL PBS for up to 48 h in an incubator under shaking at 37 °C. The fluorescence intensity of the eluate was analyzed at time points of 1 h, 6 h, 24 h, and 48 h. As control sample, NaGG and avidin were combined without conjugation and hydrogels were formed as described above.

4.4 Cell culture

4.4.1 Ethics statement

Primary human bone marrow stromal cells (hBMSC) used in Publcation III were previously harvested, isolated, and cryo-preserved in gas phase nitrogen. This work

was carried out by the Adult Stem Cell Group, BioMediTech, Tampere University, in accordance with the Regional Ethics Committee of the Expert Responsibility area of Tampere University Hospital, ethical approval R15174. The hBMSCs were isolated from an anonymous donor (labeled 6/16) with the patient's written informed consent during surgery at the Department of Orthopaedics and Traumatology at Tampere University Hospital. The isolation of hBMSCs was performed as described previously with slight modifications (Haimi *et al.*, 2009; Kyllönen *et al.*, 2013).

Human adipose stem/stromal cells (hASC) used in Publication V were isolated from subcutaneous tissue samples obtained from three independent donors to reveal the possible biological variabilities between human donors. Tissue samples were obtained at the Tampere University Hospital Department of Plastic Surgery with the donor's written informed consent and processed under ethical approval of the Ethics Committee of the Expert Responsibility area of Tampere University Hospital (R15161). The cells were isolated as described previously (Kyllönen *et al.*, 2013).

4.4.2 Fibroblasts

Human fibroblasts WI-38 (ECACC 90020107) were obtained from the European Collection of Authenticated Cell Cultures ECACC, UK Health Security Agency and used at passage numbers between 20 and 26. They were expanded from frozen state for one week until confluent in WI-38 medium, consisting of 10% v/v fetal bovine serum (FBS, Biosera, South American origin), 25 U/mL penicillin/streptomycin (pen/strep; Lonza, Basel, Switzerland) in DMEM-F12 1:1 (Gibco, Thermo Fisher Scientific, Waltham, MA). The fibroblasts were harvested using TrypLE™ Select Enzyme (Gibco) according to standard protocol and counted after resuspension.

4.4.3 Bone-marrow stem cells

The hBMSCs (passage number 6) were isolated as previously by the Adult Stem cell group, thawed from cryo-storage, and expanded for one week in basic medium consisting of α-MEM (Gibco), 5% v/w human serum (HS, Biowest, France) and 1% v/v pen/strep (Lonza, Basel, Switzerland) until confluent. The cells were then harvested using TrypLE Select and seeded into the hydrogel *via* uniform mixing at a cell density of 950 000 cells/mL. The cells were cultured for 21 days in the hydrogels using osteogenic medium (5 vol% HS, 0.25 mM ascorbate-2-phosphate, 10 mM β-

glycerophosphate, 1% 100 U/mL pen/strep in α-MEM, with the addition of dexamethasone 5 nM), which was replaced every other day.

4.4.4 Vascular co-culture

The hASC were cultured in α-MEM (Gibco) supplemented with 5% HS (Serana), 100 U/ml penicillin, and 100 μg/ml streptomycin, expanded over 4 days and used between passages 1-3. The mesenchymal origin of hASC was confirmed by surface marker expression analysis with flow cytometry and assessment of adipogenic and osteogenic differentiation potential according to the International Society for Cellular Therapy criteria (Dominici *et al.*, 2006).

Human umbilical vein endothelial cells (HUVEC) were purchased from Cellworks (India). These cells have been pooled from several human donors and express the green fluorescent protein (GFP), thus are named GFP-HUVEC. Upon removal from cryo-storage, they were cultured in Endothelial Cell Growth Medium-2 Bullet Kit (EGM-2; Lonza) consisting of Endothelial Cell Growth Basal Medium (EBM-2) and Endothelial Cell Growth Medium-2 Supplements (0.1% GA-1000, 0.1% R-IGF-1, 0.1% VEGF, 0.1% hEGF, 0.04 % hydrocortisone, 0.4% hFGF-B, 0.1% ascorbic acid, 0.1% heparin). Instead of the fetal bovine serum supplied with the Kit, 2% HS (Serana) was used. The cells were expanded over 4 days and used between passages 4-5.

4.4.5 Cell seeding

Fibroblasts were plated on top of the hydrogel (2D), and fibroblasts, hBMSC and the vascular co-culture were encapsulated in the hydrogel (3D) with some variations in cell density as listed in **Table 1**. As a general protocol the hydrogel solutions were sterilized prior to cell culture experiments *via* filtration using Whatman® FP30/0.2 CA-S syringe filters (Cytiva, USA). For 2D experiments, the hydrogels were cast to the well plate, about 300 μL for 48-well (ø 0.95 cm^2) and incubated at 37°C for 30 min before the cell suspension and medium were added on top. For 3D experiments, cells were centrifuged and resuspended in warm hydrogel precursor at the stated final concentration, before being cast to the well plate. Also here, the hydrogel was incubated for 30 min before addition of culture medium on top of the hydrogel to assure gelation.

Table 1. Cell concentrations used throughout Publications III-V.

cell type	Publication III	Publication IV	Publication V
WI-38	(2D) 63 000 cells/cm^2 (3D) 950 000 cells/mL	(2D) 26 300 cells/cm^2 (3D) 500 000 cells /mL	—
hBMSC	(3D) 1 000 000 cells/mL	—	—
HUVEC	—	—	(3D) 5 000 000 cells/mL
hASC	—	—	(3D) 1 000 000 cells/mL

4.4.6 Staining methods

4.4.6.1 Viability staining and calculation

The viability of seeded and encapsulated was assessed using the Live/Dead™ viability/cytotoxicity assay (Molecular probes, Thermo Fisher Scientific) containing calcein acetoxymethyl ester (Ca-AM) and ethidium homodimer-1 (EthD1). Briefly, cell culture samples were washed with DPBS to remove cell culture media. The dyes were diluted in DPBS (1X, Lonza) to a final solution concentration of Ca-AM 0.8 μM and EthD1 1.0 μM, and immediately added to the appropriate wells. The stain was incubated at room temperature for 30 min and replaced with fresh DPBS. The samples were immediately imaged using Olympus IX51 inverted microscope, equipped with an Olympus DP30BW digital camera (Olympus, Tokyo, Japan). From each chosen position, a live (488 nm emission filter) and dead (700 nm emission filter) image was recorded at the identical plane of focus. The images were then evaluated with ImageJ software (U.S. National Institutes of Health, Bethesda, MD) (Doube *et al.*, 2010) through the particle counting algorithm. Cell viability was determined from the area according to formula (**F1**), while cell spreading was determined from the same data using formula (**F2**):

$$Viability = \frac{area\ of\ live\ cells}{area\ of\ live\ cells + area\ of\ dead\ cells} \quad \text{(F 1)}$$

$$Spreading = \frac{area\ of\ live\ cells}{image\ area} \quad \text{(F 2)}$$

4.4.6.2 Morphology staining

To visualize the morphology of the cytoskeleton and cell nuclei, samples were stained using TRITC-phalloidin (0.17 μg/mL in 1% bovine serum albumin BSA) and 4',6-diamidino-2-phenylindole (DAPI; dilution 1:2000 in PBS; Sigma-Aldrich). Beforehand, the samples were fixed using paraformaldehyde (PFA) and Triton X-100 (0.1% in DPBS) and blocked using BSA (1%) before staining.

4.4.6.3 Immunofluorescent staining

To label a specific functionality of the cell culture samples, immunohistochemical staining was used in Publication III, staining for fibronectin using rabbit polyclonal anti-fibronectin antibody (dilution 1:250, Abcam plc, UK) and consequently Alexa Fluor 488 conjugated to donkey anti-rabbit antibody (dilution 1:88, Abcam plc, UK). The general protocol was performed so that all samples were fixed using 4% paraformaldehyde (PFA) and unspecific binding was blocked with 10% normal donkey serum (NDS) in 1% bovine serum albumin (BSA) solution containing 0.1% Triton X-100. Intermittent washing steps were performed using DPBS.

4.5 Animal studies

4.5.1 Ethics statement

To study the materials investigated in **Publication V** *in vivo*, cell-free preformed samples were subcutaneously implanted rats from the Wistar stock (male, 60 - 90 days old, weight 250 - 350 g). The species was selected in accordance with the provisions of ISO10993-2. Experiments were carried out at the Unit of Comparative Biology at the Pontificia Universidad Javeriana (Bogota, Colombia), with the approval from the Institutional Committee for the Care and Use of Laboratory Animals (CICUAL-PUJ). The animals came from the internal colony of production which was initiated with a founding stock originating from Charles River, USA. There were 10 animals per time point (40 animals), and each animal had 1 implant of each type (4 in total, n = 10).

4.5.2 Subcutaneous implantation

Before surgery, the animals were anesthetized using inhalation of 3% isoflurane in oxygen flow set of 0.5 L/min. Rats under anesthesia were treated subcutaneously with meloxicam (1 mg/kg) and enrofloxacin (5 mg/kg) 30 min before the surgical incision. Hair was removed from the implant area and incisions were performed to create 4 pockets into the dorsal subcutaneous tissue by blunt dissection, so that the base of the pocket is at least 2 mm from the line of incision. Then, hydrogel implants (ø 10 mm and 1 mm in thickness) were inserted to the pocket. During the procedure, vital signs were monitored, and temperature support was placed. At the end of the procedure, the animals were moved to an oxygenation chamber to recover from the anesthesia. When the animals woke up showing good recovery, they were taken back to their cages. During the first three days after the procedure, the animals were medicated with meloxicam and enrifloxacin and the appearance of the incisions, signs of inflammation, infection or other events were evaluated. The animals were fed a standard diet and kept in groups of two in ventilated cages for the duration of the study. After 7, 14, 21 and 28 days of implantation, the animals were sacrificed using intraperitoneal sodium pentobarbital (50 mg/kg dose) and CO_2 inhalation. Each implant was collected separately, taking skin and subcutaneous tissues until reaching the fascia of the panniculus carnosa muscle and fixed in 10% buffered formalin. The hydrogel degradation profile was followed during the retrieval.

4.5.3 Macroscopical and histological evaluation.

Retrieved tissue samples were fixed with 10% formalin, dehydrated in a series of alcohols, and embedded in paraffin. The paraffin-embedded specimens were sectioned to a thickness of 5 μm and stained with hematoxylin and eosin (H&E). Stained sections were imaged with a Nikon Eclipse E 600 microscope and Toup Cam digital camera. Tissue lesions such as neutrophils, eosinophils, granulomatous reaction, giant cells, and neovascularization were analyzed and semi-quantitatively scored on a scale from 0 – 3.

5 RESULTS

The model polysaccharide gellan gum (GG) was modified with different approaches towards improving the hydrogel for 3D cell culture and tissue engineering purposes. Data supporting the modification success and biological effects will be presented in this chapter along the defined aims of the research.

The included publications are organized by their hierarchy of modification and application assessment. Publication I explores the basic, chemical modification strategies used herein for GG, including purification, oxidation, scissoring, and blending with chitosan. Exclusively physical hydrogels are formed by use of cationic substances, and the formulations are characterized and compared. Publication II goes into detail on how to achieve uniform samples of cation-crosslinked GG hydrogels, which results in increased compression strength based on the mixing technique alone, without the need of modification. Publication III uses purified GG for chemical functionalization to introduce the avidin-biotin strategy for a modular approach. Mechanical properties and cell response are investigated to compare the modification. Oxidized GG is used in Publication IV in combination with hydrazide-modified gelatin to achieve chemical crosslinking and enhanced bioactivation. Different formulations are characterized, tested for cytocompatibility with fibroblasts, and applied for cardiomyocyte culture. Publication V then summarizes several modifications from the previous publications I, III and IV, and compares their biological effect *in vitro* and *in vivo*.

While the hydrogels presented herein were not designed for one specific purpose, their application and applicability were investigated in several directions. For instance, Publication I demonstrates the extrusion-based 3D printing of a single layer print by using a printing bath. Publication II scrutinizes the mold casting of physical hydrogels and how to achieve consistent samples, which is relevant for various cell culture and microfluidic chip applications. More advanced *in vitro* tissue models are established with the cardiomyocyte culture in Publication IV and the vascular co-culture between HUVEC and hASC in Publication V. To build reliable tissue models for disease modeling and body-on-chip applications, the artificial matrix material must be well understood, reproducible, and provide adequate cell recognition sites and mechanical compliance. Publication V also demonstrates the subcutaneous

implantation of the four selected hydrogel materials, which has high relevance for applications such as drug and cell delivery.

5.1 Modification strategies and structural analysis

Here, a brief overview of the modification strategies will be given that have been applied to the polysaccharide GG throughout this thesis. These strategies can be distinguished by their aim encompassing to modify either the bioactivity or the mechanical behavior. A summary of the primary reactants and their applied amounts used in the synthesis is presented in **Appendix A2**, showing the nomenclature and comparison between publications. To confirm the success of functionalization, various structural analysis methods are employed, depending on the type of functionalization, including spectroscopy, titration, and chromatography.

5.1.1 Purification

GG was modified from the as-received version for Publications I, II, and IV. This method yields a large enough batch to be used throughout one or more projects. The remaining counterion concentrations were assessed using ICP-OES after digesting the sample in sulfuric acid and hydrogen peroxide. **Table 2** shows the calculated weight percentages (w/w%) of unpurified GG, two purified batches that were adjusted to pH 7.5 and 10 at the final step respectively, as well as comparison to literature values from publications of Kirchmajer and Ferris (Ferris *et al.*, 2015; Kirchmajer *et al.*, 2014).

Table 2. Counterion concentrations (Ca, K, Mg and Na)

	GG	**NaGG**			
	native	(pH 7.5)	(pH10)	*Kirchmajer et al. (2014)*	*Ferris et al. (2015)*
Ca [w/w%]	0.287	0.083	0.087	0.04	0.06
K [w/w%]	4.857	0.245	0.204	1.02	1.00
Mg [w/w%]	0.103	0.022	0.024	0.03	0.03
Na [w/w%]	0.485	2.733	2.814	2.51	2.50

Our analysis arrives at slightly different values compared to the literature, with for example the Ca content showing two-fold concentration (0.08% w/w) compared to the literature value (0.04% w/w). However, a significant reduction compared to

native GG (0.29% w/w) is observed, and thus a sufficient removal to satisfy the requirement of reducing viscosity and gelation-capacity upon cooldown. On the other hand, for example K is reduced to much lower levels compared to the literature values. This may be due to batch and origin variations of the native GG, or differences in the pre-treatment of the exchange resin. The Na content of the pH-adjusted final product is slightly higher, due to over-adjustment with NaOH, even though pH was at the appropriate value. The concentration levels of K and Na are not considered as an issue, however, because crosslinking with monovalent ions is weak (Morris *et al.*, 2012).

5.1.2 Oxidation and scissoring

Oxidized and scissored GG were investigated as stand-alone materials by ionic crosslinking with SPD or $CaCl_2$ in Publication I, and later used in combination with hydrazide-modified gelatin in Publication IV and V. The chemical crosslinking of the latter is discussed in more detail in chapter 5.1.4. Unpurified GG was oxidized *via* Malaprade reaction using sodium periodate $NaIO_4$, which oxidizes the vicinal hydroxyl groups at the rhamnose sugar and creates two aldehyde groups per repeat unit (Kristiansen *et al.*, 2010; Malaprade, 1928). Consequently, the oxidized product was used for reductive cleavage at the ring-opening site using borohydride ($NaBH_4$) reducing agent, thus achieving scissored GG, named after the scission of the polymer chain. In Publication I, different degrees of oxidation were analyzed (see **Appendix A2**) and hydrogels were formed with cations ($CaCl_2$ or SPD) or blended with chitosan, forming Schiff-base linkages for crosslinking.

To verify the success of the oxidation and the presence of aldehyde groups, several techniques were employed. In Publication IV, the infrared spectrums (FT-IR) of dried GG and GGox(3) were compared, as shown in **Figure 4A**. Due to the strong dissimilarities in water content and transmission values, as visible from the H_2O band at 3200 cm^{-1}, the two spectra were not corrected for each other. However, the shoulder on peak at 1500 cm^{-1} qualitatively proves the presence of aldehydes. On the other hand, the TNBS titration assay performed in Publication I, provides a quantitative determination of aldehyde group concentration. The assay is based on the reaction between *tert*-butyl carbazate (TBC) with aldehydes and picryl sulfonic acid (TNBS), respectively. A known amount of TBC added to oxidized sample, which forms strongly bound conjugates. Excess TBC in the solution then reacts with TNBS to form a UV-active compound (Bouhadir *et al.*, 1999). **Figure 4B** shows the

results as adjusted from TBC standard curve, with inverse relationship between GGox aldehyde concentration and UV intensity of TNBS dye. The assay shows a nearly linear relationship between $NaIO_4$ added and resulting degree of oxidation, confirming not only the presence of aldehydes, but control during the oxidation process. As control samples, both pure water and native GG show a value below zero for calculated aldehyde concentration, indicating a small error in the titration or in the standard curve.

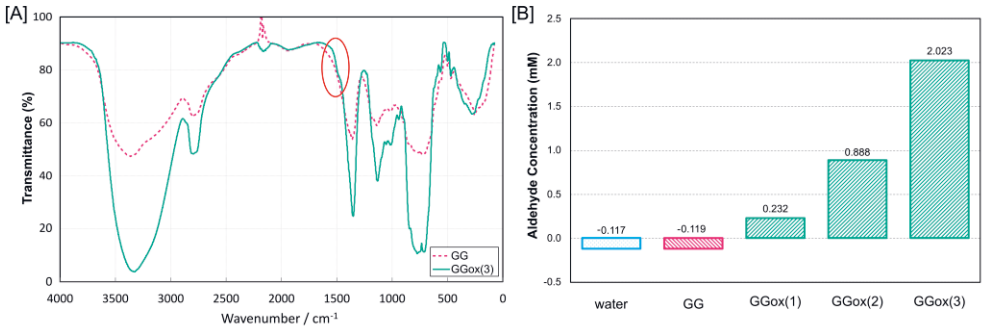

Figure 4. Determination of oxidation degree in GG. [A] IR spectrum of GG and oxidized GGox(3) [B] UV Analysis (TNBS assay).

Some of the oxidized GG batches were then scissored in a reduction reaction and referred to as GGsciss. The primary effect is the reduction in molecular weight but GGsciss retains all other structural properties of native GG. GGox is expected to have a skewed backbone because the helix is interrupted at the ring-opening. As the cleavage happens at the site of the helix fault, GG chains should recover their helical formation. Due to the reduction in molecular weight, the most notable effect is reduction of viscosity, which is discussed in more detail in chapter 5.2.1. Size exclusion chromatography (SEC) was kindly performed by Wyatt Technology and reveals the molecular weight of 326 ±5 kDa for GG, 53 ±1 kDa for GGsciss(1), 48 ±1 kDa for GGsciss(2), and polydispersity indices (PDI) of 1.7, 2.0 and 2.7, respectively. The scissored product thus indeed has a lower M_w, which is in line with the observed lower viscosity profile, but a somewhat broadening PDI. The cumulative weight fraction of the SEC results is shown in **Figure 5**. Both GGsciss(1) and (2), retain a small portion of the weight fraction with 1000 kDa or larger, which could indicate residual oxidized fragments that were not reduced and scissored. Unfortunately, it appears that aldehydes in GGox are interacting with another, leading to the aggregation of polymer chains in the used solvent. Hence, the graphs show an apparent higher molecular weight of GGox(1) than native GG, which are

agglomerated in high density. It was determined that oxidized GG would require a different protocol, solvent, and column material to be analyzed using SEC, thus the molecular weight results could not be directly compared to native and scissored GG.

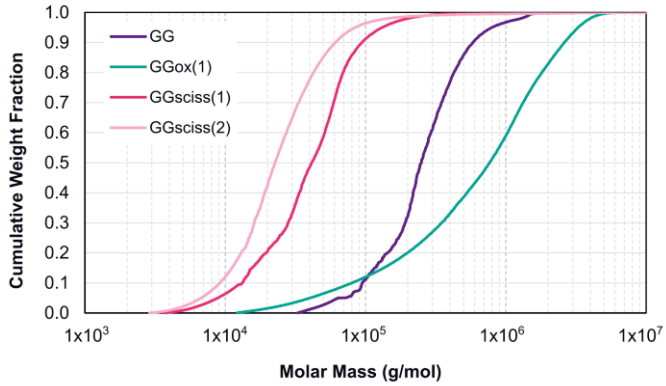

Figure 5. Cumulative weight fractions of SEC-MALS results.

5.1.3 Avidin-modification

Publication III demonstrates the coupling of avidin to GG *via* carbodiimide reaction. The final product and schematic avidin-biotin binding are shown in **Figure 6A**. To determine the final coupling yield, a fluorescence titration was employed with the specialized biotinylated fluorescence marker biotin-5-fluorescein (b5F) that is quenched when bound to avidin. From the highly distinct dip in the titration curve, the concentration of available avidin bindings sites can be deduced. Without the presence of available avidin binding sites, the titration curve is linear, as seen in **Figure 6B** NaGG and NaGG-avd blocked with biotin. As a result, the avidin concentration can be approximated to 0.075 - 0.375 µmol per 1g NaGG (0.005 mol% - 0.027 mol%) between low (L) and high (H) modification degrees. To further validate the covalent nature of the coupling between GG and avidin, the samples were subject to electrophoresis (SDS-PAGE) and an elution analysis with fluorescence detection, as shown in figure 3 within Publication III. Both electrophoresis and elution analysis validated the covalent and stable binding between NaGG and avidin.

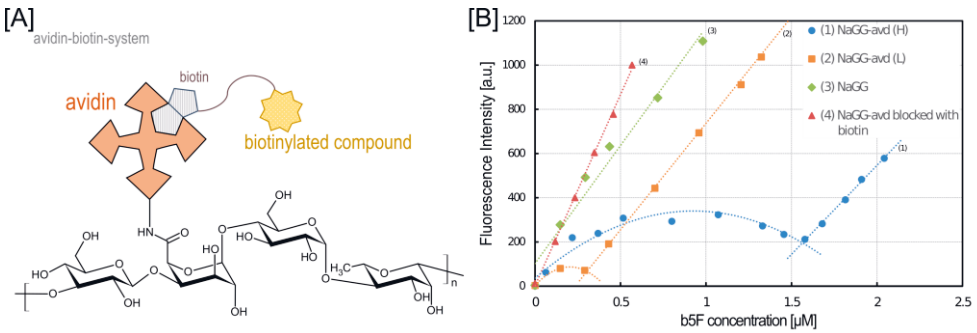

Figure 6. Avidin fluorescence titration. [A] Molecular structure of avidin-modified GG and schematic presentation of avidin-biotin binding event. [B] Fluorescence titration curve of different modified, unmodified, and blocked compounds. Biotin-5-fluorescein was used to determine the avidin concentration in NaGG-avd.

5.1.4 Chemical crosslinking of oxidized gellan gum

Oxidized GG was dissolved at high concentration and demonstrated to form self-supporting hydrogels with hydrazide-modified gelatin. These hydrogels were explored in Publication IV and V. This approach aims to achieve two goals, namely bioactivation of GG, and creation of a two-component with novel mechanical properties and increased elasticity compared to native GG. Gelatin is a hydrolysis product of collagen and known to be innately bioactive due to the presence of cell-recognizable peptide sequences, such as RGD, and is known to be bioactive and suitable for mammalian cell culture (Bello *et al.*, 2020). However, pure gelatin hydrogels typically have low stability and high degradation rates.

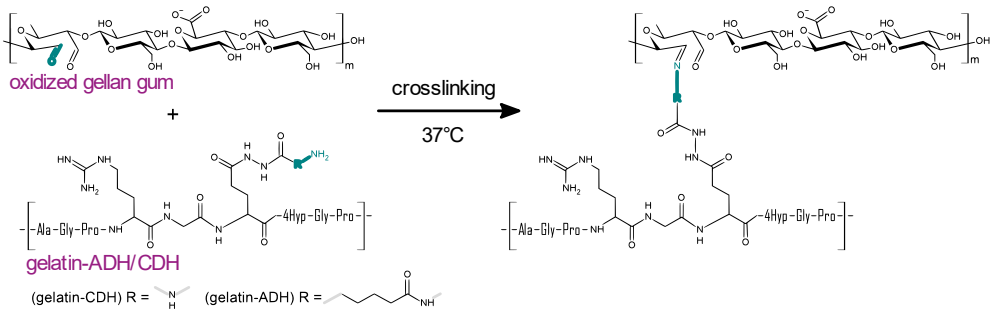

Figure 7. Crosslinking mechanism between oxidized GG and hydrazide modified gelatins.

To enable chemical crosslinking, we modified gelatin by coupling either carbohydrazide (CDH) or adipic acid hydrazide (ADH) to the glutamic acid rest *via* carbodiimide coupling using EDC and HOBt. The resulting hydrazine rest (-N-NH_2) readily reacts with aldehydes, thus forming a chemical network between the two polymers, as shown in **Figure 7**. While the reaction mechanism and preparation are identical between gelaCDH and gelaADH, the molecular spacer of ADH is considerably longer and additionally carries a carbonyl group. The chemical structure of modified gelatin was verified in publication IV using ^{1}H-NMR (figure 2 in Publication IV). No direct structural analysis was carried out for the crosslinked hydrogel, but chemical hydrogel formation was shown through gelation and recording of time sweep (chapter 5.2.2).

5.2 Mechanical and biological properties

Hydrogels are modified to alter their mechanical and bioactive properties from the original polymer, rendering the testing of these properties essential. Thus, they are a verification of the modification, as much as an initial testing for application suitability. This chapter summarizes mechanical testing results, as well as elementary cytocompatibility results from material contact with human fibroblasts. Wherever appropriate and possible, samples were prepared as described in Publication II, to assure a homogeneous distribution of crosslinker and thus a uniform specimen.

5.2.1 Compression

Pre-formed hydrogel samples were subjected to compression testing in Publication I (GG, GGox), Publication III (NaGG-avd), and Publication IV (GGox-gelatin). The samples were prepared using the mold casting technique, which produces cylindrical specimen of approximately 12 mm diameter and 0.5 mm height. Rarely, smaller molds were used, however the aspect ratio of the cylinders was respected to avoid buckling effects. All samples were incubated overnight to assure thorough network formation and covered to prevent drying. As opposed to the pure GG samples, the demolding was rather challenging for gelatin-containing formulations, as these were sticky and adhered readily to the polystyrene of the molds (refer to Figure 9C). To alleviate this issue, it was necessary to chill these samples at +4°C overnight or for several hours to facilitate demolding. If possible, all samples were

then treated in a similar manner, however an effect to the measured stiffness must be considered. A crucial aspect for compression testing is the shape fidelity of a specimen. While it is possible to load nearly any shape of sample onto the piston, the calculation for the stress-strain curve is closely dependent on the exact height and diameter. As discussed in Publication II, specimen symmetry is needed to achieve reliable result.

Besides a graphical presentation of the compression curves, some specific data points can be extracted to compare the results. These typically include the "modulus 1", also termed elastic modulus, "modulus 2", also termed fracture modulus, as well as the fracture point if one is discernible. The initial phase of hydrogel compression is the elastic region, in which it is presumed that the hydrogel will fully recover from the deformation. Evidently, this region is short for brittle material, and more extensive for elastic materials. For our physically crosslinked GG hydrogels, typically a range from 0.1 – 10% compressive strain is used to calculate the modulus from the slope of the curve. However, for the gelatin-GG hydrogels investigated in Publication IV, modulus 1 was calculated between 20-40% compressive strain and reported as compressive modulus. On the other hand, modulus 2 was reported in Publication II and III which represents the steep ramp up before the fracture point, at which the material has irreversibly deformed already. Publication I reports both moduli separately. Because the features of viscoelastic deformation and brittle fracture cannot easily be separated, compression testing does not yield information on viscoelastic properties of the hydrogels (Kocen *et al.*, 2017). Nevertheless, fracture behavior and fracture point can be compared between different hydrogel compositions and data sets. Compression testing is a convenient method to compare samples that have been subjected to different treatments or environments, because static mechanical properties of the final hydrogel are assessed, rather than hydrogel processing kinetics.

Figure 8 shows a compilation of compression graphs from different publications. In Publication IV representative curves were used to graphically represent the data, while in Publications I – III data points were averaged curves with $n \geq 3$, providing standard deviation error bars and somewhat more smooth curves. Further differences include that in Publication I the compression testing was carried out using a 22 N load sensor, while Publications II-IV used a 225 N load sensor, which is noticeable from the noise in the curves. Tabulated compression data from Publications I-IV can be found in **Appendix A4**.

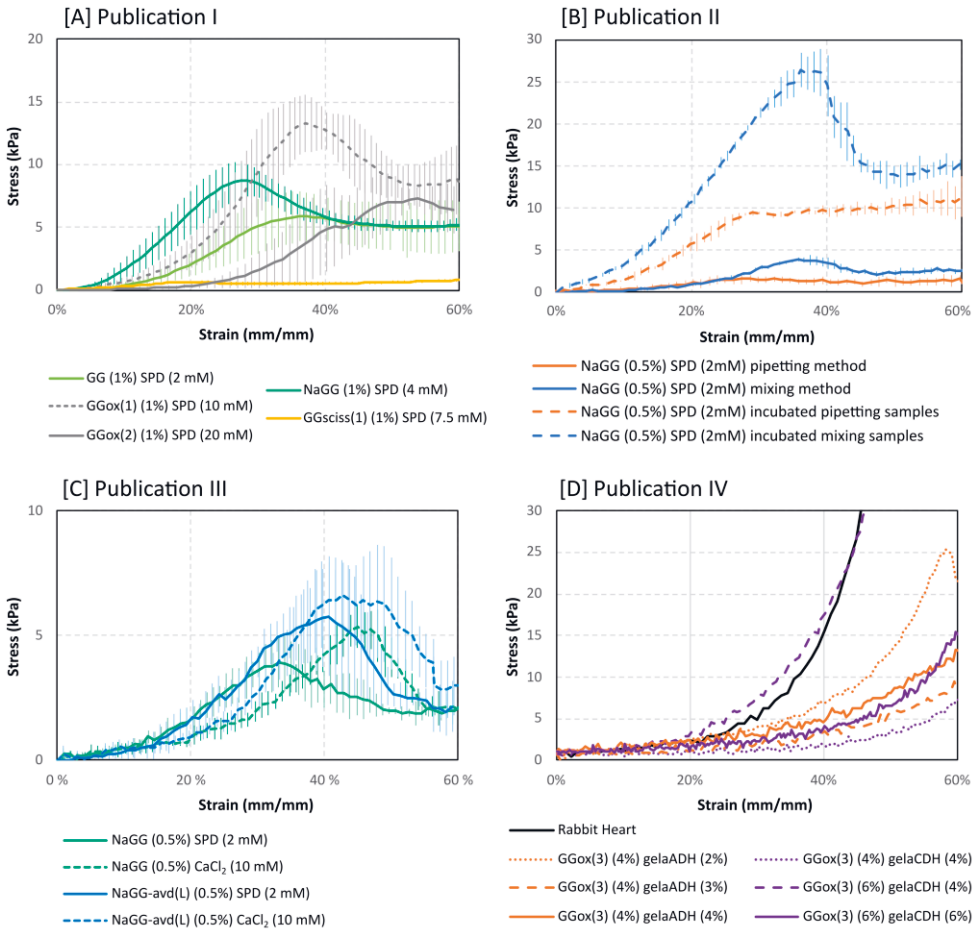

Figure 8. Compression curves of various GG-based hydrogels. Please note different scales on the stress curve.

Publication I compares different GG modifications and formulations, including native, purified, oxidized, and scissored GG, all of which were formed using either $CaCl_2$ or spermidine trihydrochloride (SPD) as cationic crosslinkers, albeit with adjusted concentrations. While it was possible to record compression curves of all modifications, GGsciss hydrogels were extremely soft and on the margin of self-supporting, as visible from the extremely shallow curve in Figure 8A. Similarly, a considerably higher crosslinker concentration was needed to gelate GGox.

Publication II explores the difference in sample preparation, with identical hydrogel composition used throughout. As is evident from the compression curves, the proposed mixing technique achieves more homogeneous samples (compare samples shown in Figure 9B), and consequently higher modulus (compare solid lines

Figure 8B). Within the same publication, the effect of basal cell culture medium (DMEM) added on top of the gelated samples was briefly investigated. This treatment aimed to mirror cell culture conditions, where culture medium is added for cell nutrition. The medium essentially provides extra crosslinking due to cationic species being present, which drastically increases the modulus and fracture point for both preparation types, but in relation to their original modulus.

The compression tests in Publication III provide evidence that the addition of avidin does not adversely affect the ability of the material to form hydrogels, as the compression curves are very similar in modulus and fracture point. A distinction is also visible for different crosslinkers, $CaCl_2$ and SPD (dashed *vs.* dotted lines in Figure 8C), used. Calcium appears to shift the fracture point towards higher compressive strains, indicating a more flexible network. The much more elastic hydrogel materials in Publication IV of GG and gelatin exhibit vastly different compression curves from the previous three publications. The curves show a fracture point at around 60% compressive strain or no fracture point at all. As mentioned above, the elastic modulus was determined between 20 - 40% compressive strain, and the fracture modulus was omitted. Crucially, the samples were compared to fresh tissue samples of rabbit heart (black line Figure 8D), which also did not exhibit a distinct fracture point, but a steep modulus exceeding 400 kPa at 65% compressive strain.

To summarize, all physically crosslinked GG hydrogels and derivates show a fracture point and steep modulus, indicating their relatively brittle nature. In contrast, the chemically crosslinked gelatin formulations, which tend to have much delayed onset of fracture and low modulus, owing to their much more elastic nature. This behavior resembles native tissues, which are known to not show a fracture point, dissipating the strain in an elastic manner, as seen with the rabbit brain tissue from Publication IV. **Figure 9** overlays compression curves of GG and NaGG hydrogels formed with 2 mM SPD from Publications I-IV, allowing the direct comparison of NaGG hydrogels between Publications II and III. The curves exhibit a high similarity in modulus and fracture stress (blue and green curve in Figure 9A), albeit with a small shift in fracture strain, which may be due to sample placement under the piston, caused by operator skill. Also depicted are native GG at 1% w/v (orange) and from Publication I and GG at 0.5% w/v (purple) from Publication IV. GG at 0.5% v/w compression is surprisingly similar to its NaGG counterpart, even though different sample preparation techniques were used. GG at 1.0% v/w has an increased fracture stress due to its higher polymer concentration, even though technically half of the crosslinking concentration in relation to GG concentration.

Overall, this comparison shows reasonably good comparison between separate studies and operators, but also highlights the limitation. Ideally, compression testing is used to compare specimen produced and tested by one operator, with standardized procedures and equipment wherever possible.

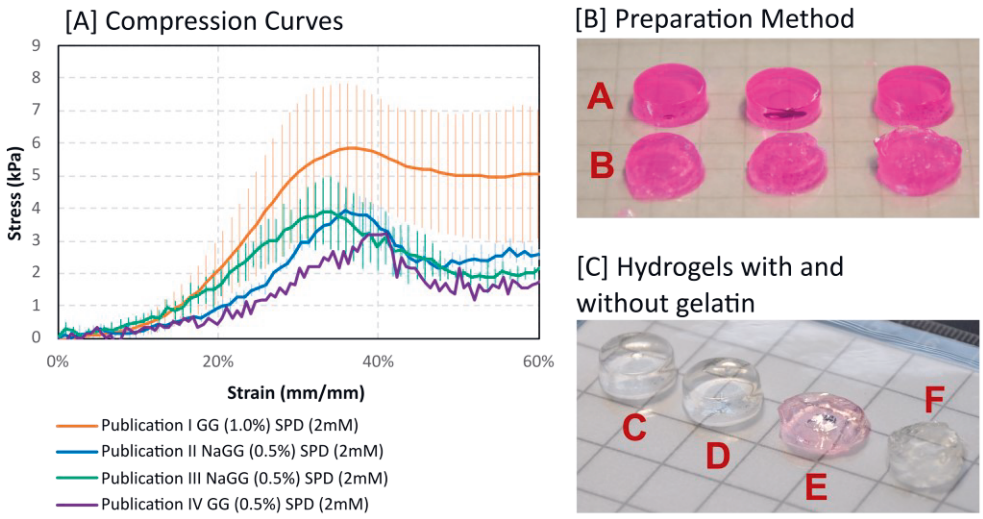

Figure 9. Comparison of compression curves and samples between publications. [A] GG and NaGG hydrogels formed with 2 mM SPD; [B] photograph of samples formed with the mixing technique (A) compared to pipetting technique (B) with 3 parallel samples each; [C] photograph of representative samples with NaGG (C), NaGG-avd (D), gelaCDH-GGox (E) and gelaADH-GGox (F) as prepared in Publication V.

Photographs in Figure 9B and C show the shape fidelity of some of the formulations. NaGG and NaGG-avd hydrogels prepared through ionotropic gelation by using the mixing technique (samples marked A, C, and D) have defined features, smooth surfaces and are straight forward to measure using calipers. NaGG samples prepared using the pipetting technique are heterogeneous and the crosslinker is not well distributed, resulting in poor shape (Figure 9B samples marked B). For GGox-gelatin samples (Figure 9C samples marked E and F), we assume the network is formed homogeneously, however the demolding process does not allow shape retention, and the sticky character of these hydrogels results in shapes as seen in the photograph.

5.2.2 Rheology

The rheology of hydrogel precursors and gelated samples was investigated minutely in Publications I and V. Publication I compares native GG, purified NaGG, oxidized GGox, scissored GGsciss, as well as some formulation with chitosan. To compare the vastly different materials in Publication V more simple time sweeps and amplitude sweeps are used. Here, the data will be presented in the order of flow sweeps characterizing the viscous precursors, time sweeps measuring the gelation procession, and finally amplitude and frequency sweeps characterizing the final, solidified hydrogels.

5.2.2.1 Flow sweeps

Flow sweeps allow for the mechanical assessment of the hydrogel precursor by continuous rotational shear, measuring the stress experienced by the substance between the plates. For example, the effect of solvent can be investigated conveniently, without the need to form self-supporting samples, and altering the system through crosslinking. Often, this type of sweep analysis is used to validate bioinks used for extrusion-based bioprinting, as their flow characteristics will determine their suitability for printing. Flow sweeps are shown in **Figure 10**, with both viscosity and shear stress as function of the applied shear rate, comparing the effect solvent (Fig. 10A) as well as comparing the effect of modification (Fig. 10B).

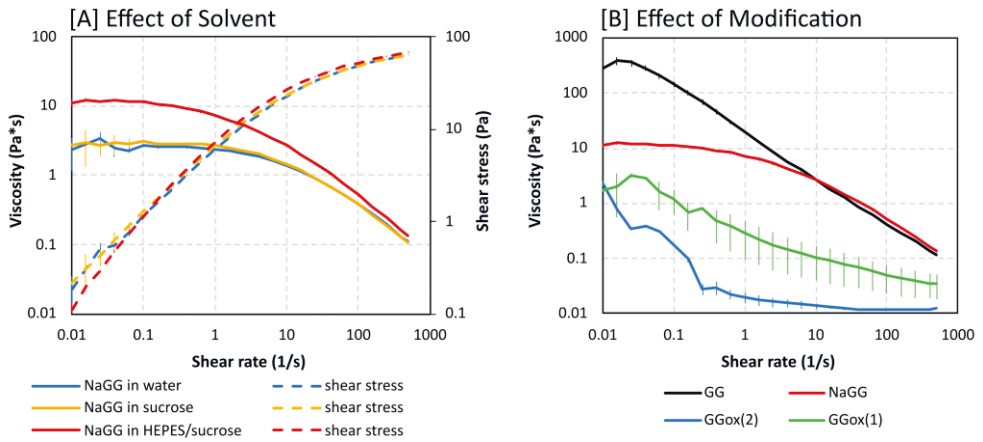

Figure 10. Flow sweeps. [A] Effect of solvent as shown for NaGG at 1% w/v (u.p. water, 10% sucrose, HEPES buffer and sucrose); [B] Effect of modification as shown for GG, NaGG, GGox(1) and GGox(2) at 1% w/v in HEPES/sucrose.

The solvent effect was investigated with the help of native and purified NaGG using flow sweeps in Publication I. The sweeps compared polymers dissolved in u.p. water, sucrose solution (10% w/v), and a combination of HEPES buffer (25 mM) and sucrose (10% w/v). The viscosity plots using water and sucrose are near identical, while the only difference is seen in the elevated viscosity profile of HEPES/sucrose solvent. This may be due to the effect of sugars and other components of the buffer, leading to molecular crowding and denser association of polymer, which has been investigated in detail (Evageliou *et al.*, 2010; Morris *et al.*, 2012). The effect of modification and degree is made clear with the viscosity profiles shown in Figure 10B. Native GG has a nearly linear profile and high viscosity, which is already clearly decreased at lower shear rates for the purified material. Oxidation further drastically reduces the viscosity in relation to the extent of oxidation, where GGox(2) was treated with 2-fold amount of iodate compared to GGox(1).

The shear behavior can be further analyzed using the shear stress *vs.* rate plot, as shown in Publication I Figure 3. There, native GG presents an initial phase of shear thinning and a yield stress range between 1.03 – 2.76 Pa, which is followed by more linear behavior above shear rates of 10 s^{-1}. This behavior can be explained using the Bingham model, which describes the flow behavior of viscoplastic material that have a yield point (Chhabra and Richardson, 2008). Similarly, the stress curves of purified NaGG exhibits shear thinning with a low yield stress between 0.02 – 0.11 Pa, as shown here in Figure 10A. In contrast, oxidized GGox and scissored GGsciss exhibit low yield stresses close to the measurement limits with values between 0.02 – 0.03 Pa and 0.01 – 0.04 Pa, respectively. Yield stress values are tabulated in **Appendix A3** from Publication I and V. Newtonian fluid behavior is exemplified by GGox above 1 s^{-1} shear rate, showing a linear trend, while a shear thickening tendency can be seen from the concave GGsciss curve. However, a steady stress sweep should be chosen for low viscosity solutions, to avoid unreliable measurements at these low stress values.

5.2.2.2 Time sweeps

The gelation of the two-component hydrogel, *i.e.*, the reaction between hydrogel precursor and crosslinker, could be observed using a time sweep in oscillation mode with low and constant amplitude and frequency. From the evolution of storage and loss modulus over time, the network formation and its kinetics can be derived (Zuidema *et al.*, 2014). The challenge is to combine these two components, generate a mixture of them, and initiate the measurement without immense delay. This was

achieved by mixing the components on the rheometer plate using the upper geometry as stirring tool as described in the Methods section. Time sweeps are useful tools for applications with time-sensitive handling, such as mold casting and cell encapsulation, and provide a more quantitative understanding of the time requirements for hydrogel setting than, for example, the tube-tilt test. **Figure 11** shows only the storage modulus over time and omits the loss modulus to avoid clutter, but they are shown in Publication I figure 4 and Publication V figure 2. **Appendix A5** lists tabulated rheology data from these publications. The plotted storage moduli all show an initial, rapid increase, but become more linear towards 30 min or 60 min mark. As quantitative data, the final modulus is reported.

All hydrogel examined herein are forming self-supporting hydrogels within their measurement period. However, typically a small slope value remains, which indicates that network development continues and ultimately justifies the longer incubation times of mechanical testing samples. The ratio between G' and G", so-called tan δ, can be used to indicate the completion of the hydrogel network formation (Chhabra and Richardson, 2008). Before the network reaches completion, during the transient phase, the viscous and elastic components (G' and G") are changing within magnitudes, but when completed tan δ reaches linearity (Zuidema *et al.*, 2014).

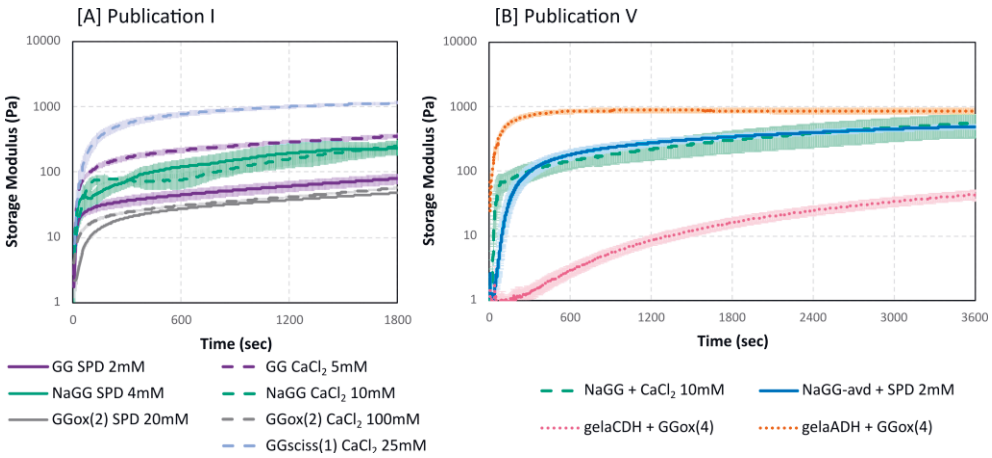

Figure 11. Time sweeps showing storage moduli. [A] Physical hydrogels from Publication I, with all GG precursors at 1.0% w/v; [B] Hydrogels from Publication V, NaGG and NaGG-avd at 0.5% w/v, gelaCDH/ADh at 4.0% w/v and GGox(4) at 4.0% v/w. Amplitude 0.75% oscillatory strain and frequency 0.75 Hz. Only storage modulus G' is shown.

Publication I compares the gelation of different GG modifications and two different ionic crosslinkers. As seen in Figure 11A, unmodified GG (purple) has a rapid

gelation and high final moduli of up to 340 Pa, but surprising differences between $CaCl_2$ and SPD in crosslinking. NaGG also shows rapid and precarious network formation but requires slightly longer time to form a stable gel. Due to the purification a larger number of crosslinking sites is available in the precursors, which could explain the shape of the curve. Oxidized GGox requires higher concentrations of crosslinker to form hydrogels and arrives at a lower final modulus, because oxidation skews the polymer backbone and impairs the ability of GG to easily form self-supporting hydrogels in the presence of ions. While scissored GGsciss(1) is able to form hydrogels with calcium and spermidine, the increased modification degree in GGsciss(2) is unable to do so (data shown in Publication I figure 4).

Publication V utilizes rheology and time sweeps to compare hydrogels of previous projects from Publication III and IV. As expected, all materials form self-supporting hydrogels within the observation time, seen in Figure 11B. NaGG and NaGG-avd exhibit similar gelation kinetics and have a final modulus of 552.8 ±219.0 Pa and 493.2 ±44.7 Pa, respectively. In contrast, the gelatin-containing formulations are dissimilar from the ionic formulations and each other, even though their chemical structure is very similar. GelaADH rapidly forms hydrogels with high final modulus of 860.9 ±6.6 Pa, while gelaCDH exhibits slower gelation kinetics and achieves a modulus of only 42.4 ±7.7 Pa after one hour.

5.2.2.3 Amplitude sweeps

Amplitude sweeps determine the material's modulus over a logarithmic increase of the oscillation amplitude with fixed frequency, observing the viscoelastic response of the fully gelated sample. Here, the presented amplitude sweeps were typically recorded from the samples prepared during the time sweep, without any further movement or adjustment, about 5 min after the time sweep had concluded. The wait period aims to assure that the network is at rest. As pointed out from the time sweeps, the hydrogel may not be fully formed within one hour and we expect it to be different to a sample that has set overnight.

The range of an amplitude sweep can be divided into a "small" and a "large" amplitude oscillatory sweep (SAOS and LAOS) regime, based on the extent of the linear region. Within the linear region (SAOS), in which the hydrogel deforms linearly, storage (G') and loss modulus (G") are reported. Although difficult to quantify, the crossover-region in LAOS can give interesting insight to how the hydrogel network distributes stress and may indicate crosslinking density. LAOS behavior is linked to the microstructure of the polymer, and can be categorized into

strain thinning, strain thickening, and strain overshoot phenomena (Hyun *et al.*, 2002). **Figure 12A** shows three examples of these different behavior types: NaGG is strain thinning, with no increase in either G' or G" before they drop; GG has a weak strain overshoot, where G' drops but G" briefly increases before dropping; and GGox exhibits a strong strain overshoot, where both G' and G" have a local maximum before dropping. Unfortunately, the GGox measurement is cut off before the crossover point is recorded. The weak strain overshoot of NaGG indicates a weakly structured material, which resists the strain and deforms before the critical strain value, after which the polymer chains disentangle, align, and start to flow. The overshoot phenomenon occurs when different components of the molecular structure within the polymer respond differently to the external strain, based on electrostatic repulsions and other intramolecular forces (Hyun *et al.*, 2002).

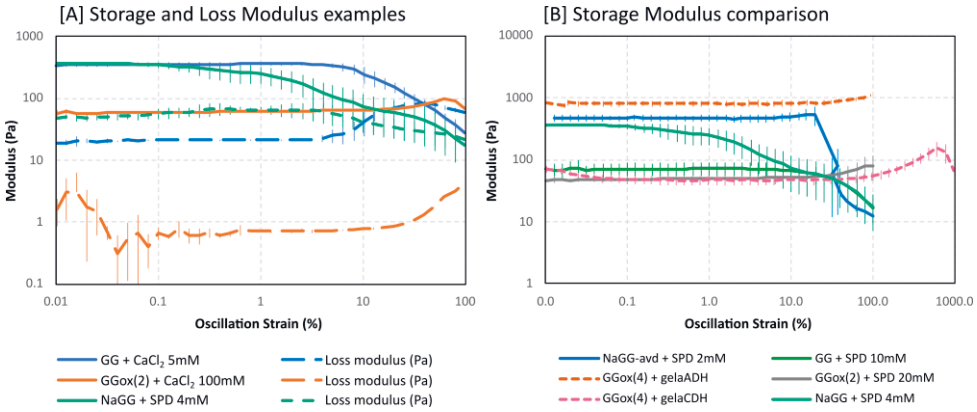

Figure 12. Amplitude sweeps. [A] Showing examples of different LAOS behavior between GG, GGox(2) and NaGG crosslinked with SPD or $CaCl_2$; [B] Storage moduli examples.

Figure 12B depicts several amplitude sweeps (G') from Publication I and V. Normally, the amplitude sweep is recorded until 100% oscillation strain. Only for GGox(4)-gelaCDH, the measurement was extended to 1000% in an attempt to observe the crossover point. A clear departure from the LVER is observed for NaGG, NaGG-avd, and GG hydrogels, and their crossover points are listed in **Appendix A5.** The observed range of oscillation strain is too short to reach the crossover-point for GGox-gelaADH, GGox-gelaCDH and GGox, indicating a higher elasticity for the hydrogels. The network density can be compared from tan δ at the LVER (see Appendix A5). For example, a tan δ of 0.07 and 0.06 for NaGG and NaGG-avd, respectively, confirms that these two hydrogels are very similar and relatively tough. In comparison, GGox-gelaCDH is extremely soft with a tan δ of

0.16, while GGox-gelaADH is even tougher at tan δ 0.04, further underlining the dissimilarity of the two gelatin-containing formulations.

5.2.2.4 Frequency sweeps

Frequency sweeps are carried out in the same manner as amplitude sweeps, except that the amplitude is constant (0.75% oscillation strain), and the frequency is ramped from 0.1 – 100 Hz. They serve to further establish the LVER of fully gelated hydrogel samples and are required to determine a suitable frequency to use in time sweeps. Frequency sweeps were recorded only in Publication I, as the LVER was found to be rather consistent and a value between 0.75 – 1.00 Hz suitable for all time and amplitude sweeps.

Figure 13 shows the storage moduli of hydrogels recorded in Publication I. Between samples formed with $CaCl_2$ and SPD, GG shows the biggest difference in modulus, while the NaGG and GGox are similar. Overall, the LVER is nearly identical between 0.1 – 1.5 Hz for all formulations.

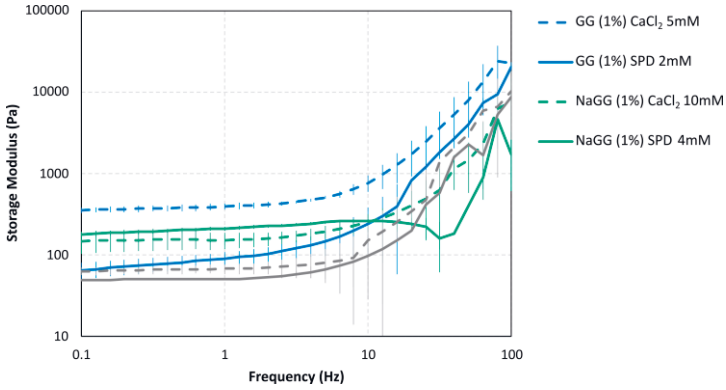

Figure 13. Frequency sweeps. Comparison of GG and NaGG crosslinked with SPD or $CaCl_2$.

5.2.3 Degradation

While not the primary focus of any of the presented studies, hydrogel degradation has been discussed in Publications IV and V as phenomenon and biomaterial design feature. There are noticeable differences between degradation profiles of cell-free degradation testing samples and cell culture experiment observations. The

degradation testing results and other observations of degradation of different GG-based hydrogels are summarized here.

Cell-free degradation of gelatin-containing formulations was demonstrated in Publication IV using collagenase to study their enzymatic degradation. To do so, hydrogels were cast to 1 mL centrifuge tubes and incubated at 37 °C in collagenase (10 U/mL) solution for up to 56 h. Aliquots were taken from the supernatant periodically and concentration was detected using fluorescamine. The fluorescence intensity is proportional to the amount of gelatin fragments in the supernatant and thus progression of degradation can be followed, as seen in Publication IV figure 3. Remarkably, the degradation rate between the different concentration formulations between one type of gelatin modification showed little difference, even though the gelatin concentration ranges from 40 – 60 mg/mL in gelaCDH hydrogels. Between gelaADH and gelaCDH formulations, however, a noticeable difference arises in the degradation rate: GGox-gelaCDH exhibits a rapid initial degradation, but plateaus after about 24 h incubation time, while GGox-gelaADH is slower to degrade initially, but reaches higher levels of fluorescence intensity. The muted degradation rate of gelaCDH was attributed to more extensive covalent and ionic crosslinking due to the use of cell culture medium as solvent as opposed to gelaADH using sucrose.

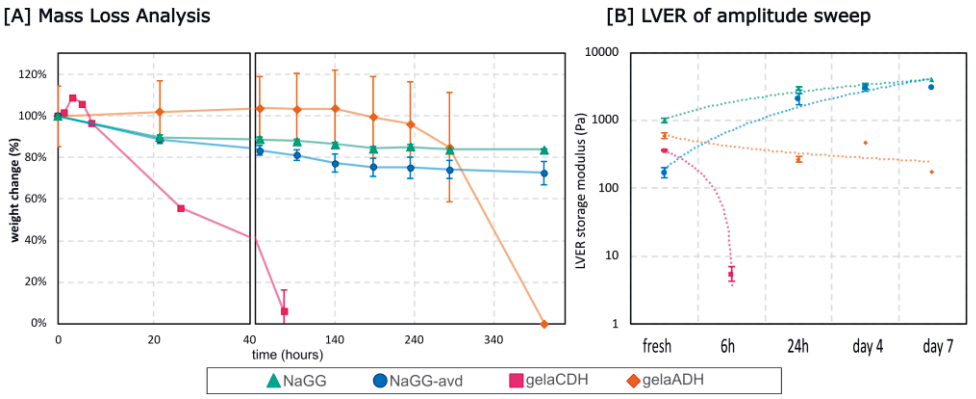

Figure 14. Cell free degradation studies. [A] Mass loss plot over 17 days; [B] Storage modulus value at LVER from amplitude sweep of pre-formed, incubated samples over 7 days.

A degradation study was carried out in Publication V to investigate the cell-free degradation in cell culture medium of the employed hydrogels. Therefore, mass loss and amplitude sweep were carried out in tandem, as shown in **Figure 14.** Of course, the sample shape and some other experimental parameters could not be reproduced exactly between the two methods. Due to the fragile nature of the degraded gelatin

samples (GGox-gelaCDH and gelaADH), the amplitude sweep could be performed only up to 7 days, while the mass loss was observed until day 17. The weight-loss graphs (Fig. 14A) exhibit both swelling and mass loss due to degradation. NaGG and NaGG-avd hydrogels lose about 20% of their mass within the first week but then remain rather stable with very small deviation between samples. This initial mass loss may be due to contraction of the network from additional crosslinking and expulsion of solvent, rather than degradation.

This is corroborated by the amplitude sweeps (Fig. 14B) in which the modulus of NaGG and NaGG-avd increases within the first week, indicating an increase in density or crosslinking. In contrast, gelatin-containing hydrogels show considerable degradation, and GGox-gelaCDH was unable to be measured using rheology after 24h of incubation already. Therefore, a separate time point at 6h was included to the graph. From the mass loss curves, however, a distinct swelling phase is visible before degradation and complete erosion of the gelatin samples. The trend of gelaCDH degradation within 10 h is replicated by gelaADH over 10 days. Hydrogels formed with gelaCDH are entirely eroded after 3 days, while gelaADH samples were weighable for 17 days, but the large difference between samples is seen from the error bars.

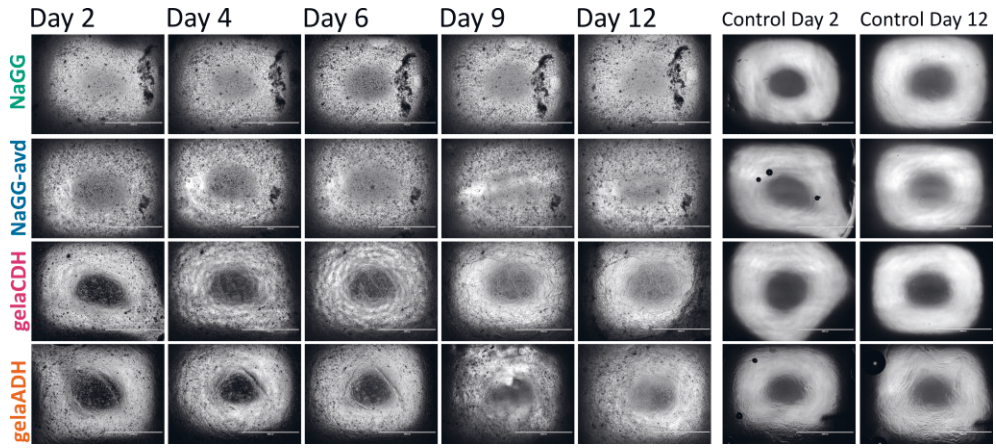

Figure 15. 2X magnification images of HUVEC-hASC encapsulated in the hydrogels over 12 days. Two right-most images are cell-free controls cultured during the same period. Scale bar 2 mm.

Indirectly, Publication V also makes use of the EVOS images used to visualize the auto-fluorescent GFP-HUVEC during the 12 days of culture period, as shown in **Figure 15**. The low magnification (2X) was used to capture an overview image of the entire well, revealing a qualitative impression of the hydrogel integrity. A similar

trend in degradation can be observed as from the cell-free study: NaGG and NaGG-avd are highly stable, but a hole quickly forms in the center of gelaCDH and gelaADH samples. Most intriguingly, however, it appears that the formation of the endothelial cell network appears to stabilize the gelatin-containing hydrogel against degradation. Already visible from these large magnification images is also that this cell network formation is much more pronounced in the gelatin formulations, while the cells remain rounded in NaGG and NaGG-avd. This increased cell activity also results in increased ECM deposition from the cells, further stabilizing the cast gels.

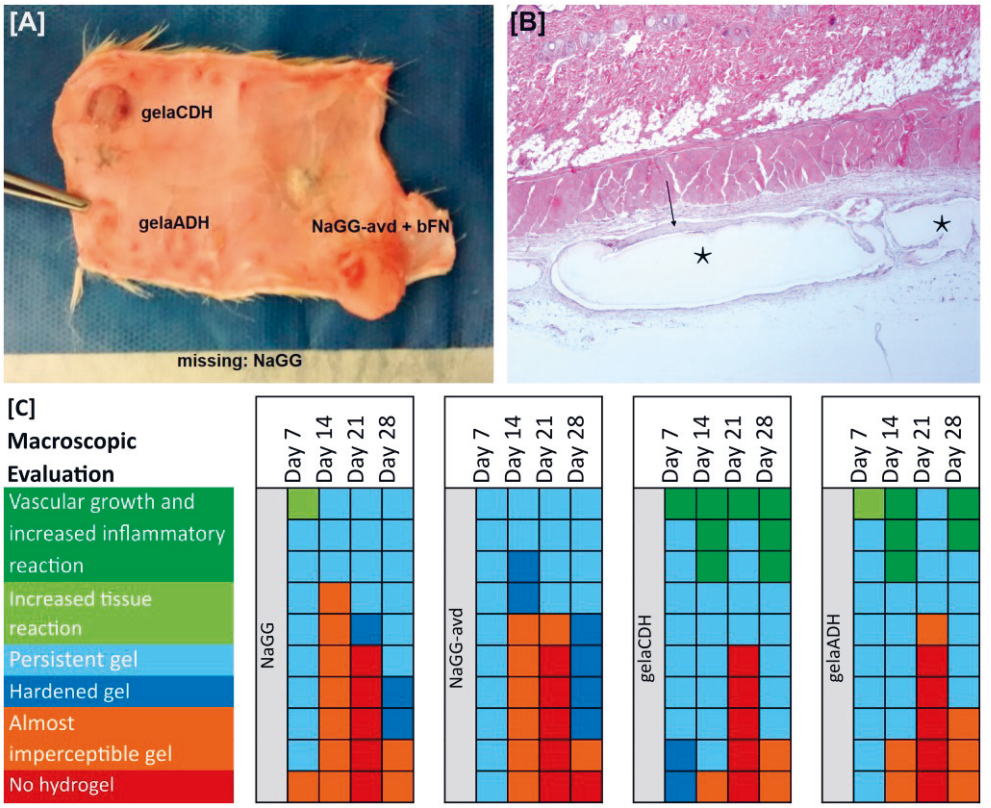

Figure 16. Degradation observations *in vivo*. [A] Photograph showing implant positioning [B] Histology slice of NaGG implant site at 2X magnification, day 28, asterisk indicates NaGG implant [C] Macroscopic evaluation of the subcutaneous implants

A qualitative observation of the subcutaneously implanted samples from Publication V is shown in **Figure 16**: Panel A shows a photograph of the entire tissue explant after its final time point, with the hydrogel implants clearly visible. Panel B shows an exemplary tissue slice with the hydrogel implant (NaGG) marked with an asterisk.

Monitoring the hydrogel degradation was not a goal of this study, and the more in-depth evaluation concerns the histology and tissue response, while hydrogel fragments were imaged rarely. However, the presence and general description of the implants was recorded by the veterinarian and a heat map of the evaluation categories is shown in Figure 16C. The heat map shows that NaGG and NaGG-avd implants were more prone to displacement and were marked as "imperceptible", however we do not attribute this to degradation. Implant movement through the subcutaneous tissue layer occurred in some of the animals and skews quantitative understanding of the data but cannot be avoided easily. Remarkably, all hydrogel types increase in this behavior towards the later time points. Noteworthy is also the description of hydrogel hardening mentioned for NaGG (day 21 and 28) and NaGG-avd (day 14 and 28), likely indicating a combination of fibrous capsule formation and hydrogel shrinkage as observed in mass-loss study. Most surprisingly is that the fast degradation rates for gelatin-GG from the cell free and cell encapsulation studies is not observed in this implantation study. Rather, it appears that the gelatin-containing hydrogels were perceived as more stable and less prone to movement.

Overall, these three approaches to study hydrogel degradation underline that neither is fully representative of *in vitro or in vivo* experimental setups. While gelatin-GGox hydrogels were persistent *in vivo* for up to four weeks, they are rarely stable enough to measure *in vitro*. While ionically crosslinked NaGG hydrogels are durable in most settings, it was challenging to assess in a biological setting. In summary, the preparation technique, components, and environment have to be carefully considered to assess hydrogel degradation.

5.2.4 Cytocompatibility

Here, the culture of human fibroblasts on or in our modified hydrogel serves to determine basic cytocompatibility and confidence to preclude cytotoxicity. The adjective "cytotoxic" is applied to any substance or process that infers detrimental changes in cell morphology, detachment, or loss of membrane integrity (ISO 10993-5, 2009). Materials are then deemed cytocompatible, if neither the material itself, nor the gelation process in the case of hydrogels, induces cytotoxicity. We use the fibroblast cell line WI-38 which was originally harvested from female embryonic lung and is best known from its use in virus vaccine production (Wadman, 2013). WI-38 were chosen for all basic cytocompatibility studies in our lab, due to their human origin, endurance of long-term cryo-storage, and reliable cell multiplication post

expansion (Hayflick and Moorhead, 1961). When viable and attached to their surrounding matrix, these cells exhibit an elongated and spindle-like shape. Fibroblast culture used to screen several hydrogel formulations and choose most promising results for other cell studies, to minimize amount of material and parallel studies needed. Hydrogels were evaluated using fibroblasts in Publication III and IV.

Plating cells in monolayer onto a relatively smooth surface is a historically relevant cell culture technique. Fibroblasts were cultured on top of hydrogel surfaces, which are macroscopically smooth but likely on the microscopic level the cells experience an undulating terrain. Regardless, this is referred to as "2D" culture because assume to be in a monolayer with only cell culture medium on top of them. Many staining assays and imaging techniques are designed and improved for this type of culturing approach, even though it disregards the biological relevance of a 3D hierarchical structuring. However, this allows for the removal of the crosslinking reaction or procedure from the equation, which may be relevant for example for photocrosslinking formulations, to avoid UV-light exposure to cells.

The left panel of **Figure 17** (A1-6) shows exemplary microscope images of fibroblasts cultured for 3 days and stained with calcein-AM (live) to EtHD-1 (dead). The qualitative microscope results highlight that attachment is crucial for fibroblasts and demonstrate best results on tissue culture plastic (TCP) without any hydrogel (Fig. 17 A1). These cells are elongated and show good cell coverage over the imaged area, indicating a natural and healthy phenotype. The 2D cultures from Publication III (Fig. 17 A2-4) compare native GG, purified NaGG and avidin-modified NaGG-avd with added biotinylated adhesive motifs, here fibronectin. All three microscope images show the aggregation of cells to large cell clusters, rather than elongation and separate cells. This indicates that the hydrogel surface is bioinert and cells cannot attach. Due to medium changes and washing steps during the staining procedure, the number of cells observed on the surface is lower than what has been plated originally. On the other hand, the gelatin-modified hydrogels investigated in Publication IV show remarkable cell elongation in 2D, as well as network formation between the cells (Fig. 17 A5-6).

The viability of the cells was quantified from Live/Dead™ stained microscope images, comparing the area covered by calcein-AM-stained cells (live) to EtHD-1-stained cells (dead). In practice, ImageJ was used to mask the areas from the separate filter images, and the calculated cell areas were compared to the sum of live and dead area covered by cells. Ideally, this assessment is carried out from microscope images of 2D plated samples. While technically 3D images can be evaluated with the same process, it is challenging to do so due to the image quality and focusing issues of 3D

images taken with a widefield microscope. Additionally, the choice of control material can skew the data interpretation.

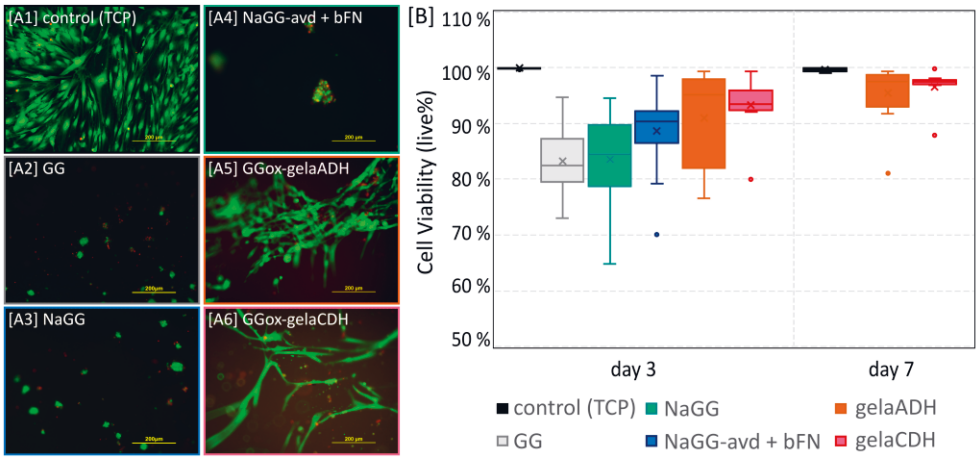

Figure 17. Fibroblasts cultured on top of hydrogel materials (2D) [A] Exemplary microscope images of Live/Dead™ stained fibroblast at 10X magnification(green Ca-AM, red EthD1); [B] Cell viability assay as counted from microscope images.

The results shown in Figure 17B demonstrate good cell viability for all materials, even native, non-bioactive GG and NaGG, with values above 80% at days 3 and 7. In Publication III, data was collected for day 3 exclusively. The lowest cell viability is observed by native GG (83.1%) and NaGG (83.5%). Even though not easily visible from the exemplary microscope image, functionalized NaGG-avd with fibronectin achieves improved viability at 88.6 % live cells. The large error values are caused by the cell aggregation and clustering of cells., which also cause noticeable difference of cell coverage between different microscope images recorded in the same well. Nonetheless, these data were determined to be significantly different through ANOVA ($p^* < 0.05$). The data for GGox-gelaCDH and ADH in Figure 17B is pooled data from the different formulations from Publication IV at day 3 and 7. On day 3, both perform better than the formulation without gelatin, at 90.8% and 93.2% live, respectively. They further exhibit an increase in cell viability at 7, likely due to increased cell proliferation. The TCP control remains stable from day 3 to day 7 with a cell viability of 99.9% to 99.6%.

The study also compared the addition of different biotinylated factors to the avidin-modified NaGG, including biotinylated RGD, biotinylated fibronectin, as well as only biotin to take up the avidin binding sites, as shown in figure 6A within Publication III. However, there was no statistical difference between these

biotinylated molecules, which was likely due to other medium and serum components taking up the functional sites before the cells are brought into contact with the material.

Encapsulating cells in a 3D matrix has increased relevance over 2D plating, as it resembles biological tissue more truthfully and provides an extended list of matrix features such as diffusion and mechanical compliance. On the other hand, the hydrogel preparation technique must be adapted for appropriate encapsulation result, achieving a homogeneous distribution with quick gelation, preventing the cells from accumulating at the bottom. These technical features can be refined using 3D fibroblast culture, as this cell type is relatively robust and abundant. While it is not trivial to adapt quantitative evaluation methods, 3D encapsulation of fibroblasts can give valuable, qualitative insight to hydrogel properties and performance for further, more complex tissue culture tasks.

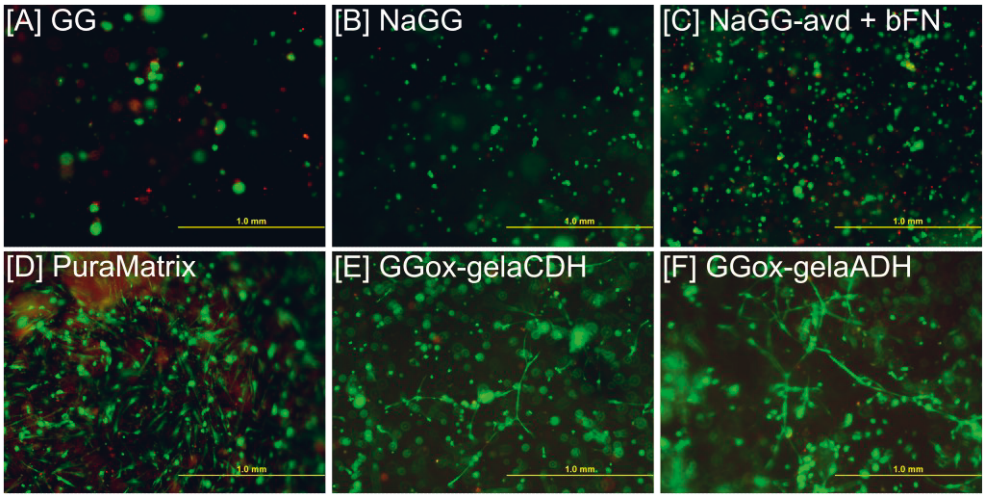

Figure 18. Fibroblasts encapsulated within 3D hydrogel materials. Cells are stained with Live/Dead™ stain (green Ca-AM, red EthD1) and images are taken at final time point of 3 or 7 days.

Exemplary microscope images in **Figure 18** show WI-38 encapsulated to different hydrogels used in Publication III and IV. Fibroblasts encapsulated in GG and NaGG remain spherical and do not elongate. Some cell aggregation can be seen in GG (Fig. 18A), indicating the possibility of cell migration. However, NaGG (Fig. 18B) appears to prevent cell migration and all cells remain separate and rounded. Regardless, the majority are stained with calcein-AM, indicating similarly good viability as in the 2D experiment. The avidin-fibronectin modified NaGG hydrogel (Fig. 18C) appears to exhibit a slightly higher cell number, with equally high live-cell ratio, however also

no significant elongation or attachment is visible. PuraMatrix™, a commercial hydrogel from decellularized basement membrane, was included as control material (Fig 18D), but unfortunately shows some issues with the EtHD-1 stain, visible from the red blurry area. Finally, considerable elongation is visible in the gelatin modified GGox hydrogels presented in Publication IV (Fig. 18E and F). While not as strong or dense as in the 2D experiments, the observed spindle-like cells were found to exceed elongation observed by other 3D studies previously reported. Additionally, almost no red-stained cells are visible in these images, confirming the viability results.

5.3 Application-based assessment

This chapter will provide a non-exhaustive list of application examples for the modified GG-based hydrogels. Rather than being fully functional tissue engineering applications, they illustrate a proof-of-concept and concise insight for further material development. However, the required properties and objectives will be highlighted with the help of these examples. Throughout the different publications herein, GG-based hydrogels were applied in extrusion printing, culture of human SC for specific tissue model, as well as implantation to an animal model.

5.3.1 Bioprinting

The additive deposition of cell-laden biomaterials, *i.e.*, the printing of bioinks, into defined volumetric shapes has been a topic of ever-increasing popularity within the field of tissue engineering (Ozbolat and Hospodiuk, 2016). Bioprinting exerts exact control over the specimen architecture by depositing the material in millimeter or better resolution and can achieve the formation of macropores, intricate shape of an implant, hierarchical material combination, or other macroscopic features. Indeed, GG-based hydrogels have been successfully used for extrusion-based bioprinting, enabling the application of GG in sophisticated tissue models (Akkineni *et al.*, 2022; Ferris *et al.*, 2015; Zhang *et al.*, 2021).

Publication I demonstrates the extrusion printing of various GG modifications as proof-of-concept. The combination of hydrogel precursor and crosslinker in the printer cartridge was not possible, because the gelation rate of the ionotropic formulation is too rapid, as established with the time sweeps shown in chapter 5.2.2.2. This gelation times does not allow for continuous extrusion but would block

the nozzle within few minutes. As an alternative approach, the precursor was extruded onto a thin layer of concentrated crosslinking solution, so that the hydrogel would be formed on the surface as deposited. The crosslinker was deposited onto a flat nylon mesh, to hold the solution in place and achieve even spreading. While this has been shown to yield good results for 2-dimensional layouts, it would be challenging to translate to volumetric printing. Nevertheless, layer printing is feasible for several application types, including skin models (Lee *et al.*, 2009). Furthermore, using this approach we were able to assess the basic requirements and feasibility for extrusion printing of our GG-based hydrogels. **Figure 19A** shows exemplary photographs of the printed structures, demonstrating the line width, accuracy, and ability to keep shape of rounded features. While both GG and NaGG present the printed image clearly, GGox formulations often depart from the instructed image and are deposited irregularly. These qualitative printing results confirm the findings from the flow sweeps shown in chapter 5.2.2.1.

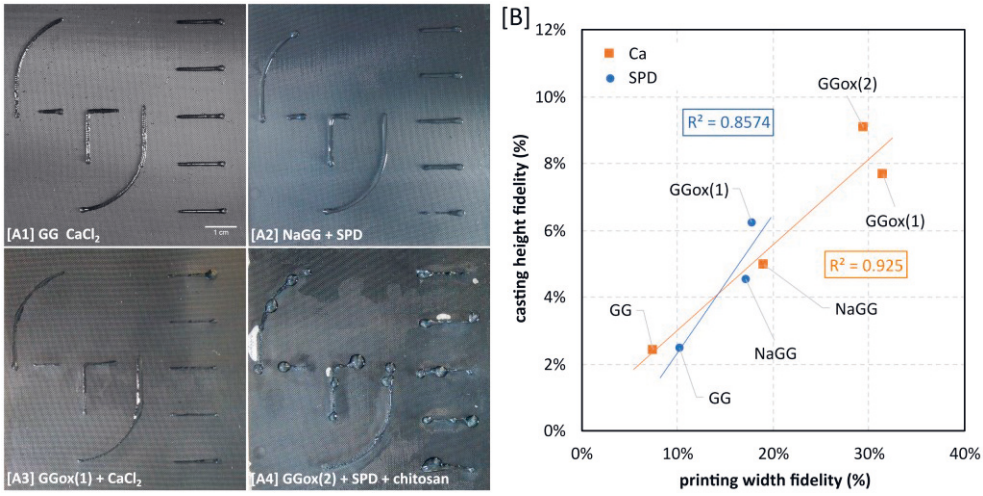

Figure 19. Results of extrusion printing. [A] Exemplary photographs of printed hydrogels on the nylon meshes wetted with crosslinker. [B] Plot of relative error from height measurement of compression samples vs. relative error of printing line width.

The printed lines were evaluated, and the printing fidelity was tabulated in table 2 of Publication I to quantify the results. This analysis indicated that hydrogel precursors with distinct shear thinning behavior, as evaluated from the flow sweeps, will yield good printing results. Further, the printing fidelity and the height measurements from the mold casting preparation could be compared. In Publication I the same formulation were mold-cast to prepare sample for compression testing, and their

height, width, and standard deviation thereof are listed in **Appendix A4**. The relative standard error of the height measurement is plotted against the printing fidelity in **Figure 19B**. Although only few data points are available, a linear relationship is apparent with a coefficient of determination (R^2) of 85.7% and 92.5 % for SPD and $CaCl_2$ crosslinked samples, respectively. This qualitatively indicates that hydrogels which are easily mold-casted and produce specimen with consistent shape, will also yield good extrusion printing results in terms of shape fidelity.

5.3.2 Bone tissue engineering

In the field of bone tissue engineering typically hard biomaterials are the focus of research to recapitulate the mechanical features of the tissue. However, even though hydrogels are mechanically resembling soft tissue specifically, they are applicable as suitable stem cell niches. Further, hydrogels can be injected easily to defects and other tissue sites, thus rendering them as excellent choice for regenerative applications and fracture repairs (Liu *et al.*, 2017). Here, human bone marrow-derived SC (hBMSC) were encapsulated in hydrogels. These hBMSC are multipotent and can differentiate to other cell types of the mesoderm, including osteoblasts, chondrocytes, and adipocytes. This differentiation towards a lineage can be induced either chemically, e.g., by adding the right growth factors, or by adjusting the stiffness of the matrix substrate. Due to this aspect of substrate control over stem cell differentiation, this cell type and system has been investigated closely by tissue engineers and biologists to reveal their molecular pathways (Discher *et al.*, 2005; Engler *et al.*, 2006).

In Publication III human bone marrow derived stromal cells (hBMSC) were encapsulated and cultured in NaGG-avd with added bRGD over 21 days. RGD (arginine-glycine-aspartate) is the peptide sequence that has been identified to be the universal amino acid motif recognized by integrin ligands of cells and responsible for anchorage between cells and their matrix. Purified NaGG served as control material, and both hydrogels were crosslinked using SPD at the same concentration. At time points of 7, 14 and 21 days the cultures were analyzed with Live/Dead™ stain to monitor their development. Additionally, at the final time point of 21 days, the cytoskeleton was stained using phalloidin, along with cell nuclei using DAPI. Exemplary images over the culture period are shown in **Figure 20**. Initially, the encapsulated cells appear viable with strong green dye and promising elongation. At 3 weeks, however, the culture appears deteriorated, and the images are poor. As seen

in the images on day 21 (third column from the left) the hydrogel material itself becomes opaque during the culture progress, hindering the image analysis. This obfuscation could be due to mineralization by the hBMSC, as was observed also in other studies (Anjum *et al.*, 2016), however we have performed no specific mineralization assay for confirmation. Cell-free hydrogels and fibroblasts at longer time points (see chapter 5.2.4) do not show this opacity, indicating it is indeed caused by the hBMSC specifically.

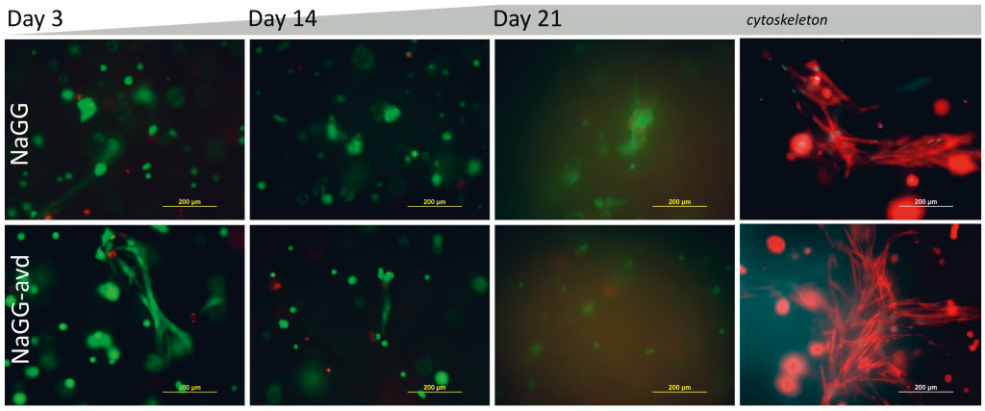

Figure 20. 3D culture of hMBSC. Images [1-3] show live/dead stain (green Ca-AM, red EthD1) on day 7, 14 and 21 respectively, while image [4] shows immunocytochemical stain (red phalloidin, blue DAPI). Top row unmodified NaGG, bottom row avidin-modified NaGG with biotinylated RGD.

Qualitatively, the bioactivated NaGG-avd-RGD hydrogel material only slightly improves the cell response and elongation. However, the visual results from the Live/Dead™ assessment are supported by the immunocytochemical stain (Figure 20, right-most panels). With a few exceptions showing elongation, the cells appear rounded in the hydrogels. Albeit not quantified, the choice of images presented in Publication III depicts visibly more elongated cells in avidin-modified NaGG than in the unmodified formulations.

5.3.3 Vascularization models

Vascularization and the presence of perfusable blood vessels is crucial for many, if not most, tissue types. Especially thick, artificial tissue constructs require higher degree of diffusion than what could be achieved through bulk hydrogel in order to guarantee a supply of oxygen and nutrients, as well as transport of waste products.

Vascularization can be achieved through the *co*-culture of endothelial cells, supported by human adipocyte SC (hASC) that express pericyte signals which facilitate the vessel formation (Sarkanen *et al.*, 2012). Formation of vascular network has been recognized to be crucial feature for both recapitulation of perfusion in *in vitro* models, as well as for the longevity and integration of regenerative medical devices (Santos *et al.*, 2019). Matrix stiffness and availability of cell attachment sites can critically steer the success of vessel formation, and thus both bioactivity and mechanical properties of the hydrogel have to be carefully designed.

Here, GFP-tagged human umbilical vein endothelial cells (HUVEC) were combined with hASC in a ratio on 5:1 and encapsulated in different hydrogels for up to 14 days. Endothelial growth factor medium was supplied in order to facilitate vessel formation of the HUVEC in static culture conditions. The cultures were observed frequently during the culture period by utilizing the autofluorescence of the GFP-tagged HUVEC and EVOS microscopy. After two weeks, the cytoskeleton was stained for α-smooth muscle actin positive (αSMA^+) cells, cell nuclei were stained using DAPI and imaged using confocal microscopy. The investigated materials from Publication V included NaGG crosslinked with calcium chloride, NaGG-avd crosslinked with spermidine and added biotinylated fibronectin, as well as oxidized GGox crosslinked with gelatin-hydrazide (gelaCDH) and gelatin-adipic acid hydrazide (gela-ADH).

The cell culture results presented in Publication V demonstrate large differences between all four materials. From the microscope images taken frequently throughout the culture period elongation of the endothelial cells is visible in the gelatin-containing formulations. The cell network at day 12 is much more pronounced as seen in **Figure 21** A3 and A4, but also occasionally in small areas in the NaGG and NaGG-avd hydrogels (Fig. 21 A1 and A2). The endothelial cells express the green-fluorescent dye, while the pericyte network is visible from the widefield image overlay. The endothelial cell coverage was quantified from EVOS images shows contrast between the material types, with gelaCDH clearly having the highest coverage. Rather than analyzing the extent and interconnectivity of vessels, the total coverage of endothelial cells in the image had to be counted, because a separately tubule network could not be distinguished. However, the endothelial cell coverage shown in Figure 21 B, demonstrates a clear difference between the materials. At day 12, GGox-gelaCDH exhibits the densest endothelial coverage with an average of 6.67 %, ahead of GGox-gelaADH with 3.34 % and far ahead of NaGG and NaGG-avd with 1.72 % and 2.52 % respectively. ANOVA test confirmed that all data are

statistically different ($p < 0.005$), but the coverage results between NaGG and NaGG-avd hydrogels are statistically the same ($p = 0.098$).

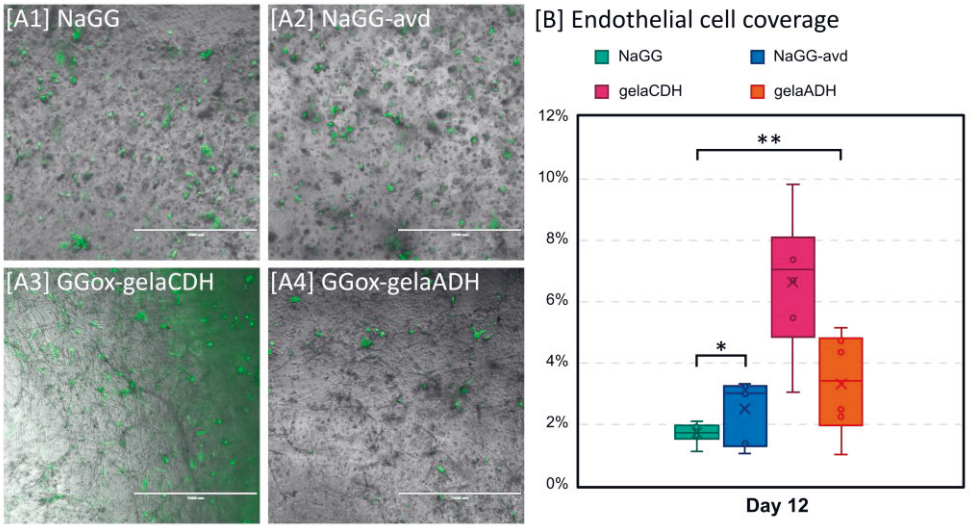

Figure 21. Endothelial cell images of the vascular co-culture. [A] EVOS images at day 12, scale bar 1 mm; [B] endothelial cell coverage from AngioTool analysis. Data marked with ** are statistically different ($p < 0.005$); and * marks data that are statistically the same ($p = 0.098$).

In Publication 5 the endothelial cell coverage was evaluated also on day 2, 4, 6, and 9 and plotted over time (data shown in figure 5 of Publication V). Carefully analyzed, the trend shows that the endothelial coverage decreases for all formulation over the two weeks, except for the GGox-gelaCDH, which shows a remarkable recovery in density after day 4. This further highlights GGox-gelaCDH to be the most suitable of the four investigated materials to support vascularization.

The confocal images of the cultures after 14 days are shown in **Figure 22**A. Encapsulated in NaGG and NaGG-avd (A1 and A2), the GFP-HUVEC as well as the αSMA$^+$ cells remain rounded. The elongated cells visible in NaGG-avd are likely cells that have migrated to the well plate bottom and adhered onto the glass surface. In contrast, the gelatin-formulations exhibit a pronounced αSMA$^+$ network formed by the hASC (Figure 22 A3 and A4). Visually, the co-location of HUVEC onto αSMA$^+$ network is noticeable, however HUVEC do not form tubular structures. Again, GGox-gelaCDH achieves the densest network, as was semi-quantitatively analyzed using the same cell counting software as for the endothelial cells (Fig. 22B). Plotting the αSMA$^+$ cell coverage follows the distribution as seen with the endothelial cell coverage: GGox-gelaCDH presents the densest coverage at 27.6%,

followed closely by GGox-gelaADG at 17.4% coverage. Again, the total coverage for NaGG and NaGG-avd hydrogels is significantly lower aa 12.0% and 5.4%, respectively. The values for NaGG-avd are unfortunately biased, due to casting issues with the hydrogel and strong degradation of the samples, leading to few confocal images taken.

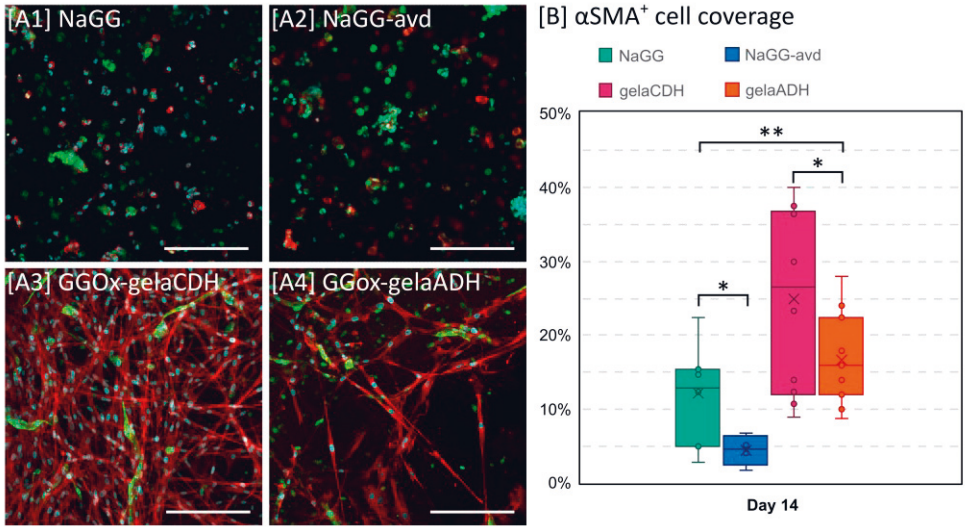

Figure 22. Confocal images of the vascular co-culture showing αSMA+ cell network. [A] EVOS images at day 12; [B] endothelial cell coverage from AngioTool analysis. Data marked with ** are statistically different ($p = 0.002$); and * marks data that are statistically the same ($p \leq 0.066$).

5.3.4 Subcutaneous implantation

The pinnacle of biomaterial assessment is to bring the material into contact with a living organism and study the tissue response. Certainly, the wholistic biological effect is more complex than any *in vitro* simulation can attempt to encompass. Nevertheless, we must appreciate the limitations within the scope of observation in regard to the biological relevance of the species, which results are monitored and external factors influencing the observations. The research question and investigated materials should be well defined before animal testing is carried out. Besides evaluating the biological response of the material, animal implantation testing also serves as a passage towards clinical testing and application of the material within a regenerative medical device.

The materials of Publication V (NaGG, NaGG-avd, GGox-gelaCDH, and GGox-gelaADH) were tested by subcutaneous implantation. Therefore, the preformed, cell-free samples were prepared in similar manner to the compression samples, except that here the samples were chilled overnight at +4°C to facilitate demolding. The rats were anaesthetized, and skin pockets were prepared in the dorsal region by incision. Four samples, one of each material type, were implanted to one animal, in order to equalize external factors, and there were 10 animals per time point. Typically, observations from implantation studies include the tissue response near the implant, the systemic response in the animal, tissue integration and vascularization of the implant, as well as material degradation. Here, tissue sections near the implant were collected, fixed, and stained with hematoxylin and eosin, thus evaluating the tissue response. Animal welfare data was collected alongside macroscopic evaluation of the implant site.

The animal welfare data can be found in appendix A4 of Publication V. Overall, it was found that the animals tolerated the surgery and the implantation period well. The animals showed no adverse reaction and behaved normally throughout the observation period. Scabbing at the incision site was absent or very mild. Only in the early time points mild oedema were observed, however these resolved entirely towards the later days. Type of implant and animal behavior could not be correlated, as each animal purposefully had each type of material implanted.

To assess tissue response, tissue slices were stained and scored on a scale of 0 - 3 by a trained veterinarian. A more complete selection of histology images, as well as the full list of scored tissue features can be found in Publication V, in appendix 5 and table 2, respectively. Overall, it can be stated that the hydrogel implants did not have an adverse effect on the epidermis, dermis or adipic panniculus. While there are some diffuse lesions visible in the subcutaneous tissue, they were deemed to have been caused by the surgery itself, rather than the implants. These tissue lesions include oedema, mononuclear cell infiltrate, and mast cells, and are evaluated also in table 2 in Publication V.

Tissue features that were evaluated in more detail include foreign body reaction, neovascularization, granulomatous reaction, giant cell presence, and lymphoplasmacytic infiltrate. Principally, the foreign body reaction of the bioactivated hydrogels was found to be more pronounced than in the inert NaGG, and even stronger in the hydrogel formulations containing gelatin. This trend is visible throughout the assessed features. For instance, the granulomatous reaction and presence of giant cells are stronger in the bioactivated hydrogels (NaGG-avd, GGox-gelaCDH and gelaADH), as compared to NaGG. Throughout the

implantation period, most implants showed mild to moderate granulomatous reaction, only for NaGG this reaction was entirely absent until day 14. In contrast, GGox-gelaADH caused a severe granulomatous reaction at later time points, indicating the high bioactivity of gelatin. The trend of giant cell presence traces the observation of the granuloma, and all samples have mild to moderate giant cell presence. On the other hand, a mild capsule formation along with the presence of multinucleated giant cells was observed for all material types.

Figure 23 summarizes the occurrence and evolution of neovascularization (A and B) and lymphocytic infiltrate (C and D), essentially confirming the trend of the general tissue response. The scoring presented in panels A and C shows absence (-) and muted (+) tissue response for all time point in NaGG. Neovascularization steeply increases for GGox-gelaADH on day 28 but is overall pronounced (++) in GGox-gelaCDH at all time points. Neovascularization score is higher in NaGG-avd samples compared to pure NaGG, likely due to the added fibronectin. There is no direct ingrowth of blood vessels observed into any of the implants, as seen in Figure 23 B1-B4, but arrows indicate vascular vessels near the implant. The occurrence of lymphocytic infiltrate behaves similarly, where NaGG is the only implant producing no score. The bioactivated hydrogels, on the other hand, induce a stronger reaction (Figure 23 C), with moderate infiltration starting from day 14. Exemplary histology slices of lymphocytic infiltrate at day 28 are shown in Figure 23 D.

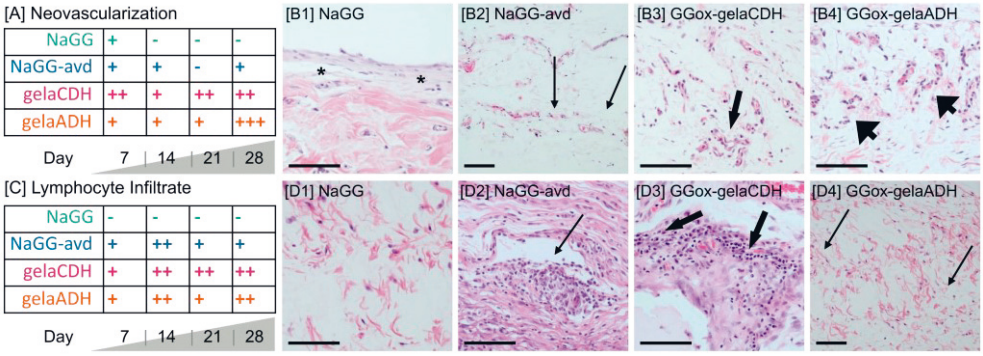

Figure 23. Tissue scoring of histology slices. [A] Tissue scores assessing neovascularization; [B] Annotated histology slices at day 28, arrows indicating neovascular structures, asterisk indicates lack of neovascularization [C] Tissue scores assessing lymphocytic infiltrate; [B] Annotated histology slices at day 28, arrows indicating lymphocyte infiltrate. Scale bar of images 100 µm.

6 DISCUSSION

The polysaccharide GG is at the core of this dissertation owing to several of its features. On one side, GG exhibits outstanding mechanical features, robust ability to form ionic hydrogels, gelation at low polymer concentration, high solubility, and favorable optical transparency. One the flip side, GG does not provide cell attachments sites and is known to be highly bioinert. This, however, should be understood as a good opportunity for modification and moreover as a chance to control the bioactivity of the hydrogel design. Thus, we aim to explore suitable modification strategies for GG, evaluate the resulting structural, mechanical, and biological properties, and finally to investigate application areas of the modified hydrogels.

6.1 Hydrogel design and modification

In this chapter the purpose and success of hydrogel modification will be deliberated. The aim of the presented modifications was to explore different modification strategies to achieve mechanically suitable and bioactive hydrogels for cell culture purposes on the basis of the polysaccharide GG. Commonly, the primary objective of biopolymer modification is to adjust the functionality of the polymer to better match the biological requirements to the purpose of the application, for example to elicit a certain cell response. However, less critical features, such as degradation, sterilization strategy, and supply, are often sidelined. The chemical modification strategies that are utilized here include counterion purification, ring-opening oxidation, reductive scissoring, carbodiimide tethering of amide compound, and Schiff-base crosslinking with hydrazide-functionalized polymer. These methods were adapted from previous literature and haven been chosen based on their relative simplicity and accessibility, but also because the modified products are projected to retain the beneficial properties of GG, such as good gelation, mechanical stability, clarity. The results and features will be discussed alongside examples from the literature for comparison.

The ion purification of GG carried out in Publications I, II, III and V was not targeted towards improvement of bioactivity but intended to aid in further functionalization and to improve viscosity and gelation features. As pointed out by Ferris *et al.* (2015), the removal of the initial mixture of counterions renders the carboxylate groups of the glucuronic acid more available for functionalization, but also prevents gelation at physiological temperatures without the addition of ionic crosslinkers (Ferris *et al.*, 2015). Indeed, we have observed this effect with the reduction in viscosity from the rheological flow sweeps (Fig. 10), and higher crosslinker concentration needed to crosslink NaGG hydrogels (for example Fig. 11). Ultimately, such ion purification presents a worthy consideration when approaching a new polymer from natural sources, such as those being expressed by bacteria. Other compounds and impurities in the formulation may affect the physicochemical, mechanical, and immunological effect of the hydrogel, and should be well accounted for in designing and modifying the hydrogel (Sondermeijer *et al.*, 2016). As is true for any polymer or biomaterial, the structural homogeneity, polydispersity, and molecular weight have to be verified to yield reliable results. Essential purification steps for polysaccharides to render them suitable for TERM have been described extensively elsewhere (Ren *et al.*, 2019). However, these were not considered necessary here for the GG used herein, due to its production process as described in chapter 2.2.1.

We have utilized the oxidation of GG to prepare hydrogel precursor with lower, perhaps more suitable, viscosity, but also to introduce aldehydes as functional groups. The oxidation products were analyzed using UV titration to determine the oxidation degree, while rheological flow testing was used for viscosity analysis. Publication I further uses the oxidized GGox to create scissored GGsciss by cleaving the polymer chain at the oxidized sites, reducing the molecular weight. Hydrogels were then formed using ionic crosslinkers, such as spermidine or calcium chloride, or by combination with hydrazide-modified gelatin. Using ionic crosslinkers was challenging to some extent and did not yield well-defined hydrogels at high oxidation degrees. The mechanical properties of hydrogels formed with GGox and GGsciss were assessed using compression testing and rheological sweeps. Our work and oxidation protocol are mostly based on the work by Gong *et al.* 2009, who demonstrated the oxidation and scissoring of GG for chondrocyte encapsulation. The authors do not report a specific degree of oxidation, only intrinsic viscosity, and molecular weight reduction, but evidently their employed reaction scheme is mild enough to retain the thermal gelation capability of GG. Chondrocytes do not rely on matrix adhesion, and thus encapsulation in GGox was demonstrated over 150 days

with improved results compared to agarose of high molecular weight. Based on the oxidation, GGox was degrading more strongly, thus allowing for a remodeling by the cells, increasing ECM deposition and cartilage tissue formation. Unfortunately, the authors did not actually demonstrate injectability, only mechanical testing is viscometry. While viscosity was determined for GGox dissolved in water, gelation tests and cell culture was established for GGox dissolved in PBS, likely affecting the gelation and mechanical properties (Gong *et al.*, 2009).

Other strategies to oxidize GG include the use of peroxide (H_2O_2) and 2,2,6,6-tetramethylpiperidinyl-1-oxyl (TEMPO) as reactive compounds, resulting in different oxidation products. Lu *et al* (2019) demonstrated the $CuSO_4$-catalyzed GG oxidation using H_2O_2. This strategy does not affect the vicinal diols at the rhamnose but targets the primary hydroxyl group at any C6 sugar atom, oxidizing it to the aldehyde form, which is immediately converted to a carboxyl group, leaving only a limited number of aldehydes in the final product. As a side reaction, also the oxidation of glycoside bonds is expected to occur, resulting in chain scission at the glycoside bond, and finally forming terminal carboxylate groups. The reaction is rapid and efficient, and none of the peroxide oxidized products retained their ability to form hydrogels in the presence of cations. The authors did not assess any mechanical properties, but focus on the gelation characteristics and the antibacterial potency of GGox films (Lu *et al.*, 2019). Similarly, using TEMPO reaction specifically oxidizes the primary hydroxyl, converting them into carboxyl groups as shown by Wang *et al* (2022). However, this reaction is milder, and the authors were able to form hydrogel beads using $CaCl_2$. These hydrogel beads were used to demonstrate drug encapsulation, and a higher oxidation degree improved the loading capacity based on increased ionic interaction and solubility of the polymer (Wang *et al.*, 2022). In summary, periodate oxidation creates aldehyde groups, which are more useful for adhesion, but results in ring opening and distortion of polymer chain. On the other hand, peroxide and TEMPO oxidation retain the chain alignment, they predominantly create carboxylate functionality. These outcomes have to be chosen carefully but offer interesting opportunities for polymer modification.

Besides GG, also the oxidation of other polysaccharides has been reported in the literature. For example, guar gum has been oxidized by Dai *et al.* (2017) using sodium periodate, creating aldehydes, and opening the sugar ring very similar to what has been described for GG. Natively, guar gum does not form hydrogels and has to be chemically crosslinked with, e.g., glutaraldehyde. But oxidized guar gum, did form hydrogels through the creation of cyclic acetals between the vicinal hydroxyl groups and carbonyl groups. While the authors proposed the materials for application in

water treatment for the removal of heavy metal ions, they report beneficial properties including self-healing based on the reversible nature of acetal formation (Dai et al., 2017).

Similarly, dextran can be oxidized using periodate. Hyon *et al.* (2013) have utilized the aldehyde groups for tethering and crosslinking of poly-L-lysine, thus forming tissue adhesive hydrogel for surgical applications. The authors were able to control the gelation time at neutral pH with the oxidation degree of dextran (Hyon et al., 2014). The same group later used the oxidized dextran to steer the degradation rate of hydrogel formed with glycidyl methacrylate. The Maillard reaction occurs when an amine compound is added to the hydrogel, and the aldehyde groups are the onset point for degradation cleaving the polymer chain. The mechanical properties are independently controlled through the crosslinking with glycidyl methacrylate, demonstrating that oxidation can be a versatile tool for hydrogel design (Nonsuwan et al., 2019).

The oxidation of hyaluronic acid and its application in TE has recently been reviewed by Pandit *et al.* (2019), and many literature examples are discussed later (Chang et al., 2021; Karvinen et al., 2017; Koivusalo et al., 2018; Martínez-Sanz et al., 2011). While the oxidation is not primarily aimed to affect the mechanical properties of hyaluronic acid, the ability to rapidly form Schiff-base linkages with amine-compounds make oxidized hyaluronic acid an intriguing biomaterial. As the review pointed out, most studies focus on in vitro results, and the step toward in vivo and clinical applications has not occurred (Pandit et al., 2019).

In a first attempt to improve the bioactivity of GG, we have coupled the protein avidin to purified NaGG using carbodiimide zero-length coupling. The functionalization has been successful, as demonstrated by fluorescence titration and electrophoresis. However, the cell response towards the bioactive functionality has been muted both in Publication III towards fibroblasts and bone marrow SC, as well as in Publication V towards the *co*-culture of endothelial cells and adipose SC. The mechanical properties and gelation ability, on the other hand, were conserved when compared to NaGG, as shown by compression testing and rheology. One of the first reports utilizing the avidin-biotin binding for biomaterial functionalization was published by the group around Prof. K. Langer at the University of Münster, who attached avidin to the surface of gelatin nanoparticles. The functionalized nanoparticles were then complemented with biotinylated antibodies to act as drug targeting ligands. The attachment of avidin was achieved through activation of surface amine groups with sulfhydryl groups using 2-iminothiolane reaction and the authors report a 56–75% coupling efficiency of avidin, where on average 2.4 out of

the 4 avidin binding sites were available to be occupied by biotinylated compounds (Balthasar *et al.*, 2005). An improved drug targeting and receptor mediated cellular uptake in lymphocytic cells was confirmed, aiming for lower systemic drug dosage. The modular avidin-biotin binding system would allow the choice and mixture of different targeting ligands in clinical applications (Dinauer *et al.*, 2005).

A very elegant, yet highly complex, application of protein-based binding was shown by Wylie *et al.* (2011), who created a spatially controlled 3D hydrogel system using two different proteins. Their orthogonal approach uses both avidin and the protein barnase, which function on similar enzyme-substrate principle, but specifically binds the peptide barstar. Both binding proteins were tethered to the same alginate network, and thus allow for an independent 3D laser patterning with biotin and barstar-conjugated compounds in a regioselective manner (Wylie *et al.*, 2011). However, a direct follow-up study and scale-up of this approach towards larger TE applications appears to be lacking. The same concept has been picked up by Leppiniemi *et al.* (2021), who used a similar charge-neutralized avidin to functionalize nanocellulose. The authors compared the addition of biotinylated fibronectin and vitronectin to the behavior of mouse embryonic fibroblasts and evaluated the adhesion marker FAK pY397 to determine the success of the functionalization. Indeed, they confirm that the fibroblasts are anchored to the nanocellulose matrix and able to produce force-dependent adhesions. They report a final concentration of 11.4 μmol/L avidin in 1.0% w/v nanocellulose and using 50 μg/mL biotinylated compound (Leppiniemi *et al.*, 2021).

When coupling avidin to GG in Publication III, we achieved a final molar concentrations 1.6 μmol/L of avidin, to which fibronectin was added at a concentration of 71.0 nmol/L in the final hydrogel. Stoichiometrically, there are 7.0 μmol/L carboxyl groups in 0.5% w/v GG solution, which leads to a total of 23% carboxyl group being functionalized with avidin. Both avidin and fibronectin are quite large in molecular size, with 57 kDa and 220 kDa respectively, and the coupling efficiency can be expected to be lower compared to small molecules due to steric effects. In contrast, Rowley *et al* (1999) demonstrated a coupling efficiency of up to 80% of the peptide sequence RGD to alginate using carbodiimide coupling. The high efficiency was achieved by precise adjustment of EDC concentration used to activate the carboxyl groups, as well as minute control over the reaction pH, in order to balance EDC/NHS efficiency and peptide pKa (Rowley *et al.*, 1999). However, other groups functionalizing GG with carbodiimide strategy have reported values similar to ours, such as 21% coupling efficiency of dopamine (Lee *et al.*, 2021), 27% for furan modification (Silva *et al.*, 2012), and a coupling efficiency range between

10-38% of G_4RGDSY to GG based on reaction setups (Ferris *et al.*, 2015). Additionally, concentrations of 92.9 nmol (Rocha *et al.*, 2020) and 304.0 nmol (Silva *et al.*, 2012) of GRGDS per mg of GG were reported, even though both groups used the same protocol.

Finally, we have attempted to improve the bioactivity of GG through the chemical crosslinking between oxidized GGox and hydrazide modified gelatin, forming hydrazone bonds *via* Schiff-base reaction. In contrast to the ionic GG hydrogels, these hydrogels proved to be very sticky, highly elastic, and had a larger range of gelation times. In terms of bioactivity, these hydrogels yielded the best results throughout Publication I-V, with noticeable fibroblast elongation and remarkable αSMA^+ cell network formation from hASC. Further, degradation was vastly increased, which can be beneficial for drug release and rearrangement by cells, but hypothetically less desired for long-term *in vitro* studies or medical implants. Blending GG with other natural or synthetic polymers has recently been reviewed by Zia *et al.* (2018). Whereas they cover a wide variety of applications apart from TE, such as food industry, waste management, printing) and GG mostly serves as stabilizer and thickener (Zia *et al.*, 2018).

Gelatin is the denaturalized hydrolysis product of collagen, however it retains the crucial peptide sequences, such as RGD, for cell recognition and binding (Bello *et al.*, 2020). While the biological properties of gelatin do not need modification in most cases, the gelation kinetics, mechanical properties, and stability have to be improved. Traditional gelation of gelatin occurs through thermal setting below 37°C, however this is mostly not suitable for TERM application. However, using gelatin as bioactive component to decorate polysaccharides has been identified as valuable strategy. For instance, Zhang *et al.* (2019) used unmodified gelatin with oxidized pullulan, a polysaccharide produced by a fungus, to form hydrogels by Schiff-base reaction. The oxidized pullulan serves to adjust the strength of the hydrogel, achieving a fracture strength of 5.8 MPa, and to limit its enzymatic degradation and swelling (Zhang *et al.*, 2019). In an alternative approach, Wen *et al.* (2014) formed interpenetrating network hydrogels from unmodified alginate and gelatin. These were based on the separate crosslinking of both polymers, where gelatin forms network through the action of microbial transglutaminase, and alginate is ionically crosslinked using $CaCl_2$. On a side note, the authors successfully sterilized their material using steam, which is not commonly seen (Wen *et al.*, 2014). The synthetic hydrogel polymer polyethylene glycol (PEG) was functionalized with gelatin and other peptides, such as YIGSR, by Su *et al.* (2019). Here, the crosslinking of gelatin and coupling

additional peptides was achieved using succinimidyl valerate conjugated PEG, which reacts with the free amine groups of the (poly)peptides (Su *et al.*, 2019).

Hydrazone crosslinking between a polymer carrying aldehydes, and another with hydrazide functionality, has been exploited for a variety of other hydrogel-forming polymers as well. One of the earliest examples of functionalizing hydrogels *via* hydrazone coupling has been demonstrated by Bouhadir *et al.* (1999). Poly(guluronate) was isolated from alginate and oxidized using sodium periodate, but then further modified using adipic dihydrazide, resulting in immediate crosslinking due to the formation between aldehydes and hydrazides. The resulting hydrogels achieved a compression modulus of up to 880 kPa and were further functionalized with GRGDY using carbodiimide functionalization (Bouhadir *et al.*, 1999). A combination of synthetic and natural polymers has been shown by Yang *et al* (2021), who oxidized PEG and functionalized chitin with adipic acid hydrazide crosslinked by aldehyde-hydrazide. The hydrogels were deemed self-healing due to the dynamic hydrazone crosslinking, injectable due to low viscosity of the separate precursors, and also enzymatically degradable with lysozyme by being based on chitin. The gelation occurs upon combination of the two components, enabling the dual extrusion and consequently injection to, *e.g.*, site of injury or cell transplantation (Yang *et al.*, 2021). This may indicate that our GGox-gela-hydrazide hydrogels could be prepared similarly. Hydrazone crosslinking also extensively used for hyaluronic acid hydrogels, either by oxidizing or reaction with hydrazides, or both. For example, Karvinen *et al.* (2018) oxidized hyaluronic acid using sodium periodate and formed hydrogels using hydrazide-modified poly-vinyl alcohol (PVA). The hydrogels were described as soft with a low second order elastic constant of 0.9 – 5.1 kPa, but comparable to rabbit midbrain tissue (Karvinen *et al.*, 2018). Alternatively, the group had previously studies hydrogels from hydrazide modified hyaluronic acid and oxidized GG, which resulted in hydrogels with a storage modulus of 8 - 9.5 kPa (Karvinen *et al.*, 2017).

A pure hyaluronic acid hydrogel based on the crosslinking between oxidized and hydrazide-modified hyaluronic acid was presented by Martínes-Sanz *et al.* (2011). The bioactivity is improved without addition of another component, based on the excess aldehyde groups after crosslinking which contribute to tissue adhesion. Additionally, the enzymatic degradation *via* hyaluronidase was demonstrated, as well as a complete bone tissue integration *in vivo* (Martínez-Sanz *et al.*, 2011). The same composition was used by Koivusalo *et al.* (2018), who developed highly transparent hydrogel for corneal applications, with compressive moduli between 0.6 – 1.6 kPa (Koivusalo *et al.*, 2018). Overall, hydrazone crosslinking offers great versatility in hydrogel design,

and a convenient approach to combine two polymers with complimentary properties.

The hydrogel modifications presented herein represent only a fraction of possible functionalization strategies and combinations. The GG modifications do not form a complete library of all possible modifications enhancing bioactivity or altering mechanical properties, and many more approaches are available. For example, the methacrylation of GG to produce photo-crosslinkable GG-based hydrogels, or the blending with inorganic particles, or functional nanoparticles, have not been explored here. Notwithstanding, there is an abundance of literature example for both methacrylation (Pacelli *et al.*, 2015; Silva-Correia *et al.*, 2013; Tsaryk *et al.*, 2014; Vilela *et al.*, 2018) and blending (Goyal *et al.*, 2011; Saranya *et al.*, 2023).

Additionally, only the polysaccharide GG in its deacetylated form was investigated. However, it was stated in the introduction that GG serves as a model polymer, contributing a simple, well-defined molecular structure, robust gelation ability, and basic cytocompatibility. Essentially, once a modification strategy is well established from the synthesis point of view, and its efficacy has been shown in application, the strategy should be able to be applied to other polysaccharides. Nevertheless, it should be considered that comparison between different base polymers and modification strategies is challenging due to the plethora of different testing approaches, and also their application targets. Moreover, to assess the success of the hydrogel modification some authors focus on *in vivo* studies above a robust analysis of mechanical and viscoelastic properties, while others derive suitable biological properties from viability studies on mouse cells. Similarly, the reporting of features and modification yields is based on the characterization method and these should be compared with caution, as has been seen with the reported efficacies of the carbodiimide coupling between polysaccharides and RGD (Ferris *et al.*, 2015; Rocha *et al.*, 2020; Rowley *et al.*, 1999; Silva *et al.*, 2012).

In many cases it appears to be so that bioactivity and mechanical support are antagonists in hydrogel properties, where if either of these aspects is pronounced and highly suitable, the other will be deficient. For instance, fibrin and collagen are superior hydrogel materials in term of cell response and attachment but degrade rapidly and shrink excessively due to cell contraction. On the other hand, synthetic hydrogel polymers such as PEG and PVA, but also GG and alginate, are robust and give strong and stable hydrogels, yet they do not natively support cell attachment. Balancing the bioactivity and mechanical support is the challenge set before biomaterial design.

Another feature of an advanced biomaterial and hydrogel is the ability of the user to control the final properties towards the application, including mechanical stiffness and availability of cell instructive features. Rather than choosing an entirely different material, with which a researcher may not have experience in handling, to match the demands of the application, it would be highly feasible to add or omit, *e.g.*, cell adhesive peptide sequences while avoiding long synthetic steps and retaining the mechanical and gelation characteristics. Such was the intent behind the avidin-modification presented in Publication III, which would allow just that with an off-the-shelf product. Another approach would be the use of smart materials, that can alter their physical properties on-demand or through external stimuli, as for example exhibited by electrically conductive materials or nanogels (Balint *et al.*, 2014; Wu and Wang, 2016). Moreover, modularity in hydrogel design should also include considerations for degradation, and user control over the degradation of a hydrogel. Again, the stability of an *in vitro* tissue construct, or the stability of an implant, has to be balanced against the ability of the material to be remodeled by the resident cells. But also, the user should have the possibility to initiate degradation and remove the hydrogel, in order to retrieve the cells without damaging them.

6.2 Hydrogel characterization

As is true for many other fields of natural sciences the characterization of created product is core issue of hydrogel design, which also determines the success of the design and functionalization. Here, we consider four important areas to fully describe a hydrogel as presented in Figure 2 in chapter 2.1.3: Structural analysis, mechanical characterization, degradation features, and biological compliance. However, an essential aspect for hydrogels is their development as 3D cell culture systems, thus they require dedicated analysis techniques for volumetric assessment, and available laboratory techniques must be amended. Conventional cell analysis methods have been developed for flat, 2D systems, but state-of-the-art must focus on the evaluation of cell-laden hydrogels. Challenges present themselves in the quantitative assessment of cell behavior, including the approach for cell DNA isolation, imaging of the full 3D volume, as well as the determination of mechanical properties and their relation to mechanotransduction phenomena.

Further, we must consider which the established mechanical and physical properties are relevant for cells. While mechanical testing is carried out on macroscopic samples, typically in centimeter range, cells are typically within

micrometers and binding ligand spacing within tens of nanometers (Walters and Gentleman, 2015). A correlation between the modulus and physical sample size has been established using bending test of bone samples of different size (Choi *et al.*, 1990). This should be understood as the difference between the size scale of cells, organoids, tissues, up to organ level. Ultimately, the size scale to which we aim to match the biological hierarchy must be considered carefully. A model will only be as good as the question it tries to answer and recapitulating the entirety of a biological system will not yield valuable answers due to high level of complexity. Simplicity in hydrogel and experiment design will aid the required characterization steps.

Structural evaluation is an essential subject in any chemical functionalization endeavor, including hydrogel modification, polymer synthesis, biomaterial development, or any other form of material chemistry. The choice of analysis technique follows the general strokes of polymer chemistry and functionalization and has to be determined according to the base polymer as well as the type of functionalization carried out. For instance, while NMR is a powerful and precise technique, the evaluation of the recorded spectrum can be challenging, and becomes more complex with advanced chemical structures and impurities. As an example, our coupling of a protein *via* carbodiimide chemistry creates a peptide bond, thus detecting another peptide bond next to a high M_w polypeptide may be ineffective.

An essential structural feature of hydrogels is their porosity and mesh size, contributing to the outstanding properties of mass transport and supply of an aqueous environment. However, it is crucial to note that these two are phenomena on vastly different length scale, and moreover they are often used intermixed and misleading. While mesh size is at the atomic structural level of the polymer chain intersection points, *i.e.*, the distance between two crosslinking sites, pores are additional, larger cavities in the macroscopic structure. In the swollen state, pores are difficult to consider altogether, because the main constituent of the network – water or any aqueous solution – should be homogeneously distributed throughout the bulk. Porosity can be considered for fibrous or solid materials, like nanocellulose or p(HEMA), but for hydrogels with truly hydrated polymer chains the phenomenon of pores is challenging to discuss.

Approaches to quantify porosity and mesh size include the theoretical calculation from mechanical behavior, diffusion observation, and imaging. The former is limited to highly uniform network meshes and can make no statement about macroscopic pores, while the latter is a poor choice when drying of the hydrated hydrogel is carried out. Measuring the diffusion properties of a sample is perhaps the ideal approach, as it accurately represents a swollen network, and yields a qualitative

understand of nutrient transport for cell encapsulation studies. This can be achieved through fluorescent imaging techniques such as fluorescence-recovery-after-photo-bleaching (FRAP) or diffusion of fluorescent dextran compounds (Soto *et al.*, 2016). Measuring either pore or mesh size has garnered little attention and discussion within this thesis, because GG is used at a low polymer density and thus good diffusion can be assumed. However, the type of diffusing substance is crucial and related to compound size, charge, partial pressure, and other affinity types.

Electron microscopy, such as scanning electron microscopy (SEM), transmission electron microscopy (TEM) and other vacuum-based methods are not suitable to image a wet and swollen hydrogels directly. They are, however, plausible to use for comparison, or to image encapsulated particles or composite structures. Imaging of hydrogels, without cells or inclusions, in their swollen state remains challenging and offers little information. Development of advanced imaging techniques such as optical projection tomography (OPT (Belay *et al.*, 2021) and selective plane illumination microscopy (SPIM) (Vuornos *et al.*, 2019) broaden the option for cell network analysis in large volumes and in three dimension, but direct hydrogel analysis remains challenging.

Using compression testing of pre-formed samples, we have assessed the static mechanical properties of most of our hydrogel formulations. The results of the compression modulus, or modulus 1, range between 1.7 ±1.6 kPa of GGox(2)-SPD (20 mM) and 14.6 ±7.9 kPa of NaGG-SPD (4 mM) for hydrogels observing a brittle fracture and up to 41.23 ±7.3 kPa for GGox-gelaCDH observing no fracture point, representing the highly elastic hydrogels. Theoretically, the values should be easily comparable between different authors as long as similar parameters for confinement, interface, and compression speed are used. However, the reported value for compression modulus depends on the range of compressive strain analyzed and can be rather subjective. Thus, comparisons to literature values have to be examined critically, but can be used to gauge the general magnitude of values. Nonetheless, there are several advantages of compression testing, such as easy comparison between fracture behavior of different samples, and facile sample fabrication, as cylindrical samples can be produced by casting and biopsy-punching. Further, compression allows for comparison between samples that have undergone different treatments as well, so long as their shape fidelity remains appropriate for compression testing. For example, Publication II demonstrates a modulus increase when NaGG hydrogels were immersed to cell culture medium for 24h from 14.2 ±1.2 kPa to 26.2 ±1.8 kPa. Finally, the testing procedure is relatively fast, and the throughput is only limited to single sample loading and measurement. On the

downside, compression testing is not suitable to establish viscoelastic properties, because viscoelastic deformation and brittle fracture features are not discernible from the graph (Kocen, *et al.*, 2017). Further, while technically any shape of sample can be loaded to the piston and compressed, but reliability of results has to be scrutinized, because the calculations depend heavily on the symmetry of the sample shape and accuracy of the area and height values of the sample.

To advance the mechanical characterization, we have incorporated rheological testing to our routine assessment of hydrogel formulations in Publication I and V. Rheological testing allows for the comparison of gelation kinetics and viscoelastic features between vastly different formulations, and through the hydrogel preparation between the geometries, overcoming the demolding issues experienced by the gelatin-containing hydrogels. Flow testing for precursors showed the reduction in viscosity due to oxidation and scissoring of GG. Amplitude sweeps demonstrated the high elasticity of the chemically crosslinked gelatin formulations, with crossover points far beyond 100% oscillation strain. And time sweeps revealed the gelation kinetics, and the transient point could be used to determine the point of gelation much more accurately than the qualitative tube-tilt test.

Rheology is a highly suitable method for a large range of hydrogel compositions, including insufficiently crosslinked hydrogels that flow, to more rigid composite hydrogels. The underlying physics and calculations are highly complex and are elaborated in more details elsewhere (Chhabra and Richardson, 2008; Larson, 1999; Zuidema *et al.*, 2014). Further, to accurately calculate the mechanical properties, two assumptions are made. Firstly, the material is in perfect contact with the upper and lower geometry while no slipping occurs, and secondly that the sample deforms homogeneously and is isotropic. This may be difficult to achieve for hydrogels that exude water and easily form a lubricating layer, or uneven samples that have been pre-formed. But even from a more practical point, rheology can be understood as an ideal method to give insight to viscoelastic properties, by utilizing different testing methods such as oscillatory amplitude and frequency sweeps, time sweeps, flow sweeps, as well as creep tests. While compression testing assesses the static mechanical properties of the final hydrogel, rheology measures the hydrogel processing kinetics. Ultimately, both techniques work in conjunction to investigate the bulk mechanical properties of hydrogels, but neither can assess the micromechanical features relevant for the cell level.

There is a large range of other testing methods that were not utilized in the studies presented here, including indentation, creep, and tensile testing. Indentation testing is, in essence, a highly localized compression test in which a cantilever indents a small

contact area on the surface, and the reduced modulus reported. The length scale of this procedure ranges within mm to μm indentation area, thus achieving the aforementioned micromechanical testing, and has been adapted from hardness measurements to be suitable for compliant, soft materials. Nowadays, commercial nanoindentation equipment can be used, but also atomic force microscopes (AFM) can be used for indentation testing. This method further eclipses other mechanical testing with its minimal sample preparation requirements, as well as ambient air and pressure requirements for topology imaging possibilities (Oyen, 2014). Indentation testing has been used to identify the effect of microscale stiffness to the expression of growth factors and proteins by endothelial cells (Santos *et al.*, 2015), as well as the force response of cardiomyocytes and cardiac fibroblasts to hydrogel environments of different stiffnesses (Bouhrira *et al.*, 2019).

Creep tests can be carried using several equipment, including rheometer, compression tester, and dynamic mechanical testing (DMA) instrument. Here, the mechanical load to the sample is fixed, and the response of the material to time and temperature is of interest (Oyen, 2014). The sample is subjected to torsional or compressive stress for a set period of time or with cyclical loading, and the following relaxation behavior after removal of the stress is observed. This stress-relaxation behavior can be applied to material compliance and could be used to estimate remodeling of the hydrogel network by cells (Kocen *et al.*, 2017). Tensile testing finds limited application for hydrogel due to their low structural integrity. The sample requires to be pulled from its ends, thus clamping presents the weak spot for this method, as a hydrogel would more readily break at the clamp than in the bulk (Oyen, 2014). For hydrogels with outstanding mechanical stability, tensile testing can be adequate regardless, as shown by Wen *et al.* (2014). From their membrane samples, the authors showed a significantly increased tensile strength with up to 600 kPa Young's modulus by dual crosslinking of gelatin with transglutaminase and alginate with calcium chloride (Wen *et al.*, 2014).

For degradation assessment, it appears that researchers design their own methods to track and investigate the temporal properties of their hydrogels, and standardization is lacking. This is appropriate in the sense that the investigation method should be developed according to research needs and material type. However, communication of best practices is desirable. Moreover, it is chiefly important to adequately describe the used procedure in publications. Certain pitfalls in degradation assessment are common, such as overestimating the accuracy of mass analysis. For example, Zustiak and Leach (2010) repeatedly weighed very small hydrogels of 50 μL (Zustiak and Leach, 2010), which can be estimated to be 50 μg,

while a typical lab typical laboratory scale has an error of maybe ±20 µg (0.02 mg) (Morse and Baer, 2004). Also, other error sources such as incomplete drying and droplets of water will easily influence the result in this case. Furthermore, da Silva *et al.* (2018) were treating their MMP-1 degradable hydrogels for one entire month with MMP-1, and still around 50% of the mass was remaining, while no considerable difference between PBS and MMP-1 was observed (da Silva *et al.*, 2018). This raises questions whether the method, or the hydrogel design, was appropriate, however the authors do not discuss it.

We have used three approaches to measuring the degradation of hydrogel samples: Supernatant analysis from spatially confined samples, weight measurement of pre-formed sample freely immersed, and rheological amplitude sweeps of the latter. The degradation samples in Publication IV were cast to centrifuge tubes, holding them in place while the incubation media containing collagenase was simply added on top. On one hand, this allows for a small and precise incubation medium, required to quantify degradation products in the supernatant. On the other hand, however, the hydrogel is poorly immersed, and the hydrogel-medium interface is limited, crudely mimicking a biological setting. Weighing of fully immersed samples is challenging if the samples lose their structural integrity, which was, however, mostly alleviated by the use of mesh holders, allowing the transport and blotting of sample without direct contact to them. The same challenge presented itself for the measurement of degraded samples for rheology. Due to the nature of the mechanical characterization, this could not be overcome, however indentation testing could be a solution as the bulk shape of the sample is of no consequence.

It is broadly understood that mass loss is the direct result of hydrogel degradation. However, there is a complex interplay between swelling induced by water uptake, shrinkage due to increasing crosslinking, and mass loss due to network erosion. A decoupling of swelling and degradation would be desirable but is difficult to achieve in practice. Specifically, a possible mass gain due to swelling and water uptake may mask initial degradation and small mass loss. Mass loss, in turn, can be either due to actual degradation and erosion of the polymer network, or due to expulsion of water from a tightening of the network, which would be evident from size measurement, but not through weighing. To exemplify, in a generic 500 µL hydrogel sample that is formed by a polymer at the concentration of 10 mg/mL (0.1% w/v), the weight of water (500 mg) would provide 99% of the total weight, greatly overshadowing changes in the polymer composition upon degradation.

Another limitation of common degradation testing setups presents itself in their simplicity. Incubation tests are merely modelling *in vitro* or *in vivo* tests, which are

themselves only models with different scales of complexity, without the ability, or intent, to recapitulate all parameters at once. For example, if a hydrogel is developed as artificial ECM or bioink for *in vitro* cell culture, its mechanical and temporal properties are usually assessed using various physiological buffers or basic cell culture media, typically omitting the more expensive growth factors and components needed strictly for the cells. Thus, the medium composition and environment of these incubation tests can be vastly different compared to cell growth experiments: For one, these components can react with the polymer, catalyze, or retard degradation reactions, and secondly the presence and action of cells, such as production of cell-own ECM, can enhance or diminish matrix stability. As mentioned in the introduction, the degradation properties and compliance to be remodeled by resident cells affects the outcome of such cell behavior experiments, but typically with inversed fates. If the hydrogel matrix is compliant, the cells will, depending on cell type of course, attach, elongate, and proliferate, while remodeling and degrading the matrix. The cell response is thus positive, but the construct typically unstable and impossible to culture for more than 1-2 weeks. If the hydrogel is stable however, typically cells will stay rounded, unable to grow into their niche. Even small cell culture medium composition changes have been shown to affect matrix behavior and stability (Eyrich *et al.*, 2007; Jarrell *et al.*, 2021), but due to experimental limitations, this is often overlooked.

Cytocompatibility results of WI-38 fibroblasts in direct contact in Publication III and IV demonstrate that none of our hydrogels induce cytotoxic effects and all are generally suitable for cell culture. We mostly aimed to show 3D cell encapsulation rather than 2D plating, in order to validate the hydrogels' application for advanced tissue models, and to incorporate the gelation step to the cytocompatibility statement. The experimental setting of this human fibroblast cell culture is calibrated so that it is simple enough to get a robust result and good understanding of cytocompatibility, but advanced enough to yield reliable statements for human organism and extrapolate to more complex systems. Hence, our routine cell culture assessment features human cell types, adequate cell number up to 1 million cells/mL in the final hydrogel, and an appropriate culture time of at least 3 days for fibroblasts. Historically, *in vitro* cell culture has been developed on mechanically hard, flat substrates such as glass and polystyrene, termed tissue culture plastic (TCP) (Justice *et al.*, 2009; Tibbitt and Anseth, 2009). Hydrogels offer the outstanding opportunity to spatially mimic the native cell environment and elevate tissue models to the third dimension. However, shrewd adaptation of established protocols is required, and many challenges still persist in comparison to 2D culture. For practical

considerations, the sample preparation strategy and required components should be tested and verified before attempting cell encapsulation, but the strategy must also be developed with requirements and limitation of the cells and aseptic technique in mind. For example, if the material requires an extra sterilization step such as filtration before being in contact with cells, then mechanical and physical characterization should be carried out with the sterilized material. Nevertheless, 2D hydrogel culture experiments remain relevant to see adhesion and separate cytotoxic effects of the crosslinking step. While the staining and imaging are comparatively quick and simple, issue can arise if the cells were not adhered to the material, as they will be removed in media change and washing steps. This can be understood as a result as well and indicates poor cell adhesion of the material. On the other hand, 3D experiments provide higher relevance for tissue models. It requires the crosslinking step to be cytocompatible, and cells must be able to adhere and remodel to the material for positive response.

Fibroblasts are attachment-dependent cells, and while they remain viable in inert materials like GG, they will not achieve their elongated morphology. To circumvent this issue, non-adherent cell types can be investigated, and the hydrogel can further be developed for this type of cells, e.g., for cartilage tissue engineering. For example, Gong *et al.* (2009) established general cytocompatibility of the oxidized GG films using human epidermis fibroblasts, which were incubated with the extractant of the hydrogel. Afterwards, they showed positive cell response of chondrocytes and encouraging ECM production over an astoundingly long culture time of 6 month, with better results compared to agarose (Gong *et al.*, 2009). Chondrocyte culture and cartilage models appear to be a popular choice for GG-based hydrogels (Bartnikowski *et al.*, 2015; Oliveira *et al.*, 2010; Tsaryk *et al.*, 2014; Vilela *et al.*, 2018).

The chosen analysis methods of the cell culture outcome must be compatible with a 3D cell culture and should not be perturbed by the material itself. For instance, if microscopy is used to visualize the cells embedded in the hydrogel throughout the culture, or at the end point, optical transparency of the hydrogel is highly advantageous, but a heterogenous texture or autofluorescence of a hydrogel can make visual analysis challenging. Qualitative observations typically include cell morphology, vacuolization, detachment, cell lysis and membrane integrity, whereas cell death, inhibition of cell growth, cell proliferation or colony formation can be quantitated with different means. Examples given by ISO-10993 for quantitative staining include the quantitative dye-uptake into lysosomes, endosomes, and vacuoles, ratio of colony formation in cell lines such as V79 compared to reference conditions, as well as the UV intensity of dye-based assay activated by metabolic

activity of cells, such as MTT, XTT, or Alamar Blue assay. Generally, a cell viability of 70% or less than control is deemed cytotoxic (ISO 10993-5, 2009).

6.3 Tissue engineering applications of hydrogels

Any discussion of design approaches and material properties of hydrogels should, of course, be conferred in the light of their final application. This chapter does not intend to thoroughly present all possible tissue models, cell types and other medical applications, but rather present a general excursion to different areas within the field, and to find the connection of our previously determined GG properties to hypothetical application requirements. Indeed, the medical application of hydrogels is a hot topic in current scientific discourse and holds great promise for future regenerative therapies (Blanco-Prieto and Garbayo, 2022; Gu, 2022; Iyengar and Atluri, 2022; Raina *et al.*, 2022). Comprehensive reviews of medical application for hydrogels in general, and GG in particular are available, and typically focused on a specific tissue or treatment type, for instance wound dressings based GG (Feketshane *et al.*, 2022), or drug delivery using thermo-responsive hydrogels (Yu *et al.*, 2021). We will broadly separate hydrogel applications to two areas: research-focused *in vitro* cell culture and medical devices for patient care. *In vitro* cell research requires hydrogels to provide a cell substrate that mimics the native environment of the cell type, does not interfere with the evaluation protocol, and evoke the desired cell response. Hydrogels for regenerative medicine, on the other hand, have a much larger variety of property demands, and can be used to delivery stem cells, tracing agents, or drugs, and be applied *via* implantation, coating, or injection. However, with the advent of personalized medicine these two areas are combined, where *in vitro* cell culture of patient-own cells will directly influence and benefit the treatment plan.

Although developed primarily for food products, GG has found application in medical devices and products for several decades, including ointments, topical dressings, and ocular suspensions. While these are not considered regenerative medical devices or tissue engineering products that are of interest here, we can associate the outstanding mechanical and inherent properties of GG to its success in the medical industry. These include the thickening and gelation properties, as well as low cost and optical transparency. For example, GG has been considered for ophthalmic drug delivery as early as 1993 (Sanzgiri *et al.*, 1993), and fluid gels have been developed for the challenging delivery of hydrophobic drugs to the eye

(Destruel *et al.*, 2020; Khare *et al.*, 2022; Vincent *et al.*, 2021). Skin wound dressings are another medical application that benefit from the pertinent gelation capacity and drug encapsulation of GG. Further, material properties such as suitable thickness, folding endurance of hydrogel sheets, swelling, inherent antibacterial and antioxidant activity (Mahmood *et al.*, 2021), as well as moderate water vapor transmission rate, good mechanical performance, excellent biocompatibility and non-toxicity (Feketshane *et al.*, 2022) contribute to the application of GG in wound dressings for skin regeneration. These same basic aspects are translated to TERM applications, where often the mechanical properties of GG are utilized to improve existing formulations, and functionalization and compounding are used to achieve desired outcome.

Hydrogels are a core aspect for 3D cell culture and a wide range of cell- and tissue engineering-related fields of research, including stem cell research and disease modeling. Essentially, the only competitors in this field are material-free suspension and organoid cultures, in which the cells form their own material matrix and 3D environment. We have demonstrated the suitability of our GG hydrogel formulations for the support and encapsulation of hBMSC, cardiomyocytes, as well as the co-culture of hASC and endothelial cells. As has been discussed previously, the properties of bioactivity and capacity of volumetric support over the desired timeframe must be carefully balanced. While our results show good viability and an absence of cytotoxicity in any GG-based hydrogel, steering the cell response and maturation of the tissue type remains challenging. The hBMSC culture in Publication III showed no extended cell network and no strong matrix deposition, and the co-culture of HUVEC and hASC in Publication V formed an αSMA^+ network rather than tubular structure from the endothelial cells. A longer cardiomyocyte culture in Publication IV is challenged by fast degradation of gelatin-containing hydrogel formulations. Nevertheless, the primary goal of achieving a sustainable, three-dimensional cell culture construct was achieved using hydrogel, encouraging further research in true-biomimicking conditions for tissue models.

The limitations of *in vitro* tissue models and design of hydrogels thereof are certainly plentiful and need to be critically discussed in the literature. For example, there appears to be a tendency of overengineering biological aspects, perhaps to the detriment of hydrogel usability and mechanical stability that would be required over the course of the analysis, as seen in fibrin and collagen-based hydrogels. A more over-arching issue is the application and interpretation of a model system, as a model is only trying to imitate certain parts of a system but can never recapitulate all. This is not a drawback in itself, as too high complexity will also sabotage the evaluation,

but a clear design choice has to be made. Biological features that are typically not fully recapitulated include the mechanical loading of cell culture constructs during growth and healing stages (Steinmetz *et al.*, 2015), consideration of genetic background and disease of different patient-derived stem cells, the oxygen supply and hypoxic conditions in hydrogel constructs (Pavlacky and Polak, 2020), and contact with other cell and tissue types.

Organs-on-chip (OOC), or body-on-chip (BOC), systems are microfluidic devices designed to increase the relevance of tissue cultures models through the addition of perfusion and the possibility of tissue interaction. They are essentially miniaturized cell culture platforms, with separate inlets and outlets to pump cell culture medium along or through the cell construct, to mimic the natural fluid flow and waste removal (Jalili-Firoozinezhad *et al.*, 2021). Within the cell culture compartment of such a chip, the investigated cell type can be plated as 2D monolayer, aggregated cell clusters, or encapsulated within a hydrogel matrix. Adequately filling the hydrogel into the small channel and ensuring its stability against the fluid flow can be challenging. From a material design perspective, OOC systems thus combine material cytocompatibility testing, adjustment of the viscosity and gelation kinetics. However, OOC models are becoming increasingly relevant and sophisticated and will be an essential tool to improve drug screening, disease modeling and replace animal models. While the use of hydrogels within OOC is not yet ubiquitous, there is range of examples and material types, such as fibrin (Glaser *et al.*, 2022; Mykuliak *et al.*, 2022), Matrigel (Hyung *et al.*, 2021), a blend of Matrigel and collagen (Veldhuizen *et al.*, 2020), hyaluronic acid (Christoffersson *et al.*, 2018; Rajan *et al.*, 2020), alginate (Sung and Shuler, 2009), and PGMatrix™ which is a commercial, nano-fibrous polypeptide hydrogel (Soltantabar *et al.*, 2021). Here, the mechanical demands on a hydrogel pertain primarily to the flow of the injected hydrogel components, rather than final bulk stiffness of the hydrogel, as it is cased in the microfluidic device. This means that the shear thinning of the hydrogel precursor, as well as the gelation time should be investigated beforehand. Further, the resistance against flow erosion for perfusion systems, minimal bubble formation during injection, and overall shape fidelity and resistance to shrinkage, have to be considered for the hydrogel design. As opposed to injectable hydrogels for, e.g., drug delivery, also the transparency and optical clarity is essential for microscopical evaluation. Indeed, our gelatin-GGox hydrogels have indeed been tested for application in a microfluidic chip in preliminary work (Kalke, 2021). While the bioactivity of these hydrogels has been deemed suitable for the cell type, the fast

gelation had been an issue that could be adjusted by reducing the polymer concentration of the precursors.

Although not directly the scope of this work, hydrogels are certainly one of the most intriguing materials for regenerative medicine and stem cell transplantation vehicles. The excellent, early review of the field by Slaughter *et al.* (2009) outlines the challenges of the research field ahead, but also indicating the exploitation the outstanding of hydrogel characteristics, such as their hydrophilic nature and chemical functionalization options. The seminal work by Tirrell, Langer and Peppas (Peppas, 1997; Tirrell and Langer, 2004) has been vastly extended in the past decade, and a large number of hydrogel reviews for drug delivery and imaging agents (Bordbar-Khiabani and Gasik, 2022; Raza *et al.*, 2021; Yu *et al.*, 2021), implant coating (Alavi *et al.*, 2022; Bjelić and Finšgar, 2022; Fu *et al.*, 2021; Liu *et al.*, 2021), and cell transplantation (Gong *et al.*, 2022; Nadine *et al.*, 2022; Xia and Chen, 2022) are available.

We have investigated the cell-free transplantation of GG-based hydrogels in Publication V, albeit not to study drug release or regenerative capacity, but strictly to observe tissue response. This is an important step for the development of any implant material, and implant integration, capsule formation and systemic effects should be analyzed. The most pronounced finding of our study was the strong distinction between the highly bioactive gelatin-formulations provoking a strong immune response, and the more bioinert plain NaGG and avidin-modified NaGG-avd. However, while strong bioactivity was desired for vascularization and the *in vitro* cell culture, from an implant material point of view a more inert material and muted immune reaction could be preferrable. Crucially, it has been somewhat challenging to correlate the results between characterization and application observations. Here, the degradation study of cell-free *in vitro* study in Publication V does not match the observations from the subcutaneous implantation, nor the observations from the cell culture study of the same materials. This forms further evidence that comparison between different assessment techniques and their final application has to be carried out with caution.

While the preparation technique of a hydrogel is not an application in itself, their development and advancement over the previous decade is worthy to note and often directly influences a hydrogel's suitability for a given application. The gelation kinetics and flow characteristics are relevant for the vast majority of hydrogel sample preparation, including extrusion bioprinting, injection, and casting. Further, it must be considered how many components and equipment are needed to create the final hydrogel. For example, bioprinting can be carried out in a support bath, or with two-

components inks and is easily adaptable to photocrosslinking, while an injectable formulation should be delivered with pre-mixed, self-crosslinking components, or at most observe thermal gelation. While the components for mold-cast hydrogels can be combined, mixed on the spot, and be highly viscous, for hydrogel coatings and film forming applications they hydrogel precursor must exhibit low viscosity and high homogeneity.

Bioprinting has received a large amount of attention in the recent years to create hydrogel structures with intricate hierarchy, several material combinations, and microscopic features with fast throughout and excellent user control. The term bioink may be defined as cells suspended in a shear thinning hydrogel for 3D printing application, and to assess the hydrogel's rheological properties, such as flow, yield stress and viscosity, is required. However, care must be taken that the addition of cells, or any particulate material, will change the rheology and stability of the hydrogel. While the micromechanical features are relevant for the cells, such bulk characteristics of a bioink must be expected to vary from a formulation without the cells, especially at high cell concentrations. Similarly, the temporal stability may also be affected by the activity of the encapsulated cells, which is not observed in cell-free immersion studies.

For extrusion-based bioprinting, the flow properties, shear-thinning, and gelation kinetics of a hydrogel and its precursor are relevant and typically assessed using rheology before any extrusion experiments. We have shown monolayer extrusion printing of simple GG modifications onto a thin layer of crosslinking solution in Publication I. While this demonstrates the extrudability of the formulations, the ionic crosslinking strategy is limiting the translation to multi-layer constructs. By itself the precursors observed too low viscosity and shear-thinning to be feasible for post-printing crosslinking and combining precursor and crosslinker in the extrusion cartridge is hampered by the gelation rate of the hydrogels, thus blocking the nozzle and cartridge. There exist many strategies to overcome these issues, such as increase in viscosity, compounding, or choice of different gelation mechanism. For example, Albrecht *et al* (2022) used native GG at 1% w/v to print ASC, simply based on the increased viscosity through hydrogel formulation in a mixture of PBS and cell culture medium. The printing resolution was further improved through the addition of the cells, and the adipose culture was shown to be viable for at least 98 days (Albrecht *et al.*, 2022). Akkineni *et al.* (2022) demonstrated the bioprinting of mesenchymal stem cells by exploiting the combination of crosslinking capacity from low acyl GG with elastic nature of high acyl GG, without any further functional modification (Akkineni *et al.*, 2022). Compounding of GG and starch has been shown to achieve good

printing results by Zhang *et al.* (2021). The starch addition acts as fiber reinforcement and the authors claim an increase in porosity as well. In a common approach to avoid processing and sterilization stress on cells, the Schwann cells were seeded onto the printed 3D grid shape (Zhang *et al.*, 2021). Alternatively, photocrosslinking can be used to aid the printability of hydrogels. Jongprasitkul *et al.* (2021) have demonstrated the dual crosslinking methacrylated GG, which is initially rendered more viscous through formulation in $CaCl_2$, and photocrosslinked immediately after printing to conserve the shape. Excellent printing fidelity has been achieved, but application onto cell culture has yet to be investigated (Jongprasitkul *et al.*, 2021).

6.4 Future prospects of hydrogels in tissue engineering

The primary aim of hydrogel design is to evoke and steer the desired response of encapsulated cells or surrounding tissue. The bioactivity and presence of cell recognition factors, such as suitable peptide sequences, is a crucial feature for cells to resume their normal function and interact with their environment and each other. Mechanotransduction has been shown to be a powerful agent in inducing different cell responses to their environment and has become a key feature for biomaterial design. Thus, the viscoelasticity, stiffness, and temporal stability of a hydrogel have to be carefully considered. A decoupling of the mechanical properties from the presentation of bioactive factors is necessary to fully understand mechano-transduction and cell response, however, this is not achieved by the publications presented herein, nor is it commonly seen in other publications. A comparative insight between bioactive features and material stiffness has been attempted in Pub V with focus towards the cells and tissue's ability to form vascular networks and signs of angiogenesis. Other publications that go into this topic do underline that both hydrogel elasticity as well as ligand presentation are crucial design parameters for regenerative therapies and stem cell differentiation (Choi and Harley, 2012; Zieris *et al.*, 2010).

Although it has been discussed and accepted for over a decade now, the need of functional biomaterials with sophisticated yet simple design remains to be a challenge. As described elegantly by Kirschner and Anseth (2013), from their inception biomaterials have developed from static, inert materials to dynamic, bioactive materials (Kirschner and Anseth, 2013). Thereafter must follow the step of cell instructiveness and user control over biological and mechanical cues. Especially the topography and control over the microstructure architecture will be

the driving endeavor in the future of biomaterials and hydrogels. For example, an improved hierarchical representation of biological tissues could be possible with bioprinting, which is being researched and reviewed heavily in the recent literature (Ding *et al.*, 2023; He *et al.*, 2016b; Ozbolat and Hospodiuk, 2016; Sola *et al.*, 2023; Tejada Jacob *et al.*, 2022).

We consider GG to be an excellent choice as model polysaccharide due to several features desirable for any hydrogels use to support cells and general TE applications, as elaborated in chapter 2.1. These features include the low cost of GG as base polymer, long-term storage, a well-characterized and consistent structure, several ways to render it sterile without polymer deterioration, its solubility in water, its adequate gelation properties, the low polymer concentration ensuring sufficient diffusion, as well as the high transparency of most GG hydrogel formulations. GG hydrogels benefit from modification to better suit the application requirements in regard to their stiffness and elasticity, but also their degradation profile, as often GG hydrogels are too stable and do not degrade.

While GG answers some of the question posed for the field of hydrogels in tissue engineering, but certainly not all. Most importantly, GG hydrogels are severely lacking in cell attachment sites and other cell instructive features, posing the need for functionalization. It is a suitable material for bioprinting applications, however, either as standalone material, but more likely it will be a supporting component in future developments in this field. Ideally, synthetic materials will replace animal-derived ECM material such as Matrigel™ in the market. This position is strengthened by regulatory and ethical aspects opposing any animal source, but also underlined by the opportunity to precisely control biological factors, rather than have a large variety of biological interactions present in native ECM. Therefore, bioactive functionalization of synthetic or inert materials may be the preferred approach for biomaterials of the future.

Other ventures for hydrogels in TE are posed by the development of more sophisticated techniques for analysis and fabrication. Especially the throughput of mechanical testing, drug screening and material-induced cell response has to be investigated. With the recent trend of creating and studying material libraries, efficiency and reliable result correlation will be especially important. Within academic research, such a material library would hold hydrogel types with versatile modifications. However, for medical and personalized healthcare applications one simple material type that covers a wide area of functionality will likely be more useful and universally accepted. This would also greatly aid and streamline the need for regulatory assessment and acceptance in different devices, in turn reducing the cost.

Hypothetically, however, the ideal solution would be to forgo hydrogel materials for cell encapsulation and transplantation altogether. It is well understood that cells have the required genetic coding and capacity to produce exactly the environment they need spatially and biologically, which no synthetic system can ever recapitulate or eclipse. Unfortunately, the currently established cell biology technology strips them of their natural surroundings, and hydrogels are required as prostheses for the foreseeable future.

7 CONCLUSIONS

Hydrogels have been established as crucial components for tissue engineering and the future of medical research. In principle, they can suspend cells in a tissue-like, 3D environment, act as instructive matrix due to biochemical and architectural features and are suitable for modern manufacturing techniques like bioprinting. However, the mechanical rigidity and bioactivity of a hydrogel material have to be carefully balanced, and the material scientist has to decide whether to improve the mechanical stability of an inherently bioactive polymer, or whether to bio-functionalize a mechanically superior hydrogel.

The aims have been addressed as follows: **(1)** An array of suitable modification techniques applied onto the polysaccharide GG has been shown. These include purification to replace the mixture of counterions with sodium, oxidation to obtain aldehyde group, chain scission to reduce molecular weight, direct chemical functionalization, as well as compounding with the bioactive polymer gelatin. Crucially, the investigated formulations were capable of forming self-supporting hydrogels and were able to be sterilized using filtration. **(2)** Moreover, the viscoelastic and mechanical properties were established for each investigated formulation, and the cytocompatibility could be assessed using human fibroblasts**.** **(3)** A wide variety of human stem cell models have been tested, including cardiomyocytes, bone-marrow derived SC, adipose SC, and vascularization model. A modest excursion to the application fields bioprinting and *in vivo* implantation have been taken as well, broadening the understanding of the hydrogels' performance within tissue engineering.

This work also established a workflow protocol for hydrogel modification and subsequent analysis. A thorough investigation of the basic mechanical and structural properties should be standard when presenting a novel hydrogel, however often crucial aspects are disregarded in the literature. This is relevant to further establish the relationship between the biomechanical features of any hydrogel and the observed cell response and tissue development. While GG answers some of the questions and demands of a hydrogel material for tissue engineering, certainly not all issues are addressed even with modification.

REFERENCES

Akkineni, A.R., Elci, B.S., Lode, A., Gelinsky, M., 2022. Addition of High Acyl Gellan Gum to Low Acyl Gellan Gum Enables the Blends 3D Bioprintable. Gels 8, 199. https://doi.org/10.3390/gels8040199

Alakpa, E. V., Jayawarna, V., Lampel, A., Burgess, K. V., West, C.C., Bakker, S.C.J., Roy, S., Javid, N., Fleming, S., Lamprou, D.A., Yang, J., Miller, A., Urquhart, A.J., Frederix, P.W.J.M., Hunt, N.T., Péault, B., Ulijn, R. V., Dalby, M.J., 2016. Tunable Supramolecular Hydrogels for Selection of Lineage-Guiding Metabolites in Stem Cell Cultures. Chem 1, 298–319. https://doi.org/10.1016/j.chempr.2016.07.001

Alavi, S.E., Panah, N., Page, F., Gholami, M., Dastfal, A., Sharma, L.A., Ebrahimi Shahmabadi, H., 2022. Hydrogel-based therapeutic coatings for dental implants. European Polymer Journal 181, 111652. https://doi.org/10.1016/j.eurpolymj.2022.111652

Albrecht, F.B., Dolderer, V., Nellinger, S., Schmidt, F.F., Kluger, P.J., 2022. Gellan Gum Is a Suitable Biomaterial for Manual and Bioprinted Setup of Long-Term Stable, Functional 3D-Adipose Tissue Models. Gels 8, 420. https://doi.org/10.3390/gels8070420

Alizadeh-Sani, M., Ehsani, A., Moghaddas Kia, E., Khezerlou, A., 2019. Microbial gums: introducing a novel functional component of edible coatings and packaging. Applied Microbiology and Biotechnology 2019 103:17 103, 6853–6866. https://doi.org/10.1007/S00253-019-09966-X

Amer, L.D., Saleh, L.S., Walker, C., Thomas, S., Janssen, W.J., Alper, S., Bryant, S.J., 2019. Inflammation via myeloid differentiation primary response gene 88 signaling mediates the fibrotic response to implantable synthetic poly(ethylene glycol) hydrogels. Acta Biomaterialia 100, 105–117. https://doi.org/10.1016/J.ACTBIO.2019.09.043

Anderson, S.B., Lin, C.-C., Kuntzler, D.V., Anseth, K.S., 2011. The performance of human mesenchymal stem cells encapsulated in cell-degradable polymer-peptide hydrogels. Biomaterials 32, 3564–3574. https://doi.org/10.1016/j.biomaterials.2011.01.064

Anjum, F., Ehrbar, M., Lienemann, P.S., Metzger, S., Biernaskie, J., Kallos, M.S., 2016. Enzyme responsive GAG-based natural-synthetic hybrid hydrogel for tunable growth factor delivery and stem cell differentiation. Biomaterials 87, 104–117. https://doi.org/10.1016/j.biomaterials.2016.01.050

Antoine, E.E., Vlachos, P.P., Rylander, M.N., 2014. Review of collagen I hydrogels for bioengineered tissue microenvironments: Characterization of mechanics, structure, and transport. Tissue Engineering - Part B: Reviews 20, 683–696. https://doi.org/10.1089/ten.teb.2014.0086

Balint, R., Cassidy, N.J., Cartmell, S.H., 2014. Conductive polymers: Towards a smart biomaterial for tissue engineering. Acta Biomaterialia 10, 2341–2353. https://doi.org/10.1016/j.actbio.2014.02.015

Balthasar, S., Michaelis, K., Dinauer, N., Briesen, H. von, Kreuter, J., Langer, K., 2005. Preparation and characterisation of antibody modified gelatin nanoparticles as drug

carrier system for uptake in lymphocytes. Biomaterials 26, 2723–2732. https://doi.org/10.1016/j.biomaterials.2004.07.047
Barbucci, R., 2009. Hydrogels - Biological Properties and Applications. Springer, Milan.
Bartnikowski, M., Wellard, R.M., Woodruff, M., Klein, T., 2015. Tailoring Hydrogel Viscoelasticity with Physical and Chemical Crosslinking. Polymers 2015, Vol. 7, Pages 2650-2669 7, 2650–2669. https://doi.org/10.3390/POLYM7121539
Belay, B., Koivisto, J.T., Parraga, J., Koskela, O., Montonen, T., Kellomäki, M., Figueiras, E., Hyttinen, J., 2021. Optical projection tomography as a quantitative tool for analysis of cell morphology and density in 3D hydrogels. Sci Rep 11, 6538. https://doi.org/10.1038/s41598-021-85996-8
Bellini, D., Cencetti, C., Meraner, J., Stoppoloni, D., D'Abusco, A.S., Matricardi, P., 2015. An in situ gelling system for bone regeneration of osteochondral defects. European Polymer Journal 72, 642–650. https://doi.org/10.1016/j.eurpolymj.2015.02.043
Bello, A.B., Kim, Deogil, Kim, Dohyun, Park, H., Lee, S.H., 2020. Engineering and Functionalization of Gelatin Biomaterials: From Cell Culture to Medical Applications. Tissue engineering. Part B, Reviews 26, 164–180. https://doi.org/10.1089/TEN.TEB.2019.0256
Berrier, A.L., Yamada, K.M., 2007. Cell–matrix adhesion. Journal of Cellular Physiology 213, 565–573. https://doi.org/10.1002/jcp.21237
Bjelić, D., Finšgar, M., 2022. Bioactive coatings with anti-osteoclast therapeutic agents for bone implants: Enhanced compliance and prolonged implant life. Pharmacological Research 176, 106060. https://doi.org/10.1016/j.phrs.2022.106060
Blanco-Prieto, M.J., Garbayo, E., 2022. Special issue on the latest advances in regenerative medicine and cancer using drug delivery systems. European Journal of Pharmaceutics and Biopharmaceutics 177, 89–90. https://doi.org/10.1016/j.ejpb.2022.06.010
Bondalapati, S., Ruvinov, E., Kryukov, O., Cohen, S., Brik, A., 2014. Rapid End-Group Modification of Polysaccharides for Biomaterial Applications in Regenerative Medicine. Macromolecular Rapid Communications 35, 1754–1762. https://doi.org/10.1002/marc.201400354
Bonifacio, M.A., Cochis, A., Cometa, S., Scalzone, A., Gentile, P., Procino, G., Milano, S., Scalia, A.C., Rimondini, L., De Giglio, E., 2020. Advances in cartilage repair: The influence of inorganic clays to improve mechanical and healing properties of antibacterial Gellan gum-Manuka honey hydrogels. Materials Science and Engineering C 108, 110444. https://doi.org/10.1016/j.msec.2019.110444
Bordbar-Khiabani, A., Gasik, M., 2022. Smart Hydrogels for Advanced Drug Delivery Systems. International Journal of Molecular Sciences 23, 3665. https://doi.org/10.3390/ijms23073665
Bouhadir, K.H., Hausman, D.S., Mooney, D.J., 1999. Synthesis of cross-linked poly(aldehyde guluronate) hydrogels. Polymer 40, 3575–3584. https://doi.org/10.1016/S0032-3861(98)00550-3
Bouhrira, N., Galie, P.A., Janmey, P.A., 2019. Hyaluronan Disrupts Cardiomyocyte Organization within 3D Fibrin-Based Hydrogels. Biophysical Journal 116, 1340–1347. https://doi.org/10.1016/J.BPJ.2019.02.018
Brandl, F., Sommer, F., Goepferich, A., 2007. Rational design of hydrogels for tissue engineering: Impact of physical factors on cell behavior. Biomaterials 28, 134–146. https://doi.org/10.1016/j.biomaterials.2006.09.017

Broguiere, N., Isenmann, L., Hirt, C., Ringel, T., Placzek, S., Cavalli, E., Ringnalda, F., Villiger, L., Züllig, R., Lehmann, R., Rogler, G., Heim, M.H., Schüler, J., Zenobi-Wong, M., Schwank, G., 2018. Growth of Epithelial Organoids in a Defined Hydrogel. Advanced Materials 30, 1801621. https://doi.org/10.3929/ethz-b-000302457

Bryant, S.J., Anseth, K.S., 2003. Controlling the spatial distribution of ECM components in degradable PEG hydrogels for tissue engineering cartilage. Journal of Biomedical Materials Research Part A 64A, 70–79. https://doi.org/10.1002/JBM.A.10319

Caddeo, S., Boffito, M., Sartori, S., 2017. Tissue Engineering Approaches in the Design of Healthy and Pathological In Vitro Tissue Models. Frontiers in Bioengineering and Biotechnology 5. https://doi.org/10.3389/fbioe.2017.00040

Caliari, S.R., Burdick, J.A., 2016. A practical guide to hydrogels for cell culture. Nature Methods 13, 405–414. https://doi.org/10.1038/nmeth.3839

Callister, W.D., Rethwisch, D.G., 2007. Materials science and engineering : an introduction, 7th edition. ed. John Wiley & Sons, Inc.

Cao, N., Chen, X.B., Schreyer, D.J., 2012. Influence of Calcium Ions on Cell Survival and Proliferation in the Context of an Alginate Hydrogel. ISRN Chemical Engineering 2012, 1–9. https://doi.org/10.5402/2012/516461

Castillo Diaz, L.A., Elsawy, M., Saiani, A., Gough, J.E., Miller, A.F., 2016. Osteogenic differentiation of human mesenchymal stem cells promotes mineralization within a biodegradable peptide hydrogel. Journal of Tissue Engineering 7. https://doi.org/10.1177/2041731416649789

Chandrasekaran, R., Millane, R.P., Arnott, S., Atkins, E.D.T., 1988. The crystal structure of gellan. Carbohydrate Research 175, 1–15. https://doi.org/10.1016/0008-6215(88)80151-4

Chang, C.Y., Johnson, H.C., Babb, O., Fishel, M.L., Lin, C.C., 2021. Biomimetic stiffening of cell-laden hydrogels via sequential thiol-ene and hydrazone click reactions. Acta Biomaterialia 130, 161–171. https://doi.org/10.1016/j.actbio.2021.05.054

Chang, H.T., Heuer, R.A., Oleksijew, A.M., Coots, K.S., Roque, C.B., Nella, K.T., McGuire, T.L., Matsuoka, A.J., 2020. An engineered three-dimensional stem cell niche in the inner ear by applying a nanofibrillar cellulose hydrogel with a sustained-release neurotrophic factor delivery system. Acta Biomaterialia 108, 111–127. https://doi.org/10.1016/J.ACTBIO.2020.03.007

Chhabra, R.P., Richardson, J.F., 2008. Chapter 2 - Rheometry for non-Newtonian fluids, in: Chhabra, R.P., Richardson, J.F. (Eds.), Non-Newtonian Flow and Applied Rheology (Second Edition). Butterworth-Heinemann, Oxford, pp. 56–109. https://doi.org/10.1016/B978-0-7506-8532-0.00002-0

Choi, J.S., Harley, B.A.C., 2012. The combined influence of substrate elasticity and ligand density on the viability and biophysical properties of hematopoietic stem and progenitor cells. Biomaterials 33, 4460–4468. https://doi.org/10.1016/j.biomaterials.2012.03.010

Choi, K., Kuhn, J.L., Ciarelli, M.J., Goldstein, S.A., 1990. The elastic moduli of human subchondral, trabecular, and cortical bone tissue and the size-dependency of cortical bone modulus. Journal of Biomechanics 23, 1103–1113. https://doi.org/10.1016/0021-9290(90)90003-L

Chopra, P., Logun, M.T., White, E.M., Lu, W., Locklin, J., Karumbaiah, L., Boons, G.J., 2019. Fully Synthetic Heparan Sulfate-Based Neural Tissue Construct That Maintains

the Undifferentiated State of Neural Stem Cells. ACS chemical biology 14, 1921. https://doi.org/10.1021/ACSCHEMBIO.9B00401

Chouhan, G., Moakes, R.J.A., Esmaeili, M., Hill, L.J., DeCogan, F., Hardwicke, J., Rauz, S., Logan, A., Grover, L.M., 2019. A self-healing hydrogel eye drop for the sustained delivery of decorin to prevent corneal scarring. Biomaterials 210, 41–50. https://doi.org/10.1016/J.BIOMATERIALS.2019.04.013

Christoffersson, J., Aronsson, C., Jury, M., Selegård, R., Aili, D., Mandenius, C.F., 2018. Fabrication of modular hyaluronan-PEG hydrogels to support 3D cultures of hepatocytes in a perfused liver-on-a-chip device. Biofabrication 11, 015013. https://doi.org/10.1088/1758-5090/AAF657

Crosby, C.O., Zoldan, J., 2019. Mimicking the physical cues of the ECM in angiogenic biomaterials. Regenerative Biomaterials 6, 61–73. https://doi.org/10.1093/rb/rbz003

Cumpstey, I., 2013. Chemical Modification of Polysaccharides 2018, 27. https://doi.org/10.1155/2013/417672

da Silva, L.P., Jha, A.K., Correlo, V.M., Marques, A.P., Reis, R.L., Healy, K.E., 2018. Gellan Gum Hydrogels with Enzyme-Sensitive Biodegradation and Endothelial Cell Biorecognition Sites. Advanced Healthcare Materials 7, 1–12. https://doi.org/10.1002/adhm.201700686

Dai, L., Zhang, L., Wang, B., Yang, B., Khan, I., Khan, A., Ni, Y., 2017. Multifunctional self-assembling hydrogel from guar gum. Chemical Engineering Journal 330, 1044–1051. https://doi.org/10.1016/j.cej.2017.08.041

DeAngelis, P.L., 2002. Evolution of glycosaminoglycans and their glycosyltransferases: Implications for the extracellular matrices of animals and the capsules of pathogenic bacteria. The Anatomical Record 268, 317–326. https://doi.org/10.1002/ar.10163

Desai, R.M., Koshy, S.T., Hilderbrand, S.A., Mooney, D.J., Joshi, N.S., 2015. Versatile click alginate hydrogels crosslinked via tetrazine–norbornene chemistry. Biomaterials 50, 30–37. https://doi.org/10.1016/j.biomaterials.2015.01.048

Destruel, P.-L., Zeng, N., Seguin, J., Douat, S., Rosa, F., Brignole-Baudouin, F., Dufaÿ, S., Dufaÿ-Wojcicki, A., Maury, M., Mignet, N., Boudy, V., 2020. Novel in situ gelling ophthalmic drug delivery system based on gellan gum and hydroxyethylcellulose: Innovative rheological characterization, in vitro and in vivo evidence of a sustained precorneal retention time. International Journal of Pharmaceutics 574, 118734. https://doi.org/10.1016/j.ijpharm.2019.118734

Dinauer, N., Balthasar, S., Weber, C., Kreuter, J., Langer, K., Briesen, H.V., 2005. Selective targeting of antibody-conjugated nanoparticles to leukemic cells and primary T-lymphocytes. Biomaterials 26, 5898–5906. https://doi.org/10.1016/j.biomaterials.2005.02.038

Ding, Y.-W., Zhang, X.-W., Mi, C.-H., Qi, X.-Y., Zhou, J., Wei, D.-X., 2023. Recent advances in hyaluronic acid-based hydrogels for 3D bioprinting in tissue engineering applications. Smart Materials in Medicine 4, 59–68. https://doi.org/10.1016/j.smaim.2022.07.003

Discher, D.E., Janmey, P., Wang, Y., 2005. Tissue Cells Feel and Respond to the Stiffness of Their Substrate. Science 310, 1139–1143. https://doi.org/10.1126/science.1116995

Dominici, M., Blanc, K.L., Mueller, I., Slaper-Cortenbach, I., Marini, F.C., Krause, D.S., Deans, R.J., Keating, A., Prockop, D.J., Horwitz, E.M., 2006. Minimal criteria for defining multipotent mesenchymal stromal cells. The International Society for

Cellular Therapy position statement. Cytotherapy 8, 315–317. https://doi.org/10.1080/14653240600855905
dos Santos, B.P., Garbay, B., Fenelon, M., Rosselin, M., Garanger, E., Lecommandoux, S., Oliveira, H., Amédée, J., 2019. Development of a cell-free and growth factor-free hydrogel capable of inducing angiogenesis and innervation after subcutaneous implantation. Acta Biomaterialia 99, 154–167. https://doi.org/10.1016/J.ACTBIO.2019.08.028
Doube, M., Kłosowski, M.M., Arganda-Carreras, I., Cordelières, F.P., Dougherty, R.P., Jackson, J.S., Schmid, B., Hutchinson, J.R., Shefelbine, S.J., 2010. BoneJ: Free and extensible bone image analysis in ImageJ. Bone 47, 1076–1079. https://doi.org/10.1016/j.bone.2010.08.023
Douglas, T.E.L., Wlodarczyk, M., Pamula, E., Declercq, H.A., Mulder, E.L.W. de, Bucko, M.M., Balcaen, L., Vanhaecke, F., Cornelissen, R., Dubruel, P., Jansen, J.A., Leeuwenburgh, S.C.G., 2012. Enzymatic mineralization of gellan gum hydrogel for bone tissue-engineering applications and its enhancement by polydopamine. Journal of Tissue Engineering and Regenerative Medicine 8, 906–918. https://doi.org/10.1002/term.1616
Drury, J.L., Mooney, D.J., 2003. Hydrogels for tissue engineering: scaffold design variables and applications. Biomaterials. https://doi.org/10.1016/S0142-9612(03)00340-5
DuBois, Michel., Gilles, K.A., Hamilton, J.K., Rebers, P.A., Smith, F., 2002. Colorimetric Method for Determination of Sugars and Related Substances. Microbial cell factories 8, 59. https://doi.org/10.1021/AC60111A017
Ellman, G.L., 1959. Tissue sulfhydryl groups. Archives of Biochemistry and Biophysics 82, 70–77. https://doi.org/10.1016/0003-9861(59)90090-6
Engler, A.J., Sen, S., Sweeney, H.L., Discher, D.E., 2006. Matrix Elasticity Directs Stem Cell Lineage Specification. Cell 126, 677–689. https://doi.org/10.1016/j.cell.2006.06.044
Ermis, M., 2021. Photo-crosslinked gelatin methacrylate hydrogels with mesenchymal stem cell and endothelial cell spheroids as soft tissue substitutes. Journal of Materials Research 36, 176–190. https://doi.org/10.1557/s43578-020-00091-4
Evageliou, V., Mazioti, M., Mandala, I., Komaitis, M., 2010. Compression of gellan gels. Part II: Effect of sugars. Food Hydrocolloids 24, 392–397. https://doi.org/10.1016/j.foodhyd.2009.11.005
Eyrich, D., Brandl, F., Appel, B., Wiese, H., Maier, G., Wenzel, M., Staudenmaier, R., Goepferich, A., Blunk, T., 2007. Long-term stable fibrin gels for cartilage engineering. Biomaterials 28, 55–65. https://doi.org/10.1016/J.BIOMATERIALS.2006.08.027
Feketshane, Z., Alven, S., Aderibigbe, B.A., 2022. Gellan Gum in Wound Dressing Scaffolds. Polymers 14, 4098. https://doi.org/10.3390/polym14194098
Ferris, C.J., Stevens, L.R., Gilmore, K.J., Mume, E., Greguric, I., Kirchmajer, D.M., Wallace, G.G., In Het Panhuis, M., 2015. Peptide modification of purified gellan gum. Journal of Materials Chemistry B 3, 1106–1115. https://doi.org/10.1039/c4tb01727g
Fialho, A.M., Moreira, L.M., Granja, A.T., Popescu, A.O., Hoffmann, K., Sá-Correia, I., 2008. Occurrence, production, and applications of gellan: Current state and perspectives. Applied Microbiology and Biotechnology 79, 889–900. https://doi.org/10.1007/s00253-008-1496-0
Fu, M., Liang, Y., Lv, X., Li, C., Yang, Y.Y., Yuan, P., Ding, X., 2021. Recent advances in hydrogel-based anti-infective coatings. Journal of Materials Science & Technology 85, 169–183. https://doi.org/10.1016/j.jmst.2020.12.070

Gantar, A., Da Silva, L.P., Oliveira, J.M., Marques, A.P., Correlo, V.M., Novak, S., Reis, R.L., 2014. Nanoparticulate bioactive-glass-reinforced gellan-gum hydrogels for bone-tissue engineering. Materials Science and Engineering: C 43, 27–36. https://doi.org/10.1016/J.MSEC.2014.06.045

Ghobril, C., Grinstaff, M.W., 2015. The chemistry and engineering of polymeric hydrogel adhesives for wound closure: a tutorial. Chemical Society Reviews 44, 1820–1835. https://doi.org/10.1039/C4CS00332B

Giavasis, I., Harvey, L.M., McNeil, B., 2000. Gellan gum. Critical Reviews in Biotechnology 20, 177–211. https://doi.org/10.1080/07388550008984169

Glaser, D.E., Curtis, M.B., Sariano, P.A., Rollins, Z.A., Shergill, B.S., Anand, A., Deely, A.M., Shirure, V.S., Anderson, L., Lowen, J.M., Ng, N.R., Weilbaecher, K., Link, D.C., George, S.C., 2022. Organ-on-a-chip model of vascularized human bone marrow niches. Biomaterials 280, 121245. https://doi.org/10.1016/J.BIOMATERIALS.2021.121245

Gong, Q., Zhao, Y., Qian, T., Wang, H., Li, Z., 2022. Functionalized hydrogels in ophthalmic applications: Ocular inflammation, corneal injuries, vitreous substitutes and intravitreal injection. Materials & Design 224, 111277. https://doi.org/10.1016/j.matdes.2022.111277

Gong, Y., Wang, C., Lai, R.C., Su, K., Zhang, F., Wang, D.-A., 2009. An improved injectable polysaccharide hydrogel: modified gellan gum for long-term cartilage regenerationin vitro. Journal of Materials Chemistry 19, 1968–1977. https://doi.org/10.1039/B818090C

Goyal, R., Tripathi, S.K., Tyagi, S., Ram, K.R., Ansari, K.M., Shukla, Y., Chowdhuri, D.K., Kumar, P., Gupta, K.C., 2011. Gellan gum blended PEI nanocomposites as gene delivery agents: Evidences from in vitro and in vivo studies. European Journal of Pharmaceutics and Biopharmaceutics 79, 3–14. https://doi.org/10.1016/j.ejpb.2011.01.009

Gu, X., 2022. Recent Progress in Biomaterials-Tissue Engineering. Engineering 13, 1. https://doi.org/10.1016/j.eng.2022.04.005

Guo, Q., Ai, L., Cui, S.W., 2018. Strategies for Structural Characterization of Polysaccharides 1–7. https://doi.org/10.1007/978-3-319-96370-9_1

Guo, W., Douma, L., Hu, M.H., Eglin, D., Alini, M., Secerovic, A., Grad, S., Peng, X., Zou, X., D'Este, M., Peroglio, M., Šećerović, A., Grad, S., Peng, X., Zou, X., D'Este, M., Peroglio, M., 2021. Hyaluronic acid-based interpenetrating network hydrogel as a cell carrier for nucleus pulposus repair. Carbohydrate Polymers 277, 118828. https://doi.org/10.1016/j.carbpol.2021.118828

Haimi, S., Suuriniemi, N., Haaparanta, A.-M., Ellä, V., Lindroos, B., Huhtala, H., Räty, S., Kuokkanen, H., Sándor, G.K., Kellomäki, M., Miettinen, S., Suuronen, R., 2009. Growth and osteogenic differentiation of adipose stem cells on PLA/bioactive glass and PLA/beta-TCP scaffolds. Tissue engineering. Part A 15, 1473–1480. https://doi.org/10.1089/ten.tea.2008.0241

Hao, Y., Zheng, W., Sun, Z., Zhang, D., Sui, K., Shen, P., Li, P., Zhou, Q., 2021. Marine polysaccharide-based composite hydrogels containing fucoidan: Preparation, physicochemical characterization, and biocompatible evaluation. International Journal of Biological Macromolecules 183, 1978–1986. https://doi.org/10.1016/J.IJBIOMAC.2021.05.190

Harimawan, A., Ting, Y.P., 2016. Investigation of extracellular polymeric substances (EPS) properties of P. aeruginosa and B. subtilis and their role in bacterial adhesion. Colloids

and Surfaces B: Biointerfaces 146, 459–467. https://doi.org/10.1016/J.COLSURFB.2016.06.039
Hayflick, L., Moorhead, P.S., 1961. The serial cultivation of human diploid cell strains. Experimental Cell Research 25, 585–621. https://doi.org/10.1016/0014-4827(61)90192-6
He, Y., Yang, F., Zhao, H., Gao, Q., Xia, B., Fu, J., 2016a. Research on the printability of hydrogels in 3D bioprinting. Scientific reports 6, 29977. https://doi.org/10.1038/srep29977
He, Y., Yang, F., Zhao, H., Gao, Q., Xia, B., Fu, J., 2016b. Research on the printability of hydrogels in 3D bioprinting. Scientific reports 6, 29977. https://doi.org/10.1038/srep29977
Hermanson, G.T., 2013. Bioconjugate Techniques: Third Edition. Bioconjugate Techniques: Third Edition 1–1146. https://doi.org/10.1016/C2009-0-64240-9
Hofman, Anton H, Van Hees, Ilse A, Yang, Juan, Kamperman, Marleen, Hofman, A H, Van Hees, I A, Kamperman, M, Yang, J, 2018. Bioinspired Underwater Adhesives by Using the Supramolecular Toolbox. Advanced Materials 30, 1704640. https://doi.org/10.1002/ADMA.201704640
Hossain, K.S., Nishinari, K., 2009. Chain Release Behavior of Gellan Gels, in: Gels: Structures, Properties, and Functions. Springer, Berlin, Heidelberg, pp. 177–186. https://doi.org/10.1007/978-3-642-00865-8_25
Hupa, L., 2018. 1 - Composition-property relations of bioactive silicate glasses, in: Ylänen, H. (Ed.), Bioactive Glasses (Second Edition), Woodhead Publishing Series in Biomaterials. Woodhead Publishing, pp. 1–35. https://doi.org/10.1016/B978-0-08-100936-9.00001-0
Hyon, S.-H., Nakajima, N., Sugai, H., Matsumura, K., 2014. Low cytotoxic tissue adhesive based on oxidized dextran and epsilon-poly-l-lysine. Journal of Biomedical Materials Research Part A 102, 2511–2520. https://doi.org/10.1002/jbm.a.34923
Hyun, K., Kim, S.H., Ahn, K.H., Lee, S.J., 2002. Large amplitude oscillatory shear as a way to classify the complex fluids. Journal of Non-Newtonian Fluid Mechanics 107, 51–65. https://doi.org/10.1016/S0377-0257(02)00141-6
Hyung, S., Lee, S.R., Kim, J., Kim, Y., Kim, S., Kim, H.N., Jeon, N.L., 2021. A 3D disease and regeneration model of peripheral nervous system–on–a–chip. Science Advances 7, 9749–9778. https://doi.org/10.1126/sciadv.abd9749
ISO 10993-1, 2009. ISO 10993 Biological evaluation of medical devices. Part 1: Evaluation and Testing within a Risk Management Process, EN ISO 10993-1:2009 (E).
ISO 10993-5, 2009. ISO 10993 Biological evaluation of medical devices. Part 5 Tests for in vitro cytotoxicity.
Iyengar, A., Atluri, P., 2022. Commentary: A multilayered stem cell sandwich? The Journal of Thoracic and Cardiovascular Surgery 163, e273–e274. https://doi.org/10.1016/j.jtcvs.2020.05.020
Jalili-Firoozinezhad, S., Miranda, C.C., Cabral, J.M.S., 2021. Modeling the Human Body on Microfluidic Chips. Trends in Biotechnology 39, 838–852. https://doi.org/10.1016/J.TIBTECH.2021.01.004
Jarrell, D.K., Vanderslice, E.J., Lennon, M.L., Lyons, A.C., VeDepo, M.C., Jacot, J.G., 2021. Increasing salinity of fibrinogen solvent generates stable fibrin hydrogels for cell delivery or tissue engineering. PLOS ONE 16, e0239242. https://doi.org/10.1371/JOURNAL.PONE.0239242

Johnson, J.A., Finn, M.G., Koberstein, J.T., Turro, N.J., 2007. Synthesis of Photocleavable Linear Macromonomers by ATRP and Star Macromonomers by a Tandem ATRP−Click Reaction: Precursors to Photodegradable Model Networks. Macromolecules 40, 3589–3598. https://doi.org/10.1021/MA062862B

Jongprasitkul, H., Turunen, S., Parihar, V.S., Annurakshita, S., Kellomäki, M., 2021. Photocross-linkable Methacrylated Polypeptides and Polysaccharides for Casting, Injecting, and 3D Fabrication. Biomacromolecules 22, 481–493. https://doi.org/10.1021/acs.biomac.0c01322

Joy, J., Aid-Launais, R., Pereira, J., Pavon-Djavid, G., Ray, A.R., Letourneur, D., Meddahi-Pellé, A., Gupta, B., 2020. Gelatin-polytrimethylene carbonate blend based electrospun tubular construct as a potential vascular biomaterial. Materials Science and Engineering: C 106, 110178. https://doi.org/10.1016/J.MSEC.2019.110178

Justice, B.A., Badr, N.A., Felder, R.A., 2009. 3D cell culture opens new dimensions in cell-based assays. Drug Discovery Today 14, 102–107. https://doi.org/10.1016/j.drudis.2008.11.006

Kalke, E., 2021. Development of organ-on-chip devices for perfusable 3D microvasculature and co-culture applications (Master Thesis). Tampere University, Tampere, Finland.

Kamath, K.R., Park, K., 1993. Biodegradable hydrogels in drug delivery. Advanced Drug Delivery Reviews 11, 59–84. https://doi.org/10.1016/0169-409X(93)90027-2

Karvinen, J., Joki, T., Ylä-Outinen, L., Koivisto, J.T., Narkilahti, S., Kellomäki, M., 2018. Soft hydrazone crosslinked hyaluronan- and alginate-based hydrogels as 3D supportive matrices for human pluripotent stem cell-derived neuronal cells. Reactive and Functional Polymers 124, 29–39. https://doi.org/10.1016/j.reactfunctpolym.2017.12.019

Karvinen, J., Koivisto, J.T., Jönkkäri, I., Kellomäki, M., 2017. The production of injectable hydrazone crosslinked gellan gum-hyaluronan-hydrogels with tunable mechanical and physical properties. Journal of the Mechanical Behavior of Biomedical Materials 71, 383–391. https://doi.org/10.1016/j.jmbbm.2017.04.006

Ke, C.-J., Chiu, K.-H., Chen, C.-Y., Huang, C.-H., Yao, C.-H., 2021. Alginate-gelatin based core-shell capsule enhances the osteogenic potential of human osteoblast-like MG-63 cells. Materials & Design 210, 110109. https://doi.org/10.1016/J.MATDES.2021.110109

Khan, M., Koivisto, J.T., Kellomäki, M., Kellomaki, M., and, B., 2022. Injectable and self-healing biobased composite hydrogels as future anticancer therapeutic biomaterials. Nano Select. https://doi.org/10.1002/NANO.202100354

Khare, P., Chogale, M.M., Kakade, P., Patravale, V.B., 2022. Gellan gum–based in situ gelling ophthalmic nanosuspension of Posaconazole. Drug Deliv. and Transl. Res. 12, 2920–2935. https://doi.org/10.1007/s13346-022-01155-0

Kim, W.J., Lee, H., Ji Roh, E., Bae An, S., Han, I.B., Hyung Kim, G., 2022. A multicellular bioprinted cell construct for vascularized bone tissue regeneration. Chemical Engineering Journal 431, 133882. https://doi.org/10.1016/J.CEJ.2021.133882

Kirchmajer, D.M., Steinhoff, B., Warren, H., Clark, R., In Het Panhuis, M., 2014. Enhanced gelation properties of purified gellan gum. Carbohydrate Research 388, 125–129. https://doi.org/10.1016/j.carres.2014.02.018

Kirschner, C.M., Anseth, K.S., 2013. Hydrogels in healthcare: From static to dynamic material microenvironments. Acta Materialia, The Diamond Jubilee Issue 61, 931–944. https://doi.org/10.1016/j.actamat.2012.10.037

Kocen, R., Gasik, M., Gantar, A., Novak, S., 2017. Viscoelastic behaviour of hydrogel-based composites for tissue engineering under mechanical load. Biomedical materials (Bristol) 12, 25004. https://doi.org/10.1088/1748-605x/aa5b00

Koivisto, J.T., Joki, T., Parraga, J.E., Pääkkönen, R., Ylä-Outinen, L., Salonen, L., Peltola, M., Ihalainen, T.O., Narkilahti, S., Kellomäki, M., 2017. Bioamine-crosslinked gellan gum hydrogel for neural tissue engineering. Biomedical Materials 12, 25014. https://doi.org/10.1088/1748-605X/aa62b0

Koivusalo, L., Karvinen, J., Sorsa, E., Jönkkäri, I., Väliaho, J., Kallio, P., Ilmarinen, T., Miettinen, S., Skottman, H., Kellomäki, M., 2018. Hydrazone crosslinked hyaluronan-based hydrogels for therapeutic delivery of adipose stem cells to treat corneal defects. Materials Science and Engineering C 85, 68–78. https://doi.org/10.1016/j.msec.2017.12.013

Kraehenbuehl, T.P., Ferreira, L.S., Zammaretti, P., Hubbell, J.A., Langer, R., 2009. Cell-responsive hydrogel for encapsulation of vascular cells. Biomaterials 30, 4318–4324. https://doi.org/10.1016/j.biomaterials.2009.04.057

Kristiansen, K.A., Potthast, A., Christensen, B.E., 2010. Periodate oxidation of polysaccharides for modification of chemical and physical properties. Carbohydrate Research, Special Issue: Selected Papers from the 15th European Carbohydrate Symposium, Vienna 2009 345, 1264–1271. https://doi.org/10.1016/j.carres.2010.02.011

Kubinová, Š., Horák, D., Vaněček, V., Plichta, Z., Proks, V., Syková, E., 2014. The use of new surface-modified poly(2-hydroxyethyl methacrylate) hydrogels in tissue engineering: Treatment of the surface with fibronectin subunits versus Ac-CGGASIKVAVS-OH, cysteine, and 2-mercaptoethanol modification. Journal of Biomedical Materials Research Part A 102, 2315–2323. https://doi.org/10.1002/jbm.a.34910

Kurisawa, M., Chung, J.E., Yang, Y.Y., Gao, S.J., Uyama, H., 2005. Injectable biodegradable hydrogels composed of hyaluronic acid–tyramine conjugates for drug delivery and tissue engineering. Chemical Communications 4312–4314. https://doi.org/10.1039/B506989K

Kyburz, K.A., Anseth, K.S., 2015. Synthetic Mimics of the Extracellular Matrix: How Simple is Complex Enough? Annals of biomedical engineering 43, 489–500. https://doi.org/10.1007/s10439-015-1297-4

Kyllönen, L., Haimi, S., Mannerström, B., Huhtala, H., Rajala, K.M., Skottman, H., Sándor, G.K., Miettinen, S., 2013. Effects of different serum conditions on osteogenic differentiation of human adipose stem cells in vitro. Stem cell research & therapy 4, 17. https://doi.org/10.1186/scrt165

Langer, R., Vacanti, J.P., 1993. Tissue Engineering. Science 260, 920–926. https://doi.org/10.1126/science.8493529

Larson, R.G., 1999. The Structure and Rheology of Complex Fluids, Topics in Chemical Engineering. Oxford University Press Inc.

Lee, F., Kurisawa, M., 2013. Formation and stability of interpenetrating polymer network hydrogels consisting of fibrin and hyaluronic acid for tissue engineering. Acta Biomaterialia 9, 5143–5152. https://doi.org/10.1016/J.ACTBIO.2012.08.036

Lee, J.W., An, H., Lee, K.Y., 2017. Introduction of N-cadherin-binding motif to alginate hydrogels for controlled stem cell differentiation. Colloids and Surfaces B: Biointerfaces 155, 229–237. https://doi.org/10.1016/j.colsurfb.2017.04.014

Lee, W., Choi, J.H., Lee, J., Youn, J., Kim, W., Jeon, G., Lee, S.W., Song, J.E., Khang, G., 2021. Dopamine-Functionalized Gellan Gum Hydrogel as a Candidate Biomaterial for a Retinal Pigment Epithelium Cell Delivery System. ACS Applied Bio Materials 4, 1771–1782. https://doi.org/10.1021/acsabm.0c01516

Lee, W., Debasitis, J.C., Lee, V.K., Lee, J.-H., Fischer, K., Edminster, K., Park, J.-K., Yoo, S.-S., 2009. Multi-layered culture of human skin fibroblasts and keratinocytes through three-dimensional freeform fabrication. Biomaterials 30, 1587–1595. https://doi.org/10.1016/j.biomaterials.2008.12.009

Leijten, J., Seo, J., Yue, K., Trujillo-de Santiago, G., Tamayol, A., Ruiz-Esparza, G.U., Shin, S.R., Sharifi, R., Noshadi, I., Álvarez, M.M., Zhang, Y.S., Khademhosseini, A., 2017. Spatially and temporally controlled hydrogels for tissue engineering. Materials Science and Engineering R: Reports 119, 1–35. https://doi.org/10.1016/j.mser.2017.07.001

Leppiniemi, J., Lahtinen, P., Paajanen, A., Mahlberg, R., Pinomaa, T., Pajari, H., Vikholm-Lundin, I., Pursula, P., 2017. 3D-Printable Bioactivated Nanocellulose-Alginate Hydrogels. ACS Applied Materials & Interfaces. https://doi.org/10.1021/acsami.7b02756

Leppiniemi, J., Mutahir, Z., Dulebo, A., Mikkonen, P., Nuopponen, M., Turkki, P., Hytönen, V.P., 2021. Avidin-Conjugated Nanofibrillar Cellulose Hydrogel Functionalized with Biotinylated Fibronectin and Vitronectin Promotes 3D Culture of Fibroblasts. Biomacromolecules 22, 4122–4137. https://doi.org/10.1021/acs.biomac.1c00579

Levental, I., Georges, P.C., Janmey, P.A., 2007. Soft biological materials and their impact on cell function. Soft Matter 3, 299–306. https://doi.org/10.1039/B610522J

Li, S., Cong, Y., Fu, J., 2021. Tissue adhesive hydrogel bioelectronics. Journal of Materials Chemistry B 9, 4423–4443. https://doi.org/10.1039/D1TB00523E

Li, S., Nih, L.R., Bachman, H., Fei, P., Li, Y., Nam, E., Dimatteo, R., Carmichael, S.T., Barker, T.H., Segura, T., 2017. Hydrogels with precisely controlled integrin activation dictate vascular patterning and permeability. Nature Materials 16, 953–961. https://doi.org/10.1038/nmat4954

Li, X., Katsanevakis, E., Liu, X., Zhang, N., Wen, X., 2012. Engineering neural stem cell fates with hydrogel design for central nervous system regeneration. Progress in Polymer Science 37, 1105–1129. https://doi.org/10.1016/j.progpolymsci.2012.02.004

Liaw, C.Y., Ji, S., Guvendiren, M., 2018. Engineering 3D Hydrogels for Personalized In Vitro Human Tissue Models. Advanced Healthcare Materials 7, 1701165. https://doi.org/10.1002/ADHM.201701165

Liu, J., Chuah, Y.J., Fu, J., Zhu, W., Wang, D.A., 2019. Co-culture of human umbilical vein endothelial cells and human bone marrow stromal cells into a micro-cavitary gelatin-methacrylate hydrogel system to enhance angiogenesis. Materials Science and Engineering: C 102, 906–916. https://doi.org/10.1016/J.MSEC.2019.04.089

Liu, J., Qu, S., Suo, Z., Yang, W., 2021. Functional hydrogel coatings. National Science Review 8, nwaa254. https://doi.org/10.1093/nsr/nwaa254

Liu, M., Zeng, X., Ma, C., Yi, H., Ali, Z., Mou, X., Li, S., Deng, Y., He, N., 2017. Injectable hydrogels for cartilage and bone tissue engineering. Bone Res 5, 1–20. https://doi.org/10.1038/boneres.2017.14

Liu, Z., Yao, P., 2015. Injectable thermo-responsive hydrogel composed of xanthan gum and methylcellulose double networks with shear-thinning property. Carbohydrate Polymers 132, 490–498. https://doi.org/10.1016/J.CARBPOL.2015.06.013

Lu, Y., Zhao, X., Fang, S., 2019. Characterization, Antimicrobial Properties and Coatings Application of Gellan Gum Oxidized with Hydrogen Peroxide. Foods 8, 31. https://doi.org/10.3390/foods8010031

Luo, B.H., Carman, C.V., Springer, T.A., 2007. Structural Basis of Integrin Regulation and Signaling. http://dx.doi.org/10.1146/annurev.immunol.25.022106.141618 25, 619–647. https://doi.org/10.1146/ANNUREV.IMMUNOL.25.022106.141618

Macková, H., Plichta, Z., Proks, V., Kotelnikov, I., Kučka, J., Hlídková, H., Horák, D., Kubinová, Š., Jiráková, K., 2016. RGDS- and SIKVAVS-Modified Superporous Poly(2-hydroxyethyl methacrylate) Scaffolds for Tissue Engineering Applications. Macromolecular Bioscience 16, 1621–1631. https://doi.org/10.1002/mabi.201600159

Madl, C.M., Heilshorn, S.C., 2018. Engineering Hydrogel Microenvironments to Recapitulate the Stem Cell Niche. https://doi.org/10.1146/annurev-bioeng-062117-120954 20, 21–47. https://doi.org/10.1146/ANNUREV-BIOENG-062117-120954

Magnusdottir, A., Vidarsson, H., Björnsson, J.M., Örvar, B.L., 2013. Barley grains for the production of endotoxin-free growth factors. Trends in Biotechnology 31, 572–580. https://doi.org/10.1016/J.TIBTECH.2013.06.002

Mahmood, H., Khan, I.U., Asif, M., Khan, R.U., Asghar, S., Khalid, I., Khalid, S.H., Irfan, M., Rehman, F., Shahzad, Y., Yousaf, A.M., Younus, A., Niazi, Z.R., Asim, M., 2021. In vitro and in vivo evaluation of gellan gum hydrogel films: Assessing the co impact of therapeutic oils and ofloxacin on wound healing. International Journal of Biological Macromolecules 166, 483–495. https://doi.org/10.1016/j.ijbiomac.2020.10.206

Malaprade, L., 1928. Action of polyalcohols on periodic acid. Analytical application. Bulletin de la Societe Chimique de France 43, 683–696.

Martens, P., Metters, A.T., Anseth, K.S., Bowman, C.N., 2001. A Generalized Bulk-Degradation Model for Hydrogel Networks Formed from Multivinyl Cross-linking Molecules. Journal of Physical Chemistry B 105, 5131–5138. https://doi.org/10.1021/JP004102N

Martínez-Sanz, E., Ossipov, D.A., Hilborn, J., Larsson, S., Jonsson, K.B., Varghese, O.P., 2011. Bone reservoir: Injectable hyaluronic acid hydrogel for minimal invasive bone augmentation. Journal of Controlled Release 152, 232–240. https://doi.org/10.1016/J.JCONREL.2011.02.003

Mason, B.N., Starchenko, A., Williams, R.M., Bonassar, L.J., Reinhart-King, C.A., 2013. Tuning three-dimensional collagen matrix stiffness independently of collagen concentration modulates endothelial cell behavior. Acta Biomaterialia 9, 4635–4644. https://doi.org/10.1016/J.ACTBIO.2012.08.007

Matricardi, P., Cencetti, C., Ria, R., Alhaique, F., Coviello, T., 2009. Preparation and characterization of novel Gellan gum hydrogels suitable for modified drug release. Molecules 14, 3376–3391. https://doi.org/10.3390/molecules14093376

McKee, C., Chaudhry, G.R., 2017. Advances and challenges in stem cell culture. Colloids and Surfaces B: Biointerfaces 159, 62–77. https://doi.org/10.1016/j.colsurfb.2017.07.051

Ménard, M., Dusseault, J., Langlois, G., Baille, W.E., Tam, S.K., Yahia, L., Zhu, X.X., Hallé, J.P., 2010. Role of protein contaminants in the immunogenicity of alginates. Journal of Biomedical Materials Research - Part B Applied Biomaterials 93, 333–340. https://doi.org/10.1002/jbm.b.31570

Mergy, J., Fournier, A., Hachet, E., Auzély-Velty, R., 2012. Modification of polysaccharides via thiol-ene chemistry: A versatile route to functional biomaterials. Journal of Polymer Science Part A: Polymer Chemistry 50, 4019–4028. https://doi.org/10.1002/pola.26201

Meybodi, Z.E., Imani, M., Atai, M., 2013. Kinetics of dextran crosslinking by epichlorohydrin: A rheometry and equilibrium swelling study. Carbohydrate Polymers 92, 1792–1798. https://doi.org/10.1016/J.CARBPOL.2012.11.030

Meyvis, T.K.L., De Smedt, S.C., Demeester, J., Hennink, W.E., 2000. Influence of the Degradation Mechanism of Hydrogels on Their Elastic and Swelling Properties during Degradation. Macromolecules 33, 4717–4725. https://doi.org/10.1021/MA992131U

Mezger, T.G., 2006. The Rheology Handbook - For Users of Rotational Rheometer (2nd edition, full), 2nd ed. Vincents Netowrk, Hannover.

Miyagi, Y., Chiu, L.L.Y.Y., Cimini, M., Weisel, R.D., Radisic, M., Li, R.-K.K., 2010. Biodegradable collagen patch with covalently immobilized VEGF for myocardial repair. Biomaterials 32, 1280–1290. https://doi.org/10.1016/j.biomaterials.2010.10.007

Moeinzadeh, S., Park, Y., Lin, S., Yang, Y.P., 2021. In-situ stable injectable collagen-based hydrogels for cell and growth factor delivery. Materialia 15, 100954. https://doi.org/10.1016/J.MTLA.2020.100954

Morris, E.R., Nishinari, K., Rinaudo, M., 2012. Gelation of gellan - A review. Food Hydrocolloids 28, 373–411. https://doi.org/10.1016/j.foodhyd.2012.01.004

Morse, D., Baer, D.M., 2004. Laboratory Balances: How They Work, Checking Their Accuracy. Laboratory Medicine 35, 48–51. https://doi.org/10.1309/QYR5UV73FRY2YBMJ

Muir, V.G., Qazi, T.H., Shan, J., Groll, J., Burdick, J.A., 2021. Influence of Microgel Fabrication Technique on Granular Hydrogel Properties. ACS Biomaterials Science and Engineering. https://doi.org/10.1021/acsbiomaterials.0c01612

Mykuliak, A., Yrjänäinen, A., Mäki, A.-J., Gebraad, A., Lampela, E., Kääriäinen, M., Pakarinen, T.-K., Kallio, P., Miettinen, S., Vuorenpää, H., 2022. Vasculogenic Potency of Bone Marrow- and Adipose Tissue-Derived Mesenchymal Stem/Stromal Cells Results in Differing Vascular Network Phenotypes in a Microfluidic Chip. Frontiers in Bioengineering and Biotechnology 0, 60. https://doi.org/10.3389/FBIOE.2022.764237

Myung, D., Waters, D., Wiseman, M., Duhamei, P.E., Noolandi, J., Ta, C.N., Frank, C.W., 2008. Progress in the development of interpenetrating polymer network hydrogels. Polymers for Advanced Technologies 19, 647–657. https://doi.org/10.1002/PAT.1134

Nadine, S., Correia, C.R., Mano, J.F., 2022. Engineering immunomodulatory hydrogels and cell-laden systems towards bone regeneration. Biomaterials Advances 140, 213058. https://doi.org/10.1016/j.bioadv.2022.213058

Nikpour, P., Salimi-Kenari, H., Fahimipour, F., Rabiee, S.M., Imani, M., Dashtimoghadam, E., Tayebi, L., 2018. Dextran hydrogels incorporated with bioactive glass-ceramic: Nanocomposite scaffolds for bone tissue engineering. Carbohydrate Polymers 190, 281–294. https://doi.org/10.1016/J.CARBPOL.2018.02.083

Nonsuwan, P., Matsugami, A., Hayashi, F., Hyon, S.H., Matsumura, K., 2019. Controlling the degradation of an oxidized dextran-based hydrogel independent of the mechanical

properties. Carbohydrate Polymers 204, 131–141. https://doi.org/10.1016/J.CARBPOL.2018.09.081
Oliveira, J.T., Martins, L., Picciochi, R., Malafaya, P.B., Sousa, R.A., Neves, N.M., Mano, J.F., Reis, R.L., 2010. Gellan gum: A new biomaterial for cartilage tissue engineering applications. Journal of Biomedical Materials Research Part A 93A, 852–863. https://doi.org/10.1002/jbm.a.32574
Oliveira, M.B., Custódio, C.A., Gasperini, L., Reis, R.L., Mano, J.F., 2016. Autonomous osteogenic differentiation of hASCs encapsulated in methacrylated gellan-gum hydrogels. Acta Biomaterialia 41, 119–132. https://doi.org/10.1016/j.actbio.2016.05.033
Osmałek, T., Froelich, A., Tasarek, S., 2014. Application of gellan gum in pharmacy and medicine. International Journal of Pharmaceutics 466, 328–340. https://doi.org/10.1016/j.ijpharm.2014.03.038
Oyen, M.L., 2014. Mechanical characterisation of hydrogel materials. International Materials Reviews 59, 44–59. https://doi.org/10.1179/1743280413Y.0000000022
Ozbolat, I.T., Hospodiuk, M., 2016. Current advances and future perspectives in extrusion-based bioprinting. Biomaterials 76, 321–343. https://doi.org/10.1016/j.biomaterials.2015.10.076
Pacelli, S., Paolicelli, P., Dreesen, I., Kobayashi, S., Vitalone, A., Casadei, M.A., 2015. Injectable and photocross-linkable gels based on gellan gum methacrylate: A new tool for biomedical application. International Journal of Biological Macromolecules 72, 1335–1342. https://doi.org/10.1016/j.ijbiomac.2014.10.046
Pacelli, S., Paolicelli, P., Moretti, G., Petralito, S., Giacomo, S.D., Vitalone, A., Casadei, M.A., 2016. Gellan gum methacrylate and laponite as an innovative nanocomposite hydrogel for biomedical applications. European Polymer Journal 77, 114–123. https://doi.org/10.1016/j.eurpolymj.2016.02.007
Pakzad, Y., Fathi, M., Omidi, Y., Mozafari, M., Zamanian, A., 2020. Synthesis and characterization of timolol maleate-loaded quaternized chitosan-based thermosensitive hydrogel: A transparent topical ocular delivery system for the treatment of glaucoma. International Journal of Biological Macromolecules 159, 117–128. https://doi.org/10.1016/J.IJBIOMAC.2020.04.274
Pan, L., Ren, Y., Cui, F., Xu, Q., 2009. Viability and differentiation of neural precursors on hyaluronic acid hydrogel scaffold. Journal of neuroscience research 87, 3207–3220. https://doi.org/10.1002/jnr.22142
Pandit, A.H., Mazumdar, N., Ahmad, S., 2019. Periodate oxidized hyaluronic acid-based hydrogel scaffolds for tissue engineering applications. International Journal of Biological Macromolecules 137, 853–869. https://doi.org/10.1016/J.IJBIOMAC.2019.07.014
Park, K.M., Gerecht, S., 2015. Polymeric hydrogels as artificial extracellular microenvironments for cancer research. European Polymer Journal 72, 507–513. https://doi.org/10.1016/j.eurpolymj.2015.06.030
Patel, R., Santhosh, M., Dash, J.K., Karpoormath, R., Jha, A., Kwak, J., Patel, M., Kim, J.H., 2019. Ile-Lys-Val-ala-Val (IKVAV) peptide for neuronal tissue engineering. Polymers for Advanced Technologies 30, 4–12. https://doi.org/10.1002/PAT.4442
Pavlacky, J., Polak, J., 2020. Technical Feasibility and Physiological Relevance of Hypoxic Cell Culture Models. Frontiers in Endocrinology 11. https://doi.org/10.3389/fendo.2020.00057

Peng, Y., Liu, Q.J., He, T., Ye, K., Yao, X., Ding, J., 2018. Degradation rate affords a dynamic cue to regulate stem cells beyond varied matrix stiffness. Biomaterials 178, 467–480. https://doi.org/10.1016/J.BIOMATERIALS.2018.04.021

Peppas, N.A., 1997. Hydrogels and drug delivery. Current Opinion in Colloid & Interface Science 2, 531–537. https://doi.org/10.1016/S1359-0294(97)80103-3

Peppas, N.A., Hilt, J.Z., Khademhosseini, A., Langer, R., 2006. Hydrogels in biology and medicine: From molecular principles to bionanotechnology. Advanced Materials 18, 1345–1360. https://doi.org/10.1002/ADMA.200501612

Prajapati, V.D., Jani, G.K., Zala, B.S., Khutliwala, T.A., 2013. An insight into the emerging exopolysaccharide gellan gum as a novel polymer. Carbohydrate Polymers 93, 670–678. https://doi.org/10.1016/j.carbpol.2013.01.030

Raina, N., Pahwa, R., Thakur, V.K., Gupta, M., 2022. Polysaccharide-based hydrogels: New insights and futuristic prospects in wound healing. International Journal of Biological Macromolecules 223, 1586–1603. https://doi.org/10.1016/j.ijbiomac.2022.11.115

Rajan, S.A.P., Aleman, J., Wan, M.M., Zarandi, N.P., Nzou, G., Murphy, S., Bishop, C.E., Sadri-Ardekani, H., Shupe, T., Atala, A., Hall, A.R., Skardal, A., 2020. Probing prodrug metabolism and reciprocal toxicity with an integrated and humanized multi-tissue organ-on-a-chip platform. Acta Biomaterialia 106, 124–135. https://doi.org/10.1016/J.ACTBIO.2020.02.015

Rasheed, A., Azizi, L., Turkki, P., Janka, M., Hytönen, V.P., Tuukkanen, S., 2021. Extrusion-based bioprinting of multilayered nanocellulose constructs for cell cultivation using in situ freezing and preprint CaCl2 cross-linking. ACS Omega 6, 569–578. https://doi.org/10.1021/acsomega.0c05036

Raza, M.A., Jeong, J.-O., Park, S.H., 2021. State-of-the-Art Irradiation Technology for Polymeric Hydrogel Fabrication and Application in Drug Release System. Frontiers in Materials 8. https://doi.org/10.3389/fmats.2021.769436

Reis, L.A., Chiu, L.L.Y., Liang, Y., Hyunh, K., Momenc, A., Radisic, M., 2012. A peptide-modified chitosan–collagen hydrogel for cardiac cell culture and delivery. Acta Biomaterialia 8, 1022–1036. https://doi.org/10.1016/j.actbio.2011.11.030

Ren, Y., Bai, Y., Zhang, Z., Cai, W., Del Rio Flores, A., 2019. The Preparation and Structure Analysis Methods of Natural Polysaccharides of Plants and Fungi: A Review of Recent Development. Molecules 24, 3122. https://doi.org/10.3390/molecules24173122

Richbourg, N.R., Peppas, N.A., 2020. The swollen polymer network hypothesis: Quantitative models of hydrogel swelling, stiffness, and solute transport. Progress in Polymer Science 105, 101243. https://doi.org/10.1016/J.PROGPOLYMSCI.2020.101243

Rocha, L.A., Gomes, E.D., Afonso, J.L., Granja, S., Baltazar, F., Silva, N.A., Shoichet, M.S., Sousa, R.A., Learmonth, D.A., Salgado, A.J., 2020. In vitro Evaluation of ASCs and HUVECs Co-cultures in 3D Biodegradable Hydrogels on Neurite Outgrowth and Vascular Organization. Frontiers in Cell and Developmental Biology 8, 1–14. https://doi.org/10.3389/fcell.2020.00489

Rouwkema, J., Khademhosseini, A., 2016. Vascularization and Angiogenesis in Tissue Engineering: Beyond Creating Static Networks. Trends in Biotechnology 34, 733–745. https://doi.org/10.1016/j.tibtech.2016.03.002

Rowley, J.A., Madlambayan, G., Mooney, D.J., 1999. Alginate hydrogels as synthetic extracellular matrix materials. Biomaterials 20, 45–53. https://doi.org/10.1016/S0142-9612(98)00107-0

Rule, P.L., Alexander, A.D., 1986. Gellan gum as a substitute for agar in leptospiral media. Journal of Clinical Microbiology 23, 500. https://doi.org/10.1128/JCM.23.3.500-504.1986

Sahoo, S., Chung, C., Khetan, S., Burdick, J.A., 2008. Hydrolytically Degradable Hyaluronic Acid Hydrogels with Controlled Temporal Structures. Biomacromolecules 9, 1088–1092. https://doi.org/10.1021/BM800051M

Samani, S., Bonakdar, S., Farzin, A., Hadjati, J., Azami, M., 2020. A facile way to synthesize a photocrosslinkable methacrylated chitosan hydrogel for biomedical applications. International Journal of Polymeric Materials and Polymeric Biomaterials 70, 730–741. https://doi.org/10.1080/00914037.2020.1760274

Santos, B.P. dos, Garbay, B., Fenelon, M., Rosselin, M., Garanger, E., Lecommandoux, S., Oliveira, H., Amédée, J., 2019. Development of a cell-free and growth factor-free hydrogel capable of inducing angiogenesis and innervation after subcutaneous implantation. Acta Biomaterialia 99, 154–167. https://doi.org/10.1016/J.ACTBIO.2019.08.028

Santos, L., Fuhrmann, G., Juenet, M., Amdursky, N., Horejs, C.M., Campagnolo, P., Stevens, M.M., 2015. Extracellular Stiffness Modulates the Expression of Functional Proteins and Growth Factors in Endothelial Cells. Advanced Healthcare Materials 4, 2056–2063. https://doi.org/10.1002/adhm.201500338

Sanzgiri, Y.D., Maschi, S., Crescenzi, V., Callegaro, L., Topp, E.M., Stella, V.J., 1993. Gellan-based systems for ophthalmic sustained delivery of methylprednisolone. Journal of Controlled Release 26, 195–201. https://doi.org/10.1016/0168-3659(93)90186-9

Saranya, M., Koivisto, J.T., Carvalho, A.C.M., Sato, F., Lassenberger, A., Porcar, L., Muchharla, B., Talapatra, S., McDonagh, B.H., Janssen, L., Pitkänen, O., Kellomäki, M., Kordas, K., Lorite, G.S., 2023. Aligned multi-walled carbon nanotube-embodied hydrogel via low magnetic field: A strategy for engineering aligned injectable scaffolds. Composites Part B: Engineering 248, 110398. https://doi.org/10.1016/j.compositesb.2022.110398

Sarkanen, J.-R., Vuorenpää, H., Huttala, O., Mannerström, B., Kuokkanen, H., Miettinen, S., Heinonen, T., Ylikomi, T., 2012. Adipose Stromal Cell Tubule Network Model Provides a Versatile Tool for Vascular Research and Tissue Engineering. Cells Tissues Organs 196, 385–397. https://doi.org/10.1159/000336679

Savina, I.N., Dainiak, M., Jungvid, H., Mikhalovsky, S. V., Galaev, I.Y., 2009. Biomimetic macroporous hydrogels: Protein ligand distribution and cell response to the ligand architecture in the scaffold. Journal of Biomaterials Science, Polymer Edition 20, 1781–1795. https://doi.org/10.1163/156856208X386390

Silva, L.P. da, Cerqueira, M.T., Sousa, R.A., Reis, R.L., Correlo, V.M., Marques, A.P., 2014. Engineering cell-adhesive gellan gum spongy-like hydrogels for regenerative medicine purposes. Acta biomaterialia 10, 4787–4797. https://doi.org/10.1016/j.actbio.2014.07.009

Silva, D.A., Poole-Warren, L.A., Martens, P.J., Panhuis, M., 2013. Mechanical characteristics of swollen gellan gum hydrogels. Journal of Applied Polymer Science 130, 3374–3383. https://doi.org/10.1002/app.39583

Silva, N.A., Cooke, M.J., Tam, R.Y., Sousa, N., Salgado, A.J., Reis, R.L., Shoichet, M.S., 2012. The effects of peptide modified gellan gum and olfactory ensheathing glia cells on neural stem/progenitor cell fate. Biomaterials 33, 6345–6354. https://doi.org/10.1016/j.biomaterials.2012.05.050

Silva-Correia, J., Zavan, B., Vindigni, V., Silva, T.H., Oliveira, J.M., Abatangelo, G., Reis, R.L., 2013. Biocompatibility Evaluation of Ionic- and Photo-Crosslinked Methacrylated Gellan Gum Hydrogels: In Vitro and In Vivo Study. Advanced Healthcare Materials 2, 568–575. https://doi.org/10.1002/adhm.201200256

Smith, A.M., Shelton, R.M., Perrie, Y., Harris, J.J., 2007. An Initial Evaluation of Gellan Gum as a Material for Tissue Engineering Applications. Journal of Biomaterials Applications 22, 241–254. https://doi.org/10.1177/0885328207076522

Sola, A., Trinchi, A., Hill, A.J., 2023. Self-assembly meets additive manufacturing: Bridging the gap between nanoscale arrangement of matter and macroscale fabrication. Smart Materials in Manufacturing 1, 100013. https://doi.org/10.1016/j.smmf.2022.100013

Soltantabar, P., Calubaquib, E.L., Mostafavi, E., Ghazavi, A., Stefan, M.C., 2021. Heart/liver-on-a-chip as a model for the evaluation of cardiotoxicity induced by chemotherapies. Organs-on-a-Chip 3, 100008. https://doi.org/10.1016/J.OOC.2021.100008

Sondermeijer, H.P., Witkowski, P., Woodland, D., Seki, T., Aangenendt, F.J., van der Laarse, A., Itescu, S., Hardy, M.A., 2016. Optimization of alginate purification using polyvinylidene difluoride membrane filtration: Effects on immunogenicity and biocompatibility of three-dimensional alginate scaffolds. J Biomater Appl 31, 510–520. https://doi.org/10.1177/0885328216645952

Soto, A.M., Koivisto, J.T., Parraga, J.E., Silva-Correia, J., Oliveira, J.M., Reis, R.L., Kellomäki, M., Hyttinen, J., Figueiras, E., 2016. Optical Projection Tomography Technique for Image Texture and Mass Transport Studies in Hydrogels Based on Gellan Gum. Langmuir : the ACS journal of surfaces and colloids 32, 5173. https://doi.org/10.1021/acs.langmuir.6b00554

Spearman, B.S., Agrawal, N.K., Rubiano, A., Simmons, C.S., Mobini, S., Schmidt, C.E., 2020. Tunable methacrylated hyaluronic acid-based hydrogels as scaffolds for soft tissue engineering applications. Journal of biomedical materials research. Part A 108, 279–291. https://doi.org/10.1002/JBM.A.36814

Sridhar, B. V., Brock, J.L., Silver, J.S., Leight, J.L., Randolph, M.A., Anseth, K.S., 2015. Development of a Cellularly Degradable PEG Hydrogel to Promote Articular Cartilage Extracellular Matrix Deposition. Advanced Healthcare Materials 4, 702–713. https://doi.org/10.1002/ADHM.201400695

Steinmetz, N.J., Aisenbrey, E.A., Westbrook, K.K., Qi, H.J., Bryant, S.J., 2015. Mechanical loading regulates human MSC differentiation in a multi-layer hydrogel for osteochondral tissue engineering. Acta Biomaterialia 21, 142–153. https://doi.org/10.1016/j.actbio.2015.04.015

Stosich, M.S., Mao, J.J., 2007. Adipose tissue engineering from human adult stem cells: clinical implications in plastic and reconstructive surgery. Plastic and reconstructive surgery 119, 71–83. https://doi.org/10.1097/01.prs.0000244840.80661.e7

Su, H., Zheng, R., Jiang, L., Zeng, N., Yu, K., Zhi, Y., Shan, S., 2021. Dextran hydrogels via disulfide-containing Schiff base formation: Synthesis, stimuli-sensitive degradation and release behaviors. Carbohydrate Polymers 265, 118085. https://doi.org/10.1016/J.CARBPOL.2021.118085

Su, J., Satchell, S.C., Wertheim, J.A., Shah, R.N., 2019. Poly(ethylene glycol)-crosslinked gelatin hydrogel substrates with conjugated bioactive peptides influence endothelial cell behavior. Biomaterials 201, 99–112. https://doi.org/10.1016/J.BIOMATERIALS.2019.02.001

Sung, J.H., Shuler, M.L., 2009. A micro cell culture analog (μCCA) with 3-D hydrogel culture of multiple cell lines to assess metabolism-dependent cytotoxicity of anti-cancer drugs. Lab on a Chip 9, 1385–1394. https://doi.org/10.1039/B901377F

Suvarna, K.S., Layton, C., Bancroft, J.D., 2019. Immunohistochemical techniques. Bancroft theory and practice of histological techniques, 8th ed. Elsevier. https://doi.org/10.1016/C2015-0-00143-5

Sze, J.H., Brownlie, J.C., Love, C.A., 2016. Biotechnological production of hyaluronic acid: a mini review. 3 Biotech 6, 1–9. https://doi.org/10.1007/S13205-016-0379-9

Tallawi, M., Rosellini, E., Cascone, M.G., Barbani, N., Rai, R., Saint-Pierre, G., Boccaccini, A.R., 2015. Strategies for the chemical and biological functionalization of scaffolds for cardiac tissue engineering: a review. Interface 12. https://doi.org/10.1098/rsif.2015.0254

Tam, R.Y., Cooke, M.J., Shoichet, M.S., 2012. A covalently modified hydrogel blend of hyaluronan-methyl cellulose with peptides and growth factors influences neural stem/progenitor cell fate. Journal of Materials Chemistry 22, 19402–19411. https://doi.org/10.1039/c2jm33680d

Tayal, A., Pai, V.B., Khan, S.A., 1999. Rheology and Microstructural Changes during Enzymatic Degradation of a Guar−Borax Hydrogel. Macromolecules 32, 5567–5574. https://doi.org/10.1021/MA990167G

Taylor, D.L., Ferris, C.J., Maniego, A.R., Castignolles, P., In Het Panhuis, M., Gaborieau, M., 2012. Characterization of gellan gum by capillary electrophoresis. Australian Journal of Chemistry 65, 1156–1164. https://doi.org/10.1071/CH12211

Tejada Jacob, G., Passamai, V.E., Katz, S., Castro, G.R., Alvarez, V., 2022. Hydrogels for extrusion-based bioprinting: General considerations. Bioprinting 27, e00212. https://doi.org/10.1016/j.bprint.2022.e00212

Thomas, L.V., VG, R., Nair, P.D., 2017. Effect of stiffness of chitosan-hyaluronic acid dialdehyde hydrogels on the viability and growth of encapsulated chondrocytes. International Journal of Biological Macromolecules 104, 1925–1935. https://doi.org/10.1016/J.IJBIOMAC.2017.05.116

Tibbitt, M.W., Anseth, K.S., 2009. Hydrogels as extracellular matrix mimics for 3D cell culture. Biotechnology and bioengineering 103, 655–663. https://doi.org/10.1002/bit.22361

Tirrell, D.A., Langer, R., 2004. Designing materials for biology and medicine. Nature 428, 487–492. https://doi.org/10.1038/nature02388

Tiwari, A., Grailer, J.J., Pilla, S., Steeber, D.A., Gong, S., 2009. Biodegradable hydrogels based on novel photopolymerizable guar gum-methacrylate macromonomers for in situ fabrication of tissue engineering scaffolds. Acta biomaterialia 5, 3441–3452. https://doi.org/10.1016/J.ACTBIO.2009.06.001

Tsaryk, R., Silva-Correia, J., Oliveira, J.M., Unger, R.E., Landes, C., Brochhausen, C., Ghanaati, S., Reis, R.L., Kirkpatrick, C.J., 2014. Biological performance of cell-encapsulated methacrylated gellan gum-based hydrogels for nucleus pulposus regeneration. Journal of Tissue Engineering and Regenerative Medicine 11, 637–648. https://doi.org/10.1002/term.1959

Tulegenovna, K.P., Negim, E.S., Al Azzam, K.M., Bustam, M.A., 2022. Modification of Xanthan Gum with Methyl Methacrylate and Investigation of Its Rheological Properties. International Journal of Technology 13, 389–397. https://doi.org/10.14716/IJTECH.V13I2.4945

Valmikinathan, C.M., Mukhatyar, V.J., Jain, A., Karumbaiah, L., Dasari, M., Bellamkonda, R.V., 2012. Photocrosslinkable chitosan based hydrogels for neural tissue engineering. Soft matter 8, 1964. https://doi.org/10.1039/C1SM06629C

Veldhuizen, J., Cutts, J., Brafman, D.A., Migrino, R.Q., Nikkhah, M., 2020. Engineering anisotropic human stem cell-derived three-dimensional cardiac tissue on-a-chip. Biomaterials 256, 120195. https://doi.org/10.1016/J.BIOMATERIALS.2020.120195

Vieira, S., da Silva Morais, A., Garet, E., Silva-Correia, J., Reis, R.L., González-Fernández, Á., Miguel Oliveira, J., 2019. Self-mineralizing Ca-enriched methacrylated gellan gum beads for bone tissue engineering. Acta Biomaterialia 93, 74–85. https://doi.org/10.1016/J.ACTBIO.2019.01.053

Vilela, C.A., Correia, C., da Silva Morais, A., Santos, T.C., Gertrudes, A.C., Moreira, E.S., Frias, A.M., Learmonth, D.A., Oliveira, P., Oliveira, J.M., Sousa, R.A., Espregueira-Mendes, J.D., Reis, R.L., 2018. In vitro and in vivo performance of methacrylated gellan gum hydrogel formulations for cartilage repair*. Journal of Biomedical Materials Research - Part A 106, 1987–1996. https://doi.org/10.1002/jbm.a.36406

Vinatier, C., Guicheux, J., 2016. Cartilage tissue engineering: From biomaterials and stem cells to osteoarthritis treatments. Annals of Physical and Rehabilitation Medicine 59, 139–144. https://doi.org/10.1016/J.REHAB.2016.03.002

Vincent, R.C., Moakes, R.J.A., Butt, G.F., Metcalfe, A.D., Williams, R.L., Wallace, G.R., Logan, A., Rauz, S., Grover, L.M., 2021. Gellan Hydrogel Eyedrop Promotes Wound Healing and Prevents Fibrosis of Cornea by Preferentially Absorbing Pro-Fibrotic Proteins. Investigative Ophthalmology & Visual Science 62, 938.

Vuornos, K., Huhtala, H., Kääriäinen, M., Kuismanen, K., Hupa, L., Kellomäki, M., Miettinen, S., 2020. Bioactive glass ions for in vitro osteogenesis and microvascularization in gellan gum-collagen hydrogels. Journal of Biomedical Materials Research Part B: Applied Biomaterials 108, 1332–1342. https://doi.org/10.1002/JBM.B.34482

Vuornos, K., Ojansivu, M., Koivisto, J.T., Häkkänen, H., Belay, B., Montonen, T., Huhtala, H., Kääriäinen, M., Hupa, L., Kellomäki, M., Hyttinen, J., Ihalainen, J.A., Miettinen, S., 2019. Bioactive glass ions induce efficient osteogenic differentiation of human adipose stem cells encapsulated in gellan gum and collagen type I hydrogels. Materials Science and Engineering: C 99, 905–918. https://doi.org/10.1016/j.msec.2019.02.035

Wadman, M., 2013. Medical research: Cell division. Nature 498, 422–426. https://doi.org/10.1038/498422a

Walters, N.J., Gentleman, E., 2015. Evolving insights in cell–matrix interactions: Elucidating how non-soluble properties of the extracellular niche direct stem cell fate. Acta Biomaterialia 11, 3–16. https://doi.org/10.1016/j.actbio.2014.09.038

Wang, P., Luo, Z., Xiao, Z., Saleh, A.S.M., 2022. Impact of calcium ions and degree of oxidation on the structural, physicochemical, and in-vitro release properties of resveratrol-loaded oxidized gellan gum hydrogel beads. International Journal of Biological Macromolecules 196, 54–62. https://doi.org/10.1016/j.ijbiomac.2021.12.043

Wang, Y., Zhang, S., Benoit, D.S.W., 2018. Degradable poly(ethylene glycol) (PEG)-based hydrogels for spatiotemporal control of siRNA/nanoparticle delivery. Journal of Controlled Release 287, 58–66. https://doi.org/10.1016/J.JCONREL.2018.08.002

Wei, J., Wang, B., Li, Z., Wu, Z., Zhang, M., Sheng, N., Liang, Q., Wang, H., Chen, S., 2020. A 3D-printable TEMPO-oxidized bacterial cellulose/alginate hydrogel with enhanced stability via nanoclay incorporation. Carbohydrate Polymers 238, 116207. https://doi.org/10.1016/J.CARBPOL.2020.116207

Wen, C., Lu, L., Li, X., 2014. Mechanically Robust Gelatin–Alginate IPNHydrogels by a Combination of Enzymaticand Ionic Crosslinking Approaches. Macromolecular Materials and Engineering 299, 504–513. https://doi.org/10.1002/MAME.201300274

Wong, L., Kumar, A., Gabela-Zuniga, B., Chua, J., Singh, G., Happe, C.L., Engler, A.J., Fan, Y., McCloskey, K.E., 2019. Substrate stiffness directs diverging vascular fates. Acta Biomaterialia 96, 321–329. https://doi.org/10.1016/j.actbio.2019.07.030

Wu, H.Q., Wang, C.C., 2016. Biodegradable smart nanogels: A new platform for targeting drug delivery and biomedical diagnostics. Langmuir 32, 6211–6225. https://doi.org/10.1021/acs.langmuir.6b00842

Wu, J., Zhang, K., Yu, X., Ding, J., Cui, L., Yin, J., 2017. Hydration of hydrogels regulates vascularization in vivo. Biomaterials Science 5, 2251–2267. https://doi.org/10.1039/c7bm00268h

Wylie, R.G., Ahsan, S., Aizawa, Y., Maxwell, K.L., Morshead, C.M., Shoichet, M.S., 2011. Spatially controlled simultaneous patterning of multiple growth factors in three-dimensional hydrogels. Nature Materials 10, 799. https://doi.org/10.1038/nmat3101

Xia, B., Chen, G., 2022. Research progress of natural tissue-derived hydrogels for tissue repair and reconstruction. International Journal of Biological Macromolecules 214, 480–491. https://doi.org/10.1016/j.ijbiomac.2022.06.137

Xu, Z., Li, Z., Jiang, S., Bratlie, K.M., 2018. Chemically Modified Gellan Gum Hydrogels with Tunable Properties for Use as Tissue Engineering Scaffolds. ACS Omega 3, 6998–7007. https://doi.org/10.1021/acsomega.8b00683

Yan, H.J., Casalini, T., Hulsart-Billström, G., Wang, S., Oommen, O.P., Salvalaglio, M., Larsson, S., Hilborn, J., Varghese, O.P., 2018. Synthetic design of growth factor sequestering extracellular matrix mimetic hydrogel for promoting in vivo bone formation. Biomaterials 161, 190–202. https://doi.org/10.1016/j.biomaterials.2018.01.041

Yan, K., Xu, F., Yang, C., Wei, W., Chen, Y., Li, X., Lu, Z., Wang, D., 2021. Interpenetrating polysaccharide-based hydrogel: A dynamically responsive versatile medium for precisely controlled synthesis of nanometals. Materials Science and Engineering: C 127, 112211. https://doi.org/10.1016/J.MSEC.2021.112211

Yang, X., Yang, H., Jiang, X., Yang, B., Zhu, K., Lai, N.C.H., Huang, C., Chang, C., Bian, L., Zhang, L., 2021. Injectable chitin hydrogels with self-healing property and biodegradability as stem cell carriers. Carbohydrate Polymers 256, 117574. https://doi.org/10.1016/J.CARBPOL.2020.117574

Yao, R., Zhang, R., Lin, F., Luan, J., 2013. Biomimetic injectable HUVEC-adipocytes/collagen/alginate microsphere co-cultures for adipose tissue engineering. Biotechnology and Bioengineering 110, 1430–1443. https://doi.org/10.1002/bit.24784

Younes, M., Aggett, P., Aguilar, F., Crebelli, R., Filipic, M., Frutos, M.J., Galtier, P., Gott, D., Gundert-Remy, U., Kuhnle, G.G., Lambré, C., Leblanc, J.C., Lillegaard, I.T., Moldeus, P., Mortensen, A., Oskarsson, A., Stankovic, I., Waalkens-Berendsen, I., Woutersen, R.A., Wright, M., Brimer, L., Mosesso, P., Christodoulidou, A., Cascio,

C., Tard, A., Lodi, F., Dusemund, B., 2018. Re-evaluation of gellan gum (E 418) as food additive. EFSA Journal 16, e05296. https://doi.org/10.2903/J.EFSA.2018.5296

Yu, Y., Cheng, Y., Tong, J., Zhang, L., Wei, Y., Tian, M., 2021. Recent advances in thermo-sensitive hydrogels for drug delivery. J. Mater. Chem. B 9, 2979–2992. https://doi.org/10.1039/D0TB02877K

Zhang, L., Liu, J., Zheng, X., Zhang, A., Zhang, X., Tang, K., 2019. Pullulan dialdehyde crosslinked gelatin hydrogels with high strength for biomedical applications. Carbohydrate Polymers 216, 45–53. https://doi.org/10.1016/J.CARBPOL.2019.04.004

Zhang, L., Zheng, T., Wu, L., Han, Q., Chen, S., Kong, Y., Li, G., Ma, L., Wu, H., Zhao, Y., Yu, Y., Yang, Y., 2021. Fabrication and characterization of 3D-printed gellan gum/starch composite scaffold for Schwann cells growth. Nanotechnology Reviews 10, 50–61. https://doi.org/10.1515/ntrev-2021-0004

Zhou, Y., Petrova, S.P., Edgar, K.J., 2021. Chemical synthesis of polysaccharide–protein and polysaccharide–peptide conjugates: A review. Carbohydrate Polymers 274, 118662. https://doi.org/10.1016/J.CARBPOL.2021.118662

Zhu, J., Tang, C., Kottke-Marchant, K., Marchant, R.E., 2009. Design and synthesis of biomimetic hydrogel scaffolds with controlled organization of cyclic RGD peptides. Bioconjugate Chemistry 20, 333–339. https://doi.org/10.1021/bc800441v

Zia, K.M., Tabasum, S., Khan, M.F., Akram, N., Akhter, N., Noreen, A., Zuber, M., 2018. Recent trends on gellan gum blends with natural and synthetic polymers: A review. International Journal of Biological Macromolecules 109, 1068–1087. https://doi.org/10.1016/j.ijbiomac.2017.11.099

Zieris, A., Prokoph, S., Levental, K.R., Welzel, P.B., Grimmer, M., Freudenberg, U., Werner, C., 2010. FGF-2 and VEGF functionalization of starPEG-heparin hydrogels to modulate biomolecular and physical cues of angiogenesis. Biomaterials 31, 7985–7994. https://doi.org/10.1016/j.biomaterials.2010.07.021

Zuidema, J.M., Rivet, C.J., Gilbert, R.J., Morrison, F.A., 2014. A protocol for rheological characterization of hydrogels for tissue engineering strategies. Journal of Biomedical Materials Research Part B: Applied Biomaterials 102, 1063–1073. https://doi.org/10.1002/jbm.b.33088

Zustiak, S.P., Leach, J.B., 2010. Hydrolytically Degradable Poly(Ethylene Glycol) Hydrogel Scaffolds with Tunable Degradation and Mechanical Properties. Biomacromolecules 11, 1348–1357. https://doi.org/10.1021/BM100137Q

APPENDIX

Table A1. Polysaccharide modifications in the literature

Polysaccharide	Purpose and Details	Mechanical Testing Results	Reference
	oxidation		
oxidized **Gellan gum** and hydrazide modified gelatin	Schiff-base crosslinking; application for general *in vitro* cell culture and cardiac cell culture	**compression**: 10 - 40 kPa compressive modulus	Koivisto *et al.*, 2019
oxidized and hydrazide-modified **Hyaluronic acid**	bone regeneration	-	Martines-Sanz *et al.*, 2011
oxidized and hydrazide-modified **Hyaluronic acid**	therapeutic delivery of corneal stem cells; ophthalmic TE	**rheology**: ~ 1 kPa storage modulus; compression: 5.4 – 11.6 kPa compressive modulus	Koivusalo *et al.*, 2018
oxidized **Hyaluronic acid** and **chitosan**	injectable hydrogel for cartilage TE	**AFM stiffness** testing: 130-199 kPa elastic modulus	Thomas *et al.*, 2017
oxidized and hydrazide-modified **Hyaluronic acid** + BMP-2, preparation pH dependent	bone regeneration by growth factor (recombinant human bone morphogenetic protein-2) delivery, which is encapsulated and stabilized by the hydrogel	-	Ji Yan *et al.*, 2018
Guar gum oxide, crosslinking between vicinal dials of neighboring chains	oxidation – diacetal modification	-	Dai *et al.*, 2017
oxidized **Dextran** and glycidyl methacrylate	aim to design a hydrogel with degradation mechanism independent of mechanical properties	**rheology**: 0.1 - 8 kPa storage modulus	Nonsuwan *et al.*, 2019
	scissoring		
oxidatively cleaved **Gellan gum**	improvement of injectability by reducing viscosity of GG through lower Mw; cartilage TE	**intrinsic viscosity**: 3.6 – 0.2 L/g and calculated Mw 1770 – 65 kDa	Gong *et al.*, 2009
	end-group modification		
Alginate-RGD-end	modification of terminal carbonyl group through oxime-mediated, aniline-catalyzed chemo-selective reaction, as to avoid functional groups in the chain	frequency **rheology**: 1 mPa*s storage modulus (compared to random in-chain modified Alg-RGD-R with 0.03 mPa*s)	Bondalapati *et al.*, 2014

Polysaccharide	Purpose and Details	Mechanical Testing Results	Reference
		methacrylation	
methacrylated **Gellan gum**	adipose SC culture towards osteogenic differentiation	**DMA compressive** probe: ~30 kPa storage modulus at 1 Hz frequency	Oliveira *et al.*, 2016
methacrylated **Gellan gum** and PEG-dimethacrylate	injectable drug delivery device	**rheology**: with low Mw PEG 0.2 - 8.7 kPa and with high Mw PEG 2.9 - 61 kPa	Pacelli *et al.*, 2015
methacrylated **Gellan gum** and laponite	nanocomposite hydrogel for drug delivery and wound dressings	frequency **rheology**: 0.9 - 4.3 kPa storage modulus at 1 Hz	Pacelli *et al.*, 2016
methacrylated **Gellan gum**	nucleus pulposus regeneration (chondrogenesis)	-	Tsaryk *et al.*, 2014
methacrylated **Gellan gum**	cartilage repair	-	Vilela *et al.*, 2018
methacrylated **Gellan gum** enriched with Ca^{2+}	bead formulation; auto-mineralization and bone TE	-	Vieira *et al.*, 2019
methacrylated collagen, gelatin, **Hyaluronic acid**, and **Alginate**	library of methacrylated polymers for 3D printing	amplitude **rheology**: gelMA 0.2 - 1.7 kPa, collagen-MA 1.6 - 2.0 kPa, HyaMA 0.8 - 3.7 kPa, AlgMA 0.3 - 3.7 kPa storage modulus	Jongprasitkul *et al.*, 2020
methacrylated **Guar gum**	modification using 4-dimethyl-amino-pyridine (DMAP)	intrinsic **viscosity**: 0.24-0.78 L/g	Tiwari *et al.*, 2009
methacrylated **Hyaluronic acid**	modification using either glycidyl methacrylate (GM) or methacrylic anhydride (MA); neural TE applications	**indentation**: GM 2.3 - 4.8 kPa and MA 4.7 - 6.1 kPa	Spearman *et al.*, 2020
methacrylated and thiol-ene modified **Gellan gum**	comparison of chain growth (metahacrylate), step growth (thiolene click) and mixed model photocrosslinking mechanism	**compression**: step-growth 7.3 kPa, chain-growth 14.6 kPa, mixed 8.1 kPa	Xu *et al.*, 2018
		thiolation	
Thiol-ene modification of **Hyaluronic acid** and **Dextran**	esterification of the hydroxyl groups using pentenoic anhydride and capping with mercaptans, forming hydrogels with PEG-$(SH)_2$ or peptide	amplitude **rheology**: 2.0 – 3.2 kPa for dextran modifcations	Mergy *et al.*, 2012
Divinyl sulfone modification of **Gellan gum** and crosslinking with MMP-1 sensitive peptide	enhanced cell degradation through bis-cysteine peptide crosslinker as well as addition of cell adhesive peptides;	oscillatory **rheology**: 0.1 – 4.9 kPa	da Silva *et al.*, 2018

Polysaccharide	Purpose and Details	Mechanical Testing Results	Reference
carbodiimide functionalization			
Carbodiimide coupling of RGD to purified **Gellan gum**	Direct coupling of RGD peptide sequence to improve cell attachment of mouse fibroblasts	amplitude **rheology**: 5.6 kPa storage modulus at LVER	Ferris *et al.*, 2015
Carbodiimide coupling of RGD to **Alginate**	direct coupling of RGD peptide sequence to improve cell attachment of mouse skeletal myoblasts	-	Rowley *et al.*, 1999
Carbodiimide coupling of dopamine to **Gellan gum**	tissue adhesion *via* catechol groups of dopamine	**compression**: 10 - 50 kPa compressive modulus	Lee *et al.*, 2021
Carbodiimide coupling of PEG, glutamic acid, or gallic acid on to **Chitosan**	injectable, therapeutic drug delivery, capacity for self-healing;	**compression**: 6 - 68 kPa compressive modulus	Khan *et al.*, 2021
carbodiimide coupling of avidin to **Nanocellulose** and blending with **Alginate** (avidin-biotin modular strategy)	avidin serves as modular functionalization point, to which any biotinylated species can be coupled without further chemical steps; application for 3D printable wound healing patches	**compression**: 22 – 44 kPa (at 30% strain)	Leppiniemi *et al.*, 2017
blending			
Gellan gum blended with the enzyme alkaline phosphatase (ALP), further incubation with polydopamine	ALP mineralizes hydrogel scaffold from calcium phosphate (CaP) in the formulation; application for bone regeneration	**compression**: hydrogels without ALP 0.75 MPa, with ALP up to 1.4 MPa, and with further incubation in PDA up to 4.5 MPa compressive modulus	Douglas *et al.*, 2012
Gellan gum blended with branched polyethylenimine (PEI)	nanocomposite formation *via* electrostatic interaction, essentially ionic crosslinking between GG^- and PEI^+; gene delivery application	-	Goyal *et al.*, 2011
Alginate blended with collagen and crosslinked with $CaSO_4$; loading with bone morphogenic protein-2 (BMP2)	In-situ stable injectable collagen-based hydrogels for cell and growth factor delivery; osteogenic differentiation of mesenchymal SC	**rheology**: 0.02 kPa (pure alginate), 0.2 – 1.6 kPa (alginate-collagen composites) storage modulus	Moeinzadeh *et al.*, 2021
Gellan gum- manuka honey (MH) blend with inorganic clay phase	no chemical modification of the gellan gum or other components; scaffolds for cartilage repair, clays: mesoporous silica, sodium-calcium bentonite, halloysite nanotubes	**compression**: only GG-MH 85 kPa, different clay composites 111 – 139 kPa compressive modulus	Bonifacio *et al.*, 2020

Polysaccharide	Purpose and Details	Mechanical Testing Results	Reference
bioactive glass (BAG) suspended in **Gellan gum**	Nanoparticulate bioactive-glass-reinforced gellan-gum hydrogels for bone-tissue engineering; formation of apatite layer; adipose SC culture	**compression**: unmodified, wet Gellan 44 kPa and BAG-Gellan gum up to 1160 kPa compressive modulus	Gantar *et al.*, 2014
nano-bioactive glass (nBAG) particles suspended to α-**Chitin** lyophilized hydrogel	preparation of porous scaffold; cell attachment of osteoblast-like cells observed	-	Peter *et al.*, 2009
chemical crosslinking			
nano-bioactive glass (nBAG) ceramic particles incorporate in **Dextran** and crosslinked with epichlorohydrin (epi)	Nanocomposite reinforced hydrogel scaffolds for bone tissue engineering; agglomeration of nBAG at high concentration reduces mechanical properties	**compression**: Dextran-epi 1.3 kPa, nBAG-Dex-ep up to 76.6 kPa compressive modulus	Nikpour *et al.*, 2018
Dextran crosslinked with epichlorohydrin (epi)	rheological study crosslinked dextran hydrogels, with observation of gelation time, storage modulus and swelling;	**rheology**: 4.6 – 31.5 kPa storage modulus after 5000 sec with epi ratio at 0.66 to dextran repeat unit, but increasing NaOH concentration (1.2 – 2.4 M)	Meybodi *et al.*, 2013
Chitosan crosslinked with **Alginate**, **Fucoidan**, or alginate and fucoidan	crosslinking in alkaline urea with epichlorohydrin (epi); inhibition of inflammatory response *in vivo*	**compression**: up to 22 kPa (chitosan-fucoidan) and 28 kPa (chitosan-alginate) compressive modulus; **frequency rheology:** 1.8 – 8 kPa (chitosan-fucoidan), 1.1 – 5 kPa (chitosan-alginate), and 0.8 kPa for chitosan-fucoidan-alginate storage modulus at 1 Hz	Hao *et al.*, 2021
Furan-modified **Gellan gum** for coupling with maleimide-modified peptide RGD	direct coupling of RGD peptide with bio-orthogonal reaction; ASCs and HUVEC co-cultures to study neurite outgrowth and vascularization; Diels-Alder cyclization chemistry	-	Rocha *et al.*, 2020
Furan-modified **Gellan gum** for coupling with maleimide-modified peptide RGD	co-culture of olfactory ensheathing glia cells and neural stem/progenitor cell fate; Diels-Alder cyclization chemistry	-	Silva *et al.*, 2012
modification of **Alginate** with norbornene (Alg-N) and tetrazine (Alg-T)	photoclick reaction between Alg-T and Alg-N forms network; post-gelation addition of thiolated peptide using unreacted Alg-N and photoreaction	**compression**: 2.5 – 15 kPa compressive modulus for 1:1 formulation	Desai *et al.*, 2015

Table A2. Overview of modified gellan gum used within the Publications I-V.

	Pub I	Pub III	Pub IV	Pub V
oxidized GG	500 mg GG	-	500 mg	500 mg GG
GGox(1)	12 mg $NaIO_4$	-	-	-
GGox(2)	24 mg $NaIO_4$	-	-	-
GGox(3)	48 mg $NaIO_4$	-	48 mg $NaIO_4$	-
GGox(4)	-	-	-	60 mg $NaIO_4$
scissored GG	100 mg GGox			
GGsciss	4 mg $NaBH_4$	-	-	-
avidin modification		100 mg NaGG		
NaGG-avd(L)	-	1.75 mg CNCA	-	-
NaGG-avd(H)	-	3.50 mg CNCA	-	-

Table A3. Yield stress from flow sweep data.

Yield Stress (Pa)	Solvent			
Hydrogel Precursor	**water**	**sucrose**	**HEPES/sucrose**	**EBM-2**
GG 1.0%	1.03 ± 0.18	2.72 ± 0.32	2.76 ± 0.51	-
NaGG 1.0%	0.02 ± 0.01	0.03 ± 0.00	0.11 ± 0.01	-
GGox(1)	-	-	0.02 ± 0.00	-
GGox(2)	-	-	0.02 ± 0.00	-
GGox(3)	-	-	0.03 ± 0.01	-
GGsciss(1)	-	-	0.01 ± 0.00	-
GGsciss(2)	-	-	0.03 ± 0.00	-
GGsciss(3)	-	-	0.02 ± 0.01	-
GGsciss(4)	-	-	0.04 ± 0.01	-
NaGG-avd 0.5%	-	-	0.03 ± 0.00	-
NaGG 0.5%	-	-	0.02 ± 0.00	-
GGox(4) 4.0%	-	0.02 ± 0.01	-	0.06 ± 0.02
gelaADH 4.0%	-	0.03 ± 0.02	-	
gelaCDH 4.0%	-	-	-	0.03 ± 0.01

Table A4. Compression data.

	Polymer	Crosslinker	Modulus 1 (1-10%)	Modulus 2 [kPa]	Fracture Strength [kPa]	Fracture Strain [%]	n	Height [mm]	Width [mm]
I	GG 1%	SPD 2mM	3.9 ±2.4	31.8 ±15.6	5.9 ±1.8	33.8 ±2.5	5	4.0 ± 0.1	12.2 ± 0.1
	GG 1%	Ca 5mM	3.7 ±0.7	34.0 ±8.7	7.0 ±1.6	37.9 ±2.1	5	4.1 ± 0.1	11.7 ± 0.3
	NaGG 1%	SPD 4mM	14.6 ±7.9	51.0 ±7.6	8.8 ±1.3	27.0 ±1.6	5	4.4 ± 0.2	12.3 ± 0.0
	NaGG 1%	Ca 10mM	3.4 ±0.6	13.6 ±2.0	4.2 ±1.1	41.9 ±4.0	5	4.0 ± 0.2	11.4 ± 0.0
	GGox(1) 1%	SPD 10mM	6.7 ±3.0	83.1 ±22.2	14.5 ±1.3	37.2 ±2.4	5	4.8 ± 0.3	11.9 ± 0.3
	GGox(1) 1%	Ca 25mM	11.2 ±2.9	220.7 ±21.5	42.1 ±2.3	44.5 ±0.8	4	5.2 ± 0.4	12.0 ± 0.2
	GGox(2) 1%	SPD 20mM	1.7 ±1.6	54.1 ±9.7	8.6 ±1.4	48.1 ±3.8	5	3.8 ± 0.4	11.9 ± 0.3
	GGox(2) 1%	Ca 100 mM	2.2 ±0.9	123.9 ±35.1	18.4 ±4.8	49.8 ±3.5	4	3.3 ± 0.3	11.8 ± 0.2
	GGsciss(1) 1%	SPD 7.5mM	2.3 ±0.4	4.9 ±0.8	0.7 ±0.1	19.4 ±2.3	3	4.8 ± 0.1	12.2 ± 0.2
	GGsciss(1) 1%	Ca 25mM	7.4 ±1.3	9.6 ±1.1	1.3 ±0.8	15.6 ±9.3	4	5.2 ± 0.1	12.3 ± 0.1
II	NaGG 0.5 %	SPD 2 mM	1.9 ± 0.7	8.9 ± 3.1	1.7 ± 0.6	28.9 ± 2.6	6	3.6 ± 0.1	11.7 ± 0.4
	NaGG 0.5 %	SPD 2 mM	2.2 ± 0.3	22.2 ± 2.8	3.9 ± 0.5	27.7 ± 3.6	3	4.1 ± 0.3	11.2 ± 0.5
	NaGG 0.5 %	SPD 2 mM	14.2 ± 1.2	50.2 ± 4.4	9.5 ± 0.8	37.7 + 2.8	5	4.6 ± 0.1	11.8 ± 0.2
	NaGG 0.5 %	SPD 2 mM	26.2 ± 1.8	105.1 ± 7.3	26.4 ± 1.8	37.2 ± 1.6	3	4.3 ± 0.1	11.4 ± 0.1
III	NaGG 0.5 %	SPD 2 mM	4.4 ± 1.1	17.1 ± 3.2	4.3 ± 1.1	32.7 ± 6.5	5	4.3 ± 0.2	11.8 ± 0.1
	NaGG 0.5 %	CaCl2 10 mM	4.2 ± 0.9	15.6 ± 4.1	5.1 ± 0.8	45.5 ± 1.0	5	4.1 ± 0.1	11.3 ± 0.2
	NaGG-avd(L) 0.5%	SPD 2 mM	3.4 ± 1.1	18.7 ± 4.4	5.5 ± 0.7	35.9 ± 4.0	5	4.0 ± 0.2	11.2 ± 0.1
	NaGG-avd(L) 0.5%	CaCl2 10 mM	4.2 ± 1.3	13.9 ± 3.3	8.6 ± 1.0	45.7 ± 2.2	5	4.0 ± 0.2	11.2 ± 0.2
IV	GGox(4) 4%	gelaADH 4%	13.60 ± 1.44	-	20.4 ± 1.8	61.7 ± 5.0	6	4.5 ± 0.4	9.3 ± 0.1
	GGox(4) 3%	gelaADH 4%	11.50 ± 1.71	-	27.5 ± 16.5	64.5 ± 9.2	4	4.4 ± 0.3	9.8 ± 0.6
	GGox(4) 2%	gelaADH 4%	13.44 ± 1.81	-	23.9 ± 2.1	58.4 ± 6.8	5	4.8 ± 0.4	10.0 ± 0.5
	GGox(4) 6%	gelaCDH 6%	8.82 ± 0.99	-	97.5 ± 18.7	74.0 ± 1.2	5	6.3 ± 0.6	10.6 ± 0.1
	GGox(4) 4%	gelaCDH 6%	41.23 ± 7.34	-	334.2 ± 145.2	62.5 ± 5.3	7	4.7 ± 0.4	10.3 ± 0.3
	GGox(4) 4%	gelaCDH 4%	14.07 ± 2.33	-	61.6 ± 14.1	69.9 ± 2.9	6	5.3 ± 0.5	10.1 ± 0.2
	Rabbit heart		21.05 ± 6.78	-	N/A	N/A	6	6.7 ± 0.2	12.3 ± 0.2

Table A5. Rheology data

		Time Sweeps				Amplitude Sweeps				Frequency Sweeps	
Polymer	**Crosslinker**	**Storage modulus (Pa)**	**Loss modulus (Pa)**	**n**	**tan δ**	**linear region**	**Storage modulus (Pa)**	**Loss modulus (Pa)**	**n**	**linear region**	
GG	SPD 2mM	74.9 ± 3.0	20.1 ± 0.4	4	0.27	0.04-6.32	70.98 ± 0.9	20.80 ± 0.3	3	0.10-1.00	77.74 ± 7.7
GG	CaCl2 5mM	339.5 ± 11.8	20.5 ± 0.4	5	0.06	0.03-3.17%	355.15 ± 4.0	21.11 ± 0.5	3	0.10-2.00	378.53 ± 18.3
NaGG	SPD 4mM	224.6 ± 3.2	39.8 ± 0.8	3	0.18	0.01-0.10	362.28 ± 8.0	51.28 ± 2.5	3	0.10-1.26	196.58 ± 11.5
NaGG	CaCl2 10mM	224.8 ± 14.0	30.6 ± 1.7	4	0.14	0.05-0.63	274.70 ± 9.5	33.40 ± 3.8	3	0.10-1.26	151.19 ± 2.3
GGox(1)	SPD 10mM	424.1 ± 6.3	18.7 ± 2.2	4	0.04	0.02-2.01%	393.77 ± 11.3	18.48 ± 2.5	3		
GGox(1)	CaCl2 25mM	695.5 ± 10.6	20.2 ± 5.6	4	0.03	0.06-0.80%	577.68 ± 9.3	17.00 ± 4.3	3		
GGsciss(1)	SPD 7.5mM	1411.6 ± 16.2	71.0 ± 0.7	3	0.05	0.01-1.00%	1606.72 ± 95.2	71.65 ± 18.3	3		
GGsciss(1)	CaCl2 25mM	1116.9 ± 17.7	34.4 ± 0.8	3	0.03	0.01-2.00	1177.58 ± 6.0	35.74 ± 2.5	3		

PUBLICATIONS

Publication I Gering, C., Rasheed, A., Koivisto, J. T., Párraga, J., Tuukkanen, S., & Kellomäki, M. (2021). Chemical modification strategies for viscosity-dependent processing of gellan gum. Carbohydrate Polymers, 269, 118335. https://doi.org/10.1016/j.carbpol.2021.118335

Publication II Gering, C., Koivisto, J.T., Parraga, J.E., Kellomäki, M. (2018). Reproducible preparation method of hydrogels for cell culture applications – case study with spermidine crosslinked gellan gum. In: Eskola, H., Väisänen, O., Viik, J., Hyttinen, J. (eds) EMBEC & NBC 2017. EMBEC NBC 2017 2017. IFMBE Proceedings, vol 65. Springer, Singapore. https://doi.org/10.1007/978-981-10-5122-7_203

Publication III Gering, C., Koivisto, J. T., Párraga, J., Leppiniemi, J., Vuornos, K., Hytönen, V. P., Miettinen, S., & Kellomäki, M. (2019). Design of modular gellan gum hydrogel functionalized with avidin and biotinylated adhesive ligands for cell culture applications. PLoS ONE, 14(8), 1–22. https://doi.org/10.1371/journal.pone.0221931

Publication IV Koivisto, J. T., Gering, C., Karvinen, J., Maria Cherian, R., Belay, B., Hyttinen, J., Aalto-Setälä, K., Kellomäki, M., & Parraga, J. (2019). Mechanically Biomimetic Gelatin-Gellan Gum Hydrogels for 3D Culture of Beating Human Cardiomyocytes. ACS Applied Materials and Interfaces, 11(23), 20589–20602. https://doi.org/10.1021/acsami.8b22343

Publication V Gering, C., Párraga, J., Vuorenpää, H., Botero, L., Miettinen, S., Kellomäki, M., 2022. Bioactivated gellan gum hydrogels affect cellular rearrangement and cell response in vascular co-culture and subcutaneous implant models. Biomaterials Advances 143, 213185. https://doi.org/10.1016/j.bioadv.2022.213185

PUBLICATION I

Chemical modification strategies for viscosity-dependent processing of gellan gum

Christine Gering, Anum Rasheed, Janne T. Koivisto, Jenny Párraga, Sampo Tuukkanen, & Minna Kellomäki

Carbohydrate Polymers, 269, 118335
https://doi.org/10.1016/j.carbpol.2021.118335

Carbohydrate Polymers 269 (2021) 118335

Contents lists available at ScienceDirect

Carbohydrate Polymers

journal homepage: www.elsevier.com/locate/carbpol

Chemical modification strategies for viscosity-dependent processing of gellan gum

Christine Gering [a,*], Anum Rasheed [a], Janne T. Koivisto [a,b], Jenny Párraga [a], Sampo Tuukkanen [a], Minna Kellomäki [a]

[a] Faculty of Medicine and Health Technology, Tampere University, 33720 Tampere, Finland
[b] Division of Pathology, Department of Laboratory Medicine, Karolinska Institute, 171 77 Stockholm, Sweden

ARTICLE INFO

Keywords:
Hydrogel
Modified gellan gum
Viscoelastic properties
Mechanical testing
Bioprinting

ABSTRACT

Recently, the hydrogel-forming polysaccharide gellan gum (GG) has gained popularity as a versatile biomaterial for tissue engineering purposes. Here, we examine the modification strategies suitable for GG to overcome processing-related limitations. We emphasize the thorough assessment of the viscoelastic and mechanical properties of both precursor solutions and final hydrogels. The investigated modification strategies include purification, oxidation, reductive chain scission, and blending. We correlate polymer flow and hydrogel forming capabilities to viscosity-dependent methods including casting, injection and printing. Native GG and purified NaGG are shear thinning and feasible for printing, being similar in gelation and compression behavior. Oxidized GGox possesses reduced viscosity, higher toughness, and aldehydes as functional groups, while scissored GGsciss has markedly lower molecular weight. To exemplify extrudability, select modification products are printed using an extrusion-based bioprinter utilizing a crosslinker bath. Our robust modification strategies have widened the processing capabilities of GG without affecting its ability to form hydrogels.

1. Introduction

Gellan gum (GG) and its derivatives have been established hydrogel materials suitable for tissue engineering and biomedical sciences (Stevens et al., 2016). Indeed, GG shows high biocompatibility, no cytotoxicity, easy processability, a similar secondary helix structure to collagen, and mechanical properties similar to soft tissue (Oliveira et al., 2010). On the other hand, GG has several limitations, such as a lack of specific cell adhesion sites (da Silva et al., 2014), a precarious gelation temperature for many cell therapy strategies (Gong et al., 2009) as well as high viscosity of precursors. These limitations complicate sterilization by filtration and the formulation of injectable medicines. To fulfill the requirements for tissue engineering, regenerative medicine, and the delivery of biomolecules, hydrogels must gelate under mild conditions. Commonly, it is required for the modification products to retain their ability to crosslink and form hydrogels. We hypothesize that GG can be modified to suit different applications and enable hydrogel formation. Therefore, we propose to modify the chemical and mechanical nature of GG using the inexpensive and gentle strategies: 1) Purification of native GG to lower solution viscosity and facilitate processing. 2) Oxidation of GG to introduce reactive sites for further functionalization and crosslinking strategies. 3) Scissoring to decrease the viscosity and improve syringeability (Fig. 1).

The purification process removes counterions from the commercial GG formulation, reduces the tendency of GG to form gels upon cool down, and decreases the viscosity of the polymer solution (Doner, 1997; Kirchmajer D et al., 2014). Oxidation via Malaprade reaction (Wang, 2010) opens the saccharide ring at the α-L-rhamnose sugar, skews the polymer backbone, and impairs formation of double helices (Morris et al., 2012). We modulate this reaction to retain gel formation capacity while providing reactive sites, namely, the aldehyde groups of oxidized rhamnose. Scissoring, i.e. oxidation and subsequent reduction of the GG polymer chain, restores the original degree of reactivity but decreases molecular weight and viscosity (Gong et al., 2009). After a rigorous analysis of the modified GG in terms of modification degree and composition, we prepare self-supporting hydrogels employing $CaCl_2$ and spermidine (SPD) as crosslinkers (Koivisto et al., 2017). To study the value of aldehyde groups in oxidized GG backbone, we introduce the cationic polysaccharide chitosan. Chitosan has previously been blended with native GG, demonstrating the ability to form electrostatic

* Corresponding author.
E-mail address: christine.gering@tuni.fi (C. Gering).

https://doi.org/10.1016/j.carbpol.2021.118335
Received 17 February 2021; Received in revised form 8 June 2021; Accepted 9 June 2021
Available online 15 June 2021

complexes (Kumar et al., 2016).

This work is the first systematic study of formulations based on modified GG with emphasis on the analysis of precursors and final hydrogels using rheological and compression measurements. Flow curves are prepared to analyze the viscosity of hydrogel precursors and the influence of solvents, and ultimately to provide an insight into extrusion behavior (Paxton et al., 2017). Time sweeps demonstrate the gelation behavior of different formulations, and amplitude sweeps complement viscoelastic characterization of fresh gels. Fully cured gels are subjected to compression testing to assess their mechanical properties. We achieve a standardized hydrogel analysis to identify network formation clues and to assess final mechanical properties resulting from the modifications. Molar mass analysis was performed using size-exclusion chromatography (SEC) coupled with multi-angle light scattering (MALS) detector and the modified compounds were assessed using ^{1}H NMR. To demonstrate the processability of the modified GG and correlate the physicochemical characteristics, we use the materials as ink for extrusion-based printing. Thus, we are proposing an easily adaptable hydrogel platform with tunable mechanical properties and known biocompatibility that suits different needs without altering the underlying material.

2. Materials and methods

2.1. Materials

Gellan gum was purchased from Sigma (Gelzan™ CM-Gelrite®, low acyl form, 1000 kg/mol), and deacetylated chitosan was acquired from NovaMatrix (Protasan UP CL 113, deacetylation degree 75–90%, water-soluble at neutral pH, M_w 50–150 kg/mol, measured as chitosan acetate). Dialysis membrane (Spectra/Por® 12–14 kDa) was purchased from Spectrum Laboratories (Rancho Dominguez, CA, USA). Other chemicals were purchased from Sigma Aldrich and used as received.

2.2. Modifications

Purification of GG is based on the protocol by (Doner, 1997). Briefly, GG was dissolved in water at 0.5% w/v and heated to 60 °C. An excess of cation exchange resin (Dowex, H^+ form, 50–100 mesh, pre-rinsed) was added and separated from the solution after 30 min. The pH was adjusted to 7.5 with NaOH (1 M). The solution was precipitated in isopropanol and the product (NaGG) was lyophilized.

For oxidation of GG, 100 mL GG (0.5% w/v in water) was heated to 40 °C. Under nitrogen atmosphere and in the dark, different amounts of sodium periodate ($NaIO_4$) were dissolved in 4 mL water and added dropwise to the GG solution. Here, we used 12 mg for GGox(1), 24 mg for GGox(2), and 48 mg for GGox(3). The reaction was kept in the dark at 40 °C for 4 h before quenching with ethylene glycol (300 µL). The product (GGox) was dialyzed (12–14 kDa MWCO) over 3 days against water and lyophilized over 4 days.

To scissor, 100 mg of oxidized GG (GGox 1, 2, or 3) was dissolved in sodium borate buffer (46 mL, 0.05 M) under stirring at 60 °C for 1 h. The solution was cooled below 10 °C and kept under nitrogen atmosphere. $NaBH_4$ (4 mL, 1 mg/mL) in sodium borate buffer (0.05 M) was added dropwise to the GGox solution and the solution was stirred overnight. The reaction was quenched by addition of an acetic acid-methanol mixture (5 mL; 1:4) and dialyzed (MWCO 12–14 kDa) against water over 2 days. The product (GGsciss) was lyophilized over 4 days. For nomenclature, scissoring transforms GGox(1) to GGsciss(1) and so forth.

2.3. Hydrogel preparation

GG and its derivates presented herein were dissolved in water (Sartorius, 0.055 µS/cm^3) at 10% w/v, sucrose (10% w/v in water) or

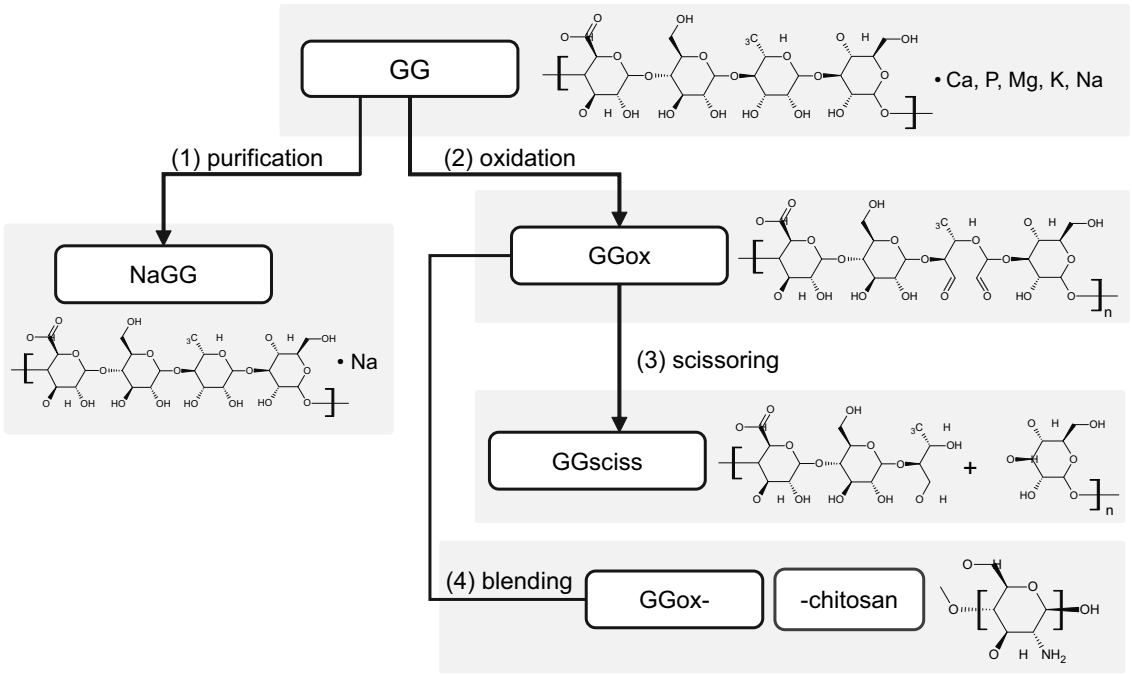

Fig. 1. Chemical structures of native and modified GG (1) Purification creates NaGG. (2) Oxidation creates aldehyde groups in GGox. (3) Subsequent scissoring produces GGsciss. (4) Blending with chitosan uses aldehydes for compounding.

HEPES/sucrose (25 mM, 10% w/v sucrose, pH 6.5), under constant stirring at 50 °C for 1 h. The solutions were stored at 4 °C and warmed to 37 °C before hydrogel preparation.

When casting gels, precursor solutions and crosslinker were mixed in a vial under constant stirring at 37 °C with a fixed volume ratio of 5:1, using either calcium chloride ($CaCl_2 \cdot H_2O$, 5–100 mM) or spermidine trihydrochloride (SPD, 2–20 mM). The hydrogel was then swiftly cast to the mold (Gering et al., 2017).

When blending oxidized GG with chitosan, the chitosan solution (5 mg/mL in HEPES/sucrose at pH 6.5) was added in 1:1 ratio to the crosslinking solution (SPD, 40 mM), and the gels were cast as described above. Essentially, chitosan is treated as component of the crosslinker and the 5:1 volume ratio is maintained for mold-cast hydrogels.

2.4. Analysis methods

Inductively coupled plasma optical emission spectroscopy (Agilent Technologies, 5110 ICP-OES) was used to verify ion concentration for native and purified GG as previously described in (Gering et al., 2019). Briefly, GG was digested in sulfuric acid (H_2SO_4, 98% w/w), cleared with hydrogen peroxide (H_2O_2, 30% w/w), and diluted with water. The solutions were analyzed for Na, Ca, Mg, and K concentrations.

The degree of oxidation was assessed using TBC-TNBS method based on (Bouhadir et al., 1999) with detailed protocol in Appendix D. Briefly, GG and GG derivatives were incubated overnight with an excess of *t*-butyl carbazate (TBC, 10 mM). Picryl sulfonic acid (TNBS, 2.5 mM) was added to each sample, incubated and quenched with hydrochloric acid (HCl, 0.5 M). The solutions were analyzed using UV–Vis-NIR spectrophotometer (Shimadzu UV-3600 Plus, maximum at 342 ± 4 nm, slit width 5 nm).

Molecular weight (M_w) and size of GG was analyzed using Agilent 1260 HPLC pump and autosampler equipped with a multiangle light scattering detector (DAWN, Wyatt Technology) and a refractive index (RI) detector (Optilab). Size separation was performed using 2 PLgel Mixed-C 300 × 7.5 mm columns. The samples were dissolved in the mobile phase (DMSO with 0.2% LiBr) overnight, then heated at 70 °C for 2 h, and filtered (0.45 μm) before injection (100 μL, flow rate 0.5 mL/min).

To record ^{1}H NMR, native and oxidized GG samples were dissolved in D_2O, treated with TBC and stirred at 37 °C for 3 h. After addition of sodium cyanoborohydride the mixture was kept stirring overnight. The product was then analyzed using Jeol 500 MHz equipment without further purification. Chemical shifts: δ 5.15 (s, 1H, CH-1 of rhamnose unit), 4.72 (s, 1H, CH-1 of glucose unit), 4.56 (s, 1H, CH-1 of glucuronic acid unit), 4.07–3.43 (m, 5H, CH-2-5 of units), 1.3 (s, 3H, CH-3 of rhamnose unit).

Rheological measurements were performed using the Discovery HR-2 rheometer and TRIOS software (TA Instruments, USA), which was equipped with a temperature control, using 20 mm plate-plate geometry throughout.

For hydrogel precursor flow comparison, the polymers were dissolved in ultra-pure water, sucrose, or HEPES/sucrose. The solutions were warmed to facilitate the manipulation of the more viscous precursors. A steady state flow shear rate sweep test was performed using 1000 μm gap, with logarithmic sweep, shear rate from 0.01 to 500 s^{-1} (5 points/s) and 25 s sampling period at 25 °C ($n = 3$). To account for wall slip, a stress-controlled flow sweep was carried out, which can be found in Appendix F.

Rheological analysis of the hydrogel formulations, i.e., precursor and crosslinking solution, was performed so that the components were combined on the rheometer plate and the geometry was used for mixing by rapid spinning. The precursor solution was dispensed to the plate at 37 °C, the geometry was lowered to 1500 μm and the crosslinker solution was added during the mixing phase (70 rad/s for 7 s at 37 °C). Consequently, the time sweep started with an amplitude of 0.75% oscillation strain, 0.75 Hz at 30 °C for 30 min ($n \geq 3$). After the sweep had concluded and the gel had formed, an amplitude sweep (30 °C, 0.75 Hz, 0.1–100% oscillation strain, $n = 3$) or frequency sweep (30 °C, 0.75% oscillation strain, 0.1–100 Hz, n = 3) was performed. A solvent trap was used to impede evaporation.

Compression behavior was analyzed using Bose BioDynamic ElectroForce Instrument 5100 and WinTest 8 software (TA Instruments, USA) equipped with 22 N load cell. Cylindrical samples (diameter≈12 mm, height≈4.5 mm, $n = 5$) were tested under uniaxial, unconfined compression in air. The sample was prevented from sliding with wet cellulose paper and compressed with a speed of 10 mm/min to 65% of the original sample height.

2.5. Printing trial

Printability of the hydrogels and the feasibility of a crosslinking bath were tested using Nordson EFD extrusion-based printer (microextruder Nordson EFD E4) and software (DispenseMotion, Nordson, Ohio, USA). The precursor solutions were extruded through a 0.15 mm stainless steel nozzle onto a nylon mesh on a glass substrate. The mesh was soaked in crosslinking solution to ensure an evenly distributed thin layer. The printed structures were in contact with crosslinker for at least 1 min to allow for gelation. The writing speed and the relative humidity were kept constant at 25 mm/s and 55% RH, respectively (Rasheed et al., 2020). Concentrations of precursor solutions and crosslinking baths are presented in Table 2. The photographs were analyzed using ImageJ software (U.S. National Institutes of Health, Bethesda, MD) by measuring the average line thickness and standard deviation of the parallel lines. The printing fidelity is determined as the ratio between standard deviation and average.

3. Results and discussion

We aimed to improve the polysaccharide gellan gum by creating a tunable hydrogel platform for different processing applications, such as extrusion-based printing, mold casting, and injection. The chosen analysis methods reflect their suitability for these different processes, and some of the formulations were printed as a proof-of-concept (see Fig. 7).

Herein, we have investigated two different crosslinking agents, calcium chloride and the bioamine spermidine, to form hydrogels from the modified GG solutions. GG has two complementary gelation mechanisms: first, upon heating and subsequent cooling, the randomly coiled GG chains form highly ordered double helices. Second, the additions of cations link the anionic helices to form a network (Grasdalen & Smidsrød, 1987). Calcium is traditionally used to crosslink a variety of hydrogels including gellan gum. Its hydrodynamic radius and charge density allow ideal intercalation between helical GG molecules. Thus, the crosslinking mechanism is understood to exceed charge screening, as monovalent ions are a weaker crosslinker even at competing charge concentration (Morris et al., 2012). Spermidine is a polyamine found in the ribosome of natural tissues. At pH values below 8.8, it carries three charged amine groups (Wang & Casero, 2006) and is thus able to crosslink the anionic GG as shown by (López-Cebral et al., 2013) and (Koivisto et al., 2017). The concentration of the crosslinking agent and respective GG derivative was chosen to ensure a self-supporting hydrogel was formed (Table 1).

The modification degree of GGox was calculated from the results of the TNBS-TBC assay, as the molar concentration of aldehydes is expected to be equivalent to the amount of consumed TBC. Hence, the percentage of oxidized rhamnose is 2.8% (GGox(1) 0.232 mM), 10.6% (GGox(2), 0.888 mM), and 24.2% (GGox(3), 2.023 mM), respectively. A graphical representation of the results is shown in Appendix D Fig. D1.

A similar TBC-derivatization was performed to detect the presence of aldehyde groups using ^{1}H NMR (Appendix C). The spectra of GGox(1) and GGox(2) show clear difference in the region of δ 1.4 ppm and 1.25 ppm compared to native GG. The presence of a peak at 1.28 ppm (9H, t-

Table 1
Tabulated values from rheology sweeps and compression tests of self-supporting hydrogel formulations. All GG derivatives are used at 1.0% w/v.

Hydrogel formulation		Amplitude sweep				Frequency sweep	Time sweep	Compression test			
		Linear region (oscillation strain %)	G′ storage modulus (Pa)	G″ loss modulus (Pa)	Tan δ	Linear region (Hz)	End of transient phase (min)	Modulus 1 (kPa)	Modulus 2 (kPa)	Fracture strength (kPa)	Fracture strain (mm/mm)
GG	SPD 10 mM	0.0–6.3	71.0 ± 0.9	20.8 ± 0.3	0.29	0.1–1.0	12.5	3.9 ± 2.4	31.8 ± 15.6	5.9 ± 1.8	33.8 ± 2.5
	$CaCl_2$ 5 mM	0.0–3.2	355.2 ± 4.0	21.1 ± 0.5	0.06	0.1–2.0	15.0	3.7 ± 0.7	34.0 ± 8.7	7.0 ± 1.6	37.9 ± 2.1
NaGG	SPD 4 mM	0.0–0.1	362.3 ± 8.0	51.3 ± 2.5	0.14	0.1–1.3	18.3	14.6 ± 7.9	51.0 ± 7.6	8.8 ± 1.3	27.0 ± 1.6
	$CaCl_2$ 10 mM	0.1–0.6	274.7 ± 9.5	33.4 ± 3.8	0.12	0.1–1.3	20.0	3.4 ± 0.6	13.6 ± 2.0	4.2 ± 1.1	41.9 ± 4.0
GGox(1)	SPD 10 mM	0.0–0.8	398.5 ± 4.0	17.5 ± 1.4	0.04	0.1–2.5	15.0	6.7 ± 3.0	83.1 ± 22.2	14.5 ± 1.3	37.2 ± 2.4
	$CaCl_2$ 25 mM	0.1–0.8	577.7 ± 9.3	17.0 ± 4.3	0.03	0.1–2.5	15.0	11.2 ± 2.9	220.7 ± 21.5	42.1 ± 2.3	44.5 ± 0.8
GGox(2)	SPD 20 mM	0.1–7.9	49.9 ± 1.0	0.4 ± 0.0	0.01	0.1–1.6	12.5	1.7 ± 1.6	54.1 ± 9.7	8.6 ± 1.4	48.1 ± 3.8
	$CaCl_2$ 100 mM	0.5–10.0	62.7 ± 1.3	0.7 ± 0.0	0.01	0.1–1.6	15.0	2.2 ± 0.9	123.9 ± 35.1	18.4 ± 4.8	49.8 ± 3.5
GGox(2) + chitosan	SPD 20 mM	0.1–10.0	104.8 ± 2.8	1.8 ± 0.1	0.02	0.1–2.0	15.0	–	–	–	–
	$CaCl_2$ 75 mM	0.1–7.9	43.2 ± 0.4	1.4 ± 0.1	0.03	0.1–1.6	15.0	–	–	–	–
GGsciss(1)	SPD 7.5 mM	0.0–1.0	1606.7 ± 95.2	71.6 ± 18.3	0.05	–	7.5	–	–	–	–
	$CaCl_2$ 25 mM	0.0–2.0	1177.6 ± 6.0	35.7 ± 2.5	0.03	–	15.0	–	–	–	–

Boc) is partially overlapping the peak corresponding to the rhamnose 1.3 ppm (s, 3H, CH-3 of rhamnose unit), thus preventing quantification.

Ion concentration of purified NaGG has previously been determined using ICP-OES. The values show that in the purified product, low concentrations of calcium (0.08% w/w), potassium (0.25% w/w), and magnesium (0.02% w/w) are present, whereas sodium is available as a counterion (2.73% w/w). (Gering et al., 2019).

M_w and size of GG and GGsciss were determined using size exclusion chromatography (SEC) with coupled multi-angle light scattering (MALS) and refractive index (RI) detector. As shown in Fig. 2, GG has a M_w of 326 ± 5 kDa (PDI 1.7), but the scissored product is markedly smaller with GGsciss(1) 53 ± 1 kDa (PDI 2.0) and GGsciss(2) 48 ± 1 kDa (PDI 2.7). The scissored product has a lower M_w, which is in line with the observed lower viscosity profile. In GGsciss(2), a small portion of the weight fraction is 1000 kDa or larger, which could be residual oxidized fragments that were not reduced and scissored. It was not possible to analyze GGox using the same protocol due to presence of aldehydes, which leads to molecular interaction and aggregation of polymer chains, resulting in an apparent higher M_w with smaller size (Appendix E Fig. E2).

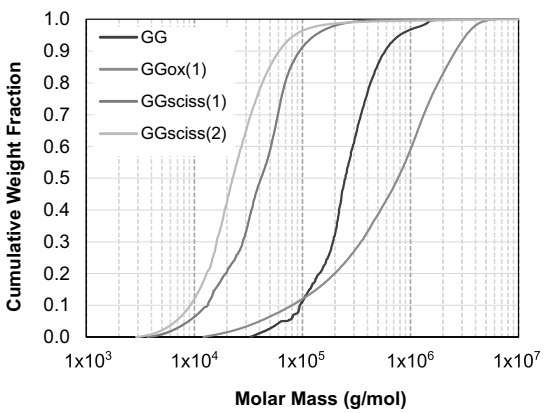

Fig. 2. Cumulative weight fractions of selected GG modifications.

A steady state stress sweep was carried out to produce flow curves of the hydrogel precursors using different solvents with a shear rate from 0.01 to 500 s^{-1}. The resulting curves of viscosity and stress are plotted as double logarithmic plots in Fig. 3.

For native and purified GG, the effect of solvent was investigated using flow sweeps comparing pure water, sucrose solution (10% w/v), and a combination of HEPES buffer (25 mM) and sucrose (10% w/v). Native GG in pure water shows visibly lower viscosity, whereas the HEPES/sucrose had a larger impact on the flow. This effect of sugars has been investigated in detail and can be attributed to molecular crowding and denser association of polymer chains (Morris et al., 2012). Different modification degrees were investigated for oxidation and subsequent scissoring, based on the amount of added reactant. From Fig. 3C and D, we can see that different oxidation degrees have a small effect on viscosity, whereas the effect for scissored GG is negligible. Comparing native and purified GG to oxidized and scissored products, however, shows a significant difference in viscosity profile.

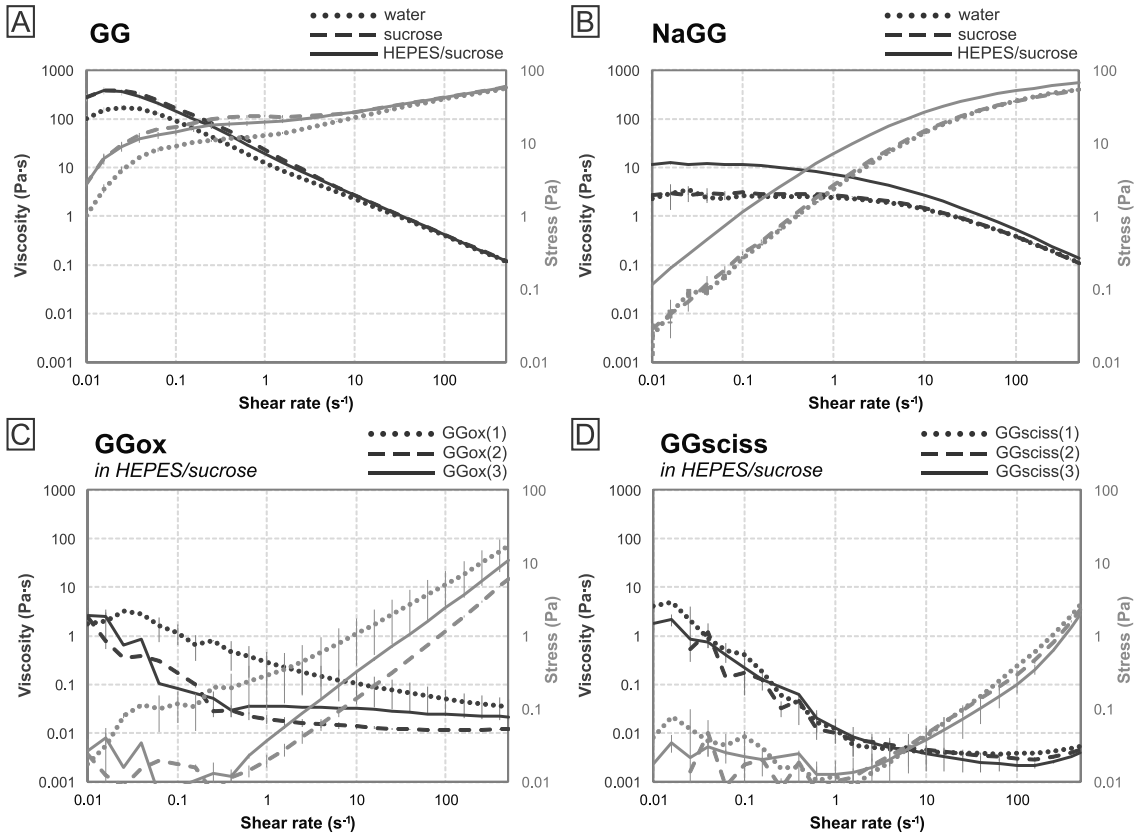

Fig. 3. Flow curves of hydrogel precursor solutions showing viscosity and stress vs. shear rate. A and B) GG and NaGG in different solvents; C and D) GGox and GGsciss with different degrees of modification. ($n = 3$).

From the stress-vs-shear rate plot, the shear behavior of hydrogel precursors can be analyzed. Native GG presents an initial phase of shear thinning behavior with a yield stress range between 1.03 Pa and 2.76 Pa (Fig. 2A). This is followed by more linear behavior above shear rates of 10 s^{-1} as defined by the Bingham model (Chhabra & Richardson, 2008). The curves of purified NaGG (Fig. 3B) clearly show its shear thinning nature, with a low yield stress between 0.02 Pa and 0.11 Pa. The Power Law can be applied for GG above 0.1 s^{-1}, and likely for NaGG above 10 s^{-1}, but not for the other modifications (Appendix G). In contrast, both oxidized GGox and scissored GGsciss (Fig. 3C and D) have near zero yield stress between 0.02 Pa and 0.03 Pa and 0.01 Pa and 0.04 Pa, respectively. Above 1 s^{-1}, GGox is fairly linear, indicating Newtonian fluid behavior, whereas GGsciss shows shear thickening tendency. At low values, measurements become unreliable, and therefore a steady stress sweep should be chosen for low viscosity solutions.

Flow curves are standard evaluation tools when considering polymer solutions for 3D printing applications, and our printing experiment confirmed our findings. Both GG and NaGG demonstrate shear thinning behavior and extruded into repeatable structures with ease. However, GGox is not shear-thinning and both GGox(1) and GGox(2) solutions required higher pressure to extrude. Moreover, due to its extremely low viscosity, GGox(2) showed poor extrudability during printing.

Rheological time sweeps (Fig. 4) provide an excellent tool for studying the network formation of hydrogels by casting the components under the geometry and performing a time sweep with low amplitude and frequency. The gelation sweep is performed so that the precursor is placed between the gap while the geometry itself carries out the mixing by rapidly spinning for a short duration. This assures even contact of the hydrogel with the geometry and prevents internal stresses in the hydrogel. Notably, this allows observation of the early gelation stages and gives an insight into gelation kinetics (Zuidema et al., 2014).

All formulations form self-supporting hydrogels within 30 min of the measurement. The curve, however, does not reach full linearity and a small slope value remains. This indicates that network development continues and justifies longer, e.g., overnight, incubation of samples for mechanical testing of final hydrogels.

Tan δ, the ratio between G′ and G″, gives further indication of the completion of network formation within the gel (Chhabra & Richardson, 2008). Mechanistically, the viscous and elastic components of the hydrogel model are shifting in magnitude related to each other during the transient phase of gelation (Appendix B). Once the gel has set, the value for tan δ should behave linearly (Zuidema et al., 2014). The end of the transient phase marks the time we understand as gelation time; however, the given value (Table 1) is rather qualitative.

The time sweep shows the gelation behavior of each formulation, which is relevant for application techniques, such as mold casting, with a critical time component for handling the hydrogel. Native GG has the highest gelation rate, causing problems for the manipulation of the setting gel components. NaGG, on the other hand, shows very rapid and precarious network formation, with slightly longer time needed to form a stable gel. This may be due to the larger number of crosslinking sites available, as purification deprives the formulation of cations, especially

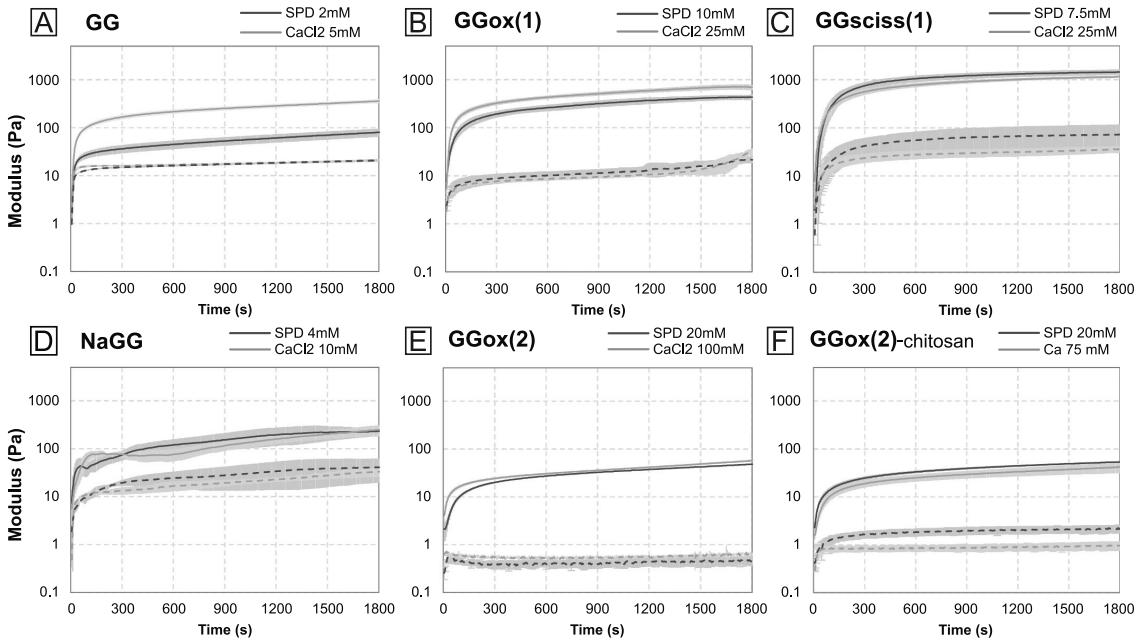

Fig. 4. Time sweeps of hydrogel-forming solutions. Shown are storage G′ (solid line) and loss G" (dashed line) modulus over time with constant amplitude (0.75% osc. strain) and frequency (0.75 Hz). Time point 0 is the end of the mixing phase (7 s) of precursor solution and crosslinker ($n = 3$).

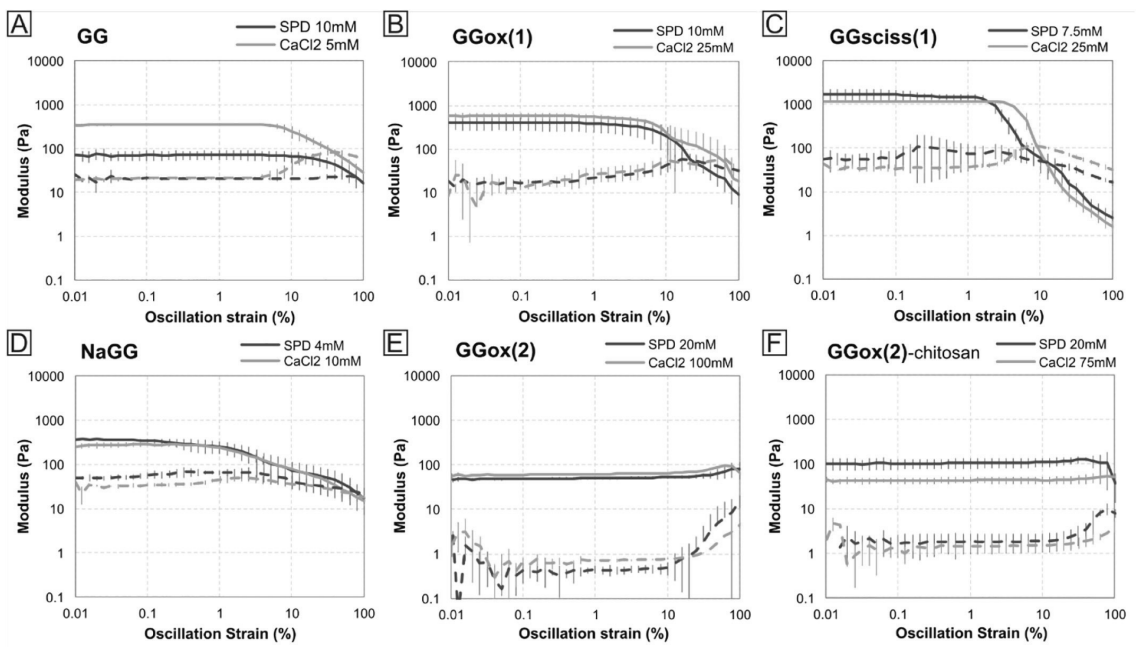

Fig. 5. Amplitude sweeps of different hydrogel formulations. Crosslinker is shown in the upper right hand side of each chart, with storage (solid line) and loss (dashed line) modulus ($n = 3$).

calcium. The oxidized GGox(1) still forms surprisingly tough hydrogels, despite polymer chain distortion, but GGox(2) already struggles to form gels even with higher concentrations of crosslinking agents. Similarly, GGsciss(1) forms gels with calcium and spermidine, but GGsciss(2) does not.

From amplitude sweep measurements we can derive: storage (G′) and loss modulus (G″) at the linear region (SAOS); the range of the linear behavior and its end point, i.e., how much the network deforms before it loses its linearity; behavior type during the non-linear region (LAOS) and in some cases, depending on the measured amplitude range, the crossover point of G″ and G′, which may indicate crosslinking density. The amplitude sweeps shown in Fig. 5 are performed after the time sweep, approximately 30 min after mixing. As previously discussed, the hydrogel at this time point may not be fully formed and is therefore expected to yield different results than a sample that has set overnight.

The linear regions, tan δ as well as G′ and G″, are listed in Table 1. Similar to time sweep, tan δ can be utilized to compare the viscoelastic nature of the formulations. In all hydrogel samples, G′ dominates G″ before the yield point, as they are elastic solids. However, the magnitude of their ratio (tan δ) reveals the extent, with larger values indicating a more associated network. The results of the frequency sweep are presented in SI Appendix A.

In discussing complex fluids, (Hyun et al., 2002) investigated the non-linear region of the amplitude sweep (LAOS) to describe different behaviors linked to the microstructure of the polymer. These behaviors include strain thinning, strain thickening, and strain overshoot phenomena, depending on how the hydrogel reacts to strain. Although we have studied viscoelastic networks rather than fluids, their observations are reflected in the sweeps shown in Fig. 5. For example, regardless of the crosslinker used, GG, NaGG, and GGox(1) all show weak strain overshoot, whereas G" increases before decreasing. This indicates a weakly structured material that experiences large deformation before a critical strain and starting to flow (Hyun et al., 2002). In Fig. 4, this can be clearly seen with GG and $CaCl_2$ as crosslinker. Conversely, GGox(2) and chitosan-containing compounds show strong strain overshoot behavior, where both G′ and G″ increase after the linear region, and before the critical strain destroys the network and both values decrease. Unfortunately, the maximum strain value of 100% oscillation strain does not show full LAOS behavior for all formulations.

Mold cast samples of different formulations were incubated at 37 °C overnight and analyzed using compression. The curves are shown in Fig. 6, whereas moduli and fracture strength are listed in Table 1. Viscoelastic properties are not directly discernable from this type of measurement, as the features of viscoelastic deformation and brittle fracture cannot be separated (Kocen et al., 2017). It is, however, straightforward to compare the fracture behavior between different compositions. Moreover, it is also possible to compare samples of the same composition that have been subjected to different treatments or environments. Therefore, compression testing assesses the static mechanical properties of the final hydrogel, whereas rheology assesses the hydrogel processing kinetics. Ultimately, both techniques work in conjunction to investigate the mechanical properties of hydrogels.

From the compression graph, three features can be assessed: modulus 1, modulus 2, and the fracture point. Modulus 1 describes the presumed elastic region of hydrogel compression. Here, the slope is taken from 1% to 10% compressive strain. Modulus 2 describes the linear region before the fracture point. All GG derivates show a fracture point, indicating their relatively brittle nature. Other hydrogels and native tissue, however, are known to not show a fracture point, dissipating the strain in an elastic manner (Karvinen et al., 2018; Koivisto et al., 2017; Koivisto et al., 2019).

Further, the fracture behavior can be evaluated to compare different

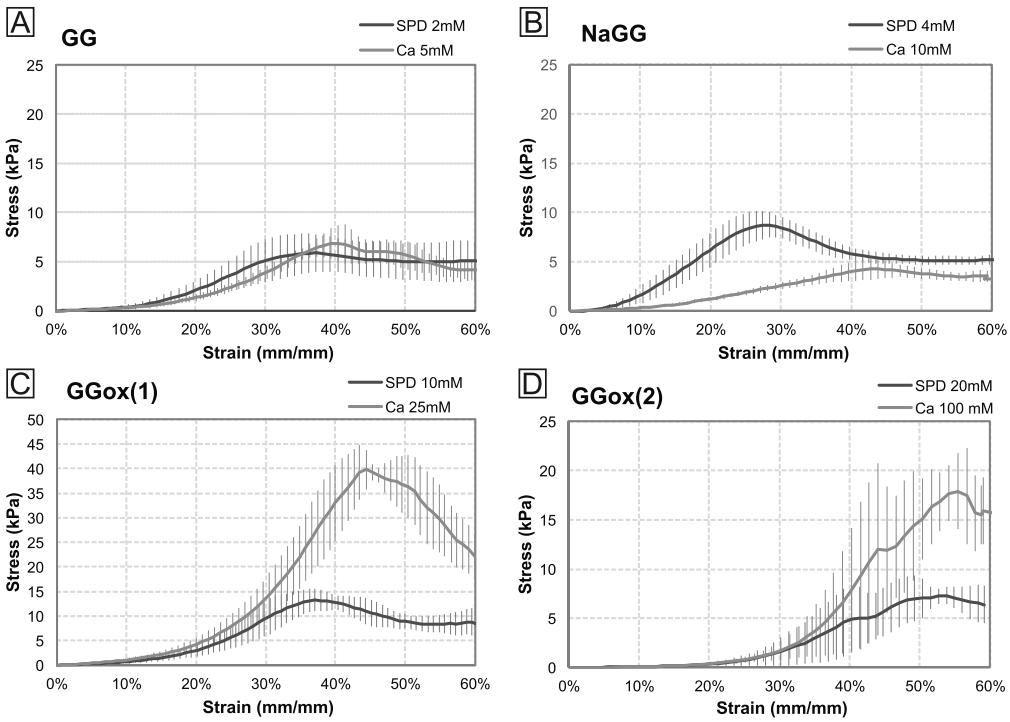

Fig. 6. Stress-strain curves of hydrogel samples under compressive load. Please note different scale of graph C ($n = 5$).

hydrogel formulations, such as the two NaGG-based hydrogels formed with $CaCl_2$ and SPD (Fig. 5B). NaGG-SPD has a steep slope and quick fracture indicating a brittle fracture. In comparison, NaGG-Ca has a shallower slope and higher ductility, which indicates extrusion of water from the surface of the gel and formation of microfractures under the compressive load (Nakamura et al., 2001). Also, GGox(1) and (2) formulated with $CaCl_2$ (25 mM and 100 mM) show very high fracture stress and modulus 2.

From the collected information on mechanical and viscoelastic properties, we can confer the application ranges of different GG modifications. For instance, scissored GG has low viscosity and loses the typical shear-thinning effect of other GG solutions due to the drastic reduction in molar weight seen from the SEC/MALS results. However, GGsciss(1) retains the ability to form self-supporting hydrogels within a short time, with the transient phase ending within 10 min (Appendix B Fig. B1). It is likely the shortened polymer chain and reduced viscosity will help the network find an equilibrium within the crosslinking architecture faster. Whereas dilation rules out printing applications, we suspect the GGsciss polymer precursor may be applicable when syringing for minimally invasive surgery, injecting body-on-chip models, filling cavities, and ophthalmic coatings. Higher degrees of scissoring, such as GGsciss(2) and (3), do not form self-supporting gels, further limiting the application range.

Oxidized GG, on the other hand, can form self-supporting gels with

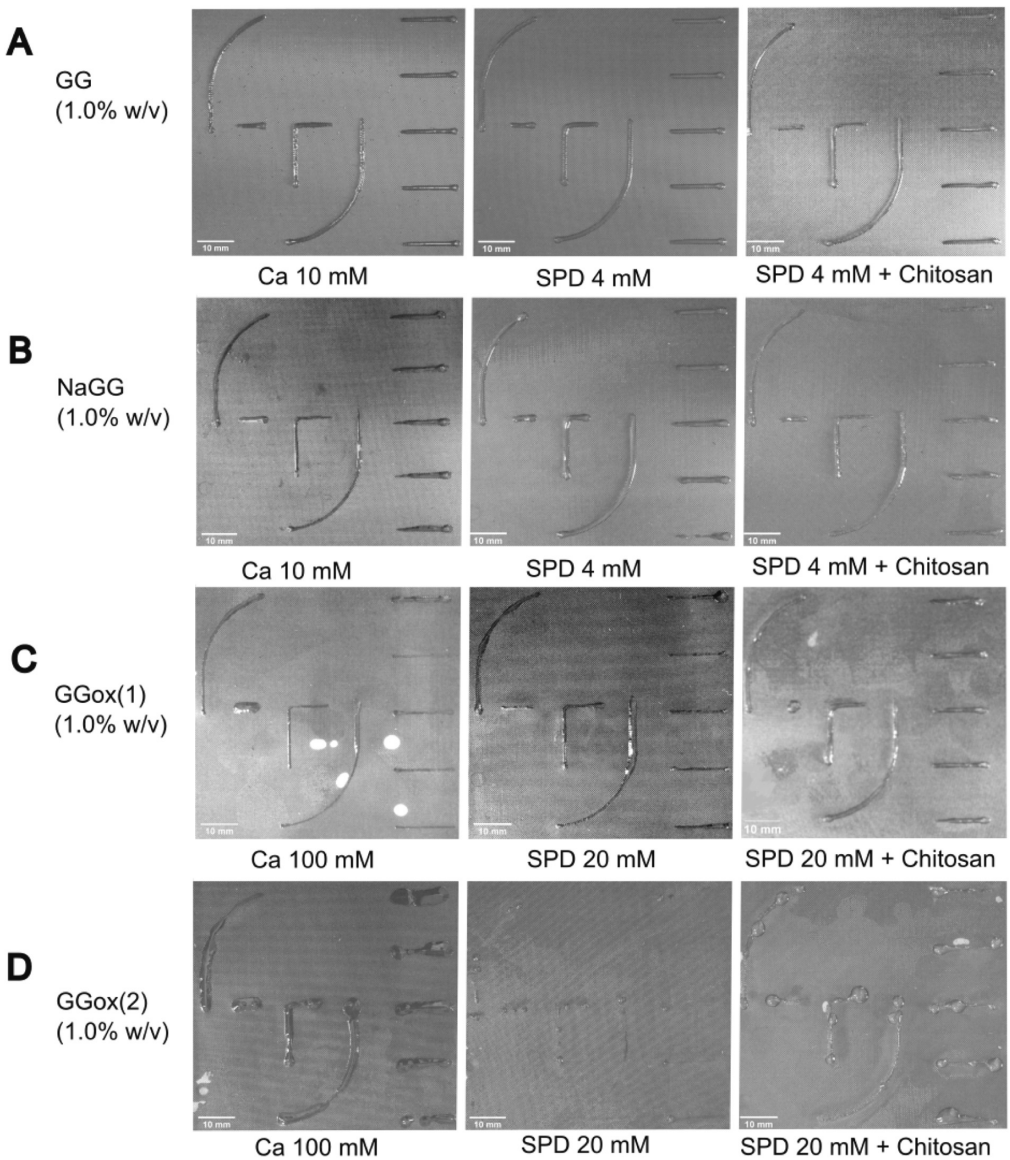

Fig. 7. Photographs of printed structures. The polymer precursor solutions were extruded from a nozzle (stainless steel 0.15 mm) at the shown pressure and constant speed (25 mm/s) onto a treated glass plate with nylon mesh coated in crosslinker solution. Ambient conditions at 20 °C and 56% RH (scale bar 10 mm).

increased crosslinker concentrations. We have demonstrated its ability to be compounded with other substances, such as chitosan, and be expanded for blending with therapeutic agents in drug delivery applications. The active sites of GGox are also beneficial for cell encapsulation, as aldehyde groups are known to be tissue adhesive, whereas native GG is known to be bioinert and does not facilitate cell attachment (Ferris et al., 2013). The oxidation degree can be fine-tuned through iodate concentration in the modification procedure. We have shown previously that a high oxidation degree can be used to compound with modified gelatin to form a chemically crosslinked, self-supporting hydrogel with good cell attachment (Koivisto et al., 2019).

Native GG and purified NaGG are good candidates for printing, which is indicated by the flow test results. Both are shear thinning, although NaGG has a more pronounced viscosity profile and dramatically lower yield stress compared to native GG. Bioprinting is a popular topic in the recent literature (Paxton et al., 2017; Rasheed et al., 2020), and therefore an understanding of hydrogel rheology and mechanical properties before, during, and after such extrusion process is needed. To demonstrate printability, we used extrusion-based bioprinting to print shapes (Fig. 7). To compare the printing behavior, we used other modifications in the trial, although, judging from the results of the flow test, they could have been disregarded. Indeed, the poor printing results are visible from Fig. 7C and D, which supports our conclusions on flow results. To render these polymer solutions suitable for extrusion-based printing, pre-crosslinking with low concentrations of crosslinkers should be considered (Rasheed et al., 2020).

Both GG (1.0% w/v) and NaGG (1.0% w/v) extruded as continuous lines at relatively low pressure (0.90 bar to 0.98 bar). GGox(1) formed a continuous line structure at a higher pneumatic pressure of 1.48 bar, whereas GGox(2) was unable to form unbroken lines at pressures as high as 2.56 bar. This further proves the increased printability of GG and NaGG. This finding is in line with the extrudable hydrogels, such as alginate and gelatin, found in the literature, and verifies that both pressure and viscosity determine printability (He et al., 2016; Paxton et al., 2017).

Table 2 summarizes the average thickness of the five parallel lines, measured from five distinct points, indicating the print fidelity and consistency.

We have shown several facile ways to chemically modify GG, impacting the mechanical and viscoelastic properties. Polymer flow and gelation kinetics are paramount for any extrusion-based processing technique, where bioprinting, casting, and injection have diverse requirements. We have correlated the flow properties and viscosity values to the printing results, while the gelation rheology results will reflect on casting and injection applications. In turn, mechanical stability and behavior of the formed hydrogel will determine the suitability for applications, such as 3D in vitro cell culture, in vivo cell carrier, drug carrier, and phantom material for imaging purposes. Although the mechanical properties of the final hydrogel may not be adequate for printing or self-supporting structures, for example GGox(3) or GGsciss (2), they may be useful in coatings and body-on-chip models. Assessing the syringeability and cavity filling of weak hydrogels, however, requires more sophisticated techniques, and therefore was not performed here.

Table 2
Setup and results of printing trial.

	Polymer	Pressure (mbar)	Crosslinking bath	Line width (mm)	Printing fidelity
A	GG	0.90	$CaCl_2$ 10 mM	1.2 ± 0.1	7.4%
			SPD 4 mM	1.3 ± 0.1	10.2%
			Chitosan 0.5% w/v -SPD 4 mM	0.9 ± 0.1	13.5%
B	NaGG	0.98	$CaCl_2$ 10 mM	1.3 ± 0.3	19.0%
			SPD 4 mM	1.3 ± 0.2	17.1%
			Chitosan 0.5% w/v -SPD 4 mM	1.1 ± 0.2	14.9%
C	GGox (1)	1.48	$CaCl_2$ 100 mM	1.0 ± 0.3	31.4%
			SPD 20 mM	0.8 ± 0.2	17.8%
			Chitosan 0.5% w/v -SPD 20 mM	1.3 ± 0.2	19.1%
D	GGox (2)	2.20–2.56	$CaCl_2$ 100 mM	3.2 ± 0.9	29.5%
			SPD 20 mM	N/A	N/A
			Chitosan 0.5% w/v -SPD 20 mM	1.9 ± 1.0	52.0%

4. Conclusion

We have confirmed our hypothesis by demonstrating suitable modification strategies for GG, resulting in a wide range of precursors which have the capacity to form hydrogels with tunable structure and properties. Modification products can have different applications and uses, depending on flow properties or precursor, and hydrogel mechanical properties. To facilitate the use of the precursors we present their systematic comparison. A significant part of this study was dedicated to the testing of viscoelastic and mechanical properties, alongside discussing the applications of the different derivatization products.

While GG and NaGG both clearly show a shear thinning profile with maximum viscosity values of 383 and 12.4 Pa·s, oxidized and scissored products have much lower viscosity (below 3.2 and 5.0 Pa·s respectively) and do not appear shear thinning. Shear thinning is an essential trait for printability, as highlighted by the good printing fidelity of GG (average 10%) and NaGG (average 17%) compared to the tested GGox modifications (average 23–41%). The SEC-MALS analysis reveals the successful chain scission, as the M_W decreases from 326 kDa (GG) to around 50 kDa for different GGsciss products. From the amplitude and time sweeps, the capacity of different modification products to form hydrogels and their apparent stiffness can be determined. For instance, GGox(1) forms hydrogels with storage modulus between 399 and 578 Pa while GGox(2) is softer with moduli between 50 and 63 Pa. On the other hand, aldehydes of GGox can interact with chitosan and other biomolecules, which can be useful for drug loading or attachment of bioactive factors. GGsciss shows greatly reduced viscosity and molar weight, predicted to be useful for injection-based applications. The results of our study indicate the suitability of GG as hydrogel material platform and our findings establish a basis on which to build a robust material library.

CRediT authorship contribution statement

Christine Gering: Methodology, Validation, Formal analysis, Investigation, Data curation, Writing – original draft, Writing – review & editing, Visualization. **Anum Rasheed:** Methodology, Validation, Formal analysis, Investigation, Data curation, Writing – original draft, Writing – review & editing, Visualization. **Janne T. Koivisto:** Conceptualization, Methodology, Writing – review & editing. **Jenny Párraga:** Conceptualization, Methodology, Validation, Investigation, Writing – original draft, Writing – review & editing, Supervision. **Sampo Tuukkanen:** Resources, Supervision, Funding acquisition. **Minna Kellomäki:** Conceptualization, Resources, Writing – review & editing, Supervision, Project administration, Funding acquisition.

Acknowledgements

This work was supported by the Academy of Finland through the Center of Excellence – Body on Chip (312409, 326587, 336663). C.G. received financial support from the Jenny and Antti Wihuri Foundation

(3a3aec) and A.R. from the TAU Doctoral School. We wish to thank Dr. Vijay Parihar for recording the ^{1}H NMR as well as the Wyatt Technology Corporation for successfully running the SEC and MALS, and Prof Michiel Postema for helpful discussion on rheology assessment.

Appendix A. Supplementary data

Supplementary data to this article can be found online at https://doi.org/10.1016/j.carbpol.2021.118335.

References

Bouhadir K. H., Hausman D. S., & Mooney D. J. (1999). Synthesis of cross-linked poly (aldehyde guluronate) hydrogels. Polymer 40, 3575–3584.

Chhabra, R. P., & Richardson, J. F. (2008). Chapter 2 - Rheometry for non-Newtonian fluids. In R. P. Chhabra, & J. F. Richardson (Eds.), *Non-Newtonian flow and applied rheology* (2nd ed., pp. 56–109). Oxford: Butterworth-Heinemann.

da Silva, L. P., Cerqueira, M. T., Sousa, R. A., Reis, R. L., Correlo, V. M., & Marques, A. P. (2014). Engineering cell-adhesive gellan gum spongy-like hydrogels for regenerative medicine purposes. *Acta Biomaterialia, 10*, 4787–4797.

Doner, L. W. (1997). Rapid purification of commercial gellan gum to highly soluble and gellable monovalent cation salts. *Carbohydrate Polymers, 32*, 245–247.

Ferris, C. J., Gilmore, K. J., Wallace, G. G., & Panhuis, M. I. H. (2013). Modified gellan gum hydrogels for tissue engineering applications. *Soft Matter, 9*, 3705–3711.

Gering, C., Koivisto, J. T., Parraga, J., Leppiniemi, J., Vuornos, K., Hytönen, V. P., … Kellomäki, M. (2019). Design of modular gellan gum hydrogel functionalized with avidin and biotinylated adhesive ligands for cell culture applications. *PLoS One, 14*, Article e0221931.

Gering, C., Koivisto, J. T., Parraga, J. E., & Kellomäki, M. (2017). Reproducible preparation method of hydrogels for cell culture applications – case study with spermidine crosslinked gellan gum. In *Anonymous Embec & Nbc 2017* (pp. 811–814). Singapore: Springer.

Gong, Y., Wang, C., Lai, R. C., Su, K., Zhang, F., & Wang, D. (2009). An improved injectable polysaccharide hydrogel: Modified gellan gum for long-term cartilage regenerationin vitro. *Journal of Materials Chemistry, 19*, 1968–1977.

Grasdalen, H., & Smidsrød, O. (1987). Gelation of gellan gum. *Carbohydrate Polymers, 7*, 371–393.

He, Y., Yang, F., Zhao, H., Gao, Q., Xia, B., & Fu, J. (2016). Research on the printability of hydrogels in 3D bioprinting. *Scientific Reports, 6*, 29977.

Hyun, K., Kim, S. H., Ahn, K. H., & Lee, S. J. (2002). Large amplitude oscillatory shear as a way to classify the complex fluids. *Journal of Non-Newtonian Fluid Mechanics, 107*, 51–65.

Karvinen, J., Joki, T., Ylä-Outinen, L., Koivisto, J. T., Narkilahti, S., & Kellomäki, M. (2018). Soft hydrazone crosslinked hyaluronan- and alginate-based hydrogels as 3D supportive matrices for human pluripotent stem cell-derived neuronal cells. *Reactive and Functional Polymers, 124*, 29–39.

Kirchmajer D. M., Steinhoff B., Warren H., Clark R., & in het Panhuis M. (2014). Enhanced gelation properties of purified gellan gum. Carbohydrate Research 388, 125–129.

Kocen, R., Gasik, M., Gantar, A., & Novak, S. (2017). Viscoelastic behaviour of hydrogel-based composites for tissue engineering under mechanical load. *Biomedical Materials (Bristol), 12*, Article 025004.

Koivisto, J. T., Gering, C., Karvinen, J., Maria Cherian, R., Belay, B., Hyttinen, J., … Parraga, J. (2019). Mechanically biomimetic gelatin–gellan gum hydrogels for 3D culture of beating human cardiomyocytes. *ACS Applied Materials & Interfaces, 11*, 20589–20602.

Koivisto, J. T., Joki, T., Parraga, J. E., Pääkkönen, R., Ylä-Outinen, L., Salonen, L., … Kellomäki, M. (2017). Bioamine-crosslinked gellan gum hydrogel for neural tissue engineering. *Biomedical Materials, 12*, Article 025014.

Kumar, S., Kaur, P., Bernela, M., Rani, R., & Thakur, R. (2016). Ketoconazole encapsulated in chitosan-gellan gum nanocomplexes exhibits prolonged antifungal activity. *International Journal of Biological Macromolecules, 93*, 988–994.

López-Cebral, R., Paolicelli, P., Romero-Caamaño, V., Seijo, B., Casadei, M. A., & Sanchez, A. (2013). Spermidine-cross-linked hydrogels as novel potential platforms for pharmaceutical applications. *Journal of Pharmaceutical Sciences, 102*, 2632–2643.

Morris, E. R., Nishinari, K., & Rinaudo, M. (2012). Gelation of gellan – A review. *Food Hydrocolloids, 28*, 373–411.

Nakamura, K., Shinoda, E., & Tokita, M. (2001). The influence of compression velocity on strength and structure for gellan gels. *Food Hydrocolloids, 15*, 247–252.

Oliveira, J. T., Martins, L., Picciochi, R., Malafaya, P. B., Sousa, R. A., Neves, N. M., … Reis, R. L. (2010). Gellan gum: A new biomaterial for cartilage tissue engineering applications. *J. Biomed. Mater. Res. Part A, 93A*, 852–863.

Paxton, N., Smolan, W., Böck, T., Melchels, F., Groll, J., & Jungst, T. (2017). Proposal to assess printability of bioinks for extrusion-based bioprinting and evaluation of rheological properties governing bioprintability. *Biofabrication, 9*, Article 044107.

Rasheed, A., Azizi, L., Turkki, P., Janka, M., Hytönen, V. P., & Tuukkanen, S. (2020). *Extrusion-based bioprinting of multilayered nanocellulose constructs for cell cultivation using in situ freezing and preprint CaCl2 cross-linking*. ACS Omega.

Stevens, L. R., Gilmore, J., Wallace, G. G., & M. in het Panhuis, G. G. (2016). Tissue engineering with gellan gum. *Biomaterials Science, 4*, 1276–1290.

Wang, J.-Y., & Casero, R. A., Jr. (2006). *Polyamine structure and synthetic analogs*. 999 Riverview Drive, Suite 208. Totowa, New Jersey 07512: 2006 Humana Press Inc.

Wang, Z. (2010). Malaprade Reaction. In Z. Wang (Ed.), *Comprehensive organic name reactions and reagents* (pp. 1807–1810). American Cancer Society.

Zuidema, J. M., Rivet, C. J., Gilbert, R. J., & Morrison, F. A. (2014). A protocol for rheological characterization of hydrogels for tissue engineering strategies. *Journal of Biomedical Materials Research Part B: Applied Biomaterials, 102*, 1063–1073.

PUBLICATION II

Reproducible preparation method of hydrogels for cell culture applications – case study with spermidine crosslinked gellan gum

Christine Gering, Janne T. Koivisto, Jenny Párraga, & Minna Kellomäki

EMBEC & NBC 2017. EMBEC NBC 2017 2017. IFMBE Proceedings, vol 65. Springer, Singapore
https://doi.org/10.1007/978-981-10-5122-7_203

Reproducible preparation method of hydrogels for cell culture applications – case study with spermidine crosslinked gellan gum

C. Gering[1], J.T. Koivisto[1, 2], J.E. Parraga[1] and M. Kellomäki[1, 2]

[1] BioMediTech Institute and Faculty of Biomedical Sciences and Engineering, Tampere University of Technology, Tampere, Finland
[2] BioMediTech Institute and Faculty of Medicine and Life Sciences, University of Tampere, Tampere, Finland

Abstract— **Hydrogels are promising materials to culture cells in 3D environment. Their mechanical properties are decisive, as cells understand the stiffness of their surroundings. Herein, a method is presented to produce ionically crosslinked hydrogel matrices. A reproducible method is needed, because conventional methods cause inconsistent properties.**

The investigated material is gellan gum, crosslinked with the bioamine spermidine. Samples were prepared with the more conventional 'pipetting' technique and with self-developed 'uniform mixing' technique. The two preparation techniques are described in detail and the obtained hydrogels are compared. The mechanical properties are analyzed with compression testing.

The obtained results show that samples by the so-called 'uniform mixing' method have more uniform dimensions and higher compression modulus. A preliminary stability test in cell culture medium was also carried out.

Keywords— **Hydrogel, gellan gum, spermidine, 3D cell culture, compression modulus.**

I. Introduction

Hydrogels have been studied for three-dimensional (3D) cell culture, owing to their ability to mimic extracellular matrix and highly tunable physical properties [1]. They exhibit a convenient time frame of gelation, for both cell culture and injectable clinical applications. Hydrogel properties and gel formation is controllable through polymer and crosslinker concentration, as well as crosslinker species [2].

Studies published over the recent years concerning 3D cell culture in hydrogels have been employing several methods, including techniques similar to the 'pipetting method' as explained in this article. To achieve reproducible and comparable results between different studies, there is a need for standardized preparation and testing of hydrogels for specific applications in tissue engineering. Some ASTM standards give guidelines on required properties and analysis methods, such as ASTM F895 for "Diffusion screening for cytotoxicity" and ASTM F2315 on "Alginate cell encapsulation" [3] [4]. However, standardized methods to produce 3D "bulk" hydrogels, or macro-gels, do not exist.

The model hydrogel investigated in this work is the bacterial polysaccharide gellan gum [5]. Gellan gum hydrogels can be obtained by crosslinking with cationic species. Ionic crosslinking can form true hydrogels *in situ* [2], without any need for further physical stimulation, e.g. UV light irradiation. Ionically crosslinked hydrogels have the benefit of simple, convenient preparation, and can form gels within seconds to minutes [2]. In essence, only the mixing of two components, polymer and crosslinker, is required. Additional additives, such as growth factors, cell attachment cues and cells, can be added to either polymer or crosslinker solution before gel formation.

However, it is crucial how the mixing is carried out, as will be discussed in this article. The preparation technique of a hydrogel has to produce consistent results. The user-related deviation of the results should be minimized and interpretation of the same protocol by different users should lead to the same results. It is beneficial for measuring and handling of the bulk sample, if the hydrogel samples to have clearly defined shape and mechanical stability. In most cases, mechanical testing requires well-defined sample dimensions. Here, compression testing of an unconfined sample between two pressure pistons is used to evaluate the mechanical properties of the final hydrogel samples [6].

Among other factors, we consider the mixing process crucial, to obtain reproducible and homogeneous hydrogels by ionic crosslinking. The physical properties of hydrogels for cell culture applications are paramount, because cells respond to the mechanical properties of their environment [7]. In turn, the properties of the hydrogel matrix depend closely on the preparation method. Consequently, the properties of the hydrogel must not deviate significantly from once-determined values, in order for the results to be meaningful.

Here, we develop a technique to produce hydrogel samples with consistent properties and shape, while accounting for cell culture restrictions. For example, all solutions can be sterile filtered and they technique is carried out at physiological temperatures. As a fundamental goal, the presented method achieves high consistency of the hydrogel samples and the repeatability of the preparation method. The samples produced with the 'uniform mixing' method have visually high quality and are easy to handle. Further, the presented results of the compression testing show clear difference between samples produced with the 'pipetting method' and the 'uniform mixing method'.

II. HYDROGEL PREPARATION

A. Materials and Methods

All reagents were acquired from Sigma-Aldrich. Solutions prepared in a HEPES/sucrose solution (HEPES 25 mM, pH 7.4 and sucrose 100 mg/mL). All solutions were sterile filtered before use through a Whatman® Puradisc FP 30/0.2 CaS syringe filter.

Gellan gum (Gelzan™ CM Gelrite) was purified to remove counter-ions and substitute them with sodium ions [8]. Solutions were prepared at 5 mg/mL in HEPES/sucrose buffer. A spermidine trihydrochloride solution in HEPES/sucrose buffer at 0.5 mg/mL was used as crosslinking agent. Gellan gum (GG) and spermidine (SPD) were combined in a volume ratio of 5:1.

During gel preparation, all used solutions were warmed on a water bath at 37°C using a magnetic stirrer with integrated heating hot plate (IKA® RCT basic). The water bath was stirred using a magnet stirrer.

B. Preparation Method 1 'pipetting method'

In this method the hydrogel is prepared by mixing the two solutions directly in the mold. The preparation steps are represented schematically in Fig. 1A.

Protocol - Method 1 'pipetting method'

1. Keep the solutions at +37°C in a water bath and maintain temperature during the whole procedure.
   a. If desired, add optional components to the polymer solution.
2. Pipette the crosslinker solution carefully into the bottom of the mold.
3. Quickly add the polymer solution directly on top of the crosslinker solution and mix gently by pipetting a few times.
4. Verify that the gelation has ended, by carefully tilting the mold and observing the flow of the gel.

C. Preparation Method 2 'uniform mixing method'

For Method 2 the gel components are combined and mixed in a glass vial, before they are transferred to the mold to yield a homogeneous gel. The preparation steps are shown in Fig. 1B. Optional gel components are added to the polymer solution before adding the crosslinking agent. The final solution should be stirred for a few seconds only and the hydrogel needs to be transferred swiftly to the mold with a pipette. The solution must not form gels too quickly and ideally the onset of gelation is 30 to 60 seconds.

Protocol – Method 2 'uniform mixing method'

1. Fill the polymer solution into a mixing vial. Let the solution warm up to +37°C in water bath under stirring.
   a. If desired, add optional components to the polymer solution.
2. Add crosslinker solution with a pipette directly into the sol, and gently pipette to increase mixing efficiency.
3. Within a few seconds, transfer the sol to the mold with a pipette.
4. Verify that the gelation has ended, by carefully tilting the mold and observing the flow of the gel.

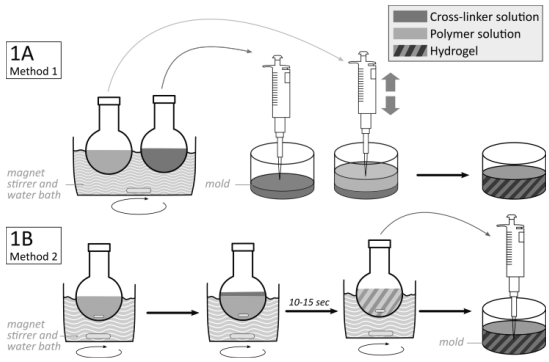

Fig. 1 Schematic explanation of gel preparation Method 1 (Fig. 1A) and Method 2 (Fig. 1B).

D. Mechanical testing

The gel samples are prepared according to the described methods and stored in an incubator, in the mold or in DMEM/F12 cell culture medium, at 37°C for 24 hours before mechanical testing. They are carefully ejected from the mold and the height and diameter of each sample are measured with a digital Vernier caliper.

Compression testing is done with a Bose BioDynamic ElectroForce Instrument 5100 using WinTest 4.1 software (TA Instruments, USA). The number of parallel compression samples (n) is 6. The testing is carried out as uniaxial, unconfined compression in air at ambient pressure and temperature. The sample is placed between two compression pistons, and prevented from sliding with wet cellulose paper.

The compression was carried out with a speed of 10 mm/min to 65% of the original sample height. From the resulting force curve the stress is calculated as force over area of the sample. The stress is plotted against the applied strain and the slope from linear region (between 15-35% strain) of the resulting curve yields the compression modulus [6].

III. Results and discussion

A. Gel preparation parameters

The protocol and the mentioned parameters should be kept constant, even if no cells are present, or the gel samples are to be analyzed with a different method, in order to produce reliable data and consistent results. This also regards the sample size for compression analysis, as the modulus is calculated based on the sample's dimensions. Thus larger cylindrical samples with sufficient height are used, whereas for cell culture flat discs with lower volume are used. Although there is a certain margin of error for the compression sample, they must neither be too flat to avoid sensitivity limitations of the measurement apparatus, nor too tall to prevent adverse failure modes such as buckling. Here, we propose the following size ratio for cylindrical 3D hydrogel samples to be used for mechanical testing:

$$\frac{height}{diameter} = 0.35 \quad (1)$$

Thus for a mold diameter of 12.12 mm (48-well plate) the height of the sample should be 4.20 mm and the volume 484 µL, assuming the gel does not experience significant shrinking or swelling upon gelation. However also smaller samples have successfully been used for compression testing. Gelation screening is carried out with smaller volume to save more precious material. The sample size can be scaled according to the height/diameter ratio in Equation 1.

The dimensions of the mixing vial should be appropriate for the final solution volume. If a narrow test tube is chosen as vial, then adequate mixing cannot be guaranteed at the top of the mixture if the filling height exceeds the reach of agitation from the magnetic stirring bar. Example parameters that have proven suitable are listed in Table 1. The material of the vial should be thin glass, to allow good heat conduction.

Table 1 Parameters for gel preparation according to the Method 2.

Parameter	Example value	Note
Water bath	+37°C	
Stirring speed	300 rpm	
Mixing vial dimension	(a) Ø 9.8 mm (sol volume 1 mL) (b) Ø 19.5 mm (sol volume 5 mL)	Choose according to total sample volume
Magnetic stirring bar	(a) Ø 2.2 mm and length 6.9 mm (b) Ø 4.6 mm and length 12.4 mm	Choose according to vial dimensions
Mold dimensions	(a) Ø 12.25 mm, volume 500 µL (b) Ø 8.75 mm, volume 183 µL	48-well cell culture plate has Ø 12.12 mm

All solutions are warmed to 37°C and are given enough time to equilibrate. This will mimic cell test conditions and allow for easier pipetting of the polymer solution. Furthermore, the water bath should be stirred to ensure even temperature distribution. It must be noted that most ionic hydrogels will form gels upon cool-down if sufficient counter-ions are present. This is the case of un-purified GG even without further addition of crosslinker solution, as residual calcium ions are present in the GG formulation [5].

The gelation time should not exceed 15 minutes, otherwise the added cells will not be evenly distributed within the gel, but will have sunken to the bottom of the mold. The gels need to be free of air bubbles and not tilted when stored to conserve sample geometry. The gelation can be observed by carefully tilting the mold as described in ASTM-F2900 [9].

Hydrogel mechanical properties are in linear relationship with water content and network density and the samples must not dry out before testing. We suggest to keep the samples in a humidity-controlled environment.

B. Sample shape and compression behavior

Hydrogel samples were prepared with GG and SPD as crosslinker according to the two different methods. The volume ratio and concentration ratio of polymer and crosslinker was the same for both methods. After the 24-hour incubation period, the dimensions of all samples were measured and compression testing was carried out. Results of the compression testing are presented numerically in Table 2 and samples of both preparation methods are shown in Fig. 2. Similarly, stability test samples (Table 2 "Method 1 and 2 in medium") were prepared according to the two protocols, but removed from the mold after 15 min and kept in cell culture medium at +37°C for 24 hours.

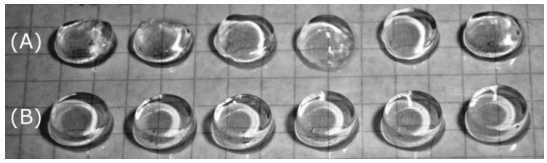

Fig. 2 Photograph of samples from (A) Method 1 and (B) Method 2.

There are clear visible differences in sample shape and homogeneity between samples of the two methods. Samples prepared with Method 2 more closely resemble the original mold shape and have clearly defined shape and sharp edges. Method 1 samples, on the other hand, show a poor shape and needed to be separated from excess liquid, before measuring.

The sample dimension and the deviation between parallel samples indicate the homogeneity and quality of the samples, which is also reflected in the compression modulus. It has to be noted that for ease of estimating their surface area Method 1 samples with irregular shape have been assumed to be round.

Table 2 Average values and standard deviation of the measured samples for Method 1 and 2, for 24 hours kept in their mold (n=6) or cell culture medium DMEM/F12 (n=3).

	Modulus [kPa]	Height [mm]	Width [mm]	Fracture strain [%]
Method 1 in mold	7.7 ± 2.1	3.6 ± 0.1	11.7 ± 0.4	28.9 ± 2.6
Method 1 in medium	46.9 ± 2.8	4.1 ± 0.3	11.2 ± 0.5	27.7 ± 3.6
Method 2 in mold	18.7 ± 2.2	4.6 ± 0.1	11.8 ± 0.2	37.7 + 2.8
Method 2 in medium	98.1 ± 9.0	4.3 ± 0.1	11.4 ± 0.1	37.2 ± 1.6

The compression modulus of Method 1 samples is significantly lower than for Method 2 samples. Similarly, the fracture point is shifted towards higher strain for Method 2 samples. Samples kept in cell culture medium for 24 hours have significantly higher compression modulus. The absorbed calcium present in the medium formulation, forms a tighter network with the polymer chains, which in turn shrinks and strengthens the GG hydrogel [5].

The thorough mixing of Method 2 forms homogeneous hydrogels with seemingly uniform network throughout the sample. If the crosslinker concentration is locally very high, it will form a heterogeneous gel, trapping some of the crosslinker in one area. The local concentration difference of crosslinker leads to a mixture of areas with true gel, weak gel and excess of water. A homogeneous network distributes the compression load evenly throughout the sample, and yields a tougher gel. Thus, higher compression modulus of samples obtained with Method 2 indicates a more uniform network. Evidently, the preparation method not only affects shape and consistency of the hydrogel samples, but also the mechanical properties of the bulk hydrogel.

A preliminary swelling test in de-ionized water of lyophilized samples showed that they disintegrate within 1 to 2 hours of immersion. Freezing the samples appears to damage the hydrogel network. To analyze swelling behavior, the samples need to be dried differently, e.g. evaporation in vacuum, or a cryoprotectant should be used.

IV. Conclusions

Here, a reproducible method to prepare hydrogel samples is proposed. The ionically crosslinked macro-gels produced with the 'uniform mixing method' (Method 2) show higher compression modulus, and smaller variation in sample dimensions. In comparison, the 'pipetting method' (Method 1) is commonly used in the literature, but yields poorly shaped gels with lower modulus.

The proposed gel preparation method ensures a thorough mixing of the gel components, by warming and stirring the sol consistently. The time frame of the gelation has to be adjusted so that mixing of polymer and a crosslinker can be carried out within a few seconds, while gelation only starts once the mixture is transferred to the mold. The results underline the importance of using a reproducible technique to create hydrogel samples.

Acknowledgment

We wish to thank the Human Spare Parts project of Tekes – the Finnish Funding Agency for Innovation, for funding this project.

Conflict of interest

The authors declare that they have no conflict of interest.

References

1. B. V. Slaughter, S. S. Khurshid, O. Z. Fisher, et al. (2009) Hydrogels in Regenerative Medicine. Adv Mater (Weinheim, Ger.) 21:3307–3329
2. J. Maitra, V. K. Shukla (2014) Cross-linking in Hydrogels - A Review. Am J Polym Sci. 4:25-31
3. ASTM Standard F2315−11 (2011) Standard Guide for Immobilization or Encapsulation of Living Cells or Tissue in Alginate Gels," *ASTM International*, West Conshohocken, United States
4. ASTM Standard F895−11 (2011) Standard Test Method for Agar Diffusion Cell Culture Screening for Cytotoxicity," ASTM International, Conshohocken, United States
5. E. R. Morris, K. Nishinari, M. Rinaudo (2012) Gelation of gellan - A review. Food Hydrocolloids 28:373-411
6. J. W. D. Callister, D. G. Rethwisch (2014) Materials Science and Engineering: An Introduction. Ringgold Inc, Beaverton
7. D. E. Discher, P. Janmey, Y.-l. Wang (2015) Tissue cells feel and respond to the stiffness of their substrate. Science 310:1139-1143
8. L. W. Doner (1997) Rapid purification of commercial gellan gum to highly soluble and gellable monovalent cation salts. Carbohyd Polym 32:245-247
9. ASTM Standard F2900−11 (2013) Standard Guide for Characterization of Hydrogels used in Regenerative Medicine," ASTM International, Conshohocken, United States

Author: Christine Gering
Institute: BioMediTech Institute and Faculty of Biomedical Sciences and Engineering, Tampere University of Technology
Street: Korkeakoulunkatu 3
City: 33720 Tampere
Country: Finland
Email: christine.gering@tut.fi

PUBLICATION III

Design of modular gellan gum hydrogel functionalized with avidin and biotinylated adhesive ligands for cell culture applications

Christine Gering, Janne T. Koivisto, Jenny Párraga, Jenni Leppiniemi, Vesa Hytönen, Kaisa Vuornos, Susanna Miettinen, & Minna Kellomäki

PLoS ONE, 14(8), 1–22
https://doi.org/10.1371/journal.pone.0221931

PLOS ONE

RESEARCH ARTICLE

Design of modular gellan gum hydrogel functionalized with avidin and biotinylated adhesive ligands for cell culture applications

Christine Gering[1]*, Janne T. Koivisto[1], Jenny Parraga[1], Jenni Leppiniemi[1], Kaisa Vuornos[1,2], Vesa P. Hytönen[1,3], Susanna Miettinen[1,2], Minna Kellomäki[1]

1 Faculty of Medicine and Health Technology, BioMediTech, Tampere University, Tampere, Finland, **2** Research, Development and Innovation Center, Tampere University Hospital, Tampere, Finland, **3** Fimlab Laboratories, Tampere, Finland

* christine.gering@tuni.fi

Citation: Gering C, Koivisto JT, Parraga J, Leppiniemi J, Vuornos K, Hytönen VP, et al. (2019) Design of modular gellan gum hydrogel functionalized with avidin and biotinylated adhesive ligands for cell culture applications. PLoS ONE 14 (8): e0221931. https://doi.org/10.1371/journal.pone.0221931

Editor: Rachael Ann Oldinski, University of Vermont, UNITED STATES

Received: November 27, 2018

Accepted: August 19, 2019

Published: August 30, 2019

Data Availability Statement: All relevant data are within the paper and its Supporting Information files.

Funding: The project was funded from several sources: the Innovation Funding Agency 'Business Finland' (formerly TEKES) as the Human Spare Parts program (MK, CG, JK, JP), by the Competitive State Research Financing of the Expert Responsibility area of Tampere University Hospital (KV, SM), by Academy of Finland project 290506

Abstract

This article proposes the coupling of the recombinant protein avidin to the polysaccharide gellan gum to create a modular hydrogel substrate for 3D cell culture and tissue engineering. Avidin is capable of binding biotin, and thus biotinylated compounds can be tethered to the polymer network to improve cell response. The avidin is successfully conjugated to gellan gum and remains functional as shown with fluorescence titration and electrophoresis (SDS-PAGE). Self-standing hydrogels were formed using bioamines and calcium chloride, yielding long-term stability and adequate stiffness for 3D cell culture, as confirmed with compression testing. Human fibroblasts were successfully cultured within the hydrogel treated with biotinylated RGD or biotinylated fibronectin. Moreover, human bone marrow stromal cells were cultured with hydrogel treated with biotinylated RGD over 3 weeks. We demonstrate a modular and inexpensive hydrogel scaffold for cell encapsulation that can be equipped with any desired biotinylated cell ligand to accommodate a wide range of cell types.

Introduction

Biomaterials are essential instruments in the field of tissue engineering and regenerative medicine that are required to support cells and mimic natural tissue.[1,2] Hydrogels are a class of biomaterials that can simulate the native, physiological, and three-dimensional (3D) environment of mammalian cells and act as an artificial extracellular matrix.[3–8] It has been well-established that 3D tissue matrices must be considered over planar, two-dimensional (2D) surfaces for cell culture applications and *in vitro* disease modeling.[5] The biomaterial should recreate all aspects of the natural cell environment, including dimensionality, physical, mechanical, and biochemical properties. These properties are then engineered to control cell attachment and cell fate.

There are several issues that need to be considered when designing a hydrogel for cell culture applications. Foremost, all components must assert their biocompatibility and the final material, as well as the reagents used in the preparation method, must be non-toxic and elicit

(VPH) and by The Doctoral Programme in Biomedical Sciences and Engineering at Tampere University (CG). The funders had no role in study design, data collection and analysis, decision to publish, or preparation of the manuscript.

Competing interests: The authors have declared that no competing interests exist.

no negative cell response.[1,5] However, rather than only providing a passive environment, hydrogels are also required to promote certain cell functions and support cell recognition and response.[5] In practice, the hydrogel should contain cell recognition moieties, such as peptide sequences or proteins like growth factors, i.e., sites that actively guide cell response. In a similar fashion, the mechanical properties and degradation profile of the hydrogel matrix must actively influence the response of the seeded cells.

Further, the stiffness of the microenvironment is directly conveyed to the cytoskeleton through cell attachment and integrin signaling. This phenomenon, called mechanotransduction, is known to affect the differentiation of cells[8–10], cell attachment, and migration.[5,11,12] In turn, mechanotransduction requires the integrin ligand to be strongly tethered to the polymeric network. This attachment is necessary to promote cell spreading and to prevent the diffusion of the cellular cues.[4]

Finally, there are a few more technical issues of hydrogel design that include the manipulation and handling as well as the availability and cost-efficiency of the material.[13] Clearly, the material must be affordable to enable its use on a more general basis. The ability to handle, transport, and analyze the final hydrogel product has definite practical advantages over more sensitive constructs. Ultimately, the design of a hydrogel must strike a balance between functional complexity and technical simplicity.

One approach to the design of hydrogels for tissue engineering applications is the conjugation of bioactive molecules to the polymer. Examples of conjugation techniques include the formation of zero-length bonds, bio-orthogonal coupling, and the use of protein-ligand binding. Zero-length bonds form a short, direct chemical bond between the polymer and the coupled compound that are achieved using carbodiimide coupling and thiol-based conjugation techniques.[14] The so-called bio-orthogonal coupling, such as the strain-promoted azide-alkyne cycloaddition[15], do not interfere with compounds found in living organisms. Here, we exploit the protein-ligand binding, which provides a simple and native tool to form substrate-ligand complexes. Certain proteins have the ability to bind small, specific molecules with high affinity and selectivity. One of the most in-depth studied protein systems is the avidin-biotin binding system.[16–18] Avidin is a protein with the capability to bind biotin with outstanding selectivity and specificity. The avidin-biotin interaction is deemed to be the strongest non-covalent bond in nature with a dissociation constant of $K_d \sim 10^{-15}$ M, and it has often been used in biochemical assays, diagnostics, and tissue engineering.[18] Furthermore, this type of protein-affinity system has been exploited for many different applications in chemistry, biosciences, and tissue engineering. Indeed, modular approaches, such as the use of nanocellulose for 3D printing [19], 2-hydroxyethyl methacrylate flat substrates[20], agarose for spatial patterning [21], and porous poly-L-lactic acid scaffolds [22], have been presented and will be discussed in chapter 4.1.

The base polymer used in this study is gellan gum (GG), which is an anionic polysaccharide that has previously been investigated for various cell culture applications.[23–26] GG is able to form self-supporting hydrogels, that do not flow and fracture under high stress and also described as "true gels" in contrast to "weak gels".[27] To form true hydrogels, GG is hereafter ionically crosslinked with the bioamine spermidine. In its native state, GG has been found to be biocompatible, but most cell types do not readily adhere to or favor the material. Previously, our research group established that functionalization of gellan gum with ECM proteins is needed to obtain better cell attachment and migration.[24]

Here, we propose the coupling of the avidin protein to gellan gum to create a modular material that can be modified through the addition of biotinylated cell cues. The cues can enable cell attachment, guide differentiation, or even present drug molecules. In this study, we use an avidin analogue called charge-neutralized chimeric avidin, which has been developed

and produced by our group. It has identical affinity for biotin, but increased stability against pH and temperature treatment compared to wild-type avidin.[28] Furthermore, we have sought suitable applications for the charge-neutralized chimeric avidin in the field of tissue engineering.[29] Biotin is a small organic compound that can be chemically coupled to a desired ligand. Before the gelation step, the hydrogel precursor can be modified without any additional chemical functionalization steps. The choice of biotinylated species can range from attachment factors, such as RGD, to drug molecules, and to growth factors (GF), such as vascular endothelial GF, which also affects differentiation. Ultimately, the goal is to design a non-specialized platform that is adaptable to different applications, while still possessing the innate ability to support cell growth and to allow for the convenient analysis of the tissue engineering construct.

To underline the suitability of the proposed modular hydrogel, we characterized the mechanical properties and avidin functionality of the gellan gum-avidin material. First, GG was purified to remove excess counter-ions, yielding sodium-purified GG (NaGG).[23,30] Then, charge-neutralized chimeric avidin (avd) was coupled to NaGG via carbodiimide conjugation using EDC and NHS[14,23], yielding NaGG-avd. True hydrogels can be formed with suitable crosslinker concentration and compression testing revealed that mechanical behavior was not impaired by the functionalization. Avidin coupled to NaGG is functional and its ability to bind biotin is not impaired by the coupling. Additionally, avidin is shown to be covalently coupled to the polymer network as it does not diffuse from the gel. Human fibroblasts were cultured in NaGG-avd and their viability was assessed. Similarly, the effect of NaGG-avd on human bone marrow-derived stem cells was studied for a total culture time of 3 weeks, highlighting the long-term stability of the gels.

Materials and methods

All materials were acquired from Sigma-Aldrich, if not otherwise stated. Charge-neutralized chimeric avidin (avd) was kindly donated by the Protein Dynamics group at the Tampere University and is commercially available for research use at Ref. [29].

Purification

Gellan gum (Gelzan^{TM}, low acyl, M_w 1 kg/mol) was purified to remove counterions in the product and to replace them with sodium ions.[30,31] Briefly, a gellan gum solution (0.5% w/v, 400 mL) in dI water (milliQ) was combined with Dowex cation exchange resin (5 g, H^+ form, 50–100 mesh, prerinsed in HCl) and stirred for 30 min at 60 ˚C. The exchange resin was removed from the solution through decantation and the pH was adjusted to 7.5 with NaOH. The purified product was then precipitated in *i*-propanol and lyophilized over 2 days.

The ion concentration of NaGG was determined with inductively coupled plasma optical emission spectrometry (ICP-OES). Hence, a part of the sample was digested in sulfuric acid and hydrogen peroxide following the protocol by Kirchmajer et al. (2014)[31] and measured with Agilent 5110 ICP-OES (Agilent Technologies).

Functionalization and structural characterization

The functionalization reaction was based on the publication by Ferris et al. who similarly activated gellan gum with 1-ethyl-3-(3-dimethylaminopropyl)-carbodiimide (EDC) and N-hydroxysuccinimide (NHS) to couple the peptide sequence RGD.[23] A solution of sodium-purified gellan gum (NaGG, 10 mg/mL, 10 or 20 mL) was dissolved in HEPES buffer (50 mM, pH 6.5) and stirred at 40 ˚C. The gellan gum was then activated with EDC (0.4 M) and sulfo-NHS (1.0 M) for 15 min and consequently quenched with β-mercapthoethanol (28 μL, final

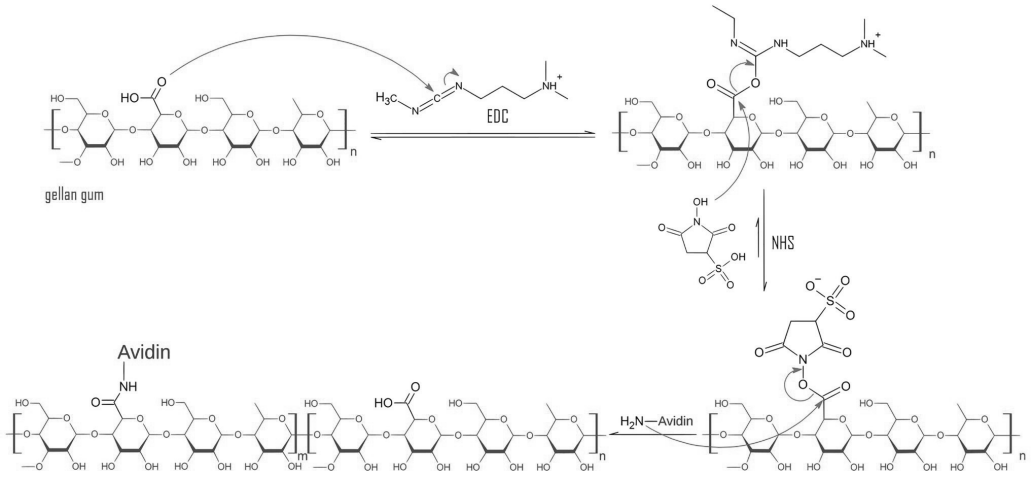

Fig 1. Reaction scheme of NaGG functionalization with avidin via activation with EDC and NHS. EDC activates the carboxyl group of NaGG, and the intermediate is stabilized with NHS to prevent activation of avidin with EDC. The final product is a combination of functionalized [m] and non-functionalized [n] NaGG repeating units.

https://doi.org/10.1371/journal.pone.0221931.g001

concentration 20 mM). Finally, charge-neutralized chimeric avidin (1 mg/mL, 3.5 mL in HEPES 50 mM, pH 6.5) was added and the mixture was stirred for 5 h at 40 ˚C. The functionalized product was dialyzed over 5 days (MWCO 12–14 kDa) and subsequently lyophilized. Two different batches of NaGG-avd were studied. Each batch differed in the amount of avidin used and the final avidin concentration in the material. Here, these modular hydrogels are termed NaGG-avd(L) for low avidin concentration (4 mg avidin/ 1 g NaGG) and NaGG-avd (H) for high avidin concentration (21 mg avidin/ 1 g NaGG).

The reaction scheme of the functionalization is shown in Fig 1. The unstable intermediate of the active ester is stabilized through the addition of NHS, which forms an amine-reactive sulfo-NHS ester. The primary amines of avidin react with the stable intermediary to form a peptide bond. Notable side reactions include the activation of the carboxyl bonds present in the protein structure of avidin. It can, however, be assumed that EDC quickly deactivates through hydrolysis in aqueous media.

The resulting structure was investigated by means of avidin-biotin binding and fluorescence spectroscopy as well as with electrophoresis (SDS-PAGE with urea) and elution analysis. A fluorescence titration curve was prepared from NaGG-avd (1 mg/mL in HEPES pH 7, 10% sucrose) and the biotinylated fluorescent dye b5F (biotin-5-fluorescein, 2 μM in DMSO and PBS). Control curves were prepared with NaGG and NaGG-avd blocked with biotin (3 μL, 0.17 mg/mL in 50 mM sodium-phosphate, 100 mM NaCl buffer, pH 7). Aliquots of 25 μL b5F were added to a 2 mL sample in a cuvette and each measured after 2 min with a QuantaMaster PTI spectrofluorometer (Photon Technology International, Inc., Lawrenceville, NJ, USA) (excitation at 495 nm, emission at 520 nm, slits 2 nm).

For elution analysis, hydrogel samples were prepared with 5 mg/mL NaGG-avd and 10 μM b5F (14 μL/mL NaGG-avd) and crosslinked with 0.5 mg/mL spermidine (SPD). The samples were incubated in the mold overnight and then placed into 500 μL PBS for up to 48 h in an incubator under shaking at 37 ˚C. The eluate was taken at time points of 1 h, 6 h, 24 h, and 48

h, and the fluorescence intensity was measured. As a reference sample, NaGG was mixed with avidin without conjugation and gels were formed as described above.

Sodium dodecyl sulfate polyacrylamide gel electrophoresis (SDS-PAGE) was used to further examine the covalent nature of the NaGG-avd conjugate through comparison with a non-covalent mixture of NaGG and avidin (avd). To improve the resolution of the SDS-PAGE, urea was added to the samples and the cast gel. The PAGE gel was cast according to standard procedure, but urea (8 M) was added. All samples were incubated with biotin (85 μg/mL final concentration) to stabilize the avidin tetramer. After addition of loading buffer, the samples were heated to 50 ˚C for 15 min. After a short cooling period, 8 M urea was added to each sample. The electrophoresis was performed at +4 ˚C for 3 h at 100 V. Finally, the gel was stained with Oriole™ fluorescent gel stain (Bio-Rad) and imaged with a ChemiDoc MP imaging system (Bio-Rad Laboratories) with Image Lab software.

Physical properties

Hydrogel samples were prepared with a uniform mixing technique, which has been described earlier[30], to yield homogenous, disc-shaped samples crosslinked with the cationic compound SPD. Gellan gum (5 mg/mL in HEPES/sucrose solution, pH 6.5) was mixed with spermidine (0.5 mg/mL) in 5:1 volume ratio. If $CaCl_2$ was used instead of spermidine crosslinker, a concentration of 10 mM was added in same volume ratio. The hydrogel solution was then warmed in a mixing vial under constant stirring (300 rpm) and the crosslinking solution was added. The solution was then swiftly transferred to the mold before the true gel was formed.

Compression behavior was analyzed with a Bose BioDynamic ElectroForce Instrument 5100 using WinTest 4.1 software (TA Instruments, USA). Disc-shaped samples with a diameter of 1.2 cm and a height of 4.5 mm were prepared in PP/PE molds, and the number of parallel samples (n) was 5. The test was carried out as uniaxial, unconfined compression in air at ambient pressure and temperature. The sample was prevented from sliding with wet cellulose paper and compressed with a speed of 10 mm/min to 65% of the original sample height. From the resulting stress-strain curve, the fracture strain and fracture strength were analyzed.

The swelling behavior of the functionalized hydrogel NaGG-avd was monitored over 3 weeks. The chosen hydrogel compositions for the swelling corresponded to the studied to compression samples. The gels were incubated in 500 μL of PBS or DMEM F-12 at 37˚C for up to 3 week. The samples were then weighed for their wet weight and consecutively lyophilized and weighed again to determine the dry mass. (Data shown in S4 Appendix).

Cell culture

Human fibroblasts WI-38 (passage 24–26, Sigma-Aldrich/Culture Collections, Public Health England) we expanded for one week in WI-38 medium, consisting of 10 vol% FBS, 25 U/mL penicillin/streptomycin (pen/strep; Lonza, Basel, Switzerland) in DMEM-F12 1:1 (Gibco, Thermo Fisher Scientific, Waltham, MA) until confluent. The hydrogel solutions of NaGG and NaGG-avd were sterilized prior to cell culture through filtration (Whatman® FP30/0.2 CA-S). The cells were seeded on top of the hydrogel (2D, 63 000 cells/cm^2) and encapsulated in the hydrogel (3D, 950 000 cells/mL) using a Greiner Cellstar 48-well plate (Sigma-Aldrich). The samples were prepared similarly as described for the compression test sample, where the NaGG-avd solution was heated and stirred in a mixing vial at 37 ˚C.[32] For cell culture purposes, the biotinylated compound was added, followed by the cell suspension and mixed gently (300 rpm) to achieve homogeneous 3D distribution. Finally, the crosslinker spermidine (0.5 mg/mL, 17 vol% of NaGG-avd) was added and the hydrogel mixture was cast into the well-plate.

The tested material compositions included NaGG-avd with biotin (0.17 mg/mL in 50 mM sodium-phosphate, 100 mM NaCl buffer, pH 7), biotinylated cyclic RGD (cyclo[Arg-Gly-Asp-D-Phe-Lys(Biotin-PEG-PEG)] 0.1 mg/mL in H_2O, 0.3 μg/mL in final gel), and biotinylated human fibronectin (bFN, 2.52 mg/mL, 33 μg/mL in final gel; fibronectin was purified by gelatin affinity chromatography from outdated plasma preparation and chemically biotinylated). The concentration of biotinylated species was set to match the number of avidin binding sites determined with fluorescence titration. As a reference, the fibroblasts were grown on the well-plate (PS) bottom. The cells were then cultured for 3 days and LIVE/DEAD® stained.

The cell culture samples were stained using the LIVE/DEAD® viability/cytotoxicity assay (Molecular probes, Thermo Fisher Scientific) containing calcein acetoxymethyl ester (Ca-AM) and ethidium homodimer-1 (EthD1). The dyes were diluted in PBS (Lonza) (final solution concentration Ca-AM 0.8 μM and EthD1 1.0 μM) and added on top of the cell culture samples. The samples were incubated for 30 min at room temperature and imaged with an Olympus IX51 inverted microscope and an Olympus DP30BW digital camera (Olympus, Tokyo, Japan). The images were then analyzed with ImageJ software (U.S. National Institutes of Health, Bethesda, MD)[33] through the particle counting algorithm. The cell viability was determined from the area according to Eq (1), while cell spreading was determined from the same data using Eq (2):

$$\text{Viability} = \frac{\text{area of live cells}}{\text{area of live cells} + \text{area of deadcells}} \quad (1)$$

$$\text{Spreading} = \frac{\text{area of live cells}}{\text{image area}} \quad (2)$$

Primary human bone marrow stromal cells (hBMSC) were previously harvested, isolated, and cryo-preserved in gas phase nitrogen by the Adult Stem Cell Group, BioMediTech, Tampere University, in accordance with the Regional Ethics Committee of the Expert Responsibility area of Tampere University Hospital, ethical approval R15174. The hBMSCs were isolated from an anonymous donor (labeled 6/16) with the patient's written informed consent during surgery at the Department of Orthopaedics and Traumatology at Tampere University Hospital. The isolation of hBMSCs was performed as described previously with slight modifications.[34,35] Briefly, the bone marrow aspirate was rinsed with DPBS (Lonza), resuspended in Ficoll (GE Healthcare, Chicago, IL, USA), centrifuged 800 g for 20 min at room temperature after which mononuclear cells were collected, washed twice with α-MEM (Gibco, Thermo Fisher Scientific) and centrifuged 400 g for 15 min at room temperature. In the following, cells were seeded into PS flasks (Nunclon; Sigma-Aldrich) in basic medium containing 5% HS (Biowest, Nuaillé, France) in α-MEM and 1% 100 U/mL pen/strep and 5 ng/mL hFGF-2 (Miltenyi Biotec, Bergisch Gladbach, Germany), and expanded until 80% confluence. The isolated hBMSCs were characterized with flow cytometry (S6 Appendix).

The hBMSCs (passage 6) were thawed and expanded for one week in T75 PS flasks (Nunclon; Sigma-Aldrich) in basic medium until confluent. The cells were then harvested and seeded into the hydrogel via uniform mixing (cell density 950 000 cells/mL), as described for the fibroblast test using spermidine as crosslinker. The studied materials were NaGG (as a reference) and NaGG-avd with the addition of biotinylated cyclic RGD (2.5 μM final solution concentration). The cells were cultured for 21 days in the hydrogels with the addition of osteogenic medium (5 vol% HS, 0.25 mM ascorbate-2-phosphate, 10 mM β-glycerophosphate, 1% 100 U/mL pen/strep in α-MEM, with the addition of dexamethasone 5 nM), which was replaced every other day.

Viability assay was carried out on day 3, 14, and 21 similar to the WI-38 experiment. Ca-AM and EtHD-1 were diluted in PBS (final solution concentration Ca-AM 0.5 μM and EthD1 0.25 μM) and added on top of the cell culture samples. On day 21, the samples were stained with phalloidin (0.17 μg/mL in 1% bovine serum albumin BSA) and 4',6-diamidino-2-phenylindole (DAPI; dilution 1:2000 in PBS; Sigma-Aldrich). The samples were then fixed (0.1% Triton x-100 and paraformaldehyde PFA) and blocked (1% BSA) before staining.

Results

GG was purified to remove counterions (Ca^{2+}, K^{+}, Mg^{2+}) and to replace them with sodium (Na^{+}). ICP-OES data can be found in S1 Appendix. The result of the ion analysis shows that the calcium content was reduced to below 0.1 wt%, closely matching reported literature values [24,29]. NaGG was successfully functionalized with the recombinant protein 'charge-neutralized chimeric avidin' (avd) through carbodiimide conjugation. NaGG-avd solution was prepared in HEPES buffer with sucrose. Hydrogel samples were prepared through gelation with SPD or $CaCl_2$ overnight in disc-shaped molds with dimensions of about 4.1 mm in height and 11.6 mm in diameter.

Success of functionalization

Fluorescence analysis was carried out in different ways to prove the binding and functionality of avidin. The biotinylated fluorescence dye biotin-5-fluorescein (b5F) was used in all cases. Fluorescence titration with b5F was carried out in order to confirm that avidin retains its ability to bind biotin after being coupled to gellan gum. Therefore, small amounts of b5F were added to the analyte. This dye shows a quenching effect to approximately 50% of fluorescence strength when bound to an avidin specific binding site, which results in a non-linear curve. The concentration of available biotin binding sites can be derived from the intersection of the quenched curve and the linear region after saturation. Fig 2 shows the curves of coupled NaGG-avd, unmodified NaGG, and coupled NaGG-avd that has been blocked with biotin. The unmodified and blocked samples show a linear increase in fluorescence intensity, whereas the avidin-modified samples show a quenched curve followed by a linear increase.

From the titration curves in Fig 2, the avidin concentration was estimated to be 0.075 (L) and 0.375 (H) μM in 1mg/mL NaGG-avd. The degree of functionalization (d_{funct}) can be calculated as the molar ratio between avidin-functionalized GG repeating units [n] and non-functionalized repeating units retaining the carboxyl (COOH) group [m]. The indices n and m refer to the reaction scheme in Fig 1, and the functionalization degrees are derived from Eq (3):

$$d_{funct} = \frac{[n]}{[m]} = \frac{mol(avidin)}{mol(GG-COOH)} \cdot 100\% \quad (3)$$

A functionalization degree of 0.005 mol% (L) and 0.027 mol% (H) was achieved between different functionalization degrees, assuming one avidin is bound to only a single carboxyl group.

To ascertain the covalent binding between gellan gum and avidin, hydrogel samples were prepared containing b5F. The samples were incubated in phosphate buffered saline (PBS) at 37 ˚C, with separate samples for each time point of 1 h, 6 h, 24 h, and 48 h, and the fluorescence intensity was measured. As a reference sample, NaGG hydrogel samples were prepared with the addition of a comparable amount of avidin. Fig 3(A) shows the resulting graph.

Initially, the fluorescence intensity of both eluates is very similar, alluding to a leaching of whole polymer chains from the gel sample carrying the b5F. However, after roughly 24 h in

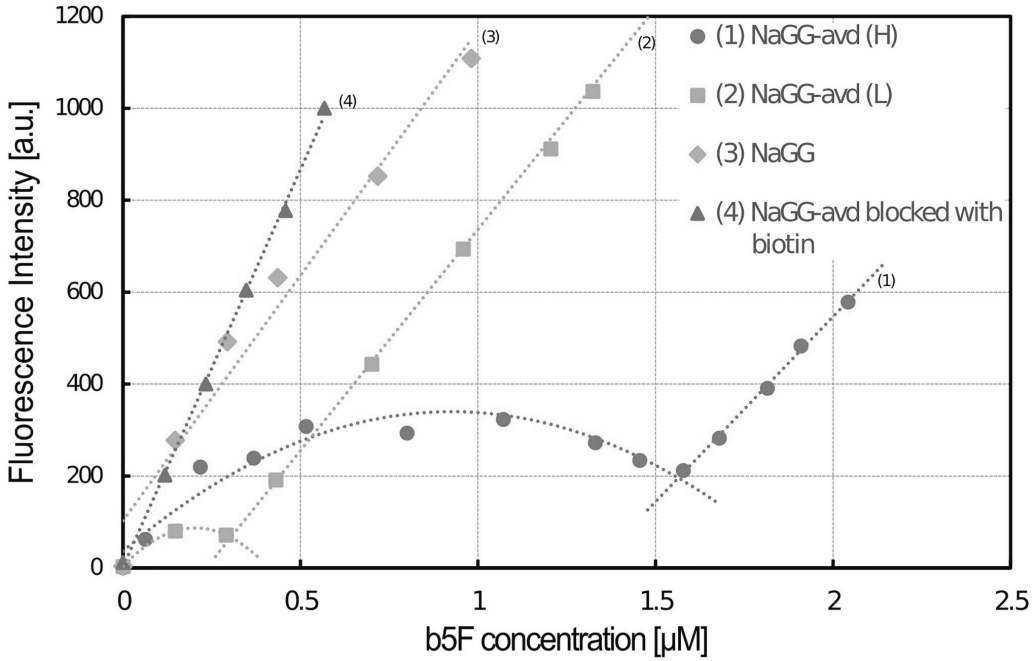

Fig 2. Fluorescence titration curves with step-wise addition of b5F. Non-functionalized NaGG (green) and functionalized NaGG-avd blocked with biotin (red) show a linear curve, whereas functionalized NaGG-avd (yellow and blue) with available biotin-binding sites show quenching behavior at low b5F concentration. From the intersection of quenched and linear parts the biotin binding site concentration can be deduced. From the intersection or linear and polynomial curves, the biotin-binding concentration was calculated.

https://doi.org/10.1371/journal.pone.0221931.g002

suspension, the fluorescence intensity of NaGG-avd starts to reach a plateau and virtually no further b5F leaves the gel. In contrast, the reference sample NaGG+avd continues to exude b5F, and after 48 h the fluorescence intensity of the eluate is considerably higher.

When choosing methods to investigate the gellan gum-avidin bonding, it was surmised that ^{1}H-NMR does not sufficiently distinguish the newly formed carbodiimide-coupled peptide bond from the already present bonds in the studied biomacromolecule. Similarly, FT-IR spectroscopy is unable to show the bond characteristics between the two macromolecules. Thus SDS-PAGE was the method of choice to confirm the gellan gum-avidin binding. The urea PAGE shows a strong band for avidin tetramer in the reference sample (NaGG+avd) and pure avidin, but a faint, diffuse band for the conjugated sample (NaGG-avd) in Fig 3(B). The dispersion of the band may be due to avidin coupled with short GG chain fragments, leading to a wider molar mass range. A very faint band for the avidin monomer can be observed for NaGG-avd, but not for the reference sample NaGG+avd. GG itself has a molecular weight of around 1000 kDa and does not appear as a band on the SDS-PAGE. The full uncropped and un-altered blot and gel image is available in S2 Appendix. A simple washing test was carried out is described in S8 Appendix, demonstrating a 4-fold increase in retained biotinylated fibronectin when comparing unfunctionalized (NaGG) and functionalized GG (NaGG-avd). This further underlines the functionality of the proposed modular hydrogel.

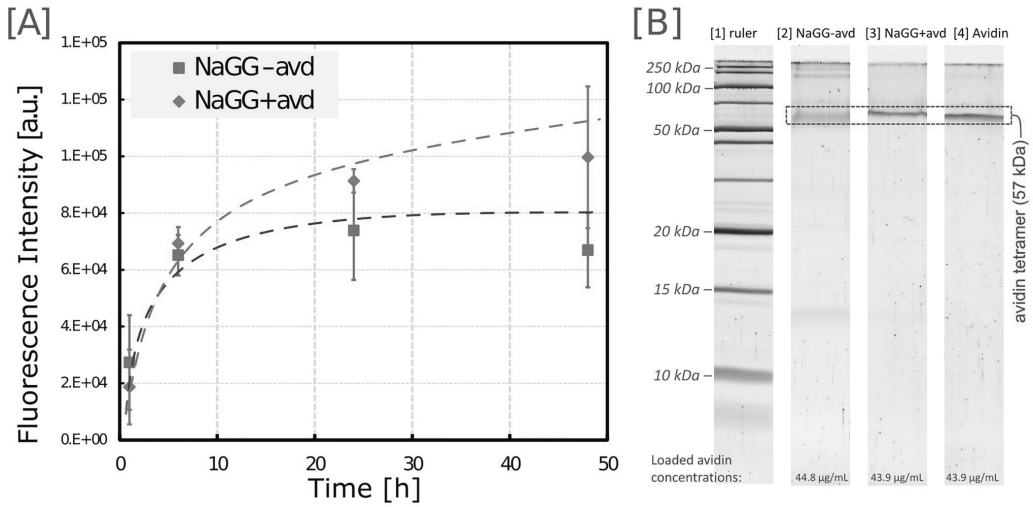

Fig 3. Avidin-GG coupling analysis. (A) Elution analysis: Fluorescence intensity of supernatants of hydrogel samples immersed in PBS. Supernatant was collected from separate samples over 2 days and analyzed with fluorescence spectrometer. Error bars represent standard deviation calculated from three independent samples, and logarithmic fit curves were added to guide the eye. (B) SDS-PAGE: Electrophoretic separation and comparison of conjugated (NaGG-avd) and unconjugated (NaGG+avd) samples. Tetrameric avidin band (57 kDa) is very faint and blurry for NaGG-avd, compared with NaGG+avd and pure avd, indicating covalent bonding between avidin and polymer.

https://doi.org/10.1371/journal.pone.0221931.g003

Physical properties

The gelation time can be estimated through a qualitative tube-tilt test. NaGG-avd forms true gels during a period of about 30 seconds to one minute after the hydrogel has been transferred to the mold. For mechanical testing, the hydrogel samples were prepared as described earlier and incubated overnight at 37 ˚C before testing. The samples were compressed once to 65% of their original height and then discarded. Representative compression curves for each sample type are shown in Fig 4(A). The results of fracture strength and strain are plotted for comparison in Fig 4(B) and shown in S3 Appendix.

From Fig 4, a significant difference in fracture point between SPD and $CaCl_2$ gels can be seen. Hydrogels formed with $CaCl_2$ are more elastic and have a higher fracture strain of ~46%, while gels formed with SPD are more brittle and have fracture occurring already at around 35% strain. However, the fracture strength values for either crosslinking method are similar. The extensive error exhibited by the strain value may be due to a manual error when positioning the sample on the compression piston. One-way analysis of variance (ANOVA) was performed assuming a confidence level of 95% ($p < 0.05$) with Microsoft Office Excel. The analysis showed that there is a significant difference between all shown samples ($p < 0.05$), but the samples prepared with SPD showed no significant difference ($p = 0.07$).

Remarkably, it appears that the addition of avidin to the polymer consistently increases both the fracture strength and fracture strain of the hydrogel samples. The samples were prepared in a buffer at pH 6.5, whereas during cell culture experiments the pH was at 7.4 determined by the cell culture medium. Although charge neutralized chimeric avidin has an isoelectric point (pI) of 6.92 (theoretical value), it can be assumed that the terminal N-acetyl glucosamine, as well as lysine and arginine groups, will carry a positive charge within the range of the mentioned pH values regardless. These positively charged amino groups aid in

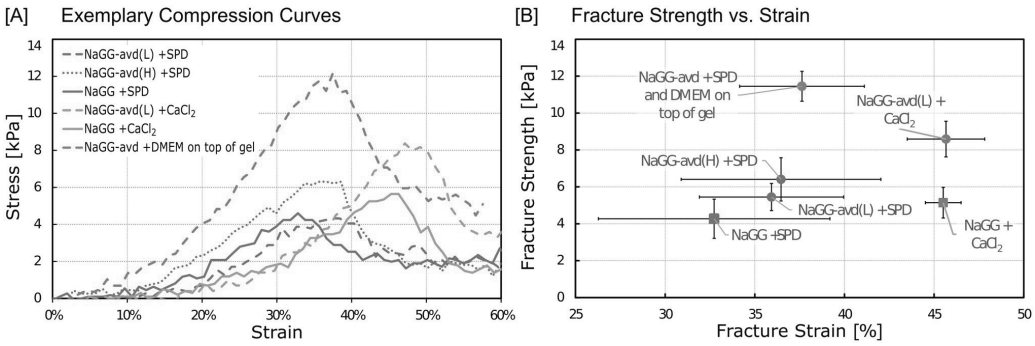

Fig 4. Compression testing results. (A) Representative compression curves of samples with different composition. (B) plot of fracture strength against fracture strain When examining all data, fracture strength ($p = 9.28 \times 10^{-11}$) and fracture strain ($p = 1.4 \times 10^{-4}$) are statistically different. Testing within samples formed with SPD, however, no significant difference is observed between fracture strength ($p = 0.06$) and fracture strain ($p = 0.54$). Error bars represent one standard deviation calculated from five independent samples.

https://doi.org/10.1371/journal.pone.0221931.g004

the crosslinking of the anionic gellan gum as additional crosslinker via charge screening. This is beneficial as the net effect of avidin functionalization is increased mechanical toughness.

An initial test with cell culture medium (DMEM) was carried out to observe the behavior of the gels in cell culture conditions. The hydrogel was crosslinked with SPD, and DMEM was added on top after the gels were formed. The samples were then incubated overnight before testing. The cationic species in DMEM diffuse into the hydrogel and increase the fracture strength of the gels significantly.

The swelling test showed no swelling of the gels, but rather a contraction over time. On average, the gels lost 3% of their original mass over 3 weeks. The results of the swelling test can be found in S4 Appendix.

Cell culture

Human WI-38 fibroblasts were cultured in avidin-modified gellan gum for three days. Three different biotinylated compounds (biotin, RGD, and fibronectin) were added to the hydrogel as separate samples. As control samples, the bare well bottom (TCP, 2D) as well as the unmodified gellan gum (3D) were used. The cells were alive when cultured on top of the hydrogel (2D) as well as when encapsulated in the matrix (3D). Fig 5 shows LIVE/DEAD® fluorescence images after three days in culture (Fig 5A1–5D1 and 5A3–5D3). The images show aggregation to large cell clusters in 2D and 3D. During encapsulation, the 3D distribution of fibroblasts was homogeneous (S9 Appendix). The most notable difference can be observed in the cell distribution and density between unmodified/unpurified GG (control) and the modified hydrogel samples (NaGG-avd). Subsequently, the samples were fixed and immuno-stained (DAPI, phalloidin, fibronectin antibody; Fig 5A2–5D2 and 5A4–5D4). Immunostaining shows no meaningful cell spreading, judging from the shape of the actin cytoskeleton (red). Fibroblasts produced their own fibronectin, as revealed by the fibronectin immunostaining in samples without added bFN.

To analyze the images statistically, images were taken of each well from random areas and the total area of live (green pixels) and dead (red pixels) cells was compared, as shown in Fig 6. Due to strong clustering of cells, the area was used rather than the number of particles. Similarly, the large error, especially for the 2D samples, was caused by aggregation of cells and the

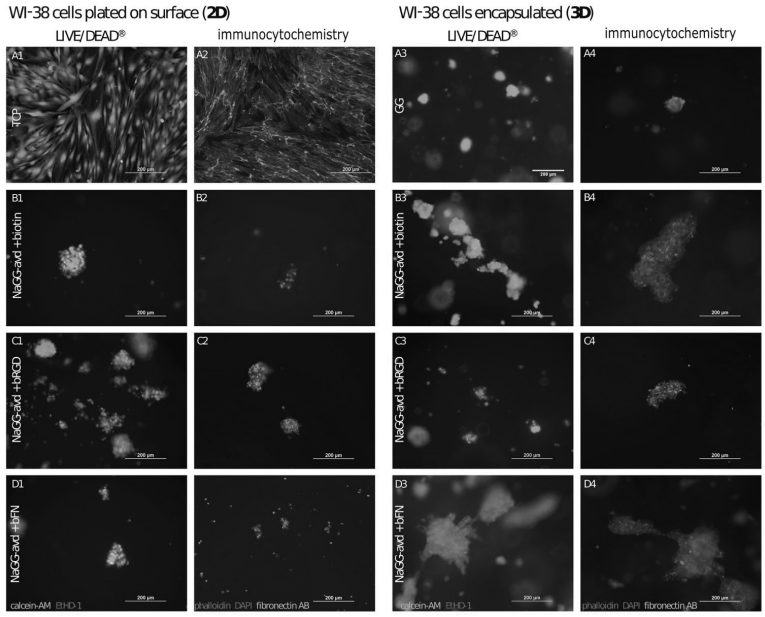

Fig 5. WI-38 fibroblasts after three days in culture. A1-D2 (left side): 2D culture with 63 000 cells/cm^2, A3-D4 (right side): 3D culture with 950 000 cells/mL in gel. Images A1-D1 and A3-D3 LIVE/DEAD® staining with live cells (Ca-AM, green channel) and dead cells (EthD1, red channel); images A2-D2 and A4-D4 actin filaments (red channel, TRITC-phalloidin), fibronectin (green channel, fibronectin antibody), cell nuclei (blue channel, DAPI).

https://doi.org/10.1371/journal.pone.0221931.g005

large difference of perceived cell density between different images of the same well. As seen in Fig 6A, all 3D samples show viability above 85% but are ultimately very similar with no statistical difference. ANOVA was performed assuming a confidence level of 95% with the result that there is a significant difference between the cell count of all the shown 2D samples, but no

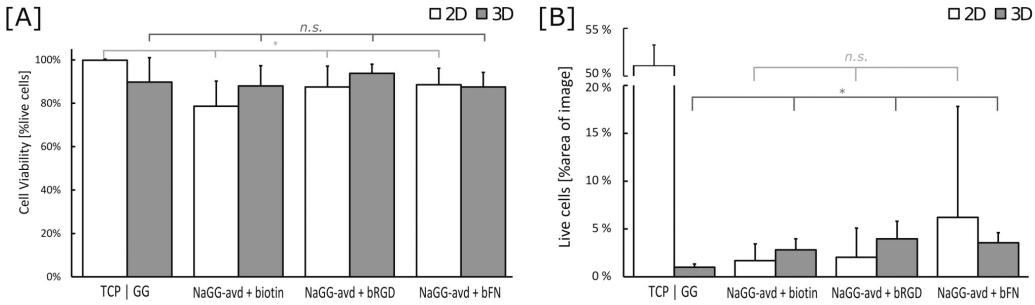

Fig 6. [A] Cell viability and [B] spreading of WI-38 fibroblasts in different materials as calculated from LIVE/DEAD® stain image analysis. Control materials are tissue culture plastic (TCP, 2D) and unmodified, unpurified GG (3D). Bars represent mean values ± SD, n ≥ 10. [A] Cell viability (%live cells vs sum of live and dead cells) demonstrates that all 3D samples (GG, NaGG-avd) are statistically the same ($p = 0.09$), while the 2D samples (TCP, NaGG-avd) are statistically different ($p^* < 0.05$). Similarly, cell spreading (area% of live cells in image) demonstrates no significant difference between 2D GG based samples ($p = 0.20$), while there is significant difference between 3D samples ($p^* = 3.94 \times 10^{-8}$).

https://doi.org/10.1371/journal.pone.0221931.g006

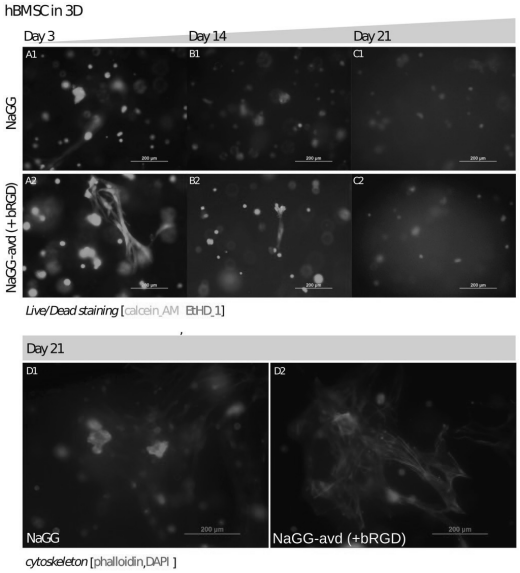

Fig 7. hBMSC encapsulation results (A1-C1 and A2-C2) LIVE/DEAD® stain of hBMSC encapsulated in NaGG (control) and NaGG-avd with bRGD over 21 days. Red stain = dead cells, Green stain = live cells. (D1-D2) Immunocytochemical cytoskeleton staining on day 21. Blue = cell nuclei (DAPI) and Red = actin filaments (phalloidin-TRITC).

https://doi.org/10.1371/journal.pone.0221931.g007

significant difference between the 3D samples. Full cell viability data from particle counting analysis is shown in S5 Appendix. Using the area% of the live cell data, cell spreading was analyzed as shown in Fig 6B, referring to the area covered by live cells on the investigated image. ANOVA test reveals no significant difference between cell spreading on or in GG-based samples (GG and NaGG-avd), due to the aforementioned large standard deviation and clustering. There is, however, a significant difference between 3D samples of GG formulations.

Consequently, human bone marrow derived stromal cells (hBMSC) were encapsulated and cultured in NaGG-avd with added bRGD for up to 21 days. Fluorescence images with LIVE/DEAD® stain of the time points 3, 14, and 21 days are shown in Fig 7. After 21 days, the samples were fixed and stained with DAPI (cell nuclei) and phalloidin (actin filaments), referred to as immunocytochemical cytoskeleton staining, as shown in Fig 7D.

The LIVE/DEAD® images demonstrate that the hBMSC are viable in both materials in 3D suspension. Evidently, the image quality degrades the longer the cells are in culture and it becomes difficult to achieve good microscope images due to opaque material. This behavior may indicate a mineralization by the hBMSC differentiating towards bone, but conclusions about differentiation cannot be drawn from actin cytoskeleton alone. In identical culture conditions, stained cell-free blank samples showed no background fluorescence after 21 days (the background image is available in S7 Appendix). Thus, the developing opacity is caused by the cells and is not due to the GG material.

Immunostaining of hBMSC samples at day 21 confirmed the observations of the LIVE/DEAD® images. A majority of the cells appear rounded, but some of them do show elongation. Visibly there are more elongated cells in NaGG-avd+bRGD than in the non-

functionalized NaGG, which is more evident with the stained actin (additional cytoskeleton images in S7 Appendix). The hBMSC culture test was analyzed with only staining and microscope images, while no quantitative analysis was carried out.

Discussion

The presented results support the concept of an avidin-modified hydrogel material for 2D and 3D cell culture applications. We have shown that the functionalized gellan gum can bind biotinylated compounds, thus equipping the hydrogel with bioactive factors and enabling cell attachment. The gellan gum-based material shows little to no degradation and has been found to be feasible for long-term cell culture. Furthermore, it has suitable mechanical properties and convenient preparation.

Functionalization strategies

There is an abundance of approaches to design hydrogels described in the literature. These approaches include the covalent functionalization of passive polymers with bioactive cues, blending with bioactive native polymers or peptides, and the use of native ECM components. [9,36] A broad selection of materials for 3D cell culture is also available commercially.

Hydrogels prepared from decellularized ECM or ECM components are a popular choice as promoting scaffolds because they naturally contain cell recognition sites. Commercially available examples include PuraMatrix® [37], a peptide sequence of arginine, alanine, and aspartic acid, and Matrigel®, a reduced growth factor basement membrane matrix.[38] Both materials provide an excellent cell environment and achieve good cell response for a vast range of mammalian cell types. Their mechanical properties are, however, poor. Bulk hydrogels have low stiffness, degrade quickly, and are rather expensive.

On the other hand, there is a plethora of synthetic and natural hydrogel materials that are conjugated with bioactive compounds. These compounds range from small peptide sequences to proteins or other large biological compounds, such as gelatin. An non-exhaustive list of examples includes the conjugation of N-cadherin to alginate[39], conjugation of the peptide sequences RGD and SIKVAV to poly(2-hydroxyethyl methacrylate)[40], or the conjugation of RGD peptide to gellan gum.[23] These attached compounds enhance cell attachment and can guide cell fate. The mechanical properties of the gels are determined by the base polymer and the stiffness can be adjusted to the cell type requirement. However, the synthesis and production of these cell culture materials are elaborate and expensive, while only a narrow application area is targeted. Usually, specific chemistry development is needed in each case of polymer modification. This means that developing a material for neural cell culture does not benefit the needs for hepatic cell culture, while both are still soft tissues.

Even though modular strategies are not as common as single molecule functionalization, avidin-biotin-based approaches have been presented by Kojima (2006), Hobzova et al. (2011), Wylie et al. (2011), and Leppiniemi et al. (2017).[19–22] Kojima et al. (2006) adsorbed avidin onto PLLA disks for the culturing of biotinylated hepatic cells. However, rigid PLLA scaffolds are a very different material type compared with soft hydrogels and their range of application. [22] Leppiniemi et al. (2017) have shown that avidin-functionalized nanocellulose combined with alginate is suitable for 3D printing. In their study, the protein was covalently bound to the cellulose fibrils and confirmed through electrophoresis. Their range of applications included biomedical devices, wearable sensors, and drug-releasing materials for wound healing, and therefore no cytotoxicity assay or cell culture experiments were presented.[19] Nanocellulose forms weak hydrogels without macroscopic hierarchy, and dimensionality was achieved by the addition of alginate and an additional freeze-drying step. On the other hand, gellan gum can

form true hydrogels applicable to long-term disease modeling.[41] Further, Wylie et al. (2011) created an advanced system using two different proteins, namely avidin and barnase, for the orthogonal functionalization of agarose hydrogels for 3D patterning. Indeed, the use of a protein-binding phenomenon enables the flexible modification of a 3D cell culture material.[21] Their approach is more complex and encompasses a more time-consuming set-up, whereas our system is applicable to larger scale use and requires no laser equipment. Hobzova et al. (2011) showed the covalent grafting of avidin to planar 2-hydroxyethyl methacrylate (pHEMA) surfaces, and they also compared non-specific surface adsorption and electrostatic interaction as a means of avidin immobilization. Their preliminary cell culture results rudimentarily show the attachment of keratinocytes on surface-modified avidin-pHEMA, but no 3D system or in-depth cell response analysis.[20] In contrast to the strategies mentioned above, our system aims to provide 3D soft tissue mimic for true cell encapsulation.

Recently, Silva et al. (2018) published their development of metalloproteinase-1 degradable GG hydrogels, which were equipped with divinyl-sulfone groups to enable modular attachment of cell-adhesive peptides, namely, T1 and C16, both derived from ECM. According to the authors, elongation of the cells is achieved when coupled with a peptide sequence from the Cyr61/CCN1 protein at a concentration of 800 μM in the gel.[42]

Structure analysis

In our project, the concentration of avidin coupled to gellan gum has been determined through fluorescence titration with a biotinylated dye. From the fluorescence titration we can conclude a concentration of 0.075 μM (L)/0.375 μM (H) avidin in 1 mg/mL NaGG solution.

In dry formulation (before dissolving and adding biotinylated species) 0.004 (L)/ 0.021 (H) mg/mg avidin:NaGG ratio. The functionalization yield is 21% (L) and 54% (H), respectively, as calculated from the total amount of CNCA used in the functionalization reaction.

Ferris et al. (2015) directly coupled RGD peptide to GG via carbodiimide coupling, report a functionalization yield of roughly 20% of carboxyl group concentration.[23] This peptide sequence (0.65 kDa) is significantly smaller than the protein avidin (57 kDa) and steric effects preventing higher coupling efficiency with carbodiimide strategy are plausible for avidin. As reported by Ferris et al. (2015), the purification of GG and the removal of divalent counterions increases activation yield with EDC and NHS, and thus convinced us to employ the same strategy.[23] The functionalization yield is further crucial for the number and density of available cell cues in the hydrogel matrix.

It has been shown that cells are sensitive to the presentation, spacing, and clustering of ligands in 2D cell culture systems and the interplay of substrate stiffness and availability of adhesion factors is well understood. In 2D, an RGD ligand spacing of less than 60 nm exhibited significantly improved adhesion and was found to be optimal.[4] However, the reality for 3D matrices is less explored and likely more complex.

One of the core issues for this study was the nature of the binding of avidin to the polymer chain because a covalent attachment of avidin is substantial for the modular approach.[4,5,10] In the literature, it has been shown that unattached compounds can also enhance cell response.[25] However, anchoring the attachment cue to the network is required to generate the mechanotransduction effect, and the ECM receptors of the cell "pull" on the cue rather than the network. If the avidin were merely entrapped via unspecific binding and electrostatic interactions, the biotinylated cell cues would not appropriately convey the matrix stiffness to the cells. Further, the diffusion of the attachment cue out of the matrix system would be anticipated. Our analysis of the functionalized material with electrophoresis showed sufficiently that avidin is covalently tethered to the polymer network.

Crosslinking and physical properties

Mechanical testing revealed that functionalization does not significantly alter the ability of the material to form gels. Forming true gels of NaGG-avd with the relevant mechanical properties for tissue engineering has proven to be uncomplicated and similar to other GG-based hydrogels.[25,43–45] The stiffness and mechanical behavior of the bulk hydrogel should mimic natural tissue, as it has been shown numerous times in the literature to influence, e.g., the differentiation of anchorage-dependent stem cells.[3,8] To prove their adequate mechanical properties, the loss modulus G" and storage modulus G' determined through rheological assessment is often reported for hydrogels. The drawbacks of rheology include problematic sample preparation, complicated data interpretation, and GG is possibly too brittle a material to be analyzed through rheology.[24] Thus, in this study we employed compression testing of the hydrogel, and thereby benefitted from easy sample preparation and straight-forward data interpretation of the fracture point. The determination of the compression modulus is, however, challenging and prone to errors due to the softness of the material and instrument limitations as well as the unclear elastic region or the nonlinear elasticity of the hydrogel material.[46,47] Regardless of the above-mentioned limitations, compression testing offers an easy and fast method of comparison between different hydrogels and hydrogel compositions, especially when comparing different compositions using the exact same test parameters, or within the same study.

Because the goal of this study is to develop a non-specialized 3D hydrogel platform for cell culture, our system needs to have the ability to adapt not only to a wide range of biochemical cues, e.g. growth factors and peptides, but also a wide range of biophysical cues and mechanical stiffness requirements. Gellan gum based hydrogels have already been shown to provide a flexible platform and an adequate stiffness range which can be adjusted by polymer concentration and crosslinker type and concentration. Koivisto et al. (2017) demonstrate a linear correlation between crosslinker concentration and final stiffness of gellan gum hydrogels using the bioamines spermine and spermidine.[24]

It must be noted that the functionalization reaction uses carboxyl groups of glucuronic acid, which are also needed to form crystalline junction zones as crosslinking sites and to form the hydrogel. However, NaGG-avd forms true gels with very similar compression behavior to non-functionalized NaGG. This clearly indicates that a sufficient number of carboxyl groups is still available for crosslinking even after the avidin-functionalization. The addition of DMEM to the gels increases their fracture strength, which can be explained by the formation of tighter crystalline junction zones in the presence of higher cation concentration. Ions present in the swelling medium increase the crosslink density, cause densification, and thus increase the fracture strength of the hydrogels.

On a more practical note, the formed NaGG-avd hydrogels can be manipulated and moved with ease. The gelation time of the hydrogels has been determined to be between 30 seconds and one minute. This indicates a possibility to use the hydrogel as an injectable scaffold, which has not yet been further explored.

Cell response

The functionalized material was tested as cell culture support, while using biotinylated RGD and biotinylated fibronectin for bioactive modification. All the required components are non-toxic and biocompatible. The crosslinking method is gentle and does not disturb cells because there are no side products of the crosslinking reaction. Further, the applied gel preparation achieves a true 3D structure, where the cells are homogeneously distributed throughout the hydrogel. This homogenous cell distribution is achieved by mixing the hydrogel sol with the

cell suspension using a magnetic stirrer at 300 rpm, before casting the mixture to the wells of the well plate. Supported by the high viability results, this treatment does not harm the cells. Indeed, the short-term test with human WI-38 fibroblasts demonstrated high cell viability throughout different compositions.

GG has previously been shown to be suitable for soft tissue culture, but it is rather bioinert.[23–26,48] Here, we have shown that after functionalization, GG retains its good mechanical properties, such as soft tissue mimicking, while adding biofunctionalization.

A direct comparison of the cell culture results is challenging due to the ubiquity of cell lines and analysis methods used in the literature. Regarding the fibroblasts, we can point out similar viability of the same WI-38 cells studied by Pacelli et al. (2016) who report 74% viability with GG-based hydrogel after 4 days.[48] However, their cells were seeded in a 2D layer for 24 h more than in our study, and viability was asserted through optical density with a so-called neutral red assay. For 3D cultures, however, dye-based assays require optimization because the hydrogel affects both light propagation and the diffusion of the dye during incubation. In the GG-based hydrogel study by da Silva et al. (2018) mentioned earlier[42], image analysis was used to determine the cell viability of human umbilical vein endothelial cells (HUVECs) in thiol-functionalized gellan gum. The authors found a 65% viability of HUVECs after 3 days encapsulated in the hydrogel. Overall, our observation of WI-38 fibroblast viability was between 85% and 90% in different formulations of NaGG-avd, which exceeds or at least matches the values found in the literature for GG-based hydrogels. Therefore, the excellent biocompatibility of NaGG-avd can be affirmed.

There appears to be no overall visible difference in WI-38 cell viability between 2D and 3D conditions, with live and dead cells being present in either culture method with substantial standard deviation. 2D culture promotes the growth of cell aggregates and the cells possibly migrate to form larger clusters, possibly due to the inert properties of the hydrogel surface. When encapsulated in 3D, the cells seemingly cannot migrate, and are therefore limited to grow within the hydrogel in the area of initial original deposition. There is no visible difference in 3D cell distribution between the different biotinylated compounds added to NaGG-avd. Overall, no statistical significance in cell spreading of could be found between all tested gellan-gum compositions (GG and NaGG-avd samples). From Fig 6B a trend is visible favoring the avidin-functionalized samples, however the large standard deviation prevents any decisive statement. A higher degree of cell adhesion and spreading would have been anticipated from the presence of ECM derived factors. However, this effect could be explained by the presence of serum proteins in the culture medium that compete with the cells to reach the provided attachment sites. This is largely due to the Vroman effect[49] that describes the mobility-dependent adsorption of proteins onto hydrophilic surfaces. Thus, serum components, such as albumin, fibrinogen, and fibronectin, attach faster to the biomaterial than the cells and favoring them may prevent the cell receptors from recognizing any available cell adhesive cues covalently bound to the biomaterial. In order to avoid the Vroman effect, some studies have successfully used serum starving conditions to show enhanced cell attachment and survival in biomaterials that contain cell adhesive cues.[50,51]

The same tendency of cell behavior was visible in hBMSC 3D culture in our functionalized gellan gum. NaGG-avd had been equipped with biotinylated RGD to stimulate cell adhesion because RGD is known to be a crucial and prevalent peptide sequence for cell integrin recognition of ECM. RGD has been used frequently for BMSC studies and positive effects have been reported in the literature[11,12,52], and thus was chosen here as a model cell adhesive site. We can correlate our findings to a study by Anjum et al. (2016) who cultured hBMSC over 14 days in their chondroitin sulfate-poly(ethylene glycol) (PEG) hydrogel and found 80% to 95% viability between different compositions.[53] The LIVE/DEAD® stained images appear similar

Table 1. Component concentration of hydrogel composition.

Component	Mass of component	Weight percent	Concentration
Avidin (L)/(H)	0.02/ 0.11 mg	0.002/0.011 wt%	0.375/ 1.875 μM
NaGG	5 mg	0.50%	10 μM
bRGD/bFn	0.3 $x10^{-3}$/0.03 mg	0.03$x10^{-3}$/0.003 wt%	0.27/ 0.08 μM
H_2O	995 mg	99.5%	

https://doi.org/10.1371/journal.pone.0221931.t001

in viability to our findings and interestingly also show a similar obfuscation with time. Similarly, Blache et al. (2016) used RGD-functionalized PEG-based hydrogel and co-cultured HUVEC+hMSC. The authors reported good cell viability and definite cell elongation with a three-times higher cell concentration compared with our study.[11] Another comparable study has been published by Tsaryk et al. (2014) using ionically crosslinked methacrylated GG (iGG-MA) with human mesenchymal stem cells (hMSC) and nasal chondrocytes. [54] They achieved good viability and adequate differentiation towards chondrogenic and osteogenic lineages. No attachment factors had been added for this encapsulation study, and the differentiation is steered solely through medium composition. After 14 days encapsulated in iGG-MA, the hMSC showed a round shape, while the hydrogel opacity increased, and the confocal microscope image clarity deteriorated similar to our study. In summary, different approaches to design hydrogels for the encapsulation of human mesenchymal stem cells have been presented in the literature.

Our proof-of-concept with avidin-functionalized NaGG provides an easy modification of hydrogel material for cell culture applications. In the laboratory, the hydrogel is rather simple to handle and requires the combination of only three components. The persisting problem in the presented results is the small amount of avidin coupled to the gellan gum network. This in turn leads to a rather low number of bioactive cues available for the cells. As a brief comparison, Broguiere et al. (2018) report that a fibrin hydrogel at 3 mg/mL provides a sufficient concentration of RGD binding sites at 75 μM, whereas our results show a concentration of 0.3 μM bRGD in the final hydrogel (Table 1).[55] Further research is therefore needed to increase functionalization degree and overcome the problem of the low number of bioactive cues in the hydrogel. A range of other functionalization reaction is conceivable, such as bio-orthogonal click reactions.[56] However, an interference of high functionalization degree with crosslinking capability must be considered. Another prospect could be the functionalization of the polymer chain end-groups to avoid blocking the carboxyl groups of gellan gum, as proposed by Bondalapati et al. (2014).[57] While considering an alternative functionalization reaction, the carbodiimide strategy will always have the advantage of being well-known and heavily used in the literature[14], and thus we can rely on its efficacy. As an example, the end-group modification strategy would have to be tested and refined for gellan gum and avidin, and additionally the cytotoxic substance aniline is used as a catalyst, which may prove problematic.

With the proposed avidin-biotin modification system, the modularity hinges solely on the availability of the biotinylated compounds. There is a multitude of these compounds already commercially available, but they can also be synthesized by biotinylating the desired compound, if such a compound is not yet available. As proof-of-concept, these results underline the viability of stromal cells in a gellan gum-based 3D hydrogel cell culture system. Our approach is suitable for disease modeling applications due to its capacity to image cells inside the hydrogel and the ability to control the 3D biochemical environment through avidin-biotin modularity. Future work will focus on the effect of biotinylated species and quantitative assessment of stromal cells encapsulated in our modular hydrogel.

Conclusions

Gellan gum was successfully functionalized with the avidin protein (charge neutralized chimeric avidin). This functionalized hydrogel provides a general, modular platform capable of tethering biotinylated compounds and aiding the attachment and proliferation of cells in 3D. Contrasting the common strategy of direct attachment, our modular hydrogel is intended to be off-the-shelf ready for any cell culture application, while still being consistent in physical properties. The current proposed avidin functionalization system is not targeted at a specific cell type or application, but rather intended to form the base material for further studies. Further modification by the addition of a cell type specific biotinylated compound is necessary to enhance the positive cell response. The presented data using two different cell types support that the avidin-modified gellan gum is a useful tool applicable for cell culture. The hydrogel is biocompatible, sterilizable, and retains adequate mechanical properties and stability over several weeks. This long-term stability is essential for disease or tissue models involving cell types with a slow metabolism and development, such as bone and cartilage derived cells.

Supporting information

S1 Appendix. ICP-OES data. Elemental composition of counterions in commercial Gelzan™ (GG) and purified product (NaGG) has been determined with ICP-OES. The ion concentration of the purified product matches values found in literature (24,28).
(PDF)

S2 Appendix. SDS PAGE. Full uncropped image of sodium dodecyl sulfate polyacrylamide gel electrophoresis (SDS PAGE) blot.
(PDF)

S3 Appendix. Compression data of functionalized and non-functionalized samples. Data are the same as presented in Fig 4B and are presented as means ± SD. The graphs (stress vs. strain) show all compression curves, from which the fracture points are averaged. The photograph shows cylindrical hydrogel samples, cell-free but incubated in DMEM.
(PDF)

S4 Appendix. Swelling degree of NaGG-avd(L) hydrogel samples. Hydrogels were prepared in Eppendorf tubes with either SPD or $CaCl_2$ as crosslinker and the initial mass of each sample was taken. Swelling media, either PBS or DMEM, were added on top after the gels had set and the samples were incubated at 37˚C up to 3 weeks. Swelling degree was calculated through monitoring change in mass according to Eq (3). Data are shown as means ± SD (n = 3).
(PDF)

S5 Appendix. Cell viability from particle counting. Averaged values of particle counting algorithm results for all LIVE/DEAD® images. The bar graph shows average values of image-by-image comparison for 'total area' value.
(PDF)

S6 Appendix. Flow cytometry surface markers analysis results of hBMSCs. n = 1. The flow cytometry analysis confirmed the mesenchymal origin of the hBMSCs.
(PDF)

S7 Appendix. Cytoskeleton images of hBMSC after 21 days. Blue channel = cell nuclei (DAPI) and red channel = actin filaments (TRITC-phalloidin). (A) Cells in NaGG and (B) NaGG-avd+bRGD.
(PDF)

S8 Appendix. Washing test and immunofluorescence straining. Description of washing test for hydrogel samples formed with NaGG and NaGG-avd using biotinylated fibronection (bFn). Immuncytochemistry staining for fibronectin shows 4-fold retention of fibronectin in avidin-functionalized gel.
(PDF)

S9 Appendix. Microscope images of WI-38 cell culture experiment for counting analysis. Exemplary images of 3D samples between day 0 (light microscope) and day 3 (LIVE/DEAD® fluorescence images) for comparison.
(PDF)

Acknowledgments

We wish to thank Tampere CellTech Laboratories and Tampere Imaging Facility (TIF) for their services, as well as the group of Assoc. Prof. Jonathan Massera for assistance with the ICP analysis.

Author Contributions

Conceptualization: Christine Gering, Janne T. Koivisto, Jenny Parraga, Jenni Leppiniemi, Kaisa Vuornos, Vesa P. Hytönen, Susanna Miettinen, Minna Kellomäki.

Formal analysis: Christine Gering, Janne T. Koivisto, Kaisa Vuornos.

Investigation: Christine Gering.

Resources: Vesa P. Hytönen, Susanna Miettinen, Minna Kellomäki.

Supervision: Vesa P. Hytönen, Susanna Miettinen, Minna Kellomäki.

Writing – original draft: Christine Gering, Janne T. Koivisto, Jenny Parraga.

Writing – review & editing: Christine Gering, Janne T. Koivisto, Jenny Parraga, Jenni Leppiniemi, Kaisa Vuornos, Vesa P. Hytönen, Susanna Miettinen, Minna Kellomäki.

References

1. Tirrell DA, Langer R. Designing materials for biology and medicine. Nature. 2004; 428: 487–492. https://doi.org/10.1038/nature02388 PMID: 15057821
2. Levental I, Georges PC, Janmey PA. Soft biological materials and their impact on cell function. Soft Matter. 2007; 3: 299–306. https://doi.org/10.1039/B610522J
3. Berrier AL, Yamada KM. Cell–matrix adhesion. Journal of Cellular Physiology. 2007; 213: 565–573. https://doi.org/10.1002/jcp.21237 PMID: 17680633
4. Walters NJ, Gentleman E. Evolving insights in cell–matrix interactions: Elucidating how non-soluble properties of the extracellular niche direct stem cell fate. Acta Biomaterialia. 2015; 11: 3–16. https://doi.org/10.1016/j.actbio.2014.09.038 PMID: 25266503
5. Tibbitt MW, Anseth KS. Hydrogels as extracellular matrix mimics for 3D cell culture. Biotechnology and bioengineering. 2009; 103: 655–663. https://doi.org/10.1002/bit.22361 PMID: 19472329
6. Drury JL, Mooney DJ. Hydrogels for tissue engineering: scaffold design variables and applications. Biomaterials. 2003; 24: 4337–4351. https://doi.org/10.1016/s0142-9612(03)00340-5 PMID: 12922147
7. Frantz C, Stewart KM, Weaver VM. The extracellular matrix at a glance. Journal of cell science. 2010; 123: 4195–4200. https://doi.org/10.1242/jcs.023820 PMID: 21123617
8. Engler AJ, Sen S, Sweeney HL, Discher DE. Matrix Elasticity Directs Stem Cell Lineage Specification. Cell. 2006; 126: 677–689. https://doi.org/10.1016/j.cell.2006.06.044 PMID: 16923388
9. McKee C, Chaudhry GR. Advances and challenges in stem cell culture. Colloids and Surfaces B: Biointerfaces. 2017; 159: 62–77. https://doi.org/10.1016/j.colsurfb.2017.07.051 PMID: 28780462

10. Oliveira MB, Custódio CA, Gasperini L, Reis RL, Mano JF. Autonomous osteogenic differentiation of hASCs encapsulated in methacrylated gellan-gum hydrogels. Acta Biomaterialia. 2016; 41: 119–132. https://doi.org/10.1016/j.actbio.2016.05.033 PMID: 27233132

11. Blache U, Metzger S, Vallmajo-Martin Q, Martin I, Djonov V, Ehrbar M. Dual Role of Mesenchymal Stem Cells Allows for Microvascularized Bone Tissue-Like Environments in PEG Hydrogels. Advanced Healthcare Materials. 2015; 5: 489–498. https://doi.org/10.1002/adhm.201500795 PMID: 26693678

12. Li S, Guan J, Chien S. Biochemistry and Biomechanics of Cell Motility. Annual Review of Biomedical Engineering. 2005; 7: 105–150. https://doi.org/10.1146/annurev.bioeng.7.060804.100340 PMID: 16004568

13. Justice BA, Badr NA, Felder RA. 3D cell culture opens new dimensions in cell-based assays. Drug Discovery Today. 2009; 14: 102–107. https://doi.org/10.1016/j.drudis.2008.11.006 PMID: 19049902

14. Hermanson GT. Chapter 4—Zero-Length Crosslinkers. In: Anonymous Bioconjugate Techniques (Third edition). Boston: Academic Press; 2013. pp. 259–273.

15. Agard NJ, Prescher JA, Bertozzi CR. A Strain-Promoted [3 + 2] Azide−Alkyne Cycloaddition for Covalent Modification of Biomolecules in Living Systems. J Am Chem Soc. 2004; 126: 15046–15047. https://doi.org/10.1021/ja044996f PMID: 15547999

16. Rosano C, Arosio P, Bolognesi M. The X-ray three-dimensional structure of avidin. Biomolecular Engineering. 1999; 16: 5–12. PMID: 10796979

17. Hytönen VP, Määttä JAE, Nyholm TKM, Livnah O, Eisenberg-Domovich Y, Hyre D, et al. Design and Construction of Highly Stable, Protease-resistant Chimeric Avidins. Journal of Biological Chemistry. 2005; 280: 10228–10233. https://doi.org/10.1074/jbc.M414196200 PMID: 15649900

18. Laitinen OH, Nordlund HR, Hytönen VP, Kulomaa MS. Brave new (strept)avidins in biotechnology. Trends in Biotechnology. 2007; 25: 269–277. https://doi.org/10.1016/j.tibtech.2007.04.001 PMID: 17433846

19. Leppiniemi J, Lahtinen P, Paajanen A, Mahlberg R, Pinomaa T, Pajari H, et al. 3D-Printable Bioactivated Nanocellulose-Alginate Hydrogels. ACS Appl Mater Interfaces. 2017; 9: 21959–21970. https://doi.org/10.1021/acsami.7b02756 PMID: 28598154

20. Hobzova R, Pradny M, Zhunusbekova NM, Sirc J, Guryca V, Michalek J. Bioactive support for cell cultivation and potential grafting. Part 1: Surface modification of 2-hydroxyethyl methacrylate hydrogels for avidin immobilization. e-Polymers. 2011; 11: 474–490. https://doi.org/10.1515/epoly.2011.11.1.474

21. Wylie RG, Ahsan S, Aizawa Y, Maxwell KL, Morshead CM, Shoichet MS. Spatially controlled simultaneous patterning of multiple growth factors in three-dimensional hydrogels. Nature Materials. 2011; 10: 799. https://doi.org/10.1038/nmat3101 PMID: 21874004

22. Kojima N, Matsuo T, Sakai Y. Rapid hepatic cell attachment onto biodegradable polymer surfaces without toxicity using an avidin–biotin binding system. Biomaterials. 2006; 27: 4904–4910. https://doi.org/10.1016/j.biomaterials.2006.05.026 PMID: 16759691

23. Ferris CJ, Stevens LR, Gilmore KJ, Mume E, Greguric I, Kirchmajer DM. Peptide modification of purified gellan gum. Journal of Materials Chemistry B. 2015; 3: 1106–1115. https://doi.org/10.1039/c4tb01727g

24. Koivisto JT, Joki T, Parraga JE, Pääkkönen R, Ylä-Outinen L, Salonen L, et al. Bioamine-crosslinked gellan gum hydrogel for neural tissue engineering. Biomed Mater. 2017; 12: 025014. https://doi.org/10.1088/1748-605X/aa62b0 PMID: 28233757

25. Silva-Correia J, Zavan B, Vindigni V, Silva TH, Oliveira JM, Abatangelo G, et al. Biocompatibility Evaluation of Ionic- and Photo-Crosslinked Methacrylated Gellan Gum Hydrogels: In Vitro and In Vivo Study. Advanced Healthcare Materials. 2013; 2: 568–575. https://doi.org/10.1002/adhm.201200256 PMID: 23184642

26. Osmałek T, Froelich A, Tasarek S. Application of gellan gum in pharmacy and medicine. International journal of pharmaceutics. 2014; 466: 328–340. https://doi.org/10.1016/j.ijpharm.2014.03.038 PMID: 24657577

27. Morris ER, Nishinari K, Rinaudo M. Gelation of gellan–A review. Food Hydrocolloids. 2012; 28: 373–411. https://doi.org/10.1016/j.foodhyd.2012.01.004

28. Ray S, Steven RT, Green FM, Höök F, Taskinen B, Hytönen VP, et al. Neutralized chimeric avidin binding at a reference biosensor surface. Langmuir: the ACS journal of surfaces and colloids. 2015; 31: 1921–1930. https://doi.org/10.1021/la503213f PMID: 25650821

29. BioMediTech F, 2018. BioMediTech protein shop. Available: http://cofa.uta.fi/med/Protein_Shop/.

30. Doner LW. Rapid purification of commercial gellan gum to highly soluble and gellable monovalent cation salts. Carbohydrate Polymers. 1997; 32: 245–247. https://doi.org/10.1016/S0144-8617(96)00168-3

31. Kirchmajer DM, Steinhoff B, Warren H, Clark R, in het Panhuis M. Enhanced gelation properties of purified gellan gum. Carbohydrate Research. 2014; 388: 125–129. https://doi.org/10.1016/j.carres.2014.02.018 PMID: 24637048

32. Gering C, Koivisto JT, Parraga JE, Kellomäki M. Reproducible preparation method of hydrogels for cell culture applications–case study with spermidine crosslinked gellan gum. In: Anonymous EMBEC & NBC 2017.: Springer, Singapore; 2017. pp. 811–814.

33. Doube M, Kłosowski MM, Arganda-Carreras I, Cordelières FP, Dougherty RP, Jackson JS, et al. BoneJ: Free and extensible bone image analysis in ImageJ. Bone. 2010; 47: 1076–1079. https://doi.org/10.1016/j.bone.2010.08.023 PMID: 20817052

34. Li Z, Kupcsik L, Yao S, Alini M, Stoddart MJ. Chondrogenesis of Human Bone Marrow Mesenchymal Stem Cells in Fibrin–Polyurethane Composites. Tissue Engineering Part A. 2008; 15: 1729–1737. https://doi.org/10.1089/ten.tea.2008.0247 PMID: 19115827

35. Gebraad A, Kornilov R, Kaur S, Miettinen S, Haimi S, Peltoniemi H, et al. Monocyte-derived extracellular vesicles stimulate cytokine secretion and gene expression of matrix metalloproteinases by mesenchymal stem/stromal cells. FEBS J. 2018; 285: 2337–2359. https://doi.org/10.1111/febs.14485 PMID: 29732732

36. Tallawi M, Rosellini E, Cascone MG, Barbani N, Rai R, Saint-Pierre G, et al. Strategies for the chemical and biological functionalization of scaffolds for cardiac tissue engineering: a review. Interface. 2015; 12.

37. Zhang S, Holmes T, Lockshin C, Rich A. Spontaneous assembly of a self-complementary oligopeptide to form a stable macroscopic membrane. PNAS. 1993; 90: 3334–3338. https://doi.org/10.1073/pnas.90.8.3334 PMID: 7682699

38. Hughes CS, Postovit LM, Lajoie GA. Matrigel: a complex protein mixture required for optimal growth of cell culture. Proteomics. 2010; 10: 1886–1890. https://doi.org/10.1002/pmic.200900758 PMID: 20162561

39. Lee JW, An H, Lee KY. Introduction of N-cadherin-binding motif to alginate hydrogels for controlled stem cell differentiation. Colloids and Surfaces B: Biointerfaces. 2017; 155: 229–237. https://doi.org/10.1016/j.colsurfb.2017.04.014 PMID: 28432956

40. Macková H, Plichta Z, Proks V, Kotelnikov I, Kučka J, Hlídková H, et al. RGDS- and SIKVAVS-Modified Superporous Poly(2-hydroxyethyl methacrylate) Scaffolds for Tissue Engineering Applications. Macromolecular Bioscience. 2016; 16: 1621–1631. https://doi.org/10.1002/mabi.201600159 PMID: 27460202

41. De France KJ, Hoare T, Cranston ED. Review of Hydrogels and Aerogels Containing Nanocellulose. Chemistry of Materials. 2017; 29: 4609–4631. https://doi.org/10.1021/acs.chemmater.7b00531

42. da Silva LP, Jha AK, Correlo VM, Marques AP, Reis RL, Healy KE. Gellan Gum Hydrogels with Enzyme-Sensitive Biodegradation and Endothelial Cell Biorecognition Sites. Adv Healthcare Mater. 2018; 7: n/a. https://doi.org/10.1002/adhm.201700686 PMID: 29388392

43. Silva DA, Poole-Warren LA, Martens PJ, Panhuis M. Mechanical characteristics of swollen gellan gum hydrogels. Journal of Applied Polymer Science. 2013; 130: 3374–3383. https://doi.org/10.1002/app.39583

44. Douglas T, Wlodarczyk M, Pamula E, Declercq HA, Mulder Ed, Bucko MM, et al. Enzymatic mineralization of gellan gum hydrogel for bone tissue-engineering applications and its enhancement by polydopamine. Journal of Tissue Engineering and Regenerative Medicine. 2012; 8: 906–918. https://doi.org/10.1002/term.1616 PMID: 23038649

45. Silva NA, Cooke MJ, Tam RY, Sousa N, Salgado AJ, Reis RL, et al. The effects of peptide modified gellan gum and olfactory ensheathing glia cells on neural stem/progenitor cell fate. Biomaterials. 2012; 33: 6345–6354. https://doi.org/10.1016/j.biomaterials.2012.05.050 PMID: 22698724

46. Oyen ML. Mechanical characterisation of hydrogel materials. International Materials Reviews. 2014; 59: 44–59. https://doi.org/10.1179/1743280413Y.0000000022

47. Storm C, Pastore JJ, MacKintosh FC, Lubensky TC, Janmey PA. Nonlinear elasticity in biological gels. Nature. 2005; 435: 191–194. https://doi.org/10.1038/nature03521 PMID: 15889088

48. Pacelli S, Paolicelli P, Moretti G, Petralito S, Di Giacomo S, Vitalone A, et al. Gellan gum methacrylate and laponite as an innovative nanocomposite hydrogel for biomedical applications. European Polymer Journal. 2016; 77: 114–123. https://doi.org/10.1016/j.eurpolymj.2016.02.007

49. Vroman L, Adams AL, Fischer GC, Munoz PC. Interaction of high molecular weight kininogen, factor XII, and fibrinogen in plasma at interfaces. Blood. 1980; 55: 156–159. PMID: 7350935

50. Lin S, Jee S, Hsiao W, Yu H, Tsai T, Chen J, et al. Enhanced cell survival of melanocyte spheroids in serum starvation condition. Biomaterials. 2006; 27: 1462–1469. https://doi.org/10.1016/j.biomaterials.2005.08.031 PMID: 16171860

51. Kraehenbuehl Thomas P., Ferreira Lino S., Zammaretti Prisca, Hubbell Jeffrey A., Langer Robert. Cell-responsive hydrogel for encapsulation of vascular cells. Biomaterials. 2009; 30: 4318–4324. https://doi.org/10.1016/j.biomaterials.2009.04.057 PMID: 19500842

52. He X, Ma J, Jabbari E. Effect of grafting RGD and BMP-2 protein-derived peptides to a hydrogel substrate on osteogenic differentiation of marrow stromal cells. Langmuir: the ACS journal of surfaces and colloids. 2008; 24: 12508–12516. https://doi.org/10.1021/la802447v PMID: 18837524

53. Anjum F, Ehrbar M, Lienemann PS, Metzger S, Biernaskie J, Kallos MS. Enzyme responsive GAG-based natural-synthetic hybrid hydrogel for tunable growth factor delivery and stem cell differentiation. Biomaterials. 2016; 87: 104–117. https://doi.org/10.1016/j.biomaterials.2016.01.050 PMID: 26914701

54. Tsaryk R, Silva-Correia J, Oliveira JM, Unger RE, Landes C, Brochhausen C, et al. Biological performance of cell-encapsulated methacrylated gellan gum-based hydrogels for nucleus pulposus regeneration. Journal of Tissue Engineering and Regenerative Medicine. 2014; 11: 637–648. https://doi.org/10.1002/term.1959 PMID: 25370800

55. Broguiere N, Isenmann L, Hirt C, Ringel T, Placzek S, Cavalli E, et al. Growth of Epithelial Organoids in a Defined Hydrogel. Advanced Materials. 2018; 30: 1801621. https://doi.org/10.3929/ethz-b-000302457

56. Desai RM, Koshy ST, Hilderbrand SA, Mooney DJ, Joshi NS. Versatile click alginate hydrogels crosslinked via tetrazine–norbornene chemistry. Biomaterials. 2015; 50: 30–37. https://doi.org/10.1016/j.biomaterials.2015.01.048 PMID: 25736493

57. Bondalapati S, Ruvinov E, Kryukov O, Cohen S, Brik A. Rapid End-Group Modification of Polysaccharides for Biomaterial Applications in Regenerative Medicine. Macromolecular Rapid Communications. 2014; 35: 1754–1762. https://doi.org/10.1002/marc.201400354 PMID: 25220432

PUBLICATION IV

Mechanically Biomimetic Gelatin-Gellan Gum Hydrogels for 3D Culture of Beating Human Cardiomyocytes

Janne T. Koivisto†, Christine Gering†, Jennika Karvinen, Reeja Maria Cherian, Birhanu Belay, Jari Hyttinen, Katriina Aalto-Setälä, Minna Kellomäki, & Jenny Párraga

ACS Applied Materials and Interfaces, 11(23), 20589–20602
https://doi.org/10.1021/acsami.8b22343

ACS APPLIED MATERIALS & INTERFACES

Research Article

Cite This: ACS Appl. Mater. Interfaces 2019, 11, 20589−20602

www.acsami.org

Mechanically Biomimetic Gelatin−Gellan Gum Hydrogels for 3D Culture of Beating Human Cardiomyocytes

Janne T. Koivisto,*[,†,‡] Christine Gering,[†] Jennika Karvinen,[†] Reeja Maria Cherian,[‡] Birhanu Belay,[§] Jari Hyttinen,[§] Katriina Aalto-Setälä,[‡,∥] Minna Kellomäki,[†] and Jenny Parraga*[,†]

[†]Biomaterials and Tissue Engineering Group, BioMediTech, Faculty of Medicine and Health Technology, Tampere University, 33720 Tampere, Finland

[‡]Heart Group, BioMediTech, Faculty of Medicine and Health Technology and [§]Computational Biophysics and Imaging Group, BioMediTech, Faculty of Medicine and Health Technology, Tampere University, 33520 Tampere, Finland

[∥]Heart Hospital, Tampere University Hospital, 33520 Tampere, Finland

Supporting Information

ABSTRACT: To promote the transition of cell cultures from 2D to 3D, hydrogels are needed to biomimic the extracellular matrix (ECM). One potential material for this purpose is gellan gum (GG), a biocompatible and mechanically tunable hydrogel. However, GG alone does not provide attachment sites for cells to thrive in 3D. One option for biofunctionalization is the introduction of gelatin, a derivative of the abundant ECM protein collagen. Unfortunately, gelatin lacks cross-linking moieties, making the production of self-standing hydrogels difficult under physiological conditions. Here, we explore the functionalization of GG with gelatin at biologically relevant concentrations using semiorthogonal, cytocompatible, and facile chemistry based on hydrazone reaction. These hydrogels exhibit mechanical behavior, especially elasticity, which resembles the cardiac tissue. The use of optical projection tomography for 3D cell microscopy demonstrates good cytocompatibility and elongation of human fibroblasts (WI-38). In addition, human-induced pluripotent stem cell-derived cardiomyocytes attach to the hydrogels and recover their spontaneous beating in 24 h culture. Beating is studied using in-house-built phase contrast video analysis software, and it is comparable with the beating of control cardiomyocytes under regular culture conditions. These hydrogels provide a promising platform to transition cardiac tissue engineering and disease modeling from 2D to 3D.

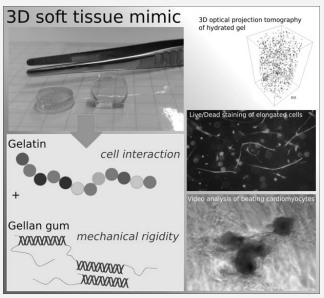

KEYWORDS: *hiPSC-derived cardiomyocytes, 3D hydrogel, gelatin, gellan gum, compression testing*

1. INTRODUCTION

The aim of tissue engineering (TE) is to create a new living tissue in vitro using a combination of biomaterial scaffolds, living tissue-specific cells, and biochemical factors.[1] In recent years, there has been a growing interest in the use of in vitro tissue and organoids as components for disease modeling, toxicology, and study of developmental biology.[2−5] In the case of cardiac disease modeling, human-induced pluripotent stem cell (hiPSC)-derived cardiomyocytes have been used to define the electrophysiological behavior of cardiomyocytes affected by specific genetic diseases.[5−8] As part of our earlier work, we reproduced the disease phenotype of genetic catecholaminergic polymorphic ventricular tachycardia in vitro and showed the proof of concept that iPSC-derived cardiomyocytes can reproduce a clinical drug response.[9] Furthermore, since cardiotoxicity is one of the most common causes of the drawbacks associated with many drugs, our group has been working on ways to improve methods for testing drug safety in 2D cardiac models.[10−12] To produce better biomimicking disease and cardiotoxicity models, however, a transition from 2D to 3D is needed to bridge the translational gap in drug discovery from single cell or 2D studies to clinical studies. A 3D disease model enables studying more intercellular interactions compared to 2D models, especially when comparing with single-cell studies.[3,13−15]

Till date, the most relevant cardiac 3D cell culture systems are engineered heart tissues, the so-called Biowire, 3D bioprinted structures, and even 3D printed organs-on-chip.[15−18] All of the above examples use an extracellular matrix (ECM) protein-based hydrogel scaffold, either Matrigel or gelatin methacrylate (GelMA), to support 3D cell culturing. In these studies, the focus is more on cardiomyocyte electrophysiology than on the relationship between the mechanical properties of the material and how cellular mechanotransduction affects the biological response.[19] Thus, more emphasis should be placed on the design and mechanical characterization of these soft biomaterial scaffolds.

Received: December 22, 2018
Accepted: May 17, 2019
Published: May 23, 2019

DOI: 10.1021/acsami.8b22343
ACS Appl. Mater. Interfaces 2019, 11, 20589−20602

To overcome the mechanical challenges of this specific biomedical application, new chemical cross-linking strategies for hydrogel production are needed. Noncovalent interactions have been used to produce hydrogels, mainly with electrostatic and hydrophobic interactions and hydrogen bonding. These hydrogels are usually relatively brittle with a narrow range of mechanical properties.[20,21] On the other hand, covalent cross-linking strategies have the ability to control the cross-linking density and, therefore, the mechanical properties. These strategies can result in higher elasticity, a key feature for the success of soft TE.

The cross-linking design should be chemoselective and efficient and should retain the biocompatibility of the polymer. In addition, gelation under physiological conditions could be beneficial for biomedical applications. Covalent hydrazone cross-linking is known to fulfil these requirements. Indeed, our previous studies have shown the elastic, biomimicking behavior of hydrogels obtained with this chemistry.[22−24]

In this work, we apply hydrazone chemistry to a combination of two well-known biopolymers in TE applications: gelatin and gellan gum (GG). Gelatin is a molecule derived from the abundant ECM protein collagen, and it is routinely used as a coating material in cardiac cell culture applications.[25,26] Gelatin hydrogel scaffolds can be formed by physical cross-linking, namely, thermal gelation. However, the gelation temperature is often below physiological requirements, and thus the use of these hydrogels in native form with cells is limited.[26] On the other hand, GG, a bacterial polysaccharide, is able to form hydrogels with tunable mechanical properties. The relatively bioinert nature of GG, however, does not support cell attachment.[21,27−29] Both GelMA and methacrylated GG (GGMA) have been photo-cross-linked into hydrogels and used to encapsulate cells.[26,30,31] They have even been combined in a double-network hydrogel with relatively good cytocompatibility.[32] However, the main limitations to using this approach for the fabrication of larger 3D tissues or organs is the phototoxicity of ultraviolet (UV) cross-linking and dependence on transparency of the hydrogel components.[33−35]

We have explored the use of these in situ cross-linkable hydrogels as biomimicking scaffolds for 3D cardiac disease modeling. In this study, we use 3D in-house-built microscopy to demonstrate the effects of hydrogel properties on cell morphology.[36] Our results show substantially more elongated fibroblast cells in 3D culture inside these hydrogels and clearly indicate better cytocompatibility than many other published cell results using the same hydrogel components.[32,37] On the basis of our findings, we used these hydrogels in a macroscale 3D culture of hiPSC-derived cardiomyocyte aggregates for the first time. The spontaneous beating behavior of the cardiomyocytes was analyzed with our previously developed motion tracking video analysis software.[11] Furthermore, we demonstrate that this rational hydrogel design supports the transition from 2D to 3D without interfering with the cardiomyocyte behavior and furthers the aim toward in vitro 3D hiPSC-derived cardiac disease modeling and drug screening.

2. EXPERIMENTAL SECTION

2.1. Materials. Gelatin A from porcine skin, GG (Gelzan CM Gelrite, M_w 1000 g mol^{-1}), spermidine trihydrochloride (SPD), sucrose, adipic dihydrazide (ADH), carbodihydrazide (CDH), dimethyl sulfoxide (DMSO), ethylene glycol, 1-ethyl-3-[3-(dimethylamino)-propyl]-carbodiimide (EDC), hydroxylamine hydrochloride, *N*-hydroxybentzotriazole (HOBt), 4-hydroxybenzaldehyde, deuterium oxide (99.9 atom % D, contains 0.05 wt % 3-(trimethylsilyl)-propionic-2,2,3,3-d4 acid, sodium salt), hydrochloric acid (HCl), sodium hydroxide (NaOH), sodium chloride (NaCl), and sodium periodate ($NaIO_4$) were purchased from Sigma-Aldrich (St. Louis, MO, USA). Dialysis membrane (Spectra/Por 12−14 kDa) was purchased from Spectrum Laboratories (Rancho Dominguez, CA, USA).

2.2. Preparation of ADH-Modified Gelatin (Gelatin-ADH). First, 300 mg of gelatin was dissolved in 100 mL of water, and 3.92 g (0.225 M) of ADH was added to this solution. The pH of the reaction mixture was adjusted to 6.8. Then, 576 mg (0.03 M) of EDC and 405 mg (0.03 M) of HOBt were dissolved in 3 mL of DMSO/water (1.5:1 v/v) and added to the reaction mixture drop by drop, while keeping the pH at 6.8 with 0.1 M NaOH and 0.1 M HCl during the mixture addition and for another 4 h. Then, the reaction was continued for another 20 h. The pH was adjusted to 7, and gelatin-ADH was exhaustively dialyzed against water for 2 d. Then, NaCl was added to produce a 7% (w/v) solution, and the product was precipitated in cold ethanol (4 vol equiv). Then, the product was dissolved in water and dialyzed against water for 2 days. Finally, the solution was lyophilized through a molecular weight cutoff 12−14 kDa dialysis membrane followed by freeze-drying.

2.3. Preparation of CDH-Modified Gelatin (Gelatin-CDH). First, 300 mg of gelatin was dissolved in 100 mL of water, and 3.6 g (0.4 M) of CDH was added to this solution. The pH of the reaction mixture was adjusted to 4.7 with 0.5 M HCl. Then, 575 mg (0.03 M) of EDC and 405 mg (0.03 M) of HOBt were dissolved in 3 mL of DMSO/water (1.5:1 v/v) and added to the reaction mixture drop by drop, while keeping the pH at 6.8 with 0.1 M NaOH and 0.1 M HCl during the mixture addition and for another 4 h. Then, the reaction was kept for another 20 h. Gelatin-CDH was exhaustively dialyzed against water for 2 days. Additional purification was carried out as described above followed by freeze-drying.

2.4. Preparation of Oxidized GG (GG-CHO). GG was modified by $NaIO_4$ oxidation according to the method previously reported by our group to produce GG-CHO at the modification degree of 25%.[22]

2.5. Polymer Characterization. To confirm the presence of hydrazide functionality, 20 mg of gelatin-ADH or gelatin-CDH was treated with 10 mL of 4-hydroxybenzaldehyde (20 mg mL^{-1}) in distilled water for 24 h at room temperature. The product was dialyzed and lyophilized as described above and analyzed by nuclear magnetic resonance (NMR) spectroscopy. All experiments were measured with a Jeol JNM-ECZR 500 MHz NMR spectrometer (Tokyo, Japan). The samples (5 mg) were dissolved in deuterium oxide (600 μL) containing an internal standard (0.05 wt % 3-(trimethylsilyl)-propionic-2,2,3,3-d4 acid, sodium salt). The samples were measured at 40 °C. The relative substitution was calculated by comparing the integral of the lysine amino acid peak at δ 3.0 ppm to the aromatic proton peak of 4-hydroxybenzaldehyde at δ 7.6 ppm. The presence of aldehyde groups in GG-CHO was qualitatively evaluated using Fourier transform infrared (FTIR) spectroscopy. FTIR-spectra from the GG-CHO polymer was measured on a PerkinElmer Spectrum One attenuated total reflection−FTIR spectrometer (Waltham, MA, USA) in the spectral range of 400−4000 cm^{-1}.

2.6. Hydrogel Preparation and Characterization. Modified gelatins and GG-CHO solutions were prepared separately by dissolving each polymer in an aqueous solution of 10% (w/w) sucrose or in Dulbecco's modified eagle medium (DMEM), as shown in Table 1. Before the hydrogel preparation, the gelatin polymer solutions were filtered using a Whatman FP 30/0.2 CA-S sterile filter (Thermo Fisher Scientific, MA, USA) at 37 °C, and the GG solutions were filtered using a Sterivex-GP 0.22 μm Millipore Express (polyethersulfone) sterile filter (Merck Millipore, MA, USA) at 60 °C. The solutions were kept at 37 °C, and then equal volumes (1:1) of the solutions were mixed for a few seconds by pipetting. The F7-SPD bioamine-GG compositions were prepared as stated previously[21]

DOI: 10.1021/acsami.8b22343
ACS Appl. Mater. Interfaces 2019, 11, 20589−20602

Table 1. Formulation of Hydrazone Cross-Linked Hydrogels Based on Gelatin and GG

formulation code	components	concentration [mg mL^{-1}]	gelation medium: 10% sucrose	gelation medium: DMEM/F-12 or PBS
F1-ADH	gelatin-ADH	40	+	
	GG-CHO	40		
F2-ADH	gelatin-ADH	40	+	
	GG-CHO	30		
F3-ADH	gelatin-ADH	40	+	
	GG-CHO	20		
F4-CDH	gelatin-CDH	60		+
	GG-CHO	60		
F5-CDH	gelatin-CDH	60		+
	GG-CHO	40		
F6-CDH	gelatin-CDH	40		+
	GG-CHO	40		
F7-SPD	unmodified GG	5	+	
	SPD	0.5	+	

with 1.5 wt % of SPD cross-linker per GG and used as the negative control.

2.7. In Vitro Hydrogel Degradation. For in vitro degradation tests, 500 μL of hydrogels were formed in Eppendorf tubes. A solution of 10 U mL^{-1} of collagenase II (Sigma-Aldrich, St. Louis, MO, USA) was added to the tubes, and aliquots were collected at the indicated time points and refreshed with fresh enzyme solution. The fluorescamine (Sigma-Aldrich, St. Louis, MO, USA) test was used to determine the presence of gelatin in the collected samples using a QuantaMaster PTI spectrofluorometer (Photon Technology International, Inc., Lawrenceville, NJ, USA) (excitation 390 nm, emission 465 nm).

2.8. Mechanical Characterization. Hydrogel samples were prepared in custom-made polydimethylsiloxane (PDMS) molds with a diameter of 12 mm and a height of 6 mm and tested at the earliest 2 h after gelation. PDMS was fabricated from the SYLGARD 184 base polymer and a curing agent (10:1, w/w, SYLGARD 184, Dow Corning, USA), acquired from Ellsworth Adhesives AB (Sweden). Mechanical testing was performed, as we have previously described in detail, using a BOSE ElectroForce BioDynamic 5100 machine equipped with a 225 N load sensor and Wintest 4.1 software (Bose Corporation, Eden Prairie, MN, USA).[21] Unconfined compression was performed with a constant 10 mm min^{-1} strain rate until 75% strain of the original height was reached. The fracture point was seen as a clear drop in the stress−strain curve.

To obtain a relevant reference for our hydrogel's biomimicry of the tissue, we used the compression testing data from fresh heart tissues of New Zealand white rabbits, based on our previous results.[22] The compression samples were cut from both the left and right heart ventricle, compressed in the direction perpendicular to the beating direction, and pooled together. The rabbit tissues were obtained from animal experiments conducted at the Tampere University Medical School.

Statistical analysis of the mechanical testing data was performed by SPSS Version 25.0 (IBM SPSS Statistics for Windows, NY, USA). The data were presented as mean ± standard deviation. One-way analysis of variance was performed with a confidence level of 95%. P values less than 0.05 were considered as statistically significant. Pair comparisons of data were done with the Tukey post-hoc test to identify significant differences between the hydrogel formulations.

2.9. Fibroblast Hydrogel Cell Culture. The commercial human lung fibroblasts (WI-38, Culture Collections, Public Health England, United Kingdom) were cultured and expanded in Nunc T75 culture flasks (Thermo Fisher Scientific, USA) with DMEM/Ham's Nutrient Mixture F-12 (F-12 1:1; Thermo Fisher Scientific, USA) supplemented with 10% fetal bovine serum (FBS; South American Origin, Biosera, Finland) and 50 U mL^{-1} penicillin/streptomycin (Pen/Strep; Thermo Fisher Scientific, USA). For cytocompatibility testing, fibroblasts were detached from the culture flask via trypsin (Lonza, Basel, Switzerland) treatment and then counted and plated with 30 000 cells cm^{-2} under 2D conditions and with 300 000 cells mL^{-1} under 3D conditions. To test the cytocompatibility of the modified gelatin, separate cell culture wells were dip-coated with gelatin-ADH or gelatin-CDH (40 mg mL^{-1}) with 1 h incubation at 37 °C.

Hydrogel cell cultures were conducted both on top of the hydrogel (2D) and encapsulated inside the hydrogel (3D), with all hydrogel compositions listed in Table 1. In the 2D experiment, the hydrogel was cast in the well plate 20 min before the cells were plated on top. In the 3D experiment, 30 μL of cell suspension was mixed with gelatin-ADH or gelatin-CDH and GG-CHO simultaneously during gelation to form a total of 330 μL of hydrogel. Cell culture medium was applied on top of the samples after ∼20 min of gelation time. Unmodified gelatin coating was used as a control in all cell experiments. All coating and hydrogel cell tests were done on a Greiner CELLSTAR 48-multiwell plate (Sigma-Aldrich).

After 3 and 7 days of culturing, the samples were stained with a Live/Dead (Thermo Fisher Scientific, USA) cell viability kit. The fluorescent calcein-AM (at 0.2 μM) stains intact cells green, and ethidium homodimer-1 (at 1.0 μM) stains dead cells red. After 1 h of incubation at room temperature with a rocker, the cells were imaged with an Olympus IX51 inverted microscope and an Olympus DP30BW digital camera (Olympus, Finland). Staining concentrations were double that recommended by the kit instructions to allow for faster diffusion under 3D hydrogel conditions. During wide-field microscopy, the 3D position in the middle of the hydrogel was verified by using the 2D cell control at the well-plate bottom as a reference point and changing the focus distance accordingly.

The cell numbers were quantified using ImageJ (Version 1.39, US National Institutes of Health, Bethesda, MD, USA)[38] particle counting algorithm based on at least three parallel Live/Dead stained images taken with 4× magnification from all studied conditions. Fibroblast viability percentage was calculated from the detected live and dead cell area according to the following equation

$$\text{Viability \%} = \frac{\text{area of live cells}}{\text{area of live cells} + \text{area of dead cells}} = \frac{\sum_{i=1}^{n} L_i}{\sum_{i=1}^{n} D_i + L_i}$$

2.10. Optical Projection Tomography Imaging. An in-house built optical projection tomography (OPT) system in transmission mode was used for imaging cells encapsulated in the hydrogel to visualize the 3D morphology of fibroblasts under selected hydrogel conditions.[36,39] Cell cultures were prepared in fluorinated ethylene propylene tubes with water matching the refractive index and submerged inside a cuvette filled with water for imaging. All OPT samples were imaged after 7 days of culture. A white light-emitting diode source (Edmund, USA) was used to illuminate the sample. The transmitted light was detected by a 5× infinity-corrected objective (Edmund, USA) with a numerical aperture of 0.14 and imaged with a sCMOS camera (ORCA-Flash 4.0, Hamamatsu, Japan). The sample was rotated 360° while a total of 400 projection images were captured at 0.9° intervals. 3D reconstruction was computed in MATLAB from projection images using standard filtered back-projection algorithm.[36] Visualization in 3D was done in Avizo software (Thermo Fisher Scientific, Waltham, MA, USA).

2.11. Cardiomyocyte Differentiation. The Ethics Committee of Pirkanmaa Hospital District gave approval to conduct research on hiPSC lines (Aalto-Setälä R08070). The hiPSC line UTA.04602.WT was cultured and characterized at the stem cell state, as previously described.[40] The cardiomyocyte differentiation was done by modulating Wnt signaling with small molecules, according to the protocol published by Lian et al. 2012.[41] In short, differentiation was initiated by plating 700 000 hiPSCs/well in a Nunc 12-multiwell plate (Thermo Fisher Scientific, USA) in feeder-free condition on Geltrex-

DOI: 10.1021/acsami.8b22343
ACS Appl. Mater. Interfaces 2019, 11, 20589−20602

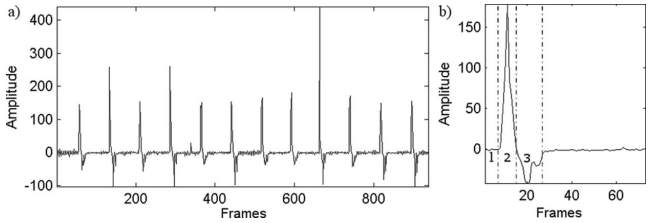

Figure 1. Beating pattern of cardiomyocyte aggregate in F4-CDH hydrogel as an example of the BeatView analysis. This is the same aggregate as in Video S8. Graph (a) shows regular beating rhythm; (b) shows the breakdown of a single beat into relaxed state (1) and contracting (2) and relaxing (3) movements.

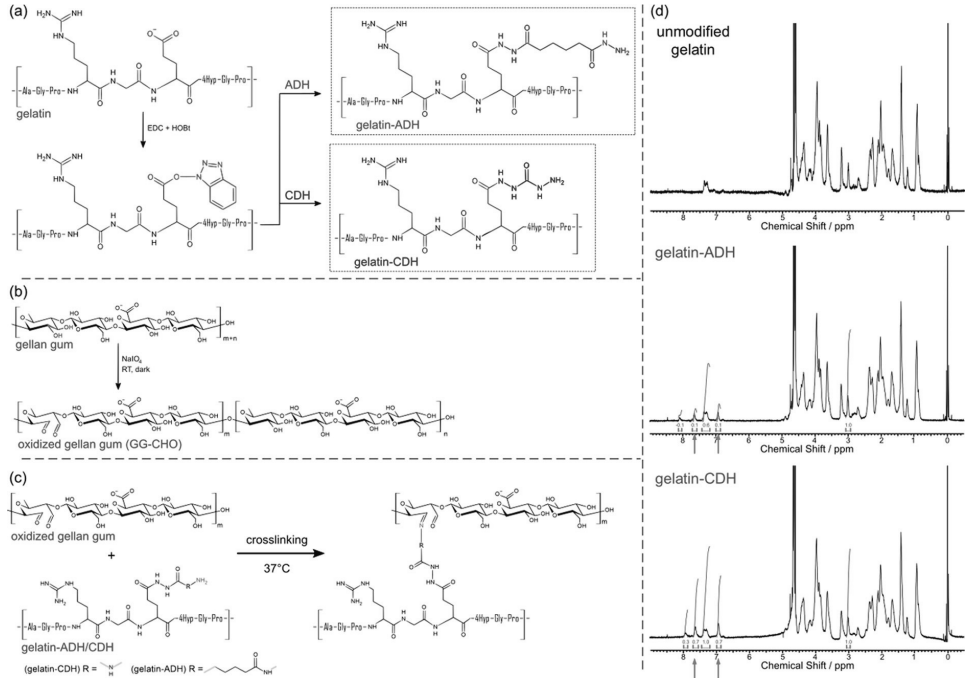

Figure 2. (a) Chemical modification of gelatin carboxylic groups with hydrazide molecules ADH (provides 10-atom bridge) and CDH (provides 5-atom bridge). (b) Periodate oxidation of vicinal diols in GG. (c) Hydrazone cross-linking reaction between gelatin-ADH/CDH and GG-CHO. (d) ^{1}H NMR-spectra of nonmodified gelatin, gelatin-ADH, and gelatin-CDH modifications. The arrows highlight the appearance of aromatic protons in gelatin-ADH and gelatin-CDH spectra after the coupling reaction of CDH and ADH with 4-hydroxybelzandehyde. Chemical modification was successful based on the appearance of extra peaks.

coating (Thermo Fisher Scientific, USA) in mTeSR1 medium (STEMCELL Technologies, Canada) supplemented with 50 U mL^{-1} Pen/Strep for 4 days. Ten days after initiation, the medium was changed to RPMI (Thermo Fisher Scientific, USA) supplemented with B27(−insulin) (Thermo Fisher Scientific, USA) and 50 U mL^{-1} Pen/Strep. During this time, on day one, 8 μM CHIR99021 (REPROCELL, United Kingdom) was applied to the cells. After 24 h, CHIR99021 was removed. On day3, 5 μM IWP-4 (R&D Bio-Techne, USA) was added for 48 h. From day 10 onwards, B27(−insulin) was changed to B27(+insulin) (Thermo Fisher Scientific, USA), and the cells were cultured in this medium until they were used for the hydrogel experiments.

2.12. Cardiomyocyte Hydrogel Cell Culture. After differentiation, beating cardiomyocyte areas were cut with a scalpel under a microscope and collected. Then, the aggregates were partially dissociated to loosen the cell-to-cell bonds inside the aggregate and to better allow the attachment on the hydrogel. Dissociation was modified from the study of Ahola et al. 2014.[11] The enzymatic dissociation buffers were applied to the cells incubated at 37 °C: First buffer for 45 min, second buffer for 15 min, and third buffer for 10 min, but no mechanical dissociation was done. The gentle dissociation treatment loosens the cardiomyocyte aggregate and makes it more susceptible to attach on to the hydrogel surface. Four aggregates were plated per well with all coating and hydrogel preparations (2D and 3D), as described above for fibroblasts. Cells were cultured with KnockOut-DMEM medium (Thermo Fisher Scientific, USA) supplemented with 20% FBS, 1% nonessential amino acids (Cambrex, NJ, USA), 2 mM GlutaMAX (Thermo Fisher Scientific, USA), and 50 U mL^{-1} Pen/Strep. The medium was changed every 3 days, always 1 day before analysis, and the cells were cultured for 7 days maximum.

DOI: 10.1021/acsami.8b22343
ACS Appl. Mater. Interfaces 2019, 11, 20589−20602

2.13. Analysis of Cardiomyocyte Hydrogel Cell Culture. The cardiomyocyte cultures were primarily analyzed by phase contrast microscopy using a Nikon Eclipse TS100 (Nikon Corporation, Japan) microscope with a Nikon accessory heating plate, and monochrome 8-bit videos were acquired with an Optika DIGI-12 (Optika Microscopes, Italy) camera. The video recording of beating cardiomyocytes was done with the same setup using 60 frames per second, recording for 30 s. The beating is temperature sensitive, and our measurement setup has been previously verified to be at 37 °C inside the well plate.[42] The videos were analyzed with BeatView software.[11] Figure 1 shows a representative beating pattern of a cardiomyocyte aggregate.

Additionally, the cardiac nature of the differentiated cardiomyocytes was verified using real time polymerase chain reaction (RT-PCR), qPCR, and immunocytochemical staining. For PCR, the total RNA from the cardiomyocyte aggregates in the hydrogel was isolated using the Qiagen RNeasy kit (Qiagen, Germany) after 2 weeks in culture. For the RNA extraction, the culture medium was removed, and the hydrogel was washed in phosphate-buffered saline (PBS) briefly three times. The cardiomyocyte aggregates in the hydrogel were cut with a scalpel under a microscope and collected in a microcentrifuge tube. The hydrogel surrounding the cluster was partially digested by adding 100 μL of pronase solution (stock 10 mg mL^{-1} in water, Sigma-Aldrich, St. Louis, MO, USA) and incubated at 37 °C for 5 min with mild shaking. The digested hydrogel solution was then added directly to the RNeasy lysis buffer and homogenized, and RNA was extracted according to the manufacturer's instructions. DNase I-treated total RNA was reverse-transcribed using a high capacity cDNA reverse transcription kit (Applied Biosystems, Foster City, CA, USA). The cDNA was amplified by the TaqMan Universal Master Mix (Applied Biosystems) using the BioRad CFX384 real-time PCR detection system. Samples were analyzed in triplicates, and glyceraldehyde 3-phosphate dehydrogenase (GAPDH) was used for normalization of expression levels of individual genes, which was calculated by the $\Delta\Delta C_T$ method.[43] TaqMan assays used in the qPCR protocol are presented in Table S1.

Immunocytochemical staining was done with the previously reported, optimized protocol for 3D cell culture.[21] In brief, cultures were fixed with 4% paraformaldehyde for 30 min. After a brief wash in PBS, nonspecific staining was blocked with 10% normal donkey serum (NDS), 0.1% Triton X-100, and 1% bovine serum albumin (BSA) (all from Sigma-Aldrich, St. Louis, MO, USA) in PBS for 1 h in room temperature, followed by another wash in 1% NDS, 0.1% Triton X-100, and 1% BSA in PBS. Then, a combination of primary antibodies, troponin T (1:1750) from goat and α-actinin (1:1250) from mouse, dissolved in 1% NDS, 0.1% Triton X-100, and 1% BSA in PBS, was applied to the cells and incubated at 4 °C for 2 days. The samples were washed three times in 1% BSA in PBS (first 5 min, followed by 2 × 1 h) and then incubated for 2 days at 4 °C with Alexa Fluor 488 conjugated to donkey anti-mouse (1:800) and Alexa Fluor 568 conjugated to donkey anti-goat (1:800) in 1% BSA in PBS. The samples were washed three times (first 5 min, followed by 2 × 1 h) in PBS. As the last step, 4′,6-diamidino-2-phenylindole (DAPI) for nuclei staining was applied at 1:2000 concentration in 1% PBS, and the samples were stored light-protected at 4 °C. The cells were imaged with an Olympus IX51 inverted microscope and an Olympus DP30BW digital camera (Olympus, Finland) similar to Live/Dead stained fibroblasts.

3. RESULTS AND DISCUSSION

3.1. Modification of Biopolymers. To form hydrazone cross-links between GG and gelatin, we hypothesized that hydrazide groups could be introduced to the gelatin backbone to form cross-links with the aldehyde groups generated in the GG molecule (Figure 2). Our results show that the carboxylic group present in the gelatin molecule can be modified with ADH or CDH, and the modifications were confirmed by ^{1}H NMR spectroscopy (Figure 2). The spectra of gelatin-ADH and gelatin-CDH after the derivatization with 4-hydroxybenzaldehyde shows the appearance of protons at δ 6.9 ppm and δ 7.6 ppm, compared with unmodified gelatin, and indicates the presence of hydrazide groups available for the cross-linking process. The integrated intensity of these protons was much higher for gelatin-CDH (0.7) than for gelatin-ADH (0.1). In addition, the peak at δ 7.3 ppm, corresponding to phenylalanine amino acid, increased in gelatin-CDH (1.0) compared with gelatin-ADH (0.6) because of the contribution of the aromatic group in 4-hydroxybenzaldehyde. As a reference, we used the amino acid lysine with a signal at δ 3.0 ppm. The degree of modification of gelatin-CDH was slightly higher than that of gelatin-ADH. This was likely due to the formation of bonds between two molecules of gelatin generating an adduct.[44] On the other hand, GG was modified through periodate oxidation (GG-CHO), and the presence of aldehyde groups was corroborated by FTIR, where a typical aldehyde shoulder was detected at 1733 cm^{-1}, as shown in Figure S1.[22]

3.2. Gelatin-GG Hydrogel Preparation. Hydrazide-modified gelatins and oxidized GG (GG-CHO) form hydrazone bonds that are capable of creating a hydrogel under physiological conditions without any external energy, cross-linkers, or catalysis. To obtain self-standing hydrogels with adequate mechanical properties, several volume ratios and polymer concentrations were tested. The detailed hydrogel formulations obtained and studied in this work are described in Table 1 in the Experimental Section. Briefly, formulations of F1−F3-ADH are composed of gelatin-ADH and GG-CHO, and formulations of F4−F6-CDH are composed of gelatin-CDH and GG-CHO. In general, poor gelation was shown by concentrations below 20 mg mL^{-1} (2%) of gelatin-ADH and 30 mg mL^{-1} (3%) gelatin-CDH. Forming the gels with components of equal concentration, the volume ratio 1:1 yielded the best gelation. When the ratio was changed by increasing the volume of the gelatin component, the gels became very weak. The maximum amount of gelatin required to produce a true hydrogel was 60% w/w in polymer weight, which was achieved with gelatin-CDH because of the higher modification degree compared with gelatin-ADH. The gelatin-ADH or gelatin-CDH with GG-CHO components form a sticky and true gel within seconds. Complete gelation is reached within 5 min for F1−F3-ADH and within 10 min for F4−F6-CDH.

Cross-linking of GG with calcium ions and PBS or DMEM to make covalently cross-linked hydrogels that are mechanically robust has been extensively explored.[27] However, these cross-linking methods lack cytocompatibility. Here, with the inclusion of gelatin, it is expected that the cell interaction with the material will improve significantly because of the natural cell adhesion motifs (e.g., RGD) and the matrix metalloproteinase-mediated degradability present in gelatin.[45] The simplicity of this cross-linking method provides the opportunity to control the mechanical properties, for example, by adjusting the ratio or concentration of the polymers in the system.

Our approach simplifies hydrogel formation relative to other gelatin cross-linking schemes because it does not require high ion concentrations, varying temperature during gelation, or UV light and enables gelation under mild, physiological conditions.[31,46,47] In general, we can state that our hydrogel production method using simple casting is an easier and biologically safer way to produce 3D culture substrates for cardiomyocytes than many of the other published methods.

DOI: 10.1021/acsami.8b22343
ACS Appl. Mater. Interfaces 2019, 11, 20589−20602

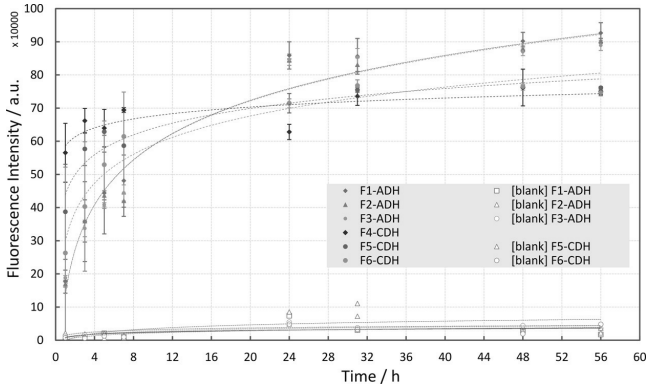

Figure 3. Degradation profiles of the tested hydrogels incubated with collagenase for 56 h. Values represent the mean and standard deviation. Sigmoidal curve fits were applied to the data.

For example, even though the layer-by-layer technique described by Amano et al. 2016 produces well-controlled 3D structures, it requires longer fabrication times per sample.[48] Moreover, the Biowire method by Nunes et al. 2013 requires a special, custom-made mold to retain the weak hydrogel until the cells produce their own ECM, and even more complex molds are required for the microphysiological system reported by Mathur et al. 2015.[16,49] In contrast, our self-supporting hydrogel can be cast, or even injected, in many different shapes for 3D cell encapsulation. Moreover, it could replace the Matrigel or GelMA used in the aforementioned 3D cardiomyocyte culture systems.[16,48,49] For future cardiac drug-screening studies, however, a high throughput study setup suitable for our gelatin-GG hydrogel would be cell-encapsulating droplets that can be studied optically and electrophysiologically, as suggested by Oliveira et al. 2016.[50]

3.3. In Vitro Hydrogel Degradation. To evaluate the degradation profile, the hydrogels were incubated at 37 °C in collagenase (10 U mL^{-1}) solution for 56 h, and sample aliquots were periodically taken. The presence of gelatin was evaluated by fluorescence. Figure 3 shows the degradation profiles of the hydrogels. The concentrations used for the ADH or CDH formulations did not show any significant differences within either chemistry type, but the degradation rate of CDH hydrogels showed a clear difference when compared with ADH hydrogels. As expected, the degradation rate decreased with F4−F6-CDH hydrogels, whereas the different degradation observed between the hydrogels based on CDH or ADH may be attributed to an increased number of cross-links (covalent and ionic) in F4−F6-CDH. Compared with the previously developed gelatin-based hydrogels exposed to similar concentrations of collagenase, our CDH gelatin-based hydrogels showed better resistant to collagenase, albeit they have been shown to be less resistant than GelMA-based hydrogels.[51,52] This lack of resistance is due to the higher cross-linking density of GelMA, which is not always beneficial for nutrient diffusion and cell spreading.

3.4. Mechanical Properties of Hydrogels. Mechanical characterization of these hydrogels was carried out as uniaxial compression testing at a compression rate of 10 mm min^{-1} under ambient conditions. The sticky characteristic of the specimens meant that they had to be cut out from their PDMS molds, and their difficult handling likely decreased the repeatability of some of the specimens.

As fresh, healthy human heart tissue is not easily available for mechanical testing, many different mammalian tissues have been used in the literature for the determination of the mechanical properties of the tissue, and we chose to use rabbit heart as the reference as it was readily available.[53−55] Figure 4 shows the representative stress−strain curves of the measured gelatin-GG hydrogel compositions and compares them with the fresh rabbit heart muscle.[22] All samples were initially very easily deformed, but the strain-hardening behavior of gelatin-CDH-based hydrogels and rabbit heart is remarkably similar and occurs at the same strain values of over 40%. The gelatin-ADH-based hydrogel's strain hardening effect is smaller and occurs at even higher strains than with gelatin-CDH-based hydrogels. Because the chemical modification does not affect the groups available for ionotropic cross-linking in GG, extra cross-linking was expected to occur in gelatin-CDH-based hydrogels as they were produced in DMEM/F-12.

The gelatin-ADH-based hydrogels had a fracture strength of 23 to 27 kPa, whereas F6-CDH had a fracture strength of 97 kPa and F5-CDH of even over 300 kPa, as can be seen in Figure 4. All tested compositions exhibited fracture between 60 and 75% strains, indicating high elasticity. For both modifications, the highest strength hydrogel was the composition with an uneven amount of gelatin to GG-CHO (F2-ADH and F5-CDH). This indicates that not all cross-linking points are used in compositions with even concentrations of both components; thus additional cross-linking occurs with the increase of hydrazide groups. Meanwhile, the increase in GG-CHO enhances the stability of the hydrogels but also makes the hydrogels slightly more brittle.

In the literature, the mechanical properties of hydrogels are too often intermixed, and the exact same parameters are not compared. For example, in the case of viscoelastic materials, different compression rates affect the material response, and in consequence, elastic regions are being defined differently.[20,56] Thus, we only compared our results with previous results from unconfined compression at 10 mm min^{-1} strain rate. When comparing the current gelatin-GG hydrogels with our previously published bioamine-GG, hyaluronic acid-GG hydrazone, and plain hyaluronic acid hydrazone hydrogels, the gelatin-ADH-based hydrogels more closely resemble the

DOI: 10.1021/acsami.8b22343
ACS Appl. Mater. Interfaces 2019, 11, 20589−20602

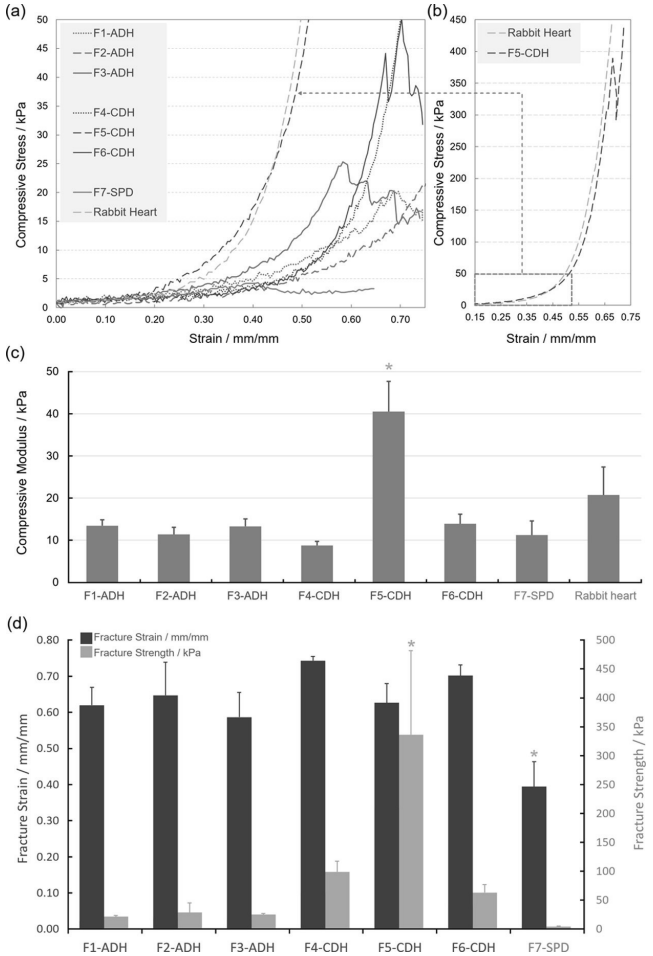

Figure 4. Representative stress−strain curves of the different hydrogel compositions and the rabbit heart tissue. (a) All representative curves with stress range 0 to 40 kPa. (b) Extended graph with the stress scale up to 450 kPa to highlight the similarities between F5-CDH and rabbit heart tissue. (c) Compressive moduli of the hydrogels compared to the rabbit heart. (d) Fracture strain and strength measured by compression testing. The *y*-axis on the left and the dark gray bars show the fracture strain relative to the original sample height. The *y*-axis on the right and the light gray bars show the fracture strength. In (c) and (d), $n = 5$; * = significantly different from other formulations at $p < 0.05$.

hyaluronic acid-based hydrogels.[21−23] The bioamine-GG, such as F7-SPD, is rather brittle in comparison to any hydrazone cross-linked hydrogels, with fracture occurring already at 35% strain. The cross-linking chemistry in all of these materials is the same and consistently produces similar mechanical behavior. This shows that the exact biopolymer concentration has only a minor effect on the mechanical behavior, whereas the chemistry used (ADH or CDH) determines the mechanical properties. At the same polymer concentration, F6-CDH is stronger than F3-ADH. However, F5-CDH has more than a 10-fold increase in fracture strength and a 2-fold increase in compressive modulus, compared to other CDH formulations, and thus substantially higher strain-hardening behavior while still being very elastic and compliant until 40% strain.

One clear effect of changing to hydrazone cross-linking from our previous ionotropic bioamine cross-linking of GG was the change in the compression behavior from being rather brittle to highly elastic. This change in compression behavior was accompanied by an increase in the fracture strength.[21] In cardiac TE, the mechanical properties of the growth substrate affect the spontaneous beating of cardiomyocytes.[57,58] In the case of a very rigid polystyrene substrate, the standard 2D well plate, the upper part of the cell is free to move, allowing for the unconstrained beating of the cell.[11] For 3D matrices, however, the cell is in contact with the surrounding scaffold material in all directions. As a result, the constant spontaneous beating of the cell while encapsulated could be prevented, if the hydrogel is not elastic and compliant enough, whereas a biomimicking hydrogel could support cell differentiation and further maturation.[57,58]

DOI: 10.1021/acsami.8b22343
ACS Appl. Mater. Interfaces 2019, 11, 20589−20602

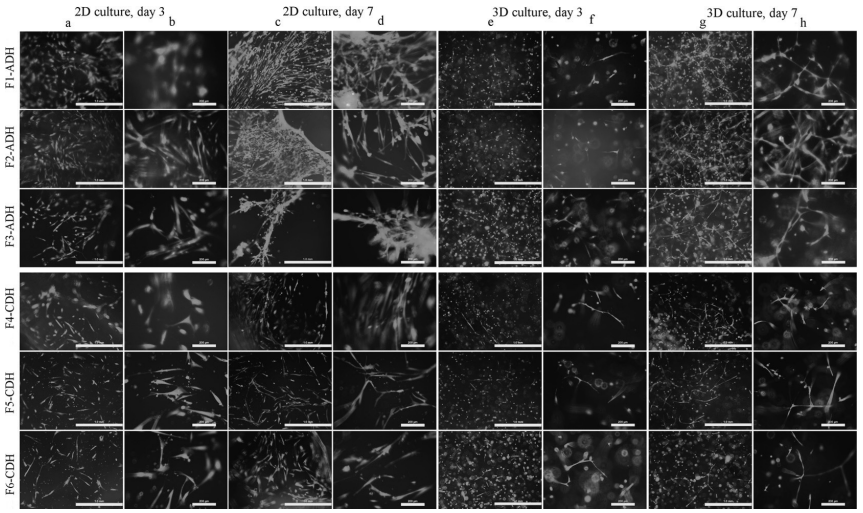

Figure 5. Representative images of Live/Dead stained fibroblast cell cultures in all tested hydrogel formulations and both 2D and 3D culture conditions at the 3-day and 7-day time points. The 3D cultures were imaged in the middle of the hydrogel. Green indicates live cells and red indicates dead cells. Rows (a), (c), (e), and (g) are with lower magnification, and the scale bar length is 1000 μm; rows (b), (d), (f), and (h) are with higher magnification with a scale bar length of 200 μm.

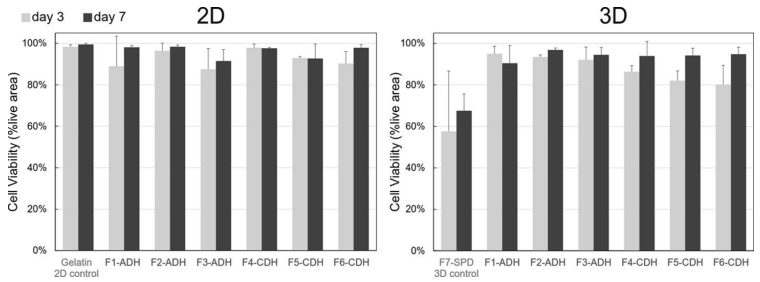

Figure 6. Measured fibroblast viability percentage based on amount of live cells compared to amount of all cells, 4× magnification images. Error bars represent mean values ± standard deviation, $n \geq 3$.

One of the earliest reports about increasing hydrogel strength by blending GG with gelatin is from US patent 4 517 216.[46] However, the patent is aimed at food applications and requires heating the components to 80 °C, which clearly exceeds the range suitable for cell encapsulation applications.[46] More suitable gelatin-GG hydrogels for cell encapsulation have been presented by Shin et al. 2012 and Melchels et al. 2014, both using GelMA that requires UV cross-linking. Both groups show a significant increase in the hydrogel fracture strength by the addition of GG to GelMA.[32,59] Shin et al. also describe a similar elasticity and strain hardening effect as shown for our hydrogels in Figure 4.[32] When compressed alone, GelMA has higher fracture strength and strain than our strongest hydrogels, whereas GGMA alone is clearly more brittle and has lower fracture strength than our hydrogels.[31,32,37,60] By combining GelMA and GGMA into a double-network GelMA-GGMA hydrogel with double the polymer concentration of ours, the fracture strength and strain are increased even further.[32] Wen et al. 2014 present another double-network hydrogel composed of GG and gelatin that utilizes enzymatic cross-linking instead of UV.[61] They report tensile, but not compressive, mechanical test results, and the measured values of fracture strength and strain are in the same range as ours, if tested without the initiation of a double network by Ca^{2+} addition. With the double network, their highest concentrations produced higher strength and elasticity than ours.[61]

3.5. Cell Culture Studies. *3.5.1. Hydrazide-Modified Gelatin Cytocompatibility.* First, native and modified gelatins (gelatin-ADH and gelatin-CDH) were used as coating at 40 mg mL^{-1} for seeding human lung fibroblast WI-38 cells to test the cytocompatibility. The WI-38 cell line was chosen for this purpose based on ISO 10993-5:2009 standard (Biological Evaluation of Medical Devices. Part 5: Tests for In Vitro Cytotoxicity) as a well-known, general purpose human cell line for initial biomaterial screening.[62] The results showed that the modifications did not alter the gelatin's inherent ability for cell attachment and proliferation. The cells attached and showed an elongated morphology after overnight culture under all gelatin-coating conditions (data not shown). In a prolonged culture, the cells became confluent in a week (Figure S2).

3.5.2. Hydrogel Cell Culture of Fibroblasts. After successful cytocompatibility tests with gelatin modifications, the fibro-

DOI: 10.1021/acsami.8b22343
ACS Appl. Mater. Interfaces 2019, 11, 20589−20602

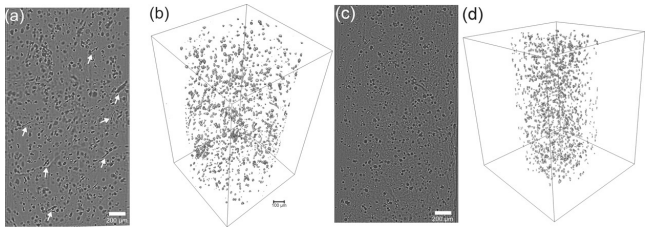

Figure 7. Bright-field OPT visualization of fibroblast cell culture under 3D hydrogel condition. (a) Single projection image of F3-ADH hydrogel, with highly elongated cells highlighted with arrows, (b) 3D reconstruction of the previous giving a view of the whole sample, (c) single projection image of negative control F7-SPD hydrogel, and (d) 3D reconstruction of the previous.

blasts were cultured on top of the hydrazone cross-linked hydrogels listed in Table 1 to study cell attachment and elongation. The fibroblasts were also encapsulated in the same hydrogels to study the cytocompatibility of the cross-linking reaction as well as viability and elongation under 3D conditions. Since gelatin has integrin binding sites and enzymatic cleavage sites, we hypothesized that the cells encapsulated in the hydrogels would be able to elongate in 3D. The initial cell response was examined after 3 days of culture and prolonged culture on day 7. Live/Dead staining was used to visually assess the viability and morphology of the fibroblasts, as shown in Figures 5 and 6. The negative control F7-SPD is shown in Figure S2. On day 3, the cells were already highly elongated and even more so at day 7.

As can be seen in Figure 5, the fibroblast cells are predominantly alive under all tested conditions and at both time points (day 3 and day 7). First, this indicates that the chemical modification is not harmful to the cells and that the cross-linking reaction is efficient and does not leave too many unreacted aldehyde groups to affect cell viability after gelation. A few dead cells were present on day 3, but the number of live cells was much higher, as seen from the viability in Figure 6 being between 80 and 95% for all hydrazone cross-linked hydrogels. Although the initial cell numbers were the same, the cultures seemed more confluent on day 7, indicating cell proliferation. Second, the cells exhibited a high degree of elongation in all directions in 3D under all tested conditions. However, a normal widefield microscope does not convey the status of the cells in a large hydrogel sample but rather gives a snapshot of the culture at a certain position. A holistic view of the sample is critical when evaluating the quality of tissue development.[63] Therefore, we use OPT to visualize several cellular features in a label-free 3D system.[39] Here, we emphasized morphology and elongation as parameters of cytocompatibility (Figure 7 and Videos S1 and S2). Moreover, both the shape and distribution of the cells throughout the hydrogel can be viewed from various angles as shown in Video S1. As can be seen with the F3-ADH hydrogel, a good proportion of the cells are elongated and uniformly distributed in 3D, indicating hydrogel homogeneity in composition and good diffusion of nutrient throughout.

As the cell morphology was well visible in the Live/Dead images, an additional phalloidin or immunocytochemical cytoskeleton staining was deemed unnecessary. The F4-6-CDH hydrogels seemed to have more elongated cells at the earlier time point, and even longer spindlelike cells were seen at the later time point compared with the F1-3-ADH hydrogels. This highly elongated cell morphology is typical for these WI-38 fibroblasts under 2D culture conditions on cell culture plastic.[64] Under 3D culture conditions and in normal cytocompatibility testing, this high degree of elongation is rarely seen. In fact, none of the gelatin-GG studies discussed in Section 2.4 report similar elongation as observed here.[32,59,61] Elongation has been previously reported with mouse fibroblasts in the click-chemistry cross-linkable gelatin hydrogel,[51] and moderate polarization of human adipose stem cells has been reported in the GG-based hydrogel, if collagen is added.[50] Qualitatively estimating the amount of elongation shown in Figure 5 is magnitudes higher compared with either of those studies.[50,51] The elongation of human fibroblast cells on top of a GG microsphere surface modified with gelatin has been previously reported by Wang et al. 2008.[65] However, they did not encapsulate the cells inside the gel microspheres because of the complexity of the cross-linking process. In summary, we have achieved a higher degree of elongation and viability of human fibroblast cells in the encapsulated condition than has been previously reported. Thus, our GELA-GG hydrogel presents an exciting step toward 3D tissue development.

3.5.3. Hydrogel Cell Culture of Cardiomyocytes. Encouraged by the fibroblast results, we studied hiPSC-derived cardiomyocyte aggregates with the hydrogels. In our group, native gelatin coating is routinely used to culture these cells. Here, we compared the modified gelatin coatings and found that the cardiomyocytes recovered their spontaneously beating phenotype after overnight culture and continued the beating as long as they were cultured. As the beating was observed, there was no need for Live/Dead staining of the cardiomyocytes.

As no difference was observed between the compositions in the fibroblast culture, we chose to use the highest and lowest ADH-formulations and all CDH-formulations, as listed in Table 1. Phase contrast microscopy showed spreading and migration of the cells from the cardiomyocyte aggregates plated on top of the hydrogel, as seen in Figure 8. The cardiac nature of the differentiated cells was verified by qPCR after 2 weeks in culture and by immunocytochemical staining after 1 week in culture, as shown in Figure 9. The expression of TNNT2 and ACTN2 on the protein level and the expression of these same markers plus MYBPC3 on the RNA level confirms the cardiac nature of our hiPSC-derived cells. The qPCR result in Figure 9a especially shows increased expression of TNNT2 in the 3D hydrogel culture compared to the 2D control, indicating positive cell response. Similarly, Figure 9d shows spreading of TNNT2 positive cells from the cell aggregate into the hydrogel.

The cardiomyocytes were also beating spontaneously under all tested conditions both on top of and encapsulated inside the hydrogels, as can be seen in Videos S6−S10. This

DOI: 10.1021/acsami.8b22343
ACS Appl. Mater. Interfaces 2019, 11, 20589−20602

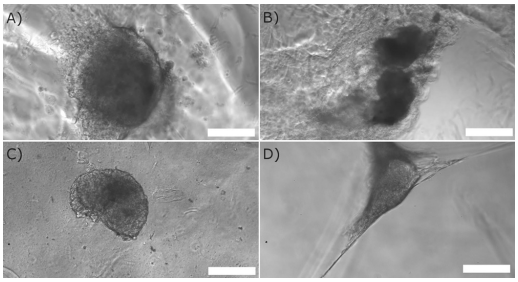

Figure 8. Microscope images of hiPSC-derived cardiomyocyte aggregates cultured under hydrogel conditions: (a) F1-ADH, (b) F3-ADH, (c) F4-CDH, and (d) F5-CDH. The scale bar length is 200 μm.

spontaneous beating is a strong indication of a positive cell response to the culture environment.

The recorded phase contrast videos of cardiomyocyte beating were analyzed with BeatView software that has already been successfully used for hiPSC-derived cardiomyocyte disease modeling in 2D.[11,40] The aggregate beating was not affected by the change of environment from a 2D natural gelatin coated surface to a chemically modified gelatin coating or by being on top of or encapsulated inside the gelatin-GG hydrogel, as shown in Table 2. Cardiomyocytes cultured in the negative control F7-SPD hydrogel did not seem to attach on the hydrogel. They looked worse than in gelatin-GG conditions and did not beat. In the hydrogel culture condition Videos S6−S10, it can be seen how the beating aggregate pulls the hydrogel with it. This observation confirms that suitable elasticity is required of the encapsulating hydrogel, otherwise the cells would be unable to manipulate their surroundings and would be entrapped inside a too rigid hydrogel network; see Videos S6−S11. In the case of two individually beating aggregates in close proximity, this transfer of movement via the hydrogel can be detrimental for the analyzability of the beating. The main beating parameters are shown in Table 2. The beating rate shows how many beats per minute (BPM) are recorded, and the contraction-relaxation duration is the length of a single beat (milliseconds). Between the contractions, the cell is at rest.

The beating behavior observed here is typical for hiPSC-derived cardiomyocytes produced with this differentiation method.[66] The beating frequency remained at ∼30 to 70 BPM, regardless of whether the aggregate was cultured on the standard unmodified gelatin coating, on the modified gelatin coating, on top of the hydrogels, or encapsulated inside the hydrogels. Culturing cardiomyocytes in the 3D-engineered heart tissue has been shown to cause their electrophysiology to have a higher resemblance to the real situation in the body.[15] However, the method uses a very weak hydrogel substrate based on Matrigel and relies on the cell's ECM production during the differentiation.[15] Our hydrogel, on the other hand, is strong enough to be handled with tweezers. Subsequently, we can use cells differentiated with any method and move them to hydrogel culture once they start beating, and they recover the beating already after 24 h. The previously discussed Biowire method is a relevant option for cardiomyocyte 3D culture. The method is, however, impeded by the mechanical weakness of Matrigel and greatly constrained by the mold shape.[16] Both of these methods would benefit from replacing the Matrigel-based substrate with our cardiomimetic gelatin-GG hydrogel.

One hurdle to overcome when developing 3D disease modeling is the maturation of hiPSC-derived cardiomyocytes.[67] It has been demonstrated that current differentiation

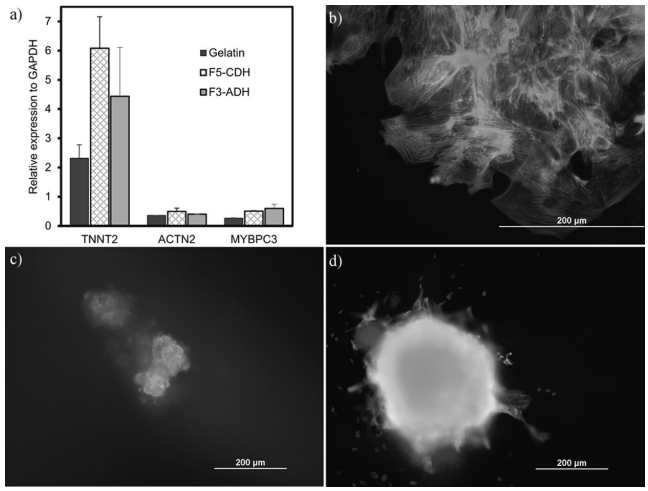

Figure 9. (a) Quantitative RT-PCR validation of cardiac specific genes expressed in hiPSC-derived cardiomyocytes cultured in the gelatin coating control, F5-CDH and F3-ADH. Shown are the expression levels of cardiac type troponin T2 (TNNT2), α-actinin 2 (ACTN2), and Myosin binding protein C (MYBPC3), relative to the housekeeping gene GAPDH. Standard deviations are from three biological replicates, each done in technical triplicate in qPCR. (b−d) Immunocytochemical staining of hiPSC-derived cardiomyocytes using red for TNNT2, green for ACTN2, and blue for DAPI. (b) 2D control on gelatin coating. (c) Aggregate 3D culture in F3-ADH. (d) Aggregate 3D culture in F5-CDH. The density of cell aggregate in F5-CDH slightly prevents antibody and fluorescent light penetration, causing blurriness in the image.

DOI: 10.1021/acsami.8b22343
ACS Appl. Mater. Interfaces 2019, 11, 20589−20602

Table 2. Contraction-Relaxation Durations and Beating Frequencies of the hiPSC-Derived Cardiomyocyte Aggregates Under All Tested Conditions, Analyzed with BeatView Software; $n = 4$

material	2D/3D	ratio[c] [mg mL^{-1}]	beating rate [BPM]	standard deviation	contraction−relaxation duration [ms]	standard deviation
gelatin coating control	2D	100:0	35.78	±20.41	568.60	±127.10[a]
GELA-ADH coating		100:0	42.35	±6.69	435.50	±154.02
GELA-CDH coating		100:0	35.60	±20.18	662.44	±268.50[a]
F7-SPD	3D	0:100	0		0	
F1−3-ADH	2D	40:40	36.71	±17.74	435.25	±113.70
		40:20	68.04	±17.01	305.21	±65.13
	3D	40:40	72.10	±15.14	264.14	±41.97
		40:20	52.70	±47.60	474.59	±303.62[a]
F4−6-CDH	2D	60:60	38.63	[b]	423.74	[b]
		60:40	37.73	±2.78[b]	434.34	±38.96[b]
		40:40	41.56	±5.33	393.14	±63.67
	3D	60:60	35.77	±7.00	403.68	±44.01
		60:40	37.99	±6.50	452.44	±32.85
		40:40	33.82	±3.02	491.88	±15.65

[a]Major prolongation in contraction−relaxation interval detected in one sample. [b]Elasticity of hydrogel transferring movement over a long distance interferes with the beating analysis; so only one or two aggregates were analyzed successfully. [c]Ratio of gelatin to GG.

protocols produce cardiomyocytes that resemble the fetal human heart in gene expression as well as on the structural and functional level.[67,68] There is a multitude of strategies that are aimed at maturing cardiomyocytes. These range from mechanical and electrical stimulations to simply longer culture times.[67] However, the physical cues from the ECM are one potential strategy that we would like to further explore in future. The correct stiffness of the culture substrate as well as its topography can provide cues that can aid the maturation process.[48,67−69] As proven by compression testing (Figure 4), our hydrogels have a biomimicking elasticity that is comparable with the heart tissue. These hydrogels are a promising tool for testing cardiomyocyte maturation. Even though gelatin-ADH-GG hydrogels had a significantly lower strain-hardening effect than gelatin-CDH-GG hydrogels, the beating and mechanotransduction of the cells occur at lower strains and thus make all hydrogel compositions equally promising in this regard.

4. CONCLUSIONS

The current trend in the development of disease models is toward transitioning from 2D cultures to the more biomimicking 3D cultures. This opens up possibilities for studying more tissuelike cellular interactions instead of only studying individual cells. We conclude that the hydrogels based on gelatin-ADH-GG and gelatin-CDH-GG presented in this study are suitable candidates for cardiac TE and 3D cardiac disease modeling. Hydrazide modification of gelatin and oxidation of GG facilitate spontaneous covalent bonding between the polymers. This aids the rapid gelation with homogeneous cross-link distribution under mild conditions suitable for the 3D encapsulation of cells. The stress−strain behavior of hydrogels based on gelatin-CDH very closely resembles the ex vivo heart tissue. The hydrogels enable cell attachment, spreading, and elongation in the encapsulated 3D culture, demonstrated first with human fibroblasts. The hiPSC-derived cardiomyocyte aggregates exhibit normal phenotypical beating behavior when plated on top of or encapsulated inside the hydrogel. On top of the hydrogel, the cardiomyocyte aggregates attached, and cell spreading and migration out of the aggregate were observed. The beating can then be quantitatively analyzed from simple phase contrast microscopy videos with BeatView software, as shown here. The beating analysis shows that cells retain their normal beating characteristics when moved from differentiation in 2D culture to 3D hydrogel culture. No significant biological difference was noticed between the formulations based on gelatin-ADH and gelatin-CDH. Overall, the results suggest the suitability of these gelatin-GG hydrogels with tunable properties for 3D soft tissue modeling and specifically to develop cardiac disease models.

■ ASSOCIATED CONTENT

Supporting Information

The Supporting Information is available free of charge on the ACS Publications website at DOI: 10.1021/acsami.8b22343.

FTIR spectra of GG-CHO compared to unmodified GG; Live/Dead micrographs of fibroblast grown on gelatin-ADH, gelatin-CDH, and unmodified gelatin coatings as well as negative control 3D fibroblast cell culture in F7-SPD composition; and table of the used TaqMan assays for qRT-PCR (PDF)

Reconstruction of bright-field OPT imaging of cultured fibroblasts encapsulated in GELA-ADH-GG 40:20 hydrogel (MPG)

Reconstruction of bright-field OPT imaging of cultured fibroblasts encapsulated in the negative control SPD cross-linked GG hydrogel (MPG)

Beating hiPSC-derived cardiomyocytes on control gelatin coating (AVI)

Beating hiPSC-derived cardiomyocytes on gelatin-ADH coating (AVI)

Beating hiPSC-derived cardiomyocytes on gelatin-CDH coating (AVI)

Beating hiPSC-derived cardiomyocytes in F1-ADH hydrogel culture conditions (AVI)

Beating hiPSC-derived cardiomyocytes in F3-ADH hydrogel culture conditions (AVI)

Beating hiPSC-derived cardiomyocytes in F4-CDH hydrogel culture conditions (AVI)

Beating hiPSC-derived cardiomyocytes in F5-CDH hydrogel culture conditions (AVI)

Beating hiPSC-derived cardiomyocytes in F6-CDH hydrogel culture conditions (AVI)

DOI: 10.1021/acsami.8b22343
ACS Appl. Mater. Interfaces 2019, 11, 20589−20602

Nonbeating hiPSC-derived cardiomyocytes in negative control F7-SPD hydrogel culture conditions (AVI)

AUTHOR INFORMATION

Corresponding Authors

*E-mail: janne.t.koivisto@tuni.fi (J.T.K.).
*E-mail: jenny.parraga@tuni.fi (J.P.).

ORCID

Janne T. Koivisto: 0000-0002-7904-4780
Jari Hyttinen: 0000-0003-1850-3055

Notes

The authors declare no competing financial interest.

ACKNOWLEDGMENTS

The authors would like to thank Alexandre Efimov Ph.D. from the Laboratory of Chemistry and Bioengineering, Faculty of Natural Sciences, Tampere University for his help related to the NMR-measurements, Mari Lehti-Polojärvi M.Sc.(Tech.) from the BioMediTech, Tampere University for the preparation of the custom-made PDMS molds for compression testing samples, Mari Hämäläinen Ph.D. from Immunopharmacology, Tampere University for providing the rabbit heart tissue samples, Eeva Laurila Ph.D. from the BioMediTech, Tampere University for help with BeatView software, and Adj. Prof. Susanna Narkilahti Ph.D., Neuro Group, BioMediTech, Tampere University for help in handling the tissue samples. Additionally, we would like to thank laboratory technicians Henna Lappi and Markus Haponen from the Heart Group, BioMediTech, Tampere University, for providing the differentiated and ready-to-use cardiomyocytes for this study. The authors acknowledge Tampere CellTech Laboratories and Tampere Imaging Facility (TIF) for their services. This work was funded by The Human Spare Parts program of Business Finland (former Tekes—Finnish Funding Agency for Innovation). J.T.K. acknowledges the support given by the Finnish Cultural Foundation Pirkanmaa Regional Fund personal grant number 50151501, and K.A.-S. acknowledges the support by the Finnish Foundation for Cardiovascular Research.

REFERENCES

(1) Langer, R.; Vacanti, J. Tissue Engineering. *Science* **1993**, *260*, 920−926.

(2) Asthana, A.; Kisaalita, W. S. Biophysical Microenvironment and 3D Culture Physiological Relevance. *Drug Discovery Today* **2013**, *18*, 533−540.

(3) Langley, G. R.; Adcock, I. M.; Busquet, F.; Crofton, K. M.; Csernok, E.; Giese, C.; Heinonen, T.; Herrmann, K.; Hofmann-Apitius, M.; Landesmann, B.; Marshall, L. J.; McIvor, E.; Muotri, A. R.; Noor, F.; Schutte, K.; Seidle, T.; van de Stolpe, A.; Van Esch, H.; Willett, C.; Woszczek, G. Towards a 21st-century roadmap for biomedical research and drug discovery: consensus report and recommendations. *Drug Discov. Today* **2017**, *22*, 327−339.

(4) Akopian, V.; Andrews, P. W.; Beil, S.; Benvenisty, N.; Brehm, J.; Christie, M.; Ford, A.; Fox, V.; Gokhale, P. J.; Healy, L.; Holm, F.; Hovatta, O.; Knowles, B. B.; Ludwig, T. E.; McKay, R. D. G.; Miyazaki, T.; Nakatsuji, N.; Oh, S. K. W.; Pera, M. F.; Rossant, J.; Stacey, G. N.; Suemori, H. Comparison of defined culture systems for feeder cell free propagation of human embryonic stem cells. *In Vitro Cell. Dev. Biol.: Anim.* **2010**, *46*, 247−258.

(5) Lu, H. R.; Whittaker, R.; Price, J. H.; Vega, R.; Pfeiffer, E. R.; Cerignoli, F.; Towart, R.; Gallacher, D. J. High Throughput Measurement of Ca++Dynamics in Human Stem Cell-Derived Cardiomyocytes by Kinetic Image Cytometery: A Cardiac Risk Assessment Characterization Using a Large Panel of Cardioactive and Inactive Compounds. *Toxicol. Sci.* **2015**, *148*, 503−516.

(6) Robertson, C.; Tran, D. D.; George, S. C. Concise Review: Maturation Phases of Human Pluripotent Stem Cell-Derived Cardiomyocytes. *Stem Cells* **2013**, *31*, 829−837.

(7) Ojala, M.; Aalto-Setälä, K. Modeling Hypertrophic Cardiomyopathy with Human Induced Pluripotent Stem Cells. In *Pluripotent Stem Cells—from the Bench to the Clinic*; Tomizawa, M., Ed.; InTech: London, U.K., 2016; pp 227−256.

(8) Liang, P.; Lan, F.; Lee, A. S.; Gong, T.; Sanchez-Freire, V.; Wang, Y.; Diecke, S.; Sallam, K.; Knowles, J. W.; Wang, P. J.; Nguyen, P. K.; Bers, D. M.; Robbins, R. C.; Wu, J. C. Drug Screening Using a Library of Human Induced Pluripotent Stem Cell-Derived Cardiomyocytes Reveals Disease-Specific Patterns of Cardiotoxicity. *Circulation* **2013**, *127*, 1677−1691.

(9) Penttinen, K.; Swan, H.; Vanninen, S.; Paavola, J.; Lahtinen, A. M.; Kontula, K.; Aalto-Setälä, K. Correction: Antiarrhythmic Effects of Dantrolene in Patients with Catecholaminergic Polymorphic Ventricular Tachycardia and Replication of the Responses Using iPSC Models. *PLoS One* **2015**, *10*, No. e0134746.

(10) Roden, D. M. Drug-Induced Prolongation of the QT Interval. *N. Engl. J. Med.* **2004**, *350*, 1013−1022.

(11) Ahola, A.; Kiviaho, A. L.; Larsson, K.; Honkanen, M.; Aalto-Setälä, K.; Hyttinen, J. Video Image-Based Analysis of Single Human Induced Pluripotent Stem Cell Derived Cardiomyocyte Beating Dynamics using Digital Image Correlation. *Biomed. Eng. Online* **2014**, *13*, 39−57.

(12) Kuusela, J.; Kujala, V. J.; Kiviaho, A.; Ojala, M.; Swan, H.; Kontula, K.; Aalto-Setälä, K. Effects of Cardioactive Drugs on Human Induced Pluripotent Stem Cell Derived Long QT Syndrome Cardiomyocytes. *Springerplus* **2016**, *5*, 234.

(13) Ribas, J.; Sadeghi, H.; Manbachi, A.; Leijten, J.; Brinegar, K.; Zhang, Y. S.; Ferreira, L.; Khademhosseini, A. Cardiovascular Organ-on-a-Chip Platforms for Drug Discovery and Development. *Appl. In Vitro Toxicol.* **2016**, *2*, 82−96.

(14) Gomes, M. E.; Rodrigues, M. T.; Domingues, R. M. A.; Reis, R. L. Tissue Engineering and Regenerative Medicine: New Trends and Directions-A Year in Review. *Tissue Eng., Part B* **2017**, *23*, 211−224.

(15) Eder, A.; Vollert, I.; Hansen, A.; Eschenhagen, T. Human Engineered Heart Tissue as a Model System for Drug Testing. *Adv. Drug Delivery Rev.* **2016**, *96*, 214−224.

(16) Nunes, S. S.; Miklas, J. W.; Liu, J.; Aschar-Sobbi, R.; Xiao, Y.; Zhang, B.; Jiang, J.; Massé, S.; Gagliardi, M.; Hsieh, A.; Thavandiran, N.; Laflamme, M. A.; Nanthakumar, K.; Gross, G. J.; Backx, P. H.; Keller, G.; Radisic, M. Biowire: a platform for maturation of human pluripotent stem cell-derived cardiomyocytes. *Nat. Methods* **2013**, *10*, 781−787.

(17) Zhu, K.; Shin, S. R.; van Kempen, T.; Li, Y.-C.; Ponraj, V.; Nasajpour, A.; Mandla, S.; Hu, N.; Liu, X.; Leijten, J.; Lin, Y.-D.; Hussain, M. A.; Zhang, Y. S.; Tamayol, A.; Khademhosseini, A. Gold Nanocomposite Bioink for Printing 3D Cardiac Constructs. *Adv. Funct. Mater.* **2017**, *27*, 1605352.

(18) Zhang, Y. S.; Arneri, A.; Bersini, S.; Shin, S.-R.; Zhu, K.; Goli-Malekabadi, Z.; Aleman, J.; Colosi, C.; Busignani, F.; Dell'Erba, V.; Bishop, C.; Shupe, T.; Demarchi, D.; Moretti, M.; Rasponi, M.; Dokmeci, M. R.; Atala, A.; Khademhosseini, A. Bioprinting 3D Microfibrous Scaffolds for Engineering Endothelialized Myocardium and Heart-on-a-Chip. *Biomaterials* **2016**, *110*, 45−59.

(19) Walters, N. J.; Gentleman, E. Evolving insights in cell-matrix interactions: Elucidating how non-soluble properties of the extracellular niche direct stem cell fate. *Acta Biomater.* **2015**, *11*, 3−16.

(20) Nakamura, K.; Shinoda, E.; Tokita, M. The Influence of Compression Velocity on Strength and Structure for Gellan Gels. *Food Hydrocoll.* **2001**, *15*, 247−252.

(21) Koivisto, J. T.; Joki, T.; Parraga, J. E.; Pääkkönen, R.; Ylä-Outinen, L.; Salonen, L.; Jönkkäri, I.; Peltola, M.; Ihalainen, T. O.; Narkilahti, S.; Kellomäki, M. Bioamine-Crosslinked Gellan Gum Hydrogel for Neural Tissue Engineering. *Biomed. Mater.* **2017**, *12*, 025014.

DOI: 10.1021/acsami.8b22343
ACS Appl. Mater. Interfaces 2019, 11, 20589−20602

(22) Karvinen, J.; Koivisto, J. T.; Jönkkäri, I.; Kellomäki, M. The Production of Injectable Hydrazone Crosslinked Gellan Gum-Hyaluronan-Hydrogels with Tunable Mechanical and Physical Properties. *J. Mech. Behav. Biomed. Mater.* **2017**, *71*, 383−391.
(23) Koivusalo, L.; Karvinen, J.; Sorsa, E.; Jönkkäri, I.; Väliaho, J.; Kallio, P.; Ilmarinen, T.; Miettinen, S.; Skottman, H.; Kellomäki, M. Hydrazone Crosslinked Hyaluronan-Based Hydrogels for Therapeutic Delivery of Adipose Stem Cells to Treat Corneal Defects. *Mater. Sci. Eng., C* **2018**, *85*, 68−78.
(24) Karvinen, J.; Joki, T.; Ylä-Outinen, L.; Koivisto, J. T.; Narkilahti, S.; Kellomäki, M. Soft Hydrazone Crosslinked Hyaluronan- and Alginate-Based Hydrogels as 3D Supportive Matrices for Human Pluripotent Stem Cell-Derived Neuronal Cells. *React. Funct. Polym.* **2018**, *124*, 29−39.
(25) Dubruel, P.; Unger, R.; Van Vlierberghe, S.; Cnudde, V.; Jacobs, P. J. S.; Schacht, E.; Kirkpatrick, C. J. Porous Gelatin Hydrogels: 2. In Vitro Cell Interaction Study. *Biomacromolecules* **2007**, *8*, 338−344.
(26) Van Den Bulcke, A. I.; Bogdanov, B.; De Rooze, N.; Schacht, E. H.; Cornelissen, M.; Berghmans, H. Structural and Rheological Properties of Methacrylamide Modified Gelatin Hydrogels. *Biomacromolecules* **2000**, *1*, 31−38.
(27) Bacelar, A. H.; Silva-Correia, J.; Oliveira, J. M.; Reis, R. L. Recent progress in gellan gum hydrogels provided by functionalization strategies. *J. Mater. Chem. B* **2016**, *4*, 6164−6174.
(28) Ferris, C. J.; Stevens, L. R.; Gilmore, K. J.; Mume, E.; Greguric, I.; Kirchmajer, D. M.; Wallace, G. G.; in het Panhuis, M. Peptide Modification of Purified Gellan Gum. *J. Mater. Chem. B* **2015**, *3*, 1106−1115.
(29) da Silva, L. P.; Jha, A. K.; Correlo, V. M.; Marques, A. P.; Reis, R. L.; Healy, K. E. Gellan Gum Hydrogels with Enzyme-Sensitive Biodegradation and Endothelial Cell Biorecognition Sites. *Adv. Healthcare Mater.* **2018**, *7*, 1700686.
(30) Silva-Correia, J.; Gloria, A.; Oliveira, M. B.; Mano, J. F.; Oliveira, J. M.; Ambrosio, L.; Reis, R. L. Rheological and Mechanical Properties of Acellular and Cell-Laden Methacrylated Gellan Gum Hydrogels. *J. Biomed. Mater. Res., Part A* **2013**, *101*, 3438−3446.
(31) Yue, K.; Trujillo-de Santiago, G.; Alvarez, M. M.; Tamayol, A.; Annabi, N.; Khademhosseini, A. Synthesis, Properties, and Biomedical Applications of Gelatin Methacryloyl (GelMA) Hydrogels. *Biomaterials* **2015**, *73*, 254−271.
(32) Shin, H.; Olsen, B. D.; Khademhosseini, A. The Mechanical Properties and Cytotoxicity of Cell-Laden Double-Network Hydrogels Based on Photocrosslinkable Gelatin and Gellan Gum Biomacromolecules. *Biomaterials* **2012**, *33*, 3143−3152.
(33) Fedorovich, N. E.; Oudshoorn, M. H.; van Geemen, D.; Hennink, W. E.; Alblas, J.; Dhert, W. J. A. The Effect of Photopolymerization on Stem Cells Embedded in Hydrogels. *Biomaterials* **2009**, *30*, 344−353.
(34) Williams, C. G.; Malik, A. N.; Kim, T. K.; Manson, P. N.; Elisseeff, J. H. Variable Cytocompatibility of Six Cell Lines with Photoinitiators used for Polymerizing Hydrogels and Cell Encapsulation. *Biomaterials* **2005**, *26*, 1211−1218.
(35) Mironi-Harpaz, I.; Wang, D. Y.; Venkatraman, S.; Seliktar, D. Photopolymerization of Cell-Encapsulating Hydrogels: Crosslinking Efficiency Versus Cytotoxicity. *Acta Biomater.* **2012**, *8*, 1838−1848.
(36) Figueiras, E.; Soto, A. M.; Jesus, D.; Lehti, M.; Koivisto, J.; Parraga, J. E.; Silva-Correia, J.; Oliveira, J. M.; Reis, R. L.; Kellomäki, M.; Hyttinen, J. Optical Projection Tomography as a Tool for 3D Imaging of Hydrogels. *Biomed. Opt. Express* **2014**, *5*, 3443−3449.
(37) Coutinho, D. F.; Sant, S. V.; Shin, H.; Oliveira, J. T.; Gomes, M. E.; Neves, N. M.; Khademhosseini, A.; Reis, R. L. Modified Gellan Gum Hydrogels with Tunable Physical and Mechanical Properties. *Biomaterials* **2010**, *31*, 7494−7502.
(38) Schneider, C. A.; Rasband, W. S.; Eliceiri, K. W. NIH Image to ImageJ: 25 Years of Image Analysis. *Nat. Methods* **2012**, *9*, 671−675.
(39) Belay, B.; Koivisto, J. T.; Vuornos, K.; Montonen, T.; Koskela, O.; Lehti-Polojärvi, M.; Miettinen, S.; Kellomäki, M.; Figueiras, E.; Hyttinen, J. Optical Projection Tomography Imaging of Single Cells in 3D Gellan Gum Hydrogel. In *EMBEC & NBC 2017: Joint Conference of the European Medical and Biological Engineering Conference (EMBEC) and the Nordic-Baltic Conference on Biomedical Engineering and Medical Physics (NBC), Tampere, Finland, June 2017*; Eskola, H., Väisänen, O., Viik, J., Hyttinen, J., Eds.; Springer Singapore: Singapore, 2018; pp 996−999.
(40) Kiviaho, A. L.; Ahola, A.; Larsson, K.; Penttinen, K.; Swan, H.; Pekkanen-Mattila, M.; Venäläinen, H.; Paavola, K.; Hyttinen, J.; Aalto-Setälä, K. Distinct Electrophysiological and Mechanical Beating Phenotypes of Long QT Syndrome Type 1-Specific Cardiomyocytes Carrying Different Mutations. *Int. J. Cardiol. Heart Vasc.* **2015**, *8*, 19−31.
(41) Lian, X.; Zhang, J.; Azarin, S. M.; Zhu, K.; Hazeltine, L. B.; Bao, X.; Hsiao, C.; Kamp, T. J.; Palecek, S. P. Directed cardiomyocyte differentiation from human pluripotent stem cells by modulating Wnt/β-catenin signaling under fully defined conditions. *Nat. Protoc.* **2012**, *8*, 162−175.
(42) Laurila, E.; Ahola, A.; Hyttinen, J.; Aalto-Setälä, K. Methods for in vitro functional analysis of iPSC derived cardiomyocytes - Special focus on analyzing the mechanical beating behavior. *Biochim. Biophys. Acta, Mol. Cell Res.* **2016**, *1863*, 1864−1872.
(43) Livak, K. J.; Schmittgen, T. D. Analysis of Relative Gene Expression Data Using Real-Time Quantitative PCR and the 2−ΔΔCT Method. *Methods* **2001**, *25*, 402−408.
(44) Prestwich, G. D.; Marecak, D. M.; Marecek, J. F.; Vercruysse, K. P.; Ziebell, M. R. Controlled Chemical Modification of Hyaluronic Acid: Synthesis, Applications, and Biodegradation of Hydrazide Derivatives. *J. Controlled Release* **1998**, *53*, 93−103.
(45) Vandooren, J.; Van den Steen, P. E.; Opdenakker, G. Biochemistry and Molecular Biology of Gelatinase B Or Matrix Metalloproteinase-9 (MMP-9): The Next Decade. *Crit. Rev. Biochem. Mol. Biol.* **2013**, *48*, 222−272.
(46) Shim, J. L. N. J.. U.S. Patent 4,517,216. Gellan gum/gelatin blends, 1985.
(47) Kozlov, P. V.; Burdygina, G. I. The Structure and Properties of Solid Gelatin and the Principles of their Modification. *Polymer* **1983**, *24*, 651−666.
(48) Amano, Y.; Nishiguchi, A.; Matsusaki, M.; Iseoka, H.; Miyagawa, S.; Sawa, Y.; Seo, M.; Yamaguchi, T.; Akashi, M. Development of Vascularized iPSC Derived 3D-Cardiomyocyte Tissues by Filtration Layer-by-Layer Technique and their Application for Pharmaceutical Assays. *Acta Biomater.* **2016**, *33*, 110−121.
(49) Mathur, A.; Loskill, P.; Shao, K.; Huebsch, N.; Hong, S.; Marcus, S. G.; Marks, N.; Mandegar, M.; Conklin, B. R.; Lee, L. P.; Healy, K. E. Human iPSC-Based Cardiac Microphysiological System for Drug Screening Applications. *Sci. Rep.* **2015**, *5*, 8883.
(50) Oliveira, M. B.; Custódio, C. A.; Gasperini, L.; Reis, R. L.; Mano, J. F. Autonomous Osteogenic Differentiation of hASCs Encapsulated in Methacrylated Gellan-Gum Hydrogels. *Acta Biomater.* **2016**, *41*, 119−132.
(51) Koshy, S. T.; Desai, R. M.; Joly, P.; Li, J.; Bagrodia, R. K.; Lewin, S. A.; Joshi, N. S.; Mooney, D. J. Click-Crosslinked Injectable Gelatin Hydrogels. *Adv. Healthcare Mater.* **2016**, *5*, 541−547.
(52) Zhao, X.; Lang, Q.; Yildirimer, L.; Lin, Z. Y.; Cui, W.; Annabi, N.; Ng, K. W.; Dokmeci, M. R.; Ghaemmaghami, A. M.; Khademhosseini, A. Photocrosslinkable Gelatin Hydrogel for Epidermal Tissue Engineering. *Adv. Healthcare Mater.* **2016**, *5*, 108−118.
(53) Mirsky, I.; Parmley, W. W. Assessment of Passive Elastic Stiffness for Isolated Heart Muscle and the Intact Heart. *Circ. Res.* **1973**, *33*, 233−243.
(54) Levental, I.; Georges, P. C.; Janmey, P. A. Soft Biological Materials and their Impact on Cell Function. *Soft Matter* **2007**, *3*, 299−306.
(55) Neal, R. A.; Jean, A.; Park, H.; Wu, P. B.; Hsiao, J.; Engelmayr, G. C., Jr.; Langer, R.; Freed, L. E. Three-Dimensional Elastomeric Scaffolds Designed with Cardiac-Mimetic Structural and Mechanical Features. *Tissue Eng., Part A* **2013**, *19*, 793−807.

DOI: 10.1021/acsami.8b22343
ACS Appl. Mater. Interfaces 2019, 11, 20589−20602

(56) Oyen, M. L. Mechanical Characterisation of Hydrogel Materials. *Int. Mater. Rev.* **2014**, *59*, 44−59.
(57) Bashir, B.; Iyer, R. K.; Chen Wen, L. K.; Ruogang, Z.; Sider, K. L.; Morakot, L.; Simmons, C. A.; Milica, R. Influence of Substrate Stiffness on the Phenotype of Heart Cells. *Biotechnol. Bioeng.* **2010**, *105*, 1148−1160.
(58) Engler, A. J.; Carag-Krieger, C.; Johnson, C. P.; Raab, M.; Tang, H.-Y.; Speicher, D. W.; Sanger, J. W.; Sanger, J. M.; Discher, D. E. Embryonic Cardiomyocytes Beat Best on a Matrix with Heart-Like Elasticity: Scar-Like Rigidity Inhibits Beating. *J. Cell Sci.* **2008**, *121*, 3794−3802.
(59) Melchels, F. P. W.; Dhert, W. J. A.; Hutmacher, D. W.; Malda, J. Development and Characterisation of a New Bioink for Additive Tissue Manufacturing. *J. Mater. Chem. B* **2014**, *2*, 2282−2289.
(60) Nichol, J. W.; Koshy, S. T.; Bae, H.; Hwang, C. M.; Yamanlar, S.; Khademhosseini, A. Cell-Laden Microengineered Gelatin Methacrylate Hydrogels. *Biomaterials* **2010**, *31*, 5536−5544.
(61) Wen, C.; Lu, L.; Li, X. An Interpenetrating Network Biohydrogel of Gelatin and Gellan Gum by using a Combination of Enzymatic and Ionic Crosslinking Approaches. *Polym. Int.* **2014**, *63*, 1643−1649.
(62) *SFS-EN ISO 10993-5 Biological Evaluation of Medical Devices. Part 5: Tests for in Vitro Cytotoxicity*; Finnish Standards Association: Helsinki, Finland, 2009.
(63) Appel, A. A.; Anastasio, M. A.; Larson, J. C.; Brey, E. M. Imaging Challenges in Biomaterials and Tissue Engineering. *Biomaterials* **2013**, *34*, 6615−6630.
(64) Hayflick, L.; Moorhead, P. S. The Serial Cultivation of Human Diploid Cell Strains. *Exp. Cell Res.* **1961**, *25*, 585−621.
(65) Wang, C.; Gong, Y.; Lin, Y.; Shen, J.; Wang, D.-A. A Novel Gellan Gel-Based Microcarrier for Anchorage-Dependent Cell Delivery. *Acta Biomater.* **2008**, *4*, 1226−1234.
(66) Vuorenpää, H.; Penttinen, K.; Heinonen, T.; Pekkanen-Mattila, M.; Sarkanen, J.-R.; Ylikomi, T.; Aalto-Setälä, K. Maturation of Human Pluripotent Stem Cell Derived Cardiomyocytes is Improved in Cardiovascular Construct. *Cytotechnology* **2017**, *69*, 785−800.
(67) Tan, S. H.; Ye, L. Maturation of Pluripotent Stem Cell-Derived Cardiomyocytes: a Critical Step for Drug Development and Cell Therapy. *J Cardiovasc Transl Res* **2018**, *11*, 375−392.
(68) Tzatzalos, E.; Abilez, O. J.; Shukla, P.; Wu, J. C. Engineered Heart Tissues and Induced Pluripotent Stem Cells: Macro- and Microstructures for Disease Modeling, Drug Screening, and Translational Studies. *Adv. Drug Delivery Rev.* **2016**, *96*, 234−244.
(69) Besser, R. R.; Ishahak, M.; Mayo, V.; Carbonero, D.; Claure, I.; Agarwal, A. Engineered Microenvironments for Maturation of Stem Cell Derived Cardiac Myocytes. *Theranostics* **2018**, *8*, 124−140.

DOI: 10.1021/acsami.8b22343
ACS Appl. Mater. Interfaces 2019, 11, 20589−20602

PUBLICATION V

Bioactivated gellan gum hydrogels affect cellular rearrangement and cell response in vascular co-culture and subcutaneous implant models

Christine Gering, Jenny Párraga, Hanna Vuorenpää, Lucía Botero, Susanna Miettinen, & Minna Kellomäki

Biomaterials Advances 143, 213185
https://doi.org/10.1016/j.bioadv.2022.213185

143 (2022) 213185

Contents lists available at ScienceDirect

Biomaterials Advances

journal homepage: www.journals.elsevier.com/materials-science-and-engineering-c

Bioactivated gellan gum hydrogels affect cellular rearrangement and cell response in vascular co-culture and subcutaneous implant models

Christine Gering [a,*], Jenny Párraga [a,1], Hanna Vuorenpää [a,b], Lucía Botero [c], Susanna Miettinen [a,b], Minna Kellomäki [a]

[a] Faculty of Medicine and Health Technology, Tampere University, Tampere, Finland
[b] Research, Development and Innovation Centre, Tampere University Hospital, Tampere, Finland
[c] Facultad de Medicina Veterinaria y de Zootecnia, Universidad Nacional de Colombia, Bogotá, Colombia

ARTICLE INFO

Keywords:
Vascularization
HUVEC and hASC co-culture
Gellan gum hydrogels
Biofunctionalization
Mechanical and viscoelastic properties

ABSTRACT

Hydrogels are suitable soft tissue mimics and capable of creating pre-vascularized tissues, that are useful for *in vitro* tissue engineering and *in vivo* regenerative medicine. The polysaccharide gellan gum (GG) offers an intriguing matrix material but requires bioactivation in order to support cell attachment and transfer of biomechanical cues. Here, four versatile modifications were investigated: Purified NaGG; avidin-modified NaGG combined with biotinylated fibronectin (NaGG-avd); oxidized GG (GGox) covalently modified with carbohydrazide-modified gelatin (gelaCDH) or adipic hydrazide-modified gelatin (gelaADH). All materials were subjected to rheological analysis to assess their viscoelastic properties, using a time sweep for gelation analysis, and subsequent amplitude sweep of the formed hydrogels. The sweeps show that NaGG and NaGG-avd are rather brittle, while gelatin-based hydrogels are more elastic. The degradation of preformed hydrogels in cell culture medium was analyzed with an amplitude sweep and show that gelatin-containing hydrogels degrade more dramatically. A co-culture of GFP-tagged HUVEC and hASC was performed to induce vascular network formation in 3D for up to 14 days. Immunofluorescence staining of the αSMA^+ network showed increased cell response to gelatin-GG networks, while the NaGG-based hydrogels did not allow for the elongation of cells. Preformed, 3D hydrogels disks were implanted to subcutaneous rat skin pockets to evaluate biological *in vivo* response. As visible from the hematoxylin and eosin-stained tissue slices, all materials are biocompatible, however gelatin-GG hydrogels produced a stronger host response. This work indicates, that besides the biochemical cues added to the GG hydrogels, also their viscoelasticity greatly influences the biological response.

1. Introduction

Hydrogels have extensively been studied for vascular tissue engineering, due to their innate soft material properties, ability to allow encapsulation and nutrient diffusion. Moreover, hydrogels are designed to guide tissue formation for various applications including artificial tissue mimics and *in vivo* regenerative implants. Vascularization, the formation of a perfusable vessel network in artificial tissues, is among the top challenges that impede the clinical application of engineered transplantable tissues [1]. Likewise, *in vitro* models and organ-on-chip applications require vasculature to adequately model living tissues and organs. To create cell support matrix for those, biomaterial design has to be balanced between high bioactivity and rapid cell resorption [2–4], and adequate mechanical and viscoelastic properties [5].

Mechanical and rheological properties are furthermore a concern for the stability of the cell-laden hydrogel and manipulation for different applications, such as injection and casting [5] and others [6–8]. The effect of hydrogel stiffness and elasticity is finding increasing appreciation in tissue engineering literature, and the phenomenon of mechanotransduction from the extracellular network to the cell is essential to biomaterial design [3,9]. Independent of cell adhesive motifs, it is well known that substrate stiffness can direct stem cell differentiation [10]. Moreover, vascular network models have been found to require surrounding matrices that are compliant enough to allow remodeling by cells, but also strong enough to confer mechanical information to the cells [5].

* Corresponding author at: Faculty of Medicine and Health Technology, Korkeaoulunkatu 3, 33720 Tampere, Finland.
E-mail address: christine.gering@tuni.fi (C. Gering).
[1] Currently at IamFluidics BV, High Tech Factory, Enschede, the Netherlands.

https://doi.org/10.1016/j.bioadv.2022.213185
Received 7 June 2022; Received in revised form 28 October 2022; Accepted 1 November 2022
Available online 8 November 2022

Gellan gum (GG) has been investigated for cell and drug delivery due to its gelation properties and cytocompatibility [11–14]. However, only few studies investigate GG hydrogels for vascularization models. One excellent example is given by Rocha et al. who use RGD-conjugated GG (GG-GRGDS) to develop a material for spinal cord injury (SCI) treatment [15]. This GG modification with the peptide sequence RGD *via* furan modification was first described by Silva et al. (2012) [16]. The SCI trauma site has increased need for oxygenation, which can be addressed only with functional vascular network in the transplant. A large array of other biomaterials has been investigated in the literature for vascularization, where the most prominent examples are fibrin and collagen I. In combination with collagen [17] and gelatin-based matrices [18], Human adipose-derived stem/stromal cells (hASC) have been shown to support the formation of formidable tubular networks when in co-culture with an endothelial cell type [15,17,19–21].

To establish stable vascularization, the stromal cell type is needed to support the vascular network formed by endothelial cells (EC). Here, we demonstrate the vascularization potential of a co-culture between human umbilical vein EC (HUVEC) and hASC. hASC are known to promote vascular growth, maturation and stabilization by secreting angiogenic factors and by differentiating into vessel lining supporting cells [19]. Furthermore, high proliferation and differentiation capacity of hASC makes them an ideal component for tissue engineering [19], and they have shown pericytic function when co-cultured with HUVEC. HUVEC are a robust source of EC with relatively easy access and proven capability for capillary morphogenesis. Despite their venous and macrovascular origin, they are the most widely used EC type in tissue engineering application with biomaterials [22]. Recently, we reported the vasculogenic potency of both bone marrow- and adipose tissue-derived mesenchymal stem/stromal in establishing a stable vascular network in fibrin hydrogel [23].

Herein, four different GG hydrogel formulations and modifications are investigated. These materials have been developed and published by us previously, and we considered these four most valuable for comparison and further study. Purified (NaGG) (Fig. 1A) and avidin-modified purified (NaGG-avd) (Fig. 1B) have previously been investigated by us for a modular design [24]. Similarly, the gelatin-gellan gum compound hydrogels, achieved *via* hydrazone crosslinking of oxidized GG and carbohydrazide (gelaCDH) (Fig. 1C) or adipic acid hydrazide (gelaADH) (Fig. 1D) functionalized gelatin, have been investigated for iPSC-derived cardiomyocyte culture by us [25]. While all four materials are based on the polysaccharide GG there are inherent mechanical differences as well. NaGG and NaGG-avd exhibit almost identical brittle compression behavior, but our gelatin-GG hydrogels exhibit an elastic component in their stress–strain curve, closely resembling heart tissue. Though biocompatible, native GG is highly bioinert [26,27], but bioactive functionalization has been shown to improve cell response while maintaining mechanical stability [24,25,28].

2. Materials and methods

GG (Gelzan™ CM-Gelrite®, low acyl form, 1000 kg/mol, CAS 71010-52-1), crosslinkers spermidine trihydrochloride (SPD, 99 %, CAS 334-50-9) and $CaCl_2$ xH_2O (CAS 22691-02-7) as well as other chemicals we purchased from Sigma (now Merck Sigma). Gelatin was purchased from Rousselot (X-Pure®) and Sigma (Gelatin from porcine skin, Type A, gel strength 300). Cytocompatibility of the different gelatin sources was assessed as shown in Appendix 6. Charge-neutralized chimeric avidin (avd) was synthesized and kindly donated by the Protein Dynamics group at Tampere University [29]. Cell culture supplies used for expansion and culture include αMEM (Gibco™, ref. 22561-021), EGM-2 (endothelial cell growth medium-2 BulletKit™, CC-3156, Lonza Group Ltd., Switzerland), and human serum (HS, Serana Europe GmbH, ref. S-HU-EU-011). Reagents for immunohistochemical staining and other analysis were purchased from Merck.

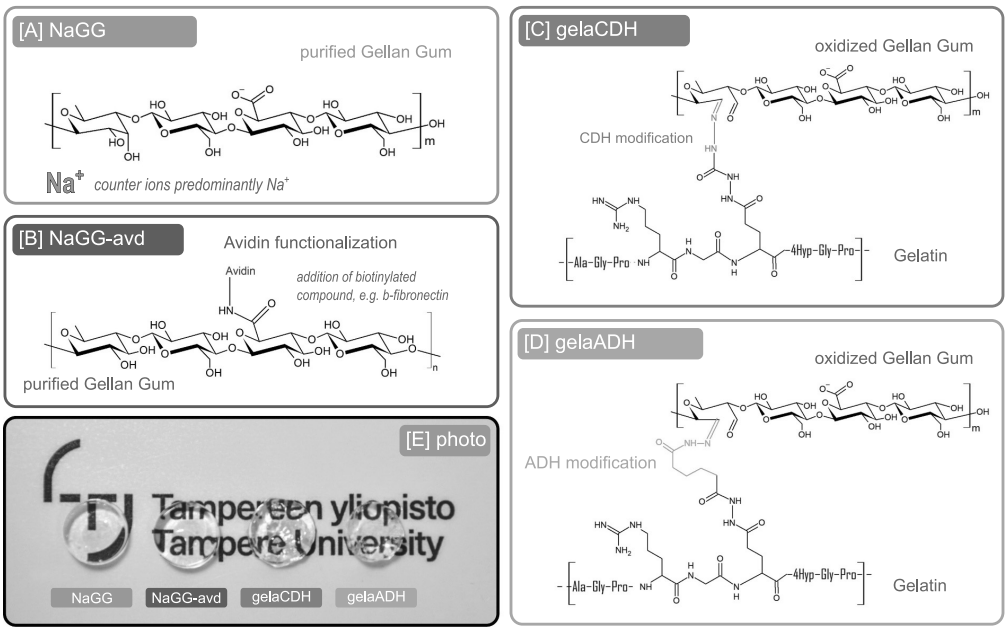

Fig. 1. Chemical structures and exemplary photographs of the investigated materials. [A] Sodium-purified gellan gum (NaGG); [B] purified gellan gum further functionalized with charge-neutralized chimeric avidin (NaGG-avd); [C] Oxidized gellan gum coupled to carbohydrazide-modified gelatin (gelaCDH-GGox); [D] Oxidized gellan gum coupled to adipic acid hydrazide-modified gelatin (gelaADH-GGox). [E] shows a photograph of cell-free hydrogel samples, depicting their ability to self-support and transparency.

2.1. Hydrogel modification and preparation

GG was purified and coupled with avidin according to [24]. Briefly, counterions were removed from commercial GG formulations using exchange resin (Dowex cation exchange resin, H+ form, 50–100 mesh, prerinsed in HCl) and replaced with sodium (Na^+) to a solution pH of 7.5. NaGG was precipitated in isopropanol and lyophilized. GG was oxidized using Malaprade oxidation, for which a hot (40 °C) GG solution is treated with $NaIO_4$ in a ratio of 50 mg GG to 6 mg $NaIO_4$. The reaction was quenched after 4 h using ethylene glycol and dialyzed (12–14 kDa MWCO) against deionized (DI) water for 3 days before lyophilization [24,25,30].

The gelatin modification protocol was adapted from Koivisto et al. (2019) [25]. Briefly, gelatin was dissolved in ultra-pure water at 2.0 g/L and kept in N_2 environment at room temperature. An excess of carbohydrazide (CDH) or adipic hydrazide (ADH) and the pH was adjusted to 4.7 and 5.0 respectively. A mixture of EDC (100 mg) and HOBT (70 mg) was dissolved in DMSO and dropwise but swiftly added to the gelatin solution. The EDC-HOBT addition was repeated 2 times, to achieve a total molar ratio of 3.8 mM EDC to 21.9 mM CDH or 43.4 mM ADH, respectively. The reaction is kept overnight, and the product is precipitated *via* salting-out using cold ethanol. The precipitate is collected, centrifuged and redissolved into ultra-pure water for dialysis over 2 days. Before lyophilization, the solution is sterile filtered using 0.2 μm syringe filter (Whatman FP30/0.2 CA-S). Hydrogel compositions are based on our previous publications [24,25,30].

Hydrogels were prepared by combination of component 1 (gellan gum) and component 2 (crosslinker) with ratios as listed in Table 1. The components were either mixed in a separate vial (Hydrogel 1 and 2) and cast to the mold or mixed directly in the mold (Hydrogel 3 and 4) to achieve homogenous, bubble-free samples. For cell encapsulation, the cell pellet was resuspended in either component 1 (NaGG and NaGG-avd for Hydrogel 1 and 2), or component 2 (gelaCDH and gelaADH) based on volume and ease of pipetting, and the hydrogels were formed as described above. Only for cell culture experiments, biotinylated fibronectin (2.5 mg/mL stock), synthesized and kindly donated by the Protein Dynamics group at Tampere University, was added to NaGG-avd to achieve a final concentration of 31 μg per mL hydrogel. After casting, the hydrogels are left to set at 37 °C for at least 20 min to 4 h before further manipulation. All components were sterile filtered using a 0.2 μm syringe filter (Whatman FP30/0.2 CA-S).

2.2. Mechanical analysis and degradation

For all rheological experiments, Rheometer DHR-2 (TA Instruments) and 20 mm stainless steel flat geometry were used. To flow test the hydrogel precursors, 370 μL of each solution was pipetted onto the bottom plate and tested using a gap of 1000 μm and analyzed from 0.1 to 500 Hz. Gel formation was observed using a time sweep. The first component of the gel, (NaGG, NaGG-avd, gelaCDH, or gelaADH, was placed to the plate at 37 °C and the geometry was lowered to a gap of 1500 μm. The second component ($CaCl_2$, SPD, or GGox) was added while the geometry was spinning at 7 rad/s for 7 s in order to facilitate mixing, after which the temperature is lowered to 30 °C. The time sweep measurement is started immediately after the spinning step, and run with constant amplitude (0.75 % oscillation strain) and frequency (0.75 Hz) for 3600 s. Consequently, the sample formed during the time sweep was left to rest in place for 5 min and then used for an amplitude sweep. The amplitude sweep was performed from 0.1 % to up to 500 % oscillation strain at 0.75 Hz.

Table 1
Composition of investigated hydrogels. Abbreviation of materials used throughout the text are bolded.

	Component 1 (gellan gum)	Component 2 (crosslinker)	Mixing ratio
1	**NaGG** 5 mg/mL in HEPES/ sucrose	Calcium chloride ($CaCl_2$ xH_2O) 10 mM in HEPES/sucrose	5:1
2	**NaGG-avd** 5 mg/mL in HEPES/ sucrose	Spermidine trihydrochloride (SPD) 2 mM in HEPES/sucrose	5:1
3	GGox(60) 40 mg/mL in EBM-2	**gelaCDH** 40 mg/mL in EBM-2	1:1
4	GGox(60) 40 mg/mL in sucrose	**gelaADH** 40 mg/mL in sucrose	1:1

Samples for degradation analysis were prepared as described as cell-free hydrogel in either a ø 20 mm mold for rheological testing at a volume of 500 μL (sample height ~ 2 mm), or in ø 8.8 mm mold for mass loss analysis at a volume of 300 μL (sample height ~ 5 mm). After the hydrogels were fully set (4 h at 37 °C), the samples were chilled overnight at +4 °C to facilitate demolding. Mass loss samples were placed on mesh ring holder, while rheology samples were kept in their molds, and the samples were then incubated with cell culture on top. Mass loss samples were periodically weighed, and new medium was placed on top of the same samples. Rheology samples were finally demolded and analyzed using an amplitude sweep (0.01–500 %) with a fixed frequency of 0.75 Hz and plate temperature of 30 °C. Samples were carefully placed on the bottom geometry and the upper one was brought into contact with the sample so that the axial force was about 0.1 N, ensuring good contact between sample and geometry, without loading too high stress onto the material.

2.3. Cell isolation and culture

Human adipose stem/stromal cells (hASC) were isolated from subcutaneous tissue samples obtained from three independent donors to reveal the possible biological variabilities between human donors. Tissue samples were obtained at the Tampere University Hospital Department of Plastic Surgery with the donor's written informed consent and processed under ethical approval of the Ethics Committee of the Expert Responsibility area of Tampere University Hospital (R15161). The cells were isolated as described previously [31]. The hASC were cultured in α-MEM (Thermo Scientific #22561054) supplemented with 5 % HS (HS, Serana Europe GmbH, ref. S-HU-EU-011), 100 U/mL penicillin, and 100 μg/mL streptomycin, expanded over 4 days and used between passages 1–3. The mesenchymal origin of hASC was confirmed by surface marker expression analysis with flow cytometry and assessment of adipogenic and osteogenic differentiation potential according to the International Society for Cellular Therapy criteria [32].

Human umbilical vein endothelial cells (HUVEC) pooled from several human donors were expressing green fluorescent protein (GFP) and were commercially obtained from Cellworks. GFP-HUVEC were cultured in Endothelial Cell Growth Medium-2 consisting of Endothelial Cell Growth Basal Medium (EBM-2, Lonza #CC-3156 and CC-3162) and Endothelial Cell Growth Medium-2 Supplements (EGM-2, Lonza CC-4176) with 0.1 % GA-1000, 0.1 % R-IGF-1, 0.1 % VEGF, 0.1 % hEGF, 0.04 % hydrocortisone, 0.4 % hFGF-B, 0.1 % ascorbic acid, 0.1 % heparin). Instead of the fetal bovine serum supplied with the Kit, 2 % HS was used. The cells were expanded over 4 days and used between passages 4–5.

2.4. Cellular co-cultures for vascular network formation

The cells were harvested, split to aliquots, combined to yield 0.75 mio GFP-HUVEC and 0.15 mio hASC per sample (cell ratio 5:1) and centrifuged. The cell pellet was resuspended in NaGG, NaGG-avd, gelaCDH or gelaADH and placed into the well-plate (ibidi μ-slide 8-well, ibidi GmbH). The other component of each hydrogel was added and mixed swiftly using the pipette tip. The hydrogels were left to gelate at 37 °C for 30 min before adding 200 μL of EGM-2 on top. Media were changed three times a week. The samples were imaged live during the

culture period using EVOS microscope (EVOS FL Cell imaging system, Thermo Fisher Scientific) with brightfield view and GFP filter.

2.5. Immunofluorescent staining and image analysis

At day 14, co-culture samples were fixed using 4 % paraformaldehyde (PFA, Sigma, #158127) and unspecific binding was blocked with 10 % normal donkey serum (NDS, Sigma, #S30) in 1 % bovine serum albumin (BSA, Sigma, #A7906) solution containing 0.1 % TritonX-100 (Sigma, #T8787). All washing steps were performed using DPBS. The samples were consecutively treated with primary antibody (mouse monoclonal, α-smooth muscle actin, dilution 1:200, Abcam #ab7817) for 2 days, secondary antibody (Goat anti-Mouse IgG Alexa Fluor 568, dilution 1:400, Invitrogen # A-11004) overnight and finally DAPI (1:1000 in DPBS for 2 h). The GFP-HUVEC are visible due to their expressed GFP (GFP tagged HUVEC). The samples were imaged using confocal microscope Zeiss LSM 780 with 10× magnification objective and imaging approximately 200 μm per z-stack and EVOS images were clipped to remove the scale bar, and selected images were used for image analysis with AngioTool64 (Version 0.6a). The average vessel thickness was adjusted to around 10.4 ± 4.0 pixel units (confocal) and 4.2 ± 0.9 pixel units (EVOS). From the results, "vessels area" was used for further evaluation for endothelial cell coverage, which is the ratio of vessel area to explant ratio determined by the software.

2.6. Subcutaneous implantation

To study the materials *in vivo*, preformed samples were subcutaneously implanted to 40 male rats from the Wistar stock (60–90 days old), weighing 250–350 g. The species was selected in accordance the provisions of ISO10993-2. Experiments were carried out at the Unit of Comparative Biology at the Pontificia Universidad Javeriana (Bogota, Colombia), with the approval from the Institutional Committee for the Care and Use of Laboratory Animals (CICUAL-PUJ). The animals came from the internal colony of production which was initiated with a founding stock originating from Charles River, USA. There were 10 animals per time point, and each animal had 1 implant of each type (4 in total, $n = 10$). Before surgery, the animals were anesthetized using inhalation of 3 % isoflurane in oxygen flow set of 0.5 L/min. Rats under anesthesia were treated subcutaneously with meloxicam (1 mg/kg) and enrofloxacin (5 mg/kg) 30 min before the surgical incision. Hair was removed from the implant area and incisions were performed to create 4 pockets into the dorsal subcutaneous tissue by blunt dissection, so that the base of the pocket is at least 2 mm from the line of incision. Then, hydrogel implants (ø 10 mm and 1 mm in thickness) were inserted to the pocket. During the procedure, vital signs were monitored, and temperature support was placed. At the end of the procedure, the animals were allocated to the oxygenation chamber to recover from anesthesia. When the animals woke up showing good recovery, they were taken back to their cages. During the first three days after the procedure, the animals were medicated with meloxicam and enrifloxacin and the appearance of the incisions, signs of inflammation, infection or other events were evaluated. The animals were fed a standard diet and kept in groups of two in ventilated cages for the duration of the study. After 7, 14, 21 and 28 days of implantation, the animals were sacrificed using intraperitoneal sodium pentobarbital (50 mg/kg dose) and CO_2 inhalation. Each implant was collected separately, taking skin and subcutaneous tissues until reaching the fascia of the panniculus carnosa muscle and fixed in 10 % buffered formalin. The hydrogel degradation profile was followed during the retrieval.

2.7. Macroscopical and histological evaluation

Retrieved tissue samples were fixed with 10 % formalin, dehydrated in a series of alcohols, and embedded in paraffin. The paraffin-embedded specimens were sectioned to a thickness of 5 μm, and stained with hematoxylin and eosin (H&E). Stained sections were imaged with a Nikon Eclipse E 600 microscope and Toup Cam digital camera. Tissue lesions such as neutrophils, eosinophils, granulomatous reaction, giant cells and neovascularization were analyzed and semi-quantitatively scored on a scale from 0 to 3.

2.8. Statistical methods

Data from AngioTool evaluation were subjected to one-way ANOVA using Microsoft Excel Data Analysis ToolPak to test for significance. The results are displayed in Fig. 5. Normality of the data was assessed using chi-square test using a random data sample set with $n > 10$ from confocal image AngioTool analysis. With a p-value larger than 0.5 ($p = 0.97$), we assume the data to be normally distributed, and apply the same behavior also for data sets with low number of points that could not be tested.

3. Results

The scope of our work was to highlight and investigate the role of the material in cellular rearrangement and neovascularization. Firstly, we assessed the mechanical properties of the cell-free hydrogel materials. Though all materials investigated herein are based on GG (see Fig. 1), their crosslinking and viscoelastic behavior is drastically different. Rheological properties of the forming and formed hydrogels assessed by conducting time sweeps of the forming hydrogels and amplitude sweeps of fresh and degraded samples Similarly, their biochemical environment is different due to the addition of gelatin and fibronectin. Secondly, we observed the cell response of co-culture between hASC and HUVEC, which are well known to interact and form vascular networks, continuously monitored over 12 days, then fixed and stained on day 14. Finally, we investigated the *in vivo* tissue responses elicited by cell-free, preformed hydrogel samples after subcutaneous implantation in rats to observe acute tissue response within 4 weeks.

3.1. Rheological testing and degradation

In the pursuit to provide a thorough assessment and understanding of the viscoelastic properties, the materials were analyzed using rheology. A time sweep, with constant amplitude and frequency, gives the ability to observe time-dependent change of the hydrogel formation, *i.e.* the gelation. Gelation occurs as expected, as is shown in the previous publications [24,25,30]. Time point zero in Fig. 2A depicts few seconds after mixing of the two components, showing how long the hydrogel components take to form a solid network and suspend encapsulated cells. All materials form true hydrogels within the observation time of 1 h. While the gelation kinetics of NaGG and NaGG-avd, with final modulus of 552.8 ± 219.0 Pa and 493.2 ± 44.7 Pa respectively, are very similar, there is a stark difference between gelaCDH and gelaADH hydrogels. Though it could be expected these to be very similar judging from their chemical structure, gelaADH rapidly forms hydrogels with high modulus of 860.9 ± 6.6 Pa. GelaCDH has a delayed network formation and achieves a modulus of only 42.4 ± 7.7 Pa after 1 h.

In direct succession of the gelation sweep, after the sample was at rest for 5 min, an amplitude sweep was performed from 0.01 to 100 % oscillation strain as shown in Fig. 2B. The resting period ensures that the network is stress-free. Because storage (G') is larger than loss modulus (G'') before the critical cross-over points, all materials are elastic solids. Before this crossover point of G' and G'', where the moduli are constant, lies the linear viscoelastic region which indicates the elasticity of a hydrogel and reversible deformation. While a crossover point is observed for NaGG (48 % osc. strain) and NaGG-avd (32 % osc. strain) hydrogels, the observed range of oscillation strain is too short to reach irreversible deformation point for gelaCDH and gelaADH. The ratio between G'' and G', *i.e.* tan δ, is proportional to the network density. A tan δ of 0.8 and 0.6 for NaGG and NaGG-avd, respectively, confirms the

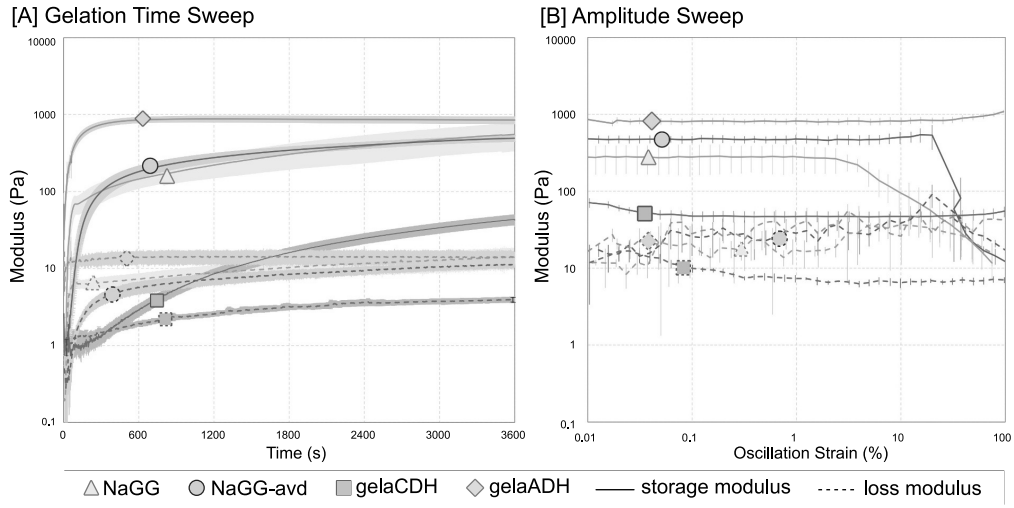

Fig. 2. Rheological assessment of cell-free hydrogels. (A) Time sweeps of hydrogels combined at $t = 7$ s. (B) Amplitude sweeps of samples just after gelation sweep. Solid line = storage modulus, dashed line = loss modulus.

finding of the time sweep that these two hydrogels are very similar and relatively tough. A comparison between the two gelatin-gels shows that CDH is softer (tan δ 0.16) and elastic than the very tough gelaADH gels presenting a very dense network (tan δ 0.04).

The flow behavior of the hydrogel precursors has been analyzed as well, showing again very similar flow behavior between NaGG and NaGG-avd precursors, while gelaADH dissolved in sucrose is slightly more viscous than gelaCDH dissolved in EBM-2. Surprisingly, the solvent has a great effect on GGox, resulting in higher viscosity and shear stress for sucrose solvent over cell culture medium, likely due to the effect of sugars on polysaccharides [33,34]. No direct comparison between precursor solution between the groups can be drawn here, as the respective solution concentrations are markedly different, with NaGG and NaGG-avd at 5 mg/mL, gelatin solutions at 40 mg/mL and oxidized GGox at 40 mg/mL. The data can be found in Appendix A1–1.

Cell-free samples were prepared similar to *in vivo* implantation procedure and incubated in EBM-2 at 37 °C for the specified time and their weight was observed, showing both swelling and mass loss due to degradation. NaGG and NaGG-avd hydrogels prove to be very stable, while gelatin-GG hydrogels quickly diminish in weight. This is also observed from the rheology analysis, where NaGG and NaGG-avd are stable and slightly increase their storage modulus, while the gelatin-based hydrogels quickly deteriorate. While measuring preformed samples with an amplitude sweep yields slightly different results compared to the method displayed in Fig. 2 and measuring highly degraded samples can have caveats. Nonetheless, when plotting the average value of the storage modulus at the linear viscoelastic region (LVER), shows expected behavior of sample types as seen in Fig. 3A. Both NaGG and NaGG-avd hydrogels show almost no degradation effects. Most noticeable is the increase in modulus, which is due to an increase in crosslinking by the medium and formation of more rigid network [33]. In contrast, the gelatin-GG hydrogels show rapid degradation. The modulus of gelaADH hydrogels declines rapidly and the measured samples were highly deformed. Unfortunately, it was not possible to measure the degradation products of gelaCDH at the other time points, and also the 6 h time point sample was delicate to measure.

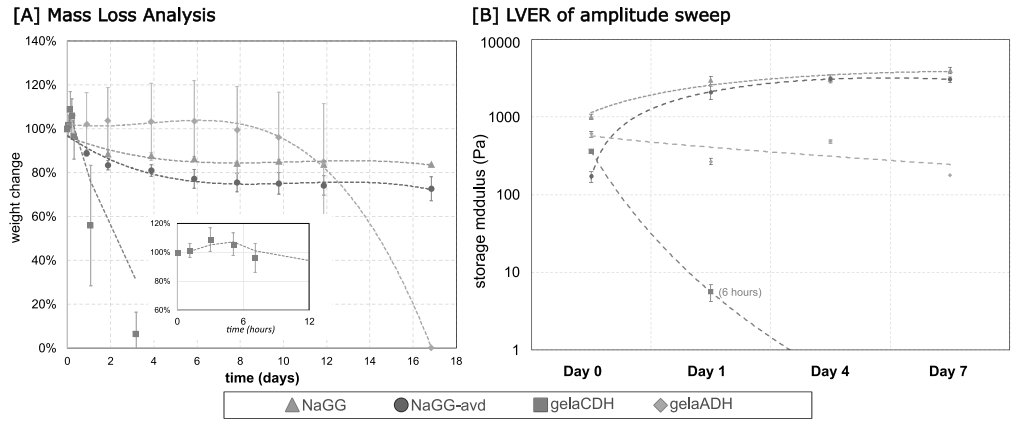

Fig. 3. Degradation of the investigated materials. [A] Mass loss analysis of cell-free materials in DMEM. Small inset image shows gelaCDH in degradation curve from 0 to 8 h. [B] Evolution of storage modulus at LVER in cell-free samples incubated in EBM-2 over 7 days.

Degradation of the hydrogels can also be observed from the EVOS images taken during the co-culture experiment. The low magnification (2×) captures the entire well and images are shown in Appendix A2–1. Upon close inspection a similar trend can be observed, where NaGG and NaGG-avd are highly stable, but a hole quickly forms in the center of gelaCDH and gelaADH samples. Hydrogel casting issues can lead to a premature degradation also for the NaGG and NaGG-avd hydrogels, but cell network formation appears to stabilize the hydrogel against degradation.

3.2. In vitro co-culture results

The encapsulation experiments show that HUVEC-hASC can be cultured in all four investigated materials up to 14 days, however with greatly varying results. Progression of the cell culture was monitored using EVOS microscope with brightfield and GFP filter on day 2, 4, 6, 9, and 12, example images of which can be viewed in Appendix A2–2. Already in the EVOS images, partial HUVEC elongation and network formation can be seen in the gelatin-gellan gum, but only sporadically for NaGG and NaGG-avd hydrogels (Appendix A2–2). Remarkably, also the progression of hydrogel degradation can be followed from 2× magnification in EVOS images (Appendix A2–1). Representative images of the confocal images at day 14 are shown in Fig. 4.

In the confocal images of NaGG and NaGG-avd the stained cells appear rounded and GFP-HUVEC are scattered and rounded. Modest elongation is visible in some of the NaGG-avd samples, but likely cells have migrated to the bottom of the well plate. The final molar concentrations of fibronectin protein modification in NaGG-avd were 71.0 nmol/L in the final hydrogel, compared to the avidin concentration of 1.6 μmol/L as determined in our previous publication [24]. The gelatin-containing samples (gelaCDH and gelaADH) on the other hand present a strong hASC network stained with αSMA. This network appears slightly denser in gelaCDH than gelaADH, but in both cases it is very pronounced. However, even in gelaCDH hydrogels the GFP-HUVEC do not form long, connected tubular structures, but alignment among the αSMA^{+} network can be observed in several locations.

AngioTool was used to measure the endothelial cell (EC) coverage from the EVOS images (Fig. 5A), as well as the αSMA^{+} cell coverage of the confocal images (Fig. 5B). Because presence of interconnected tubule network was not observed, the total coverage of ECs and αSMA cells was considered. NaGG shows a fast loss of EC coverage between day 2 and 4, and no recovery, while NaGG-avd presents an initial increase in EC coverage from day 2 to 4, followed by a steady decline. The gelaCDH hydrogels produce a small initial dip in EC coverage, but an increase from day 6 onward is visible. Finally, gelaADH shows an initial decline, but between day 4 and day 12 there are no significant differences ($p < 0.5$).

The cell coverage assessment of the αSMA^{+} network from the confocal images confirms the visual observations. While gelaCDH presents a dense network (27.6 % coverage), and gelaADH is near similar in strength (17.4 % coverage), the total coverage for NaGG and NaGG-avd hydrogels is significantly lower (12.0 % and 5.4 %). Due to degradation issues, only few samples of NaGG-avd could be assessed, likely leading to skewed values towards the lower end. Remarkably, the plots of EVOS

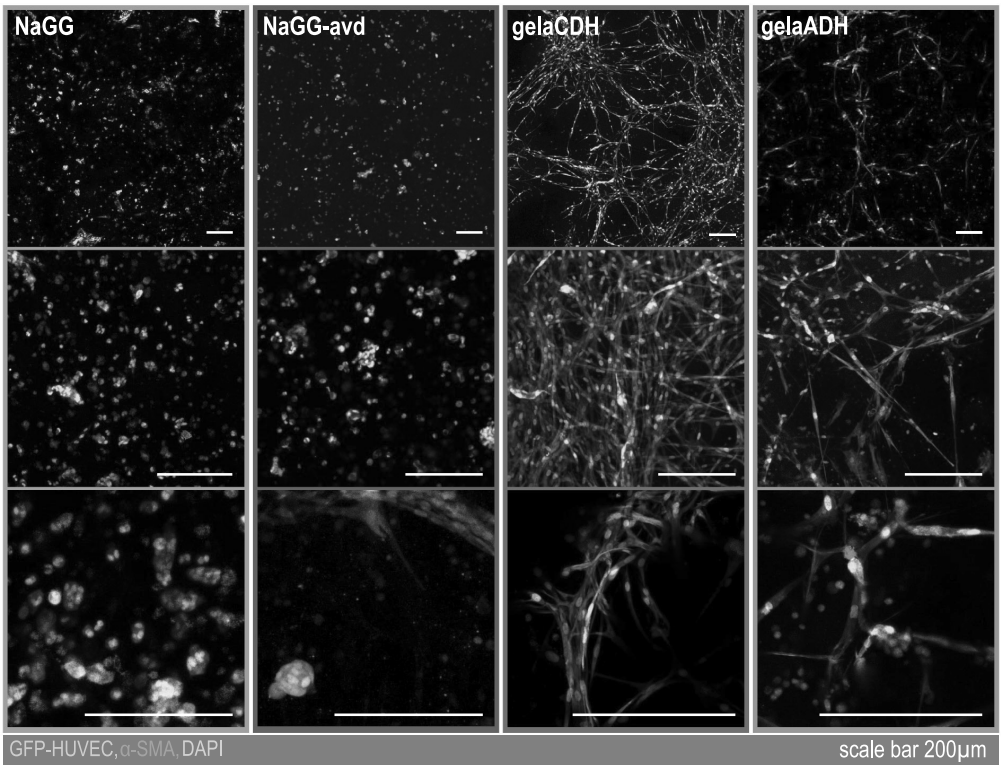

Fig. 4. Confocal microscope images of *in vitro* co-culture samples at day 14 after encapsulation. Red = αSMA, green = GFP-HUVEC, blue = DAPI cell nuclei, scale bar is 200 μm. All images were taken with 10× objective, top row shows a tile stack (1790 × 1790 μm), center row standard stack (639 × 639 μm), and bottom row small stack (310 × 310 μm).

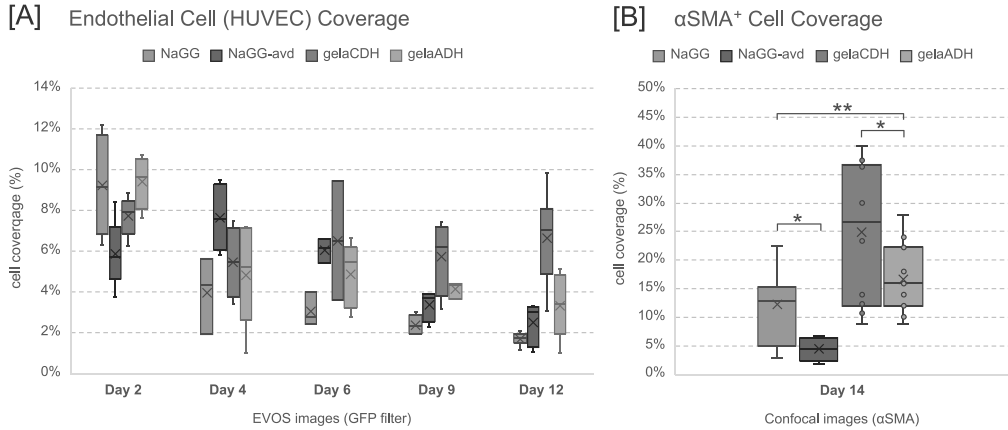

Fig. 5. Percentage of images covered with (A) endothelial and (B) αSMA positive cells, representing network formation. (A) GFP-HUVEC channel/signal from 4× magnification images on day 2, 4, 6, 9 and 12. (B) αSMA signal from confocal microscope images (pooled) at day 14. Images were analyzed using AngioTool.

day 12 and confocal day 14 seem to resemble each other in distribution between the investigated materials.

3.3. Macroscopic and histologic evaluation of the hydrogel implants

The animals tolerated the implantation procedure well and did not show adverse reaction (Appendix A4). All the animals behaved normally throughout the observation period after the implant surgery and scabbing was absent or lightweight. None of the animals developed severe oedema, and signs of oedema were entirely absent towards final time points. The hydrogel implants decrease in size between 70 and 50 % during the 28 days evaluation period. Some of the implants moved in the subcutaneous area during the evaluation period. The microscopical evaluation indicated that the implants did not affect the epidermis, dermis or adipic panniculus. The subcutaneous tissue showed diffuse lesions not related with the implant but with the surgical procedure, like oedema, infiltration of mononuclear cells and mast cells. Macroscopic assessment of the retrieved samples and their presence is tabulated in Appendix A3.

The findings from the tissue scoring associated with the implant are summarized in Table 2, where cell presence was rated on a scale from 0 to 3. Tissue slices for day 28 and examples of evaluated features are shown in Fig. 6. A more complete selection of histology images can be found in Appendix A5. In general, foreign body reaction was found to be more pronounced in the bioactivated formulations (NaGG-avd, gelaCDH, gelaADH), and even more so in the gelatin-containing formulations (gelaCDH, gelaADH).

Most prominently, neovascularization around the implant is much more pronounced in both gelatin-composite hydrogels. While gelaCDH shows steady signs of neovascular vessels throughout day 7 to 28, gelaADH has a muted response until day 28, where it achieves the highest score observed within these samples. Neovascularization is slightly more effective in NaGG-avd over pure NaGG, owing to the added fibronectin. There is no direct ingrowth of blood vessels observed into any of the implants. NaGG is the only material without lymphocytic infiltrate, while the other, bioactivated materials induce stronger reactions. Granulomatous reaction and giant cell presence are also greatly increased in the bioactivated hydrogels, especially for the gelatin-containing formulations. A mild capsule formation, indicated also by the presence of multinucleated giant cells, is observed for all implants.

Only the NaGG hydrogels at time points over 14 days showed no granulomatous reaction, all the other samples and time points had evidence of mild to moderate reaction. The gelaADH hydrogel samples showed severe granulomatous reaction at later time points. The presence of giant cells follows similar observations as granuloma, where all samples have mild to moderate giant cell presence. Only NaGG hydrogels show no evidence of giant cells at final time points, while gelaADH hydrogels induce a severe reaction at day 14. No lymphoplasmacytic (LP) infiltrate was observed for NaGG hydrogels on any evaluated time points, while the bioactivated hydrogels showed mild LP infiltrate at earlier time points, and moderate infiltrate towards 28 days.

4. Discussion

Cellular responses *in vitro* and *in vivo* are controlled by a complex combination of surrounding microenvironmental factors including biochemical cues and mechanical support. Native GG is known to be cyto- and biocompatible, albeit not bioactive and cells do not attach to

Table 2
Scoring results of subcutaneous implants. Biopsy slices were fixed in paraffin, stained with hematoxylin and eosin and scored with a scale from 0 to 3 and visualized with + and −.

	NaGG				NaGG-avd				gelaCDH				gelaADH			
Day	7	14	21	28	7	14	21	28	7	14	21	28	7	14	21	28
Neovascularization	+	−	−	−	+	+	−	+	++	+	++	++	+	+	+	+++
Diffuse mast cells	+	+	−	−	+	+	−	−	+	+	++	++	+	+	+	++
Granulomatous reaction	+	+	−	−	+	++	+	+	++	+++	++	++	++	+++	+	+++
Giant cell presence	+	+	−	−	+	++	+	+	++	++	++	++	++	+++	+	++
Neutrophils	−	−	−	−	−	−	−	−	−	−	+	−	−	−	−	−
Eosinophils	−	−	−	−	+	−	−	−	+	−	−	+	+	−	−	+
Lymphocytic infiltrate	−	−	−	−	+	++	+	+	+	++	++	++	+	++	+	++
# of retrieved samples	6	7	4	7	9	9	7	7	10	8	4	4	7	10	3	2

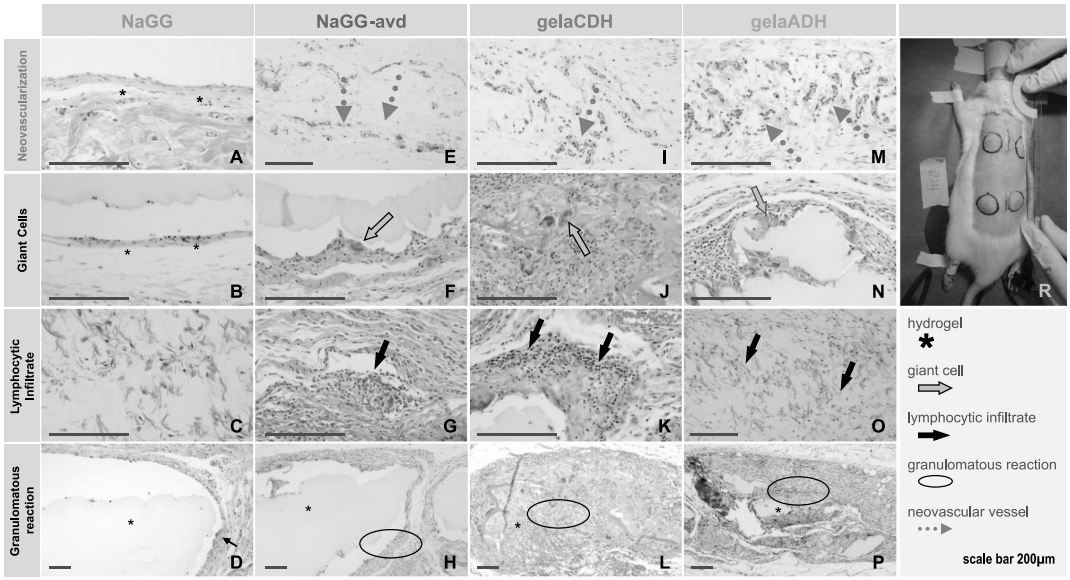

Fig. 6. Exemplary histology slices showing relevant features on day 28. Asterisk (*) indicates the implanted hydrogel. Markers show the following features: Neovascular vessel (A, E, I, M), Giant cell infiltration (B none|F mild|J, N moderate), Lymphocytic infiltrate (C none|G, O mild|K moderate), and Granulomatous reaction (D none|H mild|L moderate|P severe); Hydrogels types are A–D NaGG, E–H NaGG-avd, I–L gelaCDH, M–P gelaADH. Image R shows an example of the implantation sites immediately after surgery.

its polymer structure. To make use of its excellent mechanical properties and availability, many bioactivation strategies have been proposed [15,35–37]. Here, we aimed to investigate bioactivation strategies previously described by our lab in more detail, while directly comparing the three aspects of mechanical properties, *in vitro* cell response and *in vivo* tissue activity, in order to highlight the relation of these features. The hydrogel polymers are formulated in cell culture media, HEPES buffer or sucrose (10 %), which ensures an appropriate osmotic concentration for cell survival. After gelation, cell culture medium was added on top of the hydrogels, which readily diffuses through the hydrogels [38]. During the cell culture experiment, ionic strength and pH are both regulated by addition of cell culture medium on top, and thus they are similar for all investigated materials.

The structural analysis of the investigated materials has been reported extensively in previous publications. Ion concentration of the purified NaGG and functionalized NaGG-avd were determined using ICP-OES, with $Ca^{2+} < 0.1$ wt% and $Na^{+} \geq 2.5$ wt% [24]. The presence of ADH and CDH functional groups in modified gelatin have been confirmed by ^{1}H NMR results [25]. The oxidation degree of GGox has been determined *via* aldehyde UV titration, which showed that over 25 % of available rhamnose rests in the GG repeat unit have been oxidized [30]. Using fluorescence titration, the avidin modification degree of NaGG-avd has been determined to reach up to 0.375 µmol per mg NaGG-avd [24]. All hydrogel formulations have previously been subjected to uniaxial, unconfined compression at a rate of 10 mm/min. The recorded fracture strength of the gelatin-gellan gum formulations is much higher with 20.4 ± 1.8 kPa and 61.6 ± 14.1 kPa for gelaADH and gelaCDH (1:1 formulations with GGox) [25] as compared to the very brittle NaGG-Ca and NaGG-avd-SPD with 5.1 ± 0.8 kPa and 6.4 ± 1.2 kPa respectively. Similarly, the fracture strain is shifted to higher values for gelaCDH (69.9 ± 2.9 %) and gelaADH (61.7 ± 5.0 %) when compared to NaGG (45.5 ± 1.0 %) and NaGG-avd (36.5 ± 5.6 %), underlining the more elastic nature of the gelatin-gellan gum hydrogels.

The hydrogel formulations were analyzed using rheological amplitude and time sweep, taking advantage of the ability to investigate the viscoelastic properties of the as-prepared hydrogels. The rheological time sweep shows that NaGG and NaGG-avd hydrogels are very stiff, but they form gels reliably and fast. The gelaCDH hydrogels are softer and form slowly, while gelaADH presents a high modulus and forms hydrogels very quickly. The extent of the LVER in the amplitude sweep shows that gelatin-GG hydrogel formulations are much more elastic than NaGG-based hydrogels. Viscoelastic properties have been acknowledged to greatly affect cell response and a cell's ability to interact with the material *via* mechanotransduction [1,10,39]. However, material design is an interplay of density, stiffness, viscoelasticity, and degradation, as well presentation and concentration of bioactive and cell attachments motifs [5]. While it was reported that HUVEC have increased expression of VEGF in substrates with lower stiffness [39], angiogenic sprouting has been shown to favor stiffer matrices [40]. As confirmed in our amplitude sweep, pure NaGG hydrogels are rather brittle materials, which is often observed for ionically crosslinked hydrogels [33]. All formulations investigated here form hydrogels fast enough to effectively encapsulate cells for true 3D cell culture, but with sufficient delay to permit casting them to the well plate or into a mold. In regard to the previously assessed compressive behavior, Koivisto et al. (2019) showed that gelaCDH and gelaADH-based hydrogels have a very similar fracture strain and strength, very elastic and brittle [25], although gelaCDH is more elastic. Also NaGG and NaGG-avd have been compared using compression testing and have very similar fracture and strain behavior [24]. When comparing the mechanical properties of our presented hydrogels, their composition and total polymer concentration must be taken into account. NaGG and NaGG-avd are formulated at 8-fold lower concentration than the gelatin-containing samples yet prove to be similar in modulus with lower elasticity. Bioactivity appears to be governed through the addition of gelatin, as well as elasticity and compliance.

Preformed samples could also be analyzed for degradation testing, although measuring highly degraded samples is rather challenging. The performed test does not directly imitate neither *in vitro* nor *in vivo* experiments due to omission of cells, however, a general trend of biomaterial degradation development can be gauged. NaGG and NaGG-avd

have been found to be very stable, but this strongly depends on the success of mixing with the crosslinker, as well as the casting step. Issues were observed in the cell culture experiment with stability of NaGG and NaGG-avd formulations, but that may have been due to inadequate mixing. On the other hand, gelaCDH degrades rapidly *in vitro* without cells, even without serum in the supernatant. In turn, this hydrogel formulation was surprisingly stable in the cell culture experiments, likely due to ECM production of cells stabilizing the construct. Finally, gelaADH hydrogels are more stable, but during the rheology experiments the samples changed appearance and mechanical properties more strongly than NaGG and NaGG-avd hydrogel. Conversely, Koivisto et al. (2019) investigated the degradation of gelaCDH and gelaADH formulations using collagenase and found that ADH degrades more swiftly compared to CDH, which was concluded to be due to higher crosslinking density [25].

The co-culture of HUVEC and hASC or similar mesenchymal stem cells (hMSC) has been shown to promote vasculogenesis and self-assemble to form vascular network with and without additional biomaterial support [17,19,41]. Andree et al. (2019) showed that in serum-free conditions hASC and HUVEC are forming functional vessels in different collagen matrices, however their study provides no assessment of mechanical properties for the used materials. Interestingly, the authors conclude that this co-culture system could be used for supporting rearrangement of target cell types in *e.g.* the formation of smooth muscle cell network, which is strongly reflected by our findings [17]. Similarly, Kim et al. (2022) developed bioprinted collagen-β-TCP scaffolds and showed the co-culture of hASC and HUVEC specifically for osteogenesis and vasculogenesis [41].

Vasculogenesis is indicated by the elongation and network formation of EC, and development of an interconnected network from these. From the confocal images, we detected a formation of endothelial cell clusters and aggregates and short tubule structures but no interconnected vascular network in any hydrogel formation. However, gelatin-containing formulations included significantly more extensive endothelial cell coverage compared to NaGG-based hydrogel formulations. A more pronounced cell network was visible in NaGG-avd on day 12 (Appendix A2–2), but these samples did not endure the staining procedure and were not possible to image using confocal microscopy Overall, NaGG and NaGG-avd seemingly prevent cell network formation, but nonetheless are cytocompatible materials supporting their viability. The effective addition of biotinylated compounds to NaGG-avd at 1.5 μM per 1 mL hydrogel has been shown previously [24], but also in our originally study we concluded this concentration to be too low to achieve noticeable cell response. Surprisingly, despite the incapability to support vascular network formation, gelatin-based formulations rapidly produced an extensive αSMA-positive cellular network. The co-localization of HUVEC and αSMA-positive cells suggests close interaction of the two cell types as detected in our earlier vessel formation studies [23].

While gelaCDH and gelaADH hydrogel formulations are similar in chemical structure and in availability of gelatin, which provides cell interaction, the cell response does show significant differences in endothelial cell coverage. This is likely due to considerable difference in viscoelastic response as observed from the rheological amplitude sweeps. GelaCDH hydrogels are more elastic, while gelaADH hydrogels are quite rigid and have a higher modulus. While it has been reported that angiogenic sprouting is more pronounced in stiffer substrates [40,42], this is not observed when comparing gelaCDH and gelaADH here. However, it is also known that cells prefer a permissive matrix, which improves ability to remodel and deposit own ECM [43], seemingly favoring our gelaCDH formulation.

The results from the animal study are overall in line with the cell culture results: Hydrogels from NaGG are rather inert, NaGG-avd and its fibronectin modification shows a slight upward trend in tissue response, while a strong response is observed from both gelatin-GG formulations, as indicated by the inflammatory markers and neovascular vessel growth around the implants. There was no vascular ingrowth into any of the studied hydrogels, however the implants were cell-free and such auto-vascularization would not be expected. Interestingly, Desai et al. (2015) observed cell infiltration to cell-free hydrogel when observing their injectable, RGD-modified alginate norbornene-click hydrogels [44]. This effect was likely due to physical fragmentation of their ionically crosslinked formulations, which also have been described to be less stable than the covalent photo-crosslinked formulation. Similarly, compared to our crosslinked hydrogel formulations most injectable hydrogels in the literature are much softer, which more easily allow for cell infiltration and remodeling [45,46].

The presence of macrophages in the early time points indicates a positive, acute immune response, while their absence in later time points suggests no chronic inflammation. Similar to our study, Silva-Correia et al. (2013) reported the subcutaneous implantation of cell-free methacrylated GG (GG-MA) photo-crosslinked disks into rats [26]. In line with the expectation that GG-MA is as bioinert as native GG, they observed a moderate infiltration of granulocytes and macrophages into their hydrogels, and complete clearance of immune response markers 3 weeks of implantation.

The chosen implantation time of 28 days is too short to fully assess a mature tissue response and incorporation, but the initial implantation response and acute inflammation can be surveyed. All implanted hydrogels showed foreign body reaction to different degrees and a mild fibrosis. Absence of neutrophils indicates a successful and clean implantation procedure and no adverse inflammation reaction. Similarly, the low count of eosinophils indicates that the materials did not cause any allergic reaction. It is understood that the source of gelatin plays a significant role in immune response [47,48]. We have compared standard cell culture grade gelatin and ultra-low endotoxin gelatin in a preliminary cell culture experiment. The gelatins showed no difference in cell proliferation and morphology (Appendix 6). However, this test might not be directly translatable to *in vivo* tissue reaction. Relevant foreign body reaction was observed during tissue implantation for gelatin-containing hydrogels.

In summary, our observations show that in order to steer cell response *via* mechanotransduction, biomaterial design requires adequate mechanical properties, as defined by viscoelasticity and stiffness, as well as cell attachment, in order to convey the mechanical properties to the cell. Hence, the bioactivation strategy of GG covalently coupling functionalized gelatin (gelaCDH and gelaADH) succeeds in supporting an extensive cellular network and elicits neovascular response *in vivo* than the bioinert NaGG. The addition of fibronectin *via* avidin-biotin coupling in NaGG-avd shows a similar, albeit muted, tendency, likely due to low modification rate [24]. While this work did not aim for a decoupling of viscoelasticity and presentation of bioactive factors within the range of tested biomaterials, we present a comparative insight to vascular network formation *in vitro* and tissue response including neovascularization *in vivo*.

5. Conclusions

We have investigated the chemical modification of the bacterial polysaccharide GG, in an effort to render it more bioactive towards vascularization *in vitro* and *in vivo*. All hydrogels were tested for their rheological properties and gelation time frame, showing that NaGG and NaGG-avd are less elastic than either of the gelatin formulations, and that gelaADH is magnitudes more rigid than gelaCDH. A co-culture of HUVEC and hASC was encapsulated in each hydrogel formulation, as this combination of cell types self-assembles to vascular network. None of our investigated hydrogels formed strong endothelial networks, despite cell attachment sites being provided *via* gelatin. Instead, the gelatin-containing hydrogel strongly supported hASC proliferation and formation of αSMA^{+} cellular network. Biocompatibility of the hydrogels was surveyed by subcutaneous implantation into a rat model for up to 4 weeks. The muted immune response of NaGG and NaGG-avd-b-

fibronectin can be advantageous for inert implantation applications, while the stronger immune response of the gelatin-gellan gum hydrogels proves their general bioactivity. All materials were found to be biocompatible, and no adverse inflammation or host response was observed, but early signs of neovascularization were observed. In summary, we have presented versatile bioactivation strategies for gellan gum, as well as a thorough *in vitro* and *in vivo* testing. Our findings indicate a strong relation between biomechanical properties of a hydrogel and biological responses.

CRediT authorship contribution statement

Christine Gering: Conceptualization, Methodology, Formal analysis, Investigation, Data Curation, Writing, Review & Editing, Visualization; **Jenny Parraga**: Conceptualization, Investigation, Writing, Review & Editing; **Hanna Vuorenpää**: Conceptualization, Validation, Investigation, Writing, Review & Editing; **Lucía Botero**: Methodology, Formal analysis, Resources, Data Curation, Writing; **Susanna Miettinen**: Conceptualization, Validation, Resources, Review & Editing, Supervision, Funding acquisition; **Minna Kellomäki**: Conceptualization, Resources, Review & Editing, Supervision, Funding acquisition.

Declaration of competing interest

The authors declare that they have no known competing financial interests or personal relationships that could have appeared to influence the work reported in this paper.

Data availability

The original contributions presented in the study are included in the article and in the Supplementary materials, further inquiries can be directed to the corresponding author.

Acknowledgements

This work was financially supported by the Academy of Finland through the CoEBoC projects of Minna Kellomäki (312409 and 326587, 336663), and Susanna Miettinen (336666, 326588, 312413). We wish to thank Kirsi Penttinen for carrying out the gelatin coating test, as well as Anna-Maija Honkala and Sari Kalliokoski for their excellent technical assistance. We are further grateful to the Tampere Imaging facilities for assistance with confocal microscopy and image analysis.

Appendix A. Supplementary data

Supplementary data to this article can be found online at https://doi.org/10.1016/j.bioadv.2022.213185.

References

[1] J. Rouwkema, A. Khademhosseini, Vascularization and angiogenesis in tissue engineering: beyond creating static networks, Trends Biotechnol. 34 (9) (2016) 733–745, https://doi.org/10.1016/j.tibtech.2016.03.002.
[2] C. McKee, G.R. Chaudhry, Advances and challenges in stem cell culture, Colloids Surf. B: Biointerfaces 159 (2017) 62–77, https://doi.org/10.1016/j.colsurfb.2017.07.051.
[3] R. Chapla, J.L. West, Hydrogel biomaterials to support and guide vascularization, Prog. Biomed. Eng. 3 (1) (2021), 012002, https://doi.org/10.1088/2516-1091/abc947.
[4] R. Lanza, R. Langer, J.P. Vacanti, Principles of Tissue Engineering, Fourth edi., Academic Press, US, 2014.
[5] C.O. Crosby, J. Zoldan, Mimicking the physical cues of the ECM in angiogenic biomaterials, Regen. Biomater. 6 (2) (2019) 61–73, https://doi.org/10.1093/rb/rbz003.
[6] R. Kocen, M. Gasik, A. Gantar, S. Novak, Viscoelastic behaviour of hydrogel-based composites for tissue engineering under mechanical load, Biomed. Mater. (Bristol, U. K.) 12 (2) (2017) 25004, https://doi.org/10.1088/1748-605x/aa5b00.
[7] F. Lee, M. Kurisawa, Formation and stability of interpenetrating polymer network hydrogels consisting of fibrin and hyaluronic acid for tissue engineering, Acta Biomater. 9 (2) (Feb. 2013) 5143–5152, https://doi.org/10.1016/J.ACTBIO.2012.08.036.
[8] R. Yao, R. Zhang, F. Lin, J. Luan, Biomimetic injectable HUVEC-adipocytes/collagen/alginate microsphere co-cultures for adipose tissue engineering, Biotechnol. Bioeng. 110 (5) (2013) 1430–1443, https://doi.org/10.1002/bit.24784.
[9] M.B. Oliveira, C.A. Custódio, L. Gasperini, R.L. Reis, J.F. Mano, Autonomous osteogenic differentiation of hASCs encapsulated in methacrylated gellan-gum hydrogels, Acta Biomater. 41 (2016) 119–132, https://doi.org/10.1016/j.actbio.2016.05.033.
[10] A.J. Engler, S. Sen, H.L. Sweeney, D.E. Discher, Matrix elasticity directs stem cell lineage specification, Cell 126 (4) (Aug. 2006) 677–689, https://doi.org/10.1016/j.cell.2006.06.044.
[11] T. Muthukumar, J.E. Song, G. Khang, Biological role of gellan gum in improving scaffold drug delivery, cell adhesion properties for tissue engineering applications, Molecules (Basel, Switzerland) 24 (24) (2019) 4514, https://doi.org/10.3390/molecules24244514.
[12] M. Das, T.K. Giri, Hydrogels based on gellan gum in cell delivery and drug delivery, J. Drug Delivery Sci. Technol. 56 (Apr. 2020), 101586, https://doi.org/10.1016/J.JDDST.2020.101586.
[13] P. Matricardi, C. Cencetti, R. Ria, F. Alhaique, T. Coviello, Preparation and characterization of novel gellan gum hydrogels suitable for modified drug release, Molecules 14 (9) (2009) 3376–3391, https://doi.org/10.3390/molecules14093376.
[14] Y. Gong, C. Wang, R.C. Lai, K. Su, F. Zhang, D. Wang, An improved injectable polysaccharide hydrogel: modified gellan gum for long-term cartilage regenerationin vitro, J. Mater. Chem. 19 (14) (2009) 1968–1977, https://doi.org/10.1039/B818090C.
[15] L.A. Rocha, et al., In vitro evaluation of ASCs and HUVECs co-cultures in 3D biodegradable hydrogels on neurite outgrowth and vascular organization, Front. Cell Dev. Biol. 8 (June) (2020) 1–14, https://doi.org/10.3389/fcell.2020.00489.
[16] N.A. Silva, et al., The effects of peptide modified gellan gum and olfactory ensheathing glia cells on neural stem/progenitor cell fate, Biomaterials 33 (27) (2012) 6345–6354, https://doi.org/10.1016/j.biomaterials.2012.05.050.
[17] B. Andrée, et al., Formation of three-dimensional tubular endothelial cell networks under defined serum-free cell culture conditions in human collagen hydrogels, Sci. Rep. 9 (1) (2019) 1–11, https://doi.org/10.1038/s41598-019-41985-6.
[18] M. Ermis, Photo-crosslinked gelatin methacrylate hydrogels with mesenchymal stem cell and endothelial cell spheroids as soft tissue substitutes, J. Mater. Res. 36 (1) (2021) 176–190, https://doi.org/10.1557/s43578-020-00091-4.
[19] J.-R. Sarkanen, et al., Adipose stromal cell tubule network model provides a versatile tool for vascular research and tissue engineering, Cells Tissues Organs 196 (5) (Oct. 2012) 385–397, https://doi.org/10.1159/000336679.
[20] J. Liu, Y.J. Chuah, J. Fu, W. Zhu, D.A. Wang, Co-culture of human umbilical vein endothelial cells and human bone marrow stromal cells into a micro-cavitary gelatin-methacrylate hydrogel system to enhance angiogenesis, Mater. Sci. Eng. C 102 (Sep. 2019) 906–916, https://doi.org/10.1016/J.MSEC.2019.04.089.
[21] U. Blache, S. Metzger, Q. Vallmajo-Martin, I. Martin, V. Djonov, M. Ehrbar, Dual role of mesenchymal stem cells allows for microvascularized bone tissue-like environments in PEG hydrogels, Adv. Healthc. Mater. 5 (4) (2016) 489–498, https://doi.org/10.1002/adhm.201500795.
[22] S. Hauser, F. Jung, J. Pietzsch, Human endothelial cell models in biomaterial research, Trends Biotechnol. 35 (3) (Mar. 2017) 265–277, https://doi.org/10.1016/J.TIBTECH.2016.09.007.
[23] A. Mykuliak, et al., Vasculogenic potency of bone marrow- and adipose tissue-derived mesenchymal stem/stromal cells results in differing vascular network phenotypes in a microfluidic Chip, Front. Bioeng. Biotechnol. (Feb. 2022) 60, https://doi.org/10.3389/FBIOE.2022.764237.
[24] C. Gering, et al., Design of modular gellan gum hydrogel functionalized with avidin and biotinylated adhesive ligands for cell culture applications, PLoS ONE 14 (8) (Aug. 2019) 1–22, https://doi.org/10.1371/journal.pone.0221931.
[25] J.T. Koivisto, et al., Mechanically biomimetic gelatin-gellan gum hydrogels for 3D culture of beating human cardiomyocytes, ACS Appl. Mater. Interfaces 11 (23) (2019) 20589–20602, https://doi.org/10.1021/acsami.8b22343.
[26] J. Silva-Correia, et al., Biocompatibility evaluation of ionic- and photo-crosslinked methacrylated gellan gum hydrogels. In vitro and in vivo study, Adv. Healthc. Mater. 2 (4) (2013) 568–575, https://doi.org/10.1002/adhm.201200256.
[27] L.R. Stevens, J. Gilmore, G.G. Wallace, G.G.M. in het Panhuis, Tissue engineering with gellan gum, Biomater. Sci 4 (9) (2016) 1276–1290, https://doi.org/10.1039/c6bm00322b.
[28] C.J. Ferris, et al., Peptide modification of purified gellan gum, J. Mater. Chem. B 3 (6) (2015) 1106–1115, https://doi.org/10.1039/c4tb01727g.
[29] V.P. Hytönen, et al., Design and construction of highly stable, protease-resistant chimeric avidins, J. Biol. Chem. 280 (11) (2005) 10228–10233, https://doi.org/10.1074/jbc.M414196200.
[30] C. Gering, A. Rasheed, J.T. Koivisto, J. Párraga, S. Tuukkanen, M. Kellomäki, Chemical modification strategies for viscosity-dependent processing of gellan gum, Carbohydr. Polym. 269 (2021), 118335, https://doi.org/10.1016/j.carbpol.2021.118335.
[31] L. Kyllönen, et al., Effects of different serum conditions on osteogenic differentiation of human adipose stem cells in vitro, Stem Cell Res Ther 4 (1) (2013) 17, https://doi.org/10.1186/scrt165.
[32] M. Dominici, et al., Minimal criteria for defining multipotent mesenchymal stromal cells. The International Society for Cellular Therapy position statement, Cytotherapy 8 (4) (Jan. 2006) 315–317, https://doi.org/10.1080/14653240600855905.

[33] E.R. Morris, K. Nishinari, M. Rinaudo, Gelation of gellan - a review, Food Hydrocoll. 28 (2) (Aug. 2012) 373–411, https://doi.org/10.1016/j.foodhyd.2012.01.004.
[34] V. Evageliou, M. Mazioti, I. Mandala, M. Komaitis, Compression of gellan gels. Part II: effect of sugars, Food Hydrocoll. 24 (4) (2010) 392–397, https://doi.org/10.1016/j.foodhyd.2009.11.005.
[35] L.P. da Silva, A.K. Jha, V.M. Correlo, A.P. Marques, R.L. Reis, K.E. Healy, Gellan gum hydrogels with enzyme-sensitive biodegradation and endothelial cell biorecognition sites, Adv. Healthc. Mater. 7 (5) (2018) 1–12, https://doi.org/10.1002/adhm.201700686.
[36] E.D. Gomes, et al., Combination of a peptide-modified gellan gum hydrogel with cell therapy in a lumbar spinal cord injury animal model, Biomaterials 105 (Supplement C) (2016) 38–51, https://doi.org/10.1016/j.biomaterials.2016.07.019.
[37] C.A. Vilela, et al., In vitro and in vivo performance of methacrylated gellan gum hydrogel formulations for cartilage repair*, J. Biomed. Mater. Res. A 106 (7) (2018) 1987–1996, https://doi.org/10.1002/jbm.a.36406.
[38] A.M. Soto, et al., Optical projection tomography technique for image texture and mass transport studies in hydrogels based on gellan gum, Langmuir 32 (20) (2016) 5173.
[39] L. Santos, et al., Extracellular stiffness modulates the expression of functional proteins and growth factors in endothelial cells, Adv. Healthc. Mater. 4 (14) (2015) 2056–2063, https://doi.org/10.1002/adhm.201500338.
[40] B.N. Mason, A. Starchenko, R.M. Williams, L.J. Bonassar, C.A. Reinhart-King, Tuning three-dimensional collagen matrix stiffness independently of collagen concentration modulates endothelial cell behavior, Acta Biomater. 9 (1) (Jan. 2013) 4635–4644, https://doi.org/10.1016/J.ACTBIO.2012.08.007.
[41] W.J. Kim, H. Lee, E. Ji Roh, S. Bae An, I.B. Han, G. Hyung Kim, A multicellular bioprinted cell construct for vascularized bone tissue regeneration, Chem. Eng. J. 431 (Mar. 2022), 133882, https://doi.org/10.1016/J.CEJ.2021.133882.
[42] J. He, Y. Du, J.L. Villa-Uribe, C. Hwang, D. Li, A. Khademhosseini, Rapid generation of biologically relevant hydrogels containing long-range chemical gradients, Adv. Funct. Mater. 20 (1) (Jan. 2010) 131–137, https://doi.org/10.1002/ADFM.200901311.
[43] M.W. Tibbitt, K.S. Anseth, Hydrogels as extracellular matrix mimics for 3D cell culture, Biotechnol. Bioeng. 103 (4) (2009) 655–663, https://doi.org/10.1002/bit.22361.
[44] R.M. Desai, S.T. Koshy, S.A. Hilderbrand, D.J. Mooney, N.S. Joshi, Versatile click alginate hydrogels crosslinked via tetrazine–norbornene chemistry, Biomaterials 50 (2015) 30–37, https://doi.org/10.1016/j.biomaterials.2015.01.048.
[45] N.A. Silva, et al., The effects of peptide modified gellan gum and olfactory ensheathing glia cells on neural stem/progenitor cell fate, Biomaterials 33 (27) (Sep. 2012) 6345–6354, https://doi.org/10.1016/j.biomaterials.2012.05.050.
[46] I. Noshadi, et al., In vitro and in vivo analysis of visible light crosslinkable gelatin methacryloyl (GelMA) hydrogels, Biomater. Sci. 5 (10) (Sep. 2017) 2093–2105, https://doi.org/10.1039/C7BM00110J.
[47] A.B. Bello, D. Kim, D. Kim, H. Park, S.H. Lee, Engineering and functionalization of gelatin biomaterials: from cell culture to medical applications, Tissue Eng. B Rev. 26 (2) (Apr. 2020) 164–180, https://doi.org/10.1089/TEN.TEB.2019.0256.
[48] A. Magnusdottir, H. Vidarsson, J.M. Björnsson, B.L. Örvar, Barley grains for the production of endotoxin-free growth factors, Trends Biotechnol. 31 (10) (Oct. 2013) 572–580, https://doi.org/10.1016/J.TIBTECH.2013.06.002.